

Bulletin of Romanian Chemical Engineering Society

1 2024



ISSN 2360-4697

Edited by SICR and Matrix Rom

The journal is included in the international database
EBSCO, PROQUEST & INDEX COPENICUS

ISSN 2360-4697

**Bulletin of Romanian Chemical
Engineering Society**

Volume 11

2024

Number 1

Contents

Roxana M. STOICA, Mişu MOSCOVICI, Cristina BÂZDOACĂ, Elena S. LAKATOS, Lucian Ionel CIOCA, <i>Studies on biosurfactant production by Bacillus mycoides strain</i>	1
Valeria POP, Alexandru OZUNU, <i>Evaluation of research interests for microplastics in Romania</i>	6
Eugenia T. IACOB TUDOSE, Marius S. SECULA, <i>Methylene blue adsorption in a rotating bed reactor</i>	18
Hüseyin İLCAN, Emircan ÖZÇELIKCI, Mustafa ŞAHMARAN, <i>Circular economy-based solutions demonstrating the efficient recovery of valuable material resources from the construction and demolition waste</i>	29
Andreea MANOLACHE, Ana M. BREZOIU, Ionuţ BANU, Glycerol conversion to lactic acid: process analysis.....	37
Angela G. MAREŞ, Romuald GYÓRGY, Adina GAVRILĂ, Ionuţ BANU, <i>Modeling and optimization of a propylene glycol production plant</i>	59
Ionuţ A. POPA, Oana C. PÂRVULESCU, Petre CHIPURICI, Tănase DOBRE, <i>Modeling of volatile organic compounds flow rate produced in painting installations from automotive industry</i>	78
Valeria DANILOVA, Liliana LAZAR, Florin BANDRABUR, Ioan MĂMĂLIGĂ, <i>The influence of mass transport on the electrocrystallisation process</i>	87
Alexandra I. CRĂCIUN, Carmen A. ROBA, Maria BIZĂU-CÂRSTEA, Alexandru OZUNU, <i>Assessment of heavy metal contamination on agricultural soils in the vicinity of a historically polluted area in Turda, Cluj County</i>	99
Dan A. VASILIU, Oana C. PÂRVULESCU, Iuliana DELEANU, Cristian E. RĂDUCANU, Tănase DOBRE, <i>Technological solutions for obtaining biocellulose membranes with large surface area</i>	105

Hussein F. HUSSEIN, Farqad R. SAEED, Jihad G. ABDULQADER, Shaalan B. AHMED, <i>Effect of surface roughness of Co-Cr alloy modified by hydroxyapatite coating</i>	112
Vasile STAICU, Justinian A. TOMESCU, Mihaela NEAGU, Daniela IONESCU, Cristina MANEA, Ioan CALINESCU, <i>Ethanollic extraction of ursolic acid by conventional methods</i>	127
Adela CIOBANU, Carmen ROBA, Cristina MODOI, Alexandru OZUNU, <i>Thermal treatment a green technology in medical waste management</i>	138
Gheorghe MARIA, <i>Application of (bio)chemical engineering concepts and tools to model genetic regulatory circuits (GRCS), and some essential CCM pathways in living cells for the in-silico re-design some GRCS to obtain GMOS</i>	157

STUDIES ON BIOSURFACTANT PRODUCTION BY *BACILLUS MYCOIDES* STRAIN

Roxana M. STOICA¹, Mișu MOSCOVICI^{1,*}, Cristina BÂZDOACĂ¹, Elena S. LAKATOS^{2,3}, Lucian I. CIOCA^{2,4}

¹National Institute for Chemical-Pharmaceutical Research and Development- ICCF, 112 Vitan Avenue, District 3, 31299, Bucharest, Romania

²Institute for Research in Circular Economy and Environment “Ernest Lupan”, 400 609 Cluj-Napoca, Cluj, Romania

³Faculty of Industrial Engineering, Robotics and Product Management, Technical University of Cluj-Napoca, 400641 Cluj-Napoca, Romania

⁴Faculty of Engineering, Lucian Blaga University of Sibiu, Industrial Engineering and Management Department, 550024 Sibiu, Romania

Abstract

Currently, there is a growing interest in exploring microorganisms and substrates to produce significant amounts of biosurfactants due to the growing demand for these bio compounds in industrial and environmental applications. This study was carried out to evaluate the ability of the Bacillus mycoides strain to produce biosurfactants and to determine a suitable substrate for their production. Two carbon sources, including waste cooking oil (2%) and whey (2%), were used as different low-cost substrates in the biosynthesis processes. Biosurfactant production was monitored by measuring the emulsification index (E₂₄). Whey proved to be the best substrate for biosurfactant production, followed by waste cooking oil. The TLC chromatographic analysis revealed that the microbial surfactants produced by the Bacillus mycoides strain were lipopeptides. Therefore, this strain represents an important biosurfactant producer, and the application of its bioproducts in bioremediation or industrial sectors should be exploited.

Key words: biosurfactant, *Bacillus mycoides*, cheap substrates, lipopeptides

1. Introduction

Biosurfactants are surface-active agents that consist of a heterogeneous group of organic compounds, including glycolipids, lipopolysaccharides, oligosaccharides, and lipopeptides [1]. Bacterial strains, as well as yeast and fungi, are used in microbial fermentation to produce biosurfactants. Because it generates a variety of cyclic lipopeptides and lipoproteins, including lichenysins,

* Corresponding author: misu_moscovici@hotmail.com

bacillomycin, fengycins, and surfactins, the genus *Bacillus* is one of the most studied among all bacteria for obtaining biosurfactants. A few examples of *Bacillus* species that produce lipopeptides include *B. subtilis*, *B. cereus*, *B. thuringiensis*, *B. globigii*, *B. amyloliquefaciens*, *B. megaterium*, *B. pumilus*, and *B. licheniformis* [2].

Research on the synthesis of bacterial biosurfactants has increased in recent years due to their important properties, such as high temperature and salinity tolerance, stability in pH variation, high degradation rate, better selectivity, and less toxicity [3, 4]. Due to these characteristics, biosurfactants have a broad range of uses in medicine, pharmaceuticals, agriculture, food, and environmental protection [5].

Several studies from literature have reported that *Bacillus* strains are able to produce biosurfactants by using a variety of inexpensive substrates as carbon sources [6, 7].

Therefore, in this paper, the ability of the *Bacillus mycoides* strain to produce biosurfactants using waste cooking oil and whey as potential low-cost substrates in the biosynthesis processes was assessed.

2. Experimental

Biologic material

The *Bacillus mycoides* ICCF 422 strain used in this study, maintained on nutritive agar medium, belongs to the Collection of Microorganisms of Industrial Importance-CMII-ICCF-WFCC 232.

Fermentation media and cultivation conditions

The bacterial strain used as the pre-inoculum was maintained until further use on nutritive agar medium with the following composition % (g/v): meat extract 3.0, bacto-peptone 1.0, NaCl 5.0, and agar 2.0, and incubated for 48-72 hours at 30°C.

To prepare the inoculum, 2.0 mL of pre-inoculum containing 9×10^8 CFU/mL (McFarland Standard No. 3) was seeded into 100 mL of liquid medium (the same composition as the biosynthesis media) in a 500 mL Erlenmeyer flask. The inoculum medium was then incubated for 24 hours at 30°C and 220 rpm on a rotary shaker.

For biosurfactant production, the following liquid media were used:

- M1 medium % (g/v): waste cooking oil 2.0, as a carbon source; corn extract 2.0, as nitrogen source.

- M2 medium % (g/v): whey 2.0, as a carbon source; corn extract 2.0, as nitrogen source.

The culture media were prepared with distilled water, pH-adjusted to 7.0-7.5, and sterilized for 30 minutes at 115°C. The biosurfactant production was performed in 500 mL Erlenmeyer flasks containing 100 mL of the liquid medium inoculated with 10% (v/v) of inoculum. The flasks were incubated at 30°C, 220 rpm, for 72 hours. The chemicals were purchased from Difco (USA) and Sigma-Aldrich (Germany). Bacterial cell growth was determined by measuring the pH and optical density of the culture medium at 550 nm.

Emulsification activity

The production of biosurfactants by the *Bacillus mycoides* ICCF 422 strain was assessed through submerged fermentations using 500 mL flasks containing 100 mL medium on a rotary shaker at 220 rpm. The strain was cultivated in M1 and M2 liquid media for 72 hours at 30 °C. After the culture broths were centrifuged for 20 minutes at 4 °C and 9000 rpm, the emulsification index (E_{24}) was calculated. In different tubes, 4 mL of the supernatant was mixed with 6 mL of heptane, octane, and sunflower oil. The tubes were then vigorously mixed for five minutes and stored for twenty-four hours [8].

Using the formula $E_{24} \% = (\text{height of the emulsified layer} / \text{total height of the liquid column}) \times 100$, the emulsification index was determined. The experiments were performed in triplicate.

3. Results and discussions

Emulsification Index

For 72 hours, bioprocesses were performed at 30 °C. The supernatants obtained at the end of the bioprocesses were evaluated for their capacity to emulsify heptane, octane, and sunflower oil (figure 1).

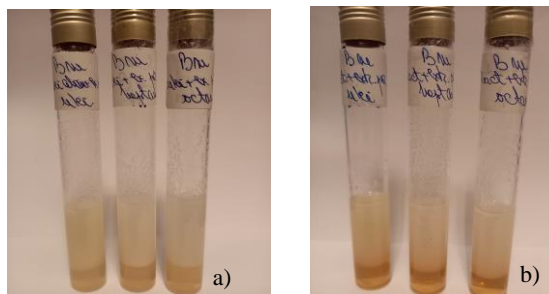


Figure 1. Emulsions obtained with heptane, octane, and sunflower oil with the supernatants of *Bacillus mycoides* ICCF 422 strain cultivated on: a) M1 liquid medium (b) M2 liquid medium

Supernatants of the *Bacillus mycoides* strain grown in M1 medium produced stable emulsions with heptane, octane, and sunflower oil.

The values of the emulsification index (E_{24}) obtained in the case of M1 medium were 67.37% for heptane, 68.96% for octane, and 66.53% for sunflower oil. Regarding the results obtained with M2 medium containing whey as a carbon source, the values of E_{24} were higher compared with M1 medium, with an emulsification index of 72.22% for heptane, 69.23% for octane, and 64.81% for sunflower oil.

The figure below presents the values of the emulsification index ($E_{24}\%$) obtained with the *Bacillus mycoides* strain on M1 and M2 liquid media (Figure 2).

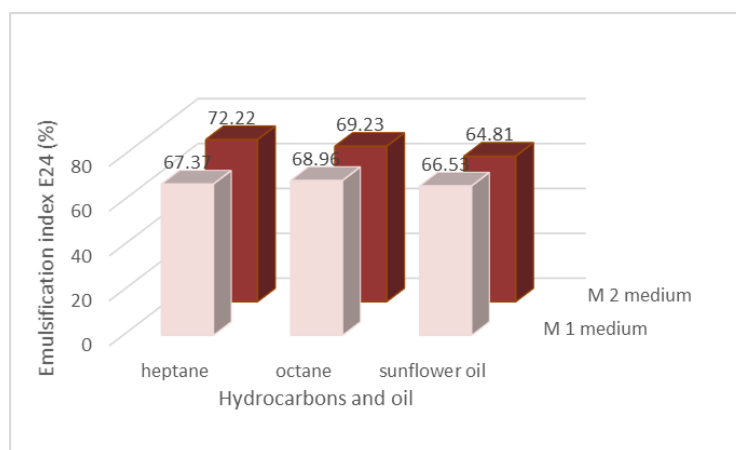


Figure 2. Emulsification index for heptane, octane, and sunflower oil obtained with supernatant of *Bacillus mycoides* ICCF 422 strain cultivated on M1 and M2 liquid media

Therefore, the supernatants of the *Bacillus mycoides* ICCF 422 strain formed emulsions with heptane, octane, and sunflower oil, with the best values of the emulsification index obtained on substrates containing whey at 2%, followed by those obtained using waste cooking oil at 2% as carbon sources. The partially purified bioactive compounds were analyzed by the TLC method, which indicated the nature of the biosurfactants produced as lipopeptides. The results show that the values of the emulsifying indices obtained are in accordance with the findings of Ali et al. [9], who reported an emulsification index of 66.4% for sunflower oil and 52.4% for heptane.

4. Conclusions

Our results demonstrate that the *Bacillus mycoides* ICCF 422 strain is a good producer of biosurfactants on substrates containing waste cooking oil or whey as carbon sources at a concentration of 2%, suggesting the possibility of

industrial production of biosurfactants using economically cheaper substrates. The biosurfactants isolated from the fermentation media were identified by TLC analysis as lipopeptides and showed high emulsification activity, which makes them suitable for various industrial and environmental applications. The biosurfactant-producing capacity of this strain will be further increased by optimization studies.

REFERENCES

- [1] Adamu A., Ijah U.J.J., Riskuwa M.L., Ismail H.Y., Ibrahim U.B., Study on biosurfactant production by two *Bacillus* species, *International Journal of Scientific Research in Knowledge*, 3(1), (2015), 013-020.
- [2] Nawazish A, Zhengjun P., Fenghuan W., Baocai X., Hesham R.S., Lipopeptide biosurfactants from *Bacillus* spp.: Types, Production, Biological Activities, and Applications in Food, *Journal of Food Quality*, vol. 2022, (2022), 1-19, Article ID 3930112, <https://doi.org/10.1155/2022/3930112>.
- [3] Schalchli H., Lamilla C., Rubilar O., Briceño G., Gallardo F., Durán N., Huenchupan A., Diez M.C., Production and characterization of a biosurfactant produced by *Bacillus amyloliquefaciens* C11 for enhancing the solubility of pesticides, *Journal of Environmental Chemical Engineering*, 11 (6), (2023), 1-11, <https://doi.org/10.1016/j.jece.2023.111572>.
- [4] Ali F., Das S., Hossain T.J., Chowdhury S.I., Zedny S.A., Das T., Ahmed C.M.N., Uddin M.S., Production, optimization, stability and oil emulsifying potential of biosurfactants from selected bacteria isolated from oil-contaminated sites, *Royal. Society Open Science*, 8, 211003, (2021). <https://doi.org/10.1098/rsos.211003>.
- [5] Diez M.C., Llafquen C., Fincheira P., Lamilla C., Briceño G., Schalchli H. Biosurfactant production by *Bacillus amyloliquefaciens* C11 and *Streptomyces lavendulae* C27 isolated from a biopurification system for environmental applications, *Microorganisms*, 10, (2022), 1892. <https://doi.org/10.3390/microorganisms10101892>
- [6] Rane A.N., Baikar V.V., Ravi K.V., Deopurkar R.L., Agro-Industrial wastes for production of biosurfactant by *Bacillus subtilis* ANR 88 and its application in synthesis of silver and gold nanoparticles, *Frontiers in Microbiology*, 8, (2017), 1-12. doi: 10.3389/fmicb.2017.00492.
- [7] Md Badrul Hisham N.H., Ibrahim M.F., Ramli N., Abd-Aziz S., Production of biosurfactant produced from used cooking oil by *Bacillus* sp. HIP3 for heavy metals removal, *Molecules*, 24, (2019), 1-16, 2617. <https://doi.org/10.3390/molecules24142617>.
- [8] Pathak K.V., Keharia H. Application of extracellular lipopeptide biosurfactant produced by endophytic *Bacillus subtilis* K1 isolated from aerial roots of banyan (*Ficus benghalensis*) in microbially enhanced oil recovery (MEOR). *3Biotech*, 4, (2014), 41-48.
- [9] Ali N., Wang F., Xu B., Safdar B., Ullah A., Naveed M., Wang C., Rashid M.T., Production and application of biosurfactant produced by *Bacillus Licheniformis* Ali5 in enhanced oil recovery and motor oil removal from contaminated sand, *Molecules*, 24, (2019), 1-18. doi: 10.3390/molecules24244448.

Acknowledgements: This work was supported by a grant of the Ministry of Research, Innovation and Digitization, CCCDI-UEFISCDI, project number PN-III-P2-2.1-PED-2021-3528, 731PED/2022, within PNCDI III, and also, was carried out through the NUCLEU Program within the National Research and Innovation Strategic Plan 2023-2027, carried out with the support of MCID, project no. PN 23-28 01 02.

EVALUATION OF RESEARCH INTERESTS FOR MICROPLASTICS IN ROMANIA

Valeria POP^{1,*}, Alexandru OZUNU¹

¹ Faculty of Environmental Science and Engineering, University of Babeş-Bolyai,
30 Fantanele Street, RO-400294, Cluj-Napoca, Romania

Abstract

Global research was and is the engine behind the development of the economy and not least the creation of new jobs in various sectors, while at the same time having a major influence in all other spheres of development such as trade, environment, education, and health. At the European level, this research-development component is a major point of interest in development strategies. In Romania, research is carried out in higher education institutions and in national research institutes with the role of developing Science and Technology to increase the competitiveness of the Romanian economy and increase knowledge with the potential for capitalization and widening the horizon of action. This study shows that research on plastic/microplastic pollution (MPs) is at a low level, even insufficiently studied in Romania, where there are still deficiencies in household waste management. The knowledge gaps identified so far suggest new research directions in the area of MPs at a pioneering level in Romania, plastic studies, and MPs being identified in a few Institutes and Universities in Romania, through this study. At the global level, the abundance of MPs has been studied more intensively in recent years in marine and freshwater environments, and in other environments, in Romania, it is completely absent. The increase in plastic production and the large-scale use of plastic materials results in the accumulation of large amounts of plastic waste in the environment, being a global challenge that must be addressed because the natural aging process of macroplastics generates a multitude of secondary microplastic fragments that accumulates in all areas of the planet. According to the Science and Research Barometer - the State of the Nation project [1], Romanians attach importance to the field of Science and Technology, but at the same time, it does not have a counterpart in the importance given over time by the governments of Romania. The funding granted to this field is below one percent of GDP, which puts us at the bottom of the European ranking, compared to the states in the region (Hungary, Poland, Bulgaria), and the long-term impact of the underfunding of the research field in Romania is negative and difficult to estimate [2].

Key words: micro plastic particles, research interests, research gaps, Romania

¹ Corresponding author: valeria.bob.@yahoo.com

1. Introduction

One of the problems that represents a major risk to health and the environment is plastic waste. A large amount of plastic waste is generated annually worldwide, and landfills are commonly used to dispose of plastic waste. Since 1950, approximately 8300 million metric tons of plastic have been produced worldwide, of which 79% is accumulated either in landfills or in the environment [3]. However, landfilling them does not rid us of plastic waste, it leaves the problem unsolved in the future. Polyethylene (PE), polypropylene (PP), and polyethylene terephthalate (PET) are major types of polymers that are in the sights of scientists, governments, NGOs, and last but not least in the sight of the media. Microplastic (MPs) waste present in a landfill, not properly treated and without sufficient protection, can leak into the environment. MPs pollution from landfills should receive more attention [4]. Due to the increase in plastic production, the use of products, and, last but not least, plastic waste, MPs pollution is a ubiquitous and emerging environmental and health problem that affects biodiversity, water, air, and soil.

At the global level, this type of pollution could be on a downward slope if measures are taken by several poles, namely: governments, science and research, NGOs, large producers of plastic products, and last but not least, the civic spirit of the population, which could be shaped by changing attitudes and behaviors towards recycling. Global research being an engine that pushes the economy from behind could have a major influence in putting plastic pollution on the downward slope. There are worldwide studies done on plastic, micro and nano plastic, most of them being done on fresh waters, and in the other environmental factors, it could be said that the research is at a pioneering level, but in Romania, it is completely lacking for more many environmental factors.

Our study shows the development and research interests on the territory of Romania, carried out in a few Research Institutes and Universities. Plastic/microplastic pollution (MPs) is still at a low level, even insufficiently studied in Romania, with great deficiencies in household waste management, in particular. The transformational element at the national level is represented by investments in large collaboration projects between the private sector and research organizations (innovation and technology centers), which ensure the increase in the number of actors in research, fighting together with the private sector to achieve a common agenda of research, including through participation in international partnerships, will lead to the decrease of this deficiency in research in the territory of Romania in the future. The revitalization of research in Romania depends decisively on the increase of public investments in research and development, (0.17% of GDP was allocated in 2018) placing us, as a country, in last place in the European Union. There is a need for an increase in private

investment in research, development, and innovation, and for this reason, Romania aims to reach the level of 1% of GDP by 2027, in this area [5]

State of the Art

Research interests in Romania/plastic/MPs

(i) In Romania, interest in research in the MPs field is low. The southeastern part of the country is covered by the *GeoEcoMar Research Institute* with headquarters in Bucharest. The scientific activity there is focused on the following fields: geological and geophysical studies within the Danube - Danube Delta - Black Sea macro-geosystem; complex studies in the coastal area of the Black Sea; geology - paleontology, natural protected areas. The Institute is also based in Constanța and has scientific activities in the following fields: natural, mineral, energy (conventional and non-conventional), and biological resources; geochemistry, oceanography, and marine ecology.

Iulian Pojar is one of the few Romanian scientists representing GeoEcoMar who studies water pollution with MPs particles, elements that are increasingly present in the Danube and the Black Sea. In his study, conducted with German colleagues, and published in 2021, Iulian observed an average amount of seven particles of MPs and mesoplastic (larger than 5 mm) per cubic meter of seawater, sampled from the surface of the Black Sea basin. Three-quarters of the amount of plastic is textile fibers, and the rest are small foils and fragments.

The study focuses on assessing the abundance and composition of plastics on the surface of the Black Sea, especially in its west, where there is a lack of data. For this purpose, 12 surface water samples were collected near the Danube Delta and the Romanian coast using neuston nets. Organic materials were removed, and plastic particles were isolated by density separation. The results of the analysis showed an average concentration of 7 plastic particles per cubic meter, predominantly fibers, followed by foils and fragments. The types of plastic identified were mainly polypropylene and polyethylene, consistent with other similar studies. Statistical analyses revealed a significantly higher concentration of plastic near the mouth of the Danube River compared to other areas along the Romanian and Bulgarian coasts, indicating a considerable input of plastic from the river into the Black Sea.

Following visual inspection, for Mps *pyrolysis GC-MS* and *ATR-FTIR* for mesoplastics >5 mm), an average concentration of 7 plastic particles/m³ was obtained, which was dominated by fibers (~76%), followed by foils (~13%) and fragments (~11%) [6].

(ii) Professor Dr. Simona Pînzaru from the Faculty of Physics, U.B.B. Cluj-Napoca, studies MPs particles, with a team of Ph.D. students, *Ioan Ursu Research Institute*, taking water samples for which they use Raman laser technology, one of the newest technologies used in Romania. In their latest study, they took samples from two springs in the Carpathian Mountains/most MPs found were dominated by polyethylene terephthalate (PET), followed by polypropylene.

The process of degradation of macroplastics inevitably generates secondary fragments of MPs, which we can find in all the planet's ecosystems, a factor that led to an increase in the number of studies at the global level, starting with 2015, for MPs. Although MPs pollution in large water bodies such as rivers, seas, and oceans are well documented, their presence in karstic spring waters has not yet been reported. In his study, Nesterovsky [7] used *Raman microspectroscopy* to confirm the presence of MPs in water samples collected from two rural karst springs in the Apuseni Mountains, Romania (Țarina and Josani). Two sets of 1000-liter water samples, collected in the spring and fall of 2021, were filtered and analyzed. Using the Python programming language and combining two separate Raman databases, one for plastics and one for pigments, a custom database was created to identify the type of plastic and pigment present in the discovered micro-fragments. The study confirmed the presence of MPs particles in the karst spring waters, and the quantitative estimate was 0.034 fragments or fibers per liter at Josani and 0.06 at the Țarina karst spring in spring 2021. Five months later, sampling in autumn 2021 revealed 0.05 microplastics per liter.

(iii) An effective solution could be to improve recycling and waste management strategies to reduce plastic pollution in the future, according to Marica [8] from the *Ioan Ursu Institute, Cluj-Napoca, Babes Bolyai University*. Raman analyses of representative stocks of plastics aged in terrestrial or aquatic environments, up to 15 years old, were performed. All information was used to build a *Raman logic platform* for the automated sorting of plastic waste recovered from the environment.

The methodology respects the principles of FAIR (Findability, Accessibility, Interoperability, and Reuse) of scientific data, being useful to researchers, decision-makers, and stakeholders contributing to an improved management of them that can have a positive impact both economically and environmentally.

(iv) Marcel Liedermann, from the *Institute of Hydraulic Engineering and River Research, Department of Water Atmosphere and Environment, BOKU - University of Natural Resources* in collaboration with Ionut Procop researcher at the Lower Danube University, made measurements for the concentrations of MPs on the Danube River. Water samples were taken from Romania, Serbia, and Austria

and the results showed that there is a strong fluctuation, longitudinally and depending on the flow level on the Danube River, of MPs particle concentrations. Liederman [9], shows the importance of MPs study using benthic nets for MPs collection as a measurement methodology, *the multipoint method for longitudinal and transversal measurements*.

As a result of the measurements, they obtained a spatial and temporal distribution of MPs in the Danube River comparing the concentrations of MPs between different riparian countries, showing at the same time the important role of the Danube River and other rivers in the transport and accumulation of MPs.

(v) In his study, Stoica [10], *INCDPM - National Marine Research and Development Institute Grigore Antipa Constanta*, presents the results of seasonal research on marine waste carried out over a period between 2018 and 2019, a study based on the degree of tourism exploitation and urbanization on three sandy beaches along the Romanian coast of the Black Sea. The assessment of the abundance and composition of the large waste (> 2.5 cm) and microplastics (1-5 mm) was carried out according to the monitoring methodology described in the EU MSFD TG10 guideline [11], where 55 types of waste were monitored, the main with cigarette butts and pieces of plastic making up the bulk, contributing over 50% of the total waste. Mean MP abundance varied between 4 and 272 particles per square meter between sites. The tourist beaches of the Mamaia resort (Marina Regia and Malibu) recorded an abundance of MP with a variation between 2 and 30 times higher than the protected wild areas (Vadu). The highest concentrations of waste MPs results from the study were recorded in the south of the Mamaia summer resort area (Malibu beach), results that show a more accelerated development of coastal infrastructure, seasonal tourists during the summer, and not least the density of the local population are important factors that influence the level of marine waste pollution on Romanian beaches.

(vi) Batrănescu [12] from the National Research and Development Institute for Industrial Ecology-ECOIND, Department of Environmental Technology and Technological Transfer, Bucharest, analyzes three water samples: the first from a municipal treatment plant and two surface water samples from the Jiu River, upstream and downstream. By filtration and microfiltration, the presence of MPs was detected in all samples, in the form of irregular fragments, fibers, and spheres, with sizes ranging between 3.2 μm and 119.5 μm for fragments and between 3 μm and 15 μm for spheres. MPs analysis was done by electron microscopy.

(vii) A literature-based profile of plastic pollution in the Black Sea coastal area, highlighting major sources of contamination, including large river discharge, transport, and other economic activities, as well as the impact of the COVID-19 pandemic, is being carried out by Savuca [13]. The results show a significant presence of polymeric material in water, sediments, and marine organisms, which

generates concerns related to environmental protection and especially human health. Savuca [13] and his team emphasize the need for improved research on the transport, degradation, and impact of MPs in the future. An identification of the preferential accumulation areas of MPs in the Black Sea could be achieved by taking into account the specific factors that characterize this region, such as currents and salinity distribution.

(viii) The impact of plastic waste on mountain fluvial ecosystems in the Carpathian region, one of the most diverse mountain ranges in Eastern Central Europe, was debated by Liro [14] with its team also made up of Romanian researchers from the *CERNESIM Environmental Research Center Institute, Department of Exact Sciences and Natural Sciences, Interdisciplinary Research Institute, "Alexandru Ioan Cuza" University of Iasi, Iasi, Romania*. Using a detailed river network and data on mismanaged plastic waste, the researchers mapped the distribution of this waste along the 175,675 km of watercourses in this ecoregion. The results show that watercourses located below 750 m altitude are seriously affected by plastic waste, representing 81% of the total length of watercourses, and the highest concentrations of plastic waste were identified in Romania (56.6%). Hungary (23.1%) and Ukraine (16.5%).

The conclusions of this study emphasize the importance first of identifying and monitoring areas with high concentrations of plastic waste in the Carpathian region, which leads to the support and collaborative efforts between the scientific community, engineers, government authorities, and citizens in managing and reducing pollution with plastic in this region.

(ix) *Chondrostoma nasus*, following the studies carried out by Curtean-Banaduc [15], from the Applied Ecology Research Center, Lucian Blaga University in Sibiu, Romania, proved to be a perfect vector for the absorption of MPs that contained extremely dangerous chemical substances, a fact that also constitutes a danger for human food.

(x) According to Buruiana [16], from the *University Dunarea de Jos, Galati*, polypropylene and abrasive blasting sand in the hot asphalt mixture is a viable option that brings an improvement in the performance of the mixture.

Although the studies on plastic pollution and MPs in Romania are at a pioneering level, a large amount of plastic is transported to the Black Sea through the Danube River. A detailed investigation of plastic pollution and waste management in the Danube Basin and the Black Sea is imperative. According to Buruiana [17], this investigation must lead to the development of emergency plans for the future, which aim to support the learning of future generations to prevent a new environmental disaster related to water pollution. All these things can be done starting from an assessment of the population and more specifically of the young population through various market studies related to attitudes and behavior

towards this type of pollution that is related to human health and the environment with all its factors.

Technologies that have undergone rapid development, especially during the COVID-19 pandemic, have contributed to increasing water pollution with plastic. Macroplastics have a direct harmful effect on wildlife. Animals can ingest large pieces of plastic or become entangled in objects such as fishing nets, suffocating or starving (Fig. 1).

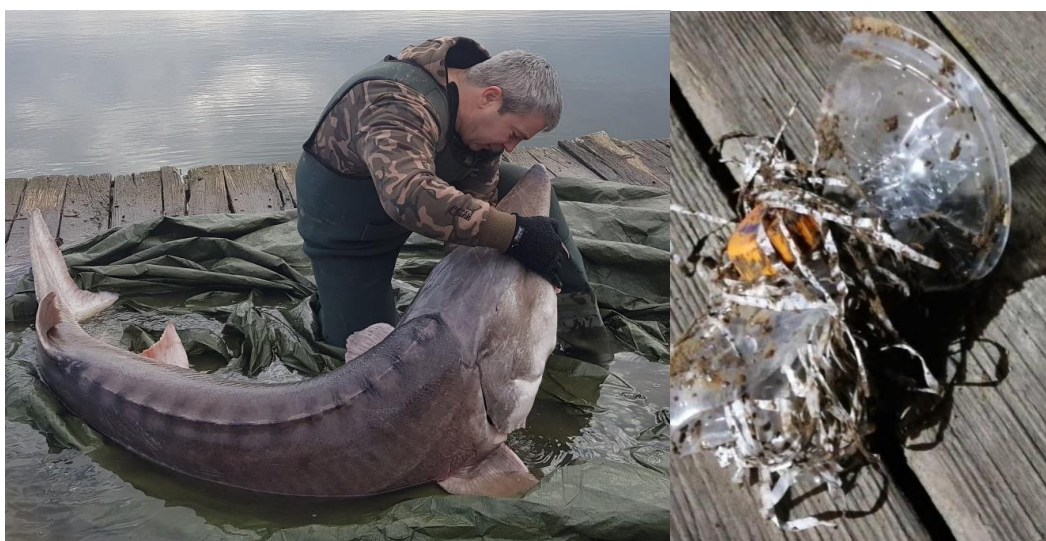


Fig. 1- Sturgeon was saved from the after he ingested plastic [18]

(xi) Dr. Scutariu is a scientific researcher at the Pollution Control Department (Laboratory for Water, soil, waste control) within the *National Institute for Research and Development for Industrial Ecology ECOIND*, Bucharest, Romania. One of her objectives is to investigate adsorption processes occurring on the surface of MPs particles using an important class of organic pollutants (organochlorine pesticides). The results showed that these compounds, being in contact with Mps particles, can be significantly adsorbed (up to 50%). In the future, the contaminated particles can be ingested by aquatic organisms, ultimately causing damage to the entire food chain [19].

As I specified above, market studies have an effect over time on the behavior and attitude of the population. In Romania, we find few studies on this type of pollution, the content of some of them being described below.

(xii) *The Grigore Antipa, Constanța National Marine Research and Development Institute (NIMRD)* is actively involved in activities related to marine waste, participating in various projects such as beach cleaning activities, education, and awareness campaigns by introducing the Marine Litter Watch mobile application that offers tools to collect and share comparable data on marine litter on beaches.

In addition to these tools, it provides a platform for marine litter communities to come together and share knowledge to create approaches that can monitor marine litter. The surveys that were carried out were done during and outside the summer season (2015), and the main waste identified were cigarette butts and plastic containers [20].

(xiii) Boca [21], aims to study or examine the effects of university students' needs and awareness on their environmental behavior. For this purpose, data were collected from 537 students at the *University of Cluj Napoca*, Romania, from the engineering and management specializations, the study being carried out through an online questionnaire regarding plastic pollution. The results obtained from the survey led to the identification of common elements of student's needs regarding their behavior and awareness regarding plastic waste.

(xiv) Pop [22], in his market study, recognizes the influential role that the mass media has in shaping public attitudes and behaviors and investigates whether the media influences awareness and perceptions of environmental and health risks in association with MPs. The results show that age and specific media narratives significantly influence MPs awareness.

Pop together with his team under the guidance of Mr. Professor Dr. Ing. Alexandru Ozunu are interested in research in the Mps area, the Someș river that drains a hydrographic basin of 15,740 km², comprising 403 water courses with a total length of 5,528 km, being the fifth largest river in the country. This would be the first study to test MPs on the Somes River, a river that has a major impact on the environment. In Romania there are many test studies on fresh waters, some of them identifying risk areas in rivers such as River Aries with heavy metal content from the main mining operations [23].

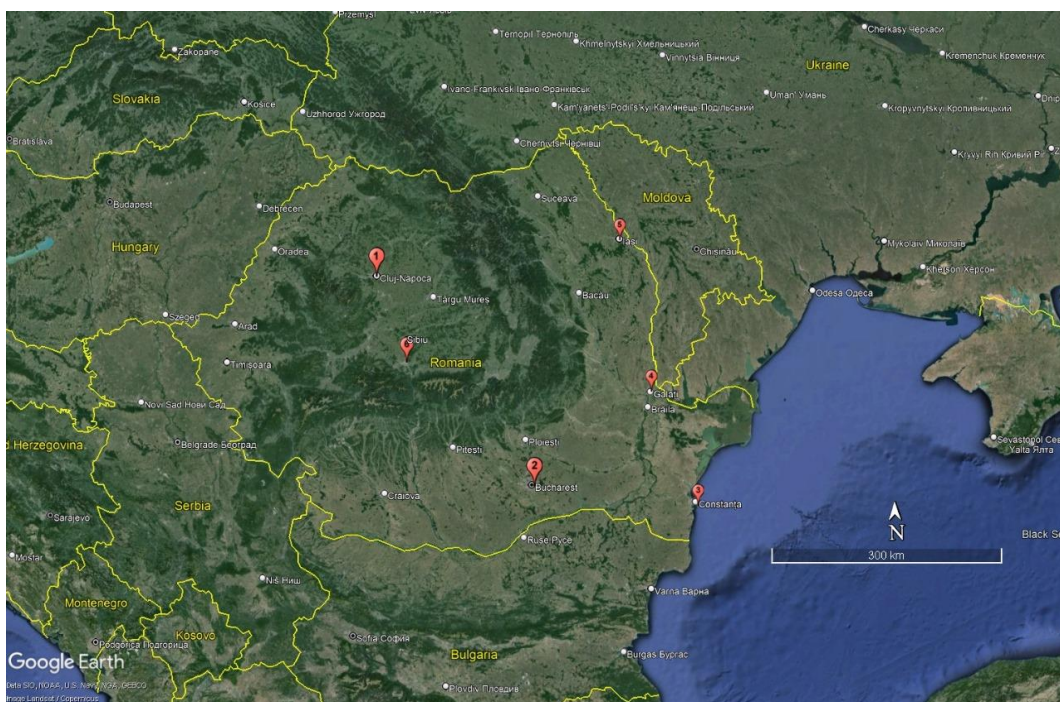


Fig. 2- Research interests - plastic/microplastic - Romania

2. Methodology: Literature search

As a methodology, I did a literature analysis for the study of plastic/microplastic in Romania (Fig. 2). The literature review was carried out in Science Direct, Web of Science, Scopus, and the Google Scholar search engine between February and March 2024. The initial stage of literature identification included the search terms: microplastic, research interests, research gaps, and Romania, which can be found in the title, abstract, and/or keywords. For the first time, I selected ISI articles, but also collected BDI articles and analyzed the results obtained. The review was done to identify future research needs in the MPs area.

3. Results and discussions

The most developed technique for micro and nano plastic research in Romania is Raman Spectroscopy from the Ioan Ursu Institute in Cluj-Napoca. The other research centers use FTIR (Fourier-Transform Infrared Spectroscopy) technology, which is an analytical method used to identify and characterize materials based on the infrared spectrum, being a common and efficient technique at the same time. It is a robust and sensitive method that can identify a wide range

of polymer types and is frequently used in microplastic pollution monitoring studies and environmental impact and public health research. Raman spectroscopy, a newer and more complex technique than FTIR spectroscopy, can provide detailed information about the chemical structure and composition of the material, including chemical bonds with a high sensitivity to subtle structural and chemical changes in the analyzed samples. In addition, it can detect multiple types of polymers and other organic or inorganic substances in a sample, as well as the potential to identify different forms of micro and nanoplastic, including changes caused by degradation or other processes. As with any technique, there are some limitations: certain materials can exhibit fluorescence that can interfere with the Raman signal and require sensitive equipment and experts to interpret the data and analyze the results.

The state-of-the-art in this field is the LDIR (Laser Direct Infrared) technique. As advantages: high sensitivity and detection capability for various types of polymers and plastics resistance to fluorescence which may make LDIR preferable for highly fluorescent samples potential to provide rapid and accurate results without the need for preparation of the samples. In general, the choice between Raman and LDIR depends on the specific objectives of the study, the type of samples analyzed, and the availability of the necessary equipment and expertise. Sometimes, it is useful to combine both techniques to obtain a comprehensive characterization of micro and nanoplastic, but the LDIR technique, used in a few research centers worldwide, has not been found in Romania until now.

Even in market studies (microplastic, nano-plastic), Romania is not leading. We have big gaps in this research area as well.

4. Conclusions:

Regarding the research and management of MPs and nanoplastics in Romania, as can be seen in our study, several limitations and gaps must be addressed to improve the situation. The first and the one that was discussed in the largest proportion in our study is the lack of *(i) the necessary infrastructure and resources* for research and adequate monitoring of MPs in Romania. Greater investment in specialized equipment and laboratories as well as staff training in MPs analysis is required.

(ii) Legislation and policies: It is extremely necessary to develop and implement effective legislation and policies to reduce and manage microplastic pollution in Romania. In recent years, huge steps have been taken in this area of policies and legislation, but this trend still needs to be continued by including restrictions on the use and elimination of single-use plastics, the promotion of alternative and sustainable solutions, as well as education and public awareness.

(iii) *Monitoring studies*: It is essential to carry out extensive microplastic monitoring studies in different aquatic and terrestrial environments in Romania. As we can see, in Romania there are no studies on several environmental factors in the area of PM pollution. These studies should identify the sources, distribution, and levels of MPs contamination, to assess environmental and public health impacts.

(iv) *Education and awareness*: It is very important at the national level to increase the level of awareness and education among the population, decision-makers, and large producers in the industry, at the same time reducing the negative impact on health and the environment. The introduction of environmental education modules in schools starting with primary grades and last but not least public information campaigns could play a crucial role in changing behavior and attitude towards the use and disposal of plastics.

(v) *Research and innovation*, the limitation that was the basis of our study is extremely necessary, contributing simultaneously to finding alternatives for plastic. Government support, EU funds, etc., could stimulate the development of more effective and sustainable solutions to combat microplastic pollution.

(vi) *Last but not least, an international operation* is essential for the global approach to the microplastic problem. A more in-depth initiative through Romania's participation in international projects for an exchange of knowledge, and good practices in the field of MPs pollution management, would be necessary in the coming years.

To reduce MPs pollution, an integrated and coordinated approach is needed at the national and international levels to address the MPs problem in Romania, protecting the environment and public health in the long term, involving the same time actions starting from the governmental and legislative level, the civic spirit, industry, and all other interested parties.

REFERENCES

- [1] Guvernul Romaniei, *Starea Națiunii Construirea unui instrument inovator pentru fundamentarea politicilor publice*, 2018. [Online]. Available: <http://starea-natiunii.ro/index.php/ro/>
- [2] Institutul National de Statistica, *Comunicat cercetare si Dezvoltare*, 2024. [Online]. Available: <https://insse.ro/cms/ro/tags/comunicat-cercetare-dezvoltare>
- [3] Geyer R., Jambeck J. R., Law, K. L., Production, use, and fate of all plastics ever made, *Sci. Adv.*, 3, 7, (2017), 1700782, doi: 10.1126/sciadv.1700782.
- [4] Wan Y., Chen X., Liu Q., Hu H., Wu C., Xue Q., Informal landfill contributes to the pollution of microplastics in the surrounding environment, *Environmental Pollution*, 293, (2022) , 118586, doi: 10.1016/j.envpol.2021.118586.
- [5] Guvernul Romaniei, *Strategia Națională de Cercetare, Inovare și Specializare Inteligentă 2022-2027*, 2021. [Online]. Available: https://www.poc.research.gov.ro/uploads/2021-2027/conditie-favorizanta/sncisi_19-iulie.pdf

- [6] Pojar I., Kochleus C., Dierkes G., Ehlers S.M., Reifferscheid G., Stock F., Quantitative and qualitative evaluation of plastic particles in surface waters of the Western Black Sea, *Environmental Pollution*, 268, (2021), 115724, doi: 10.1016/j.envpol.2020.115724.
- [7] Nesterovschi I. *et al.*, Subterranean transport of microplastics as evidenced in karst springs and their characterization using Raman spectroscopy, *Spectrochimica Acta Part A: Molecular and Biomolecular Spectroscopy*, 298, (2023), 122811, doi: 10.1016/j.saa.2023.122811.
- [8] Marica I., Aluș M., Cîntă Pinzaru S., Raman technology application for plastic waste management aligned with FAIR principle to support the forthcoming plastic and environment initiatives, *Waste Management*, 144, (2022), 479–489, doi: 10.1016/j.wasman.2022.04.021.
- [9] Liedermann M., Pessenlehner S., Gmeiner P., Mayerhofer J., Procop I., Habersack H., *Microplastic measurements at the Danube river using a multi-level approach*, 2023. doi: 10.5194/egusphere-egu23-14876.
- [10] Stoica E., *Assessment of the Marine Litter on the Romanian Black Sea Beaches*. 2021. [Online]. Available: DOI:10.55268/CM.2021.51.49
- [11] European Commission, *Guidance on Monitoring of Marine Litter in European Seas*, 2013. [Online]. Available: https://www.researchgate.net/publication/258240681_Guidance_on_Monitoring_of_Marine_Litter_in_European_Seas
- [12] Batrinescu G., Ionescu I.A., Scutariu, R.E. Chiricuta B., Surupaceanu I. C., Characterisation of Microplastics from the Effluent of a Municipal Wastewater Treatment Plant and from its Natural Receptor, *Mater. Plast.*, 58, 4, (2022) 47–54, doi: 10.37358/MP.21.4.5530.
- [13] Savuca A., Nicoara M.N., Faggio C., Comprehensive Review regarding the Profile of the Microplastic Pollution in the Coastal Area of the Black Sea, *Sustainability*, 14, 21, (2022), 14376, doi: 10.3390/su142114376.
- [14] Liro M. *et al.*, Mountains of plastic: Mismanaged plastic waste along the Carpathian watercourses, *Science of The Total Environment*, 888, (2023), 164058, doi: 10.1016/j.scitotenv.2023.164058.
- [15] Curtean-Bănăduc A., Mihuț C., Burcea A., McCall, G.S., Matei C., Bănăduc D., Freshwater ecosystems' benthic microplastic uptake in fish: the case study of *Chondrostoma nasus* (Linnaeus, 1758), In Review, preprint, Nov. 2022. doi: 10.21203/rs.3.rs-2253909/v1.
- [16] Buruiana D.L., Georgescu P.L., Carp G.B., Ghisman V., Recycling micro polypropylene in modified hot asphalt mixture, *Sci Rep*, 13, 1, (2023), 3639, doi: 10.1038/s41598-023-30857-9.
- [17] Buruiana D.L., Microplastic Pollution In The Aquatic Environment, Applying A Case Study: Lower Danube-Black Sea Area - A Review, in *MASET-22, MLHES-22, EMMLS-22, IRSET-22 & IEMSSH-22 March 2022 International Conferences*, Dignified Researchers Publication, 2022. doi: 10.17758/DIRPUB10.DIR0322105.
- [18] Descopera.ro, “Un sturion dintr-un lac din Romania ‘s-a lasat salvat’- Plastic si rafie in gura pestelui,” 2020. [Online]. Available: <https://www.descopera.ro/dnews/18785966-un-sturion-dintr-un-lac-din-romania-s-a-lasat-salvat-plastic-si-rafie-in-gura-pestelui>
- [19] Scutariu, Roxana Elena, Puiu, Diana, Nechifor, Gheorghe, Niculescu, Marcela, Pascu, Luoana Florentina, and Galaon, Toma, “In Vitro sorption study of some Organochlorine Pesticides on Polyethylene Terephthalate microplastics,” 2019, [Online]. Available: <http://hdl.handle.net/123456789/1569>
- [20] M. Golumbeanu, *Marine litter watch app as a tool for ecological education and awareness raising along the romanian Black Sea coast*. 2017. [Online]. Available: 348–362 (2017)
- [21] Boca G.D., Saraçlı S., Effects of Romanian Student's Awareness and Needs Regarding Plastic Waste Management, *Sustainability*, 15, 8, (2023), 6811, doi: 10.3390/su15086811.
- [22] Pop V., Ozunu A., Petrescu D.C., Stan A.D., Petrescu-Mag R.M., The influence of media narratives on microplastics risk perception, *PeerJ*, 11, (2023), e16338, doi: 10.7717/peerj.16338.

- [23] Ozunu A., Stefanescu L., Costan C., Miclean M., Modoi, C., Vlad S.N., Surface water pollution generated by mining activities. case study: Aries River middle catchment basin, Romania, *Environ. Eng. Manag. J.*, 8, 4, (2009) 809–815, doi: 10.30638/eej.2009.114.

METHYLENE BLUE ADSORPTION IN A ROTATING BED REACTOR

Eugenia T. IACOB TUDOSE^{1*}, Marius S. SECULA¹

¹“Cristofor Simionescu” Faculty of Chemical Engineering and Environmental Protection, “Gheorghe Asachi” Technical University of Iași

Abstract

This research investigates an intensive discontinuous process for methylene blue dye adsorption from an aqueous solution, in a rotating bed system, containing a specific adsorbent, Aquasorb L27, with enhanced retaining qualities. Experiments were conducted at two different rotational speeds of 500 and 1000 rpm, and two different temperatures, of 20 °C and 45 °C, to study the color removal efficiency in this system, for two different initial dye concentrations of 20 and respectively, 50 mg/L. For the highest MB initial concentration, discoloration of approximately 90% is attained at the largest investigated rotational speed, after 40 min at room temperature and after 16 min, at 45 °C, respectively. Based on a screening evaluation, the bed spinning speed was found to be the most significant influence parameter for the adsorption process, followed by temperature and operating time. Additionally, a modified face centered full factorial design revealed that the adsorption rate constant can be accurately predicted by Response Surface Methodology (RSM).

Key words: adsorption, rotating bed, intensive process

1. Introduction

Dye pollutants from various industries, such as textile, paper, and dye manufacturing, pose significant environmental challenges due to their persistence and potential harmful effects on ecosystems. Conventional methods for dye removal, such as chemical precipitation and filtration, often have limitations in terms of efficiency and cost-effectiveness. In recent years, there has been growing interest in alternative approaches, including adsorption-based technologies, for effective dye removal from aqueous solutions.

One such promising technology is the use of rotating adsorbent beds, which offers advantages such as enhanced mass transfer rates, and potential scalability for industrial applications [1-5]. The rotating bed configuration allows

* Corresponding author

for dynamic fluid flow patterns, promoting efficient adsorption of dyes onto the adsorbent material.

This study focuses on preliminary investigations regarding the feasibility and efficacy of dye removal using an in-house designed rotating adsorbent bed system. The initial dye concentration and three other operational parameters, namely bed rotational speed, temperature and time, are investigated to establish the most relevant parameters for the dye adsorption process. Furthermore, based on experimental data, rate constants based on a pseudo-first-order process model, for all investigated parameters, were determined and a modified face centered full factorial design was performed.

2. Experimental

Materials

Methylene Blue dye from Fluka Chemie AG, Aquasorb L27 mesh 12x40 adsorbent and distilled water were used. The activated carbon L27 was provided by PICA-Jacobi (Vierzon, France). The adsorbent has a developed total surface ($1060 \text{ m}^2 \text{ g}^{-1}$). The characteristics of the employed adsorbent are reported in prior works [6].

Experimental conditions

Preliminary tests included investigation of two initial dye concentrations of 20 mg/L and respectively, 50 mg/L, at two different rotational speeds of 500 and 1000 rpm, respectively, at 20 °C room temperature and 45 °C, respectively. The system consisted of a cylindrical bed containing the adsorbent has a diameter of 6 cm and 5 cm height. It is connected, through a rod, to a stirrer, with adjustable rotational speed. The adsorbent bed is immersed in a vessel of 10 cm internal diameter and 25 cm height. The experimental set-up is depicted in figure 1:

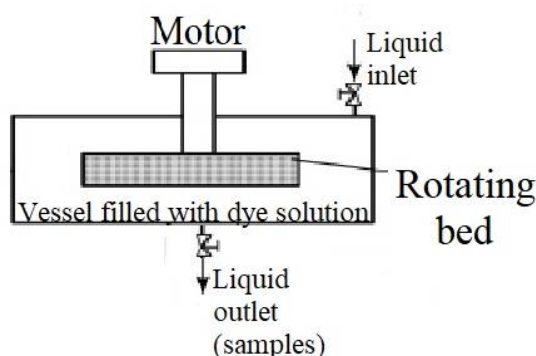


Fig.1 Experimental set-up with a self-designed rotating bed system

Experimental methodology

Experiments were conducted in a batch system, with sampling every 2 minutes to measure the absorbance. The temperature was monitored throughout each test using a thermocouple connected to a data logger. Spectrophotometry using a Hitachi U-5100 UV-VIS Spectrophotometer was applied to measure absorbance at MB characteristic wavelength of 660 nm. Also, measurements to correlate the absorbance with MB dye solutions of well-known concentrations were performed.

Analysis methods

The color removal efficiency, Y , was calculated using:

$$Y = \frac{C_o - C}{C_o} \cdot 100 \quad (1)$$

where C_o is the initial solution dye concentration (mg/L), and C is the solution dye concentration after t minutes of adsorption (mg/L).

The rate constants were determined for all investigated conditions. Considering the rate of adsorption follows a first order mechanism, the pseudo-first-order process model can be expressed by equation (1):

$$\frac{dq_t}{dt} = k_1(q_\infty - q_t) \quad (2)$$

with q_t (mg/g) the amount of dye adsorbed at time t , q_∞ (mg/g) the amount of dye adsorbed at infinite time, k_1 (min⁻¹) is the rate constant of pseudo-first order adsorption. Integration of equation (1), using the following boundary conditions of $t=0$, $q_t = 0$ and $t=t$, $q_t = q_t$, renders:

$$q_t = q_\infty(1 - e^{-k_1 t}) \quad (3)$$

An experimental design methodology for screening and response surface modeling of MB removal from aqueous solutions by adsorption was used. Initial concentration of dye, rotational speed, solution temperature and adsorption process time were considered as dependent variables whereas the removal efficiency was the response function for the screening design. To model the investigated adsorption process, a modified face centered full factorial design was also considered.

3. Results and discussions

Figures 2 and 3 show MB dye removal variation in time for a 20 mg/L initial dye concentration, at 20 °C and respectively 45 °C, for two different rotational speeds of 500 and 1000 rpm. The graphs indicate effective removal rates of approximately 90% in ~40 min time interval, at 20°C, with faster removal rates at the largest bed spinning speed. Data obtained at 45 °C show a color removal efficiency of approximately 90% for both 500 rpm (in 32 min) and 1000 rpm (in 24 min).

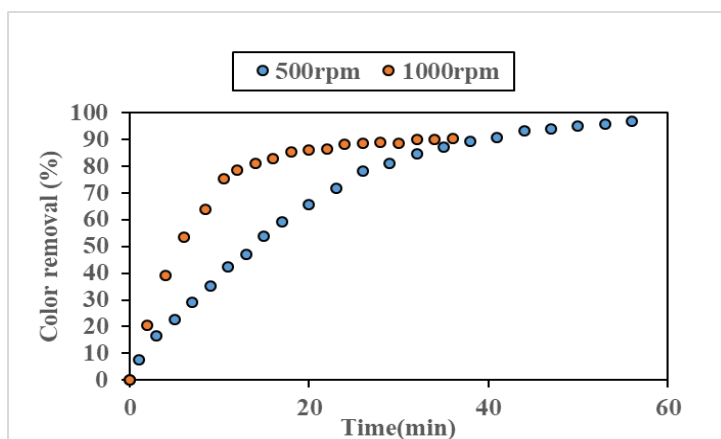


Fig.2 Color removal variation in time for a 20 mg/L MB concentration, at 20 °C, 500 and 1000 rpm rotational speed

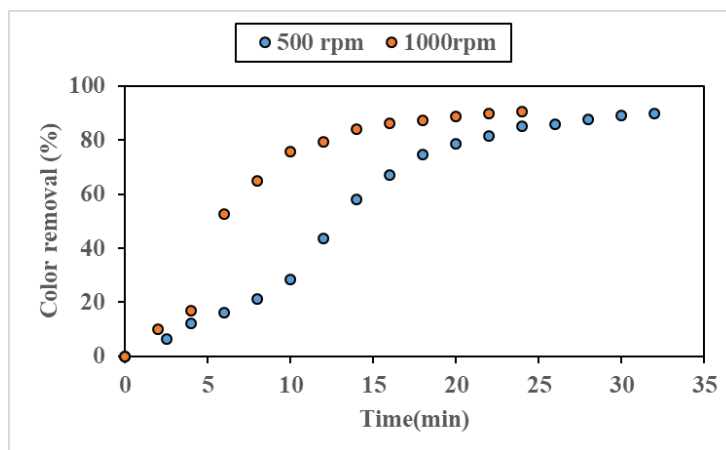


Fig.3 Color removal variation in time for a 20 mg/L MB concentration, at 45 °C, 500 and 1000 rpm rotational speed

Experimental results presented in figure 4 for MB dye initial concentration of 50 mg/L, obtained at 20 °C, for 500 and 1000 rpm, reveal ~ 90% discoloration

in approximately 39 min operation time. Figure 5 comprising data obtained for the same initial 50mg/L MB solution dye concentration, at 45 °C, at same rotational speeds of 500 and 1000 rpm, reveal 88% color removal at lower spinning speed and 94% discoloration at 1000 rpm, both after only 30 min working period. The experimental data indicates good efficiency color removal, in comparison to a regular batch system, for similar working conditions, was attained in the rotating bed adsorber used in this study.

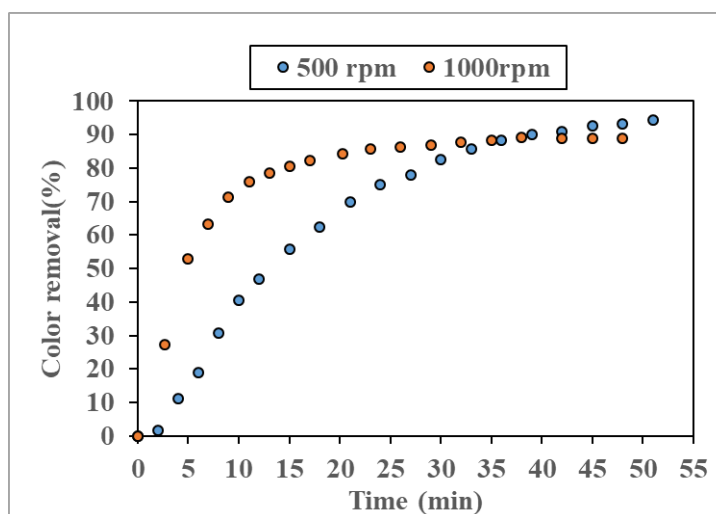


Fig.4 Color removal variation in time for a 50 mg/L MB concentration, at 20 °C, 500 and 1000 rpm rotational speed

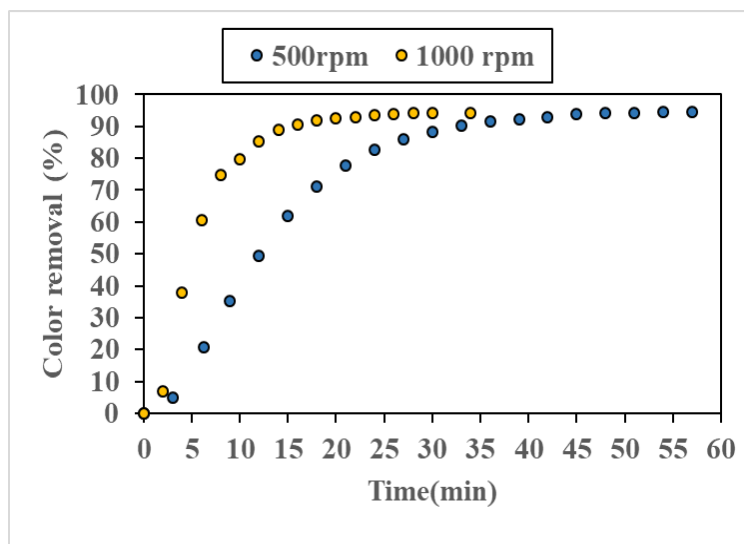


Fig.5 Color removal variation in time for a 50 mg/L MB concentration, at 45 °C, 500 and 1000 rpm rotational speed

The experimental data indicated good efficiency color removal, particularly at larger bed rotational speed and higher temperature.

To provide a better overview of the adsorption dynamics, based on a pseudo-first order process model, the rate constant, k_1 , representing the slope of the equation (2) in logarithmic form was determined. The obtained values depending on the operating conditions are presented in table 1:

Table 1

Rate constant of pseudo-first order adsorption dependence on operating parameters

Dye initial concentration (mg/L)	Temperature (°C)	Rotational bed speed (rot/min)	Rate constant (min ⁻¹)
20	20	500	0.0806
20	20	1000	0.1454
20	45	500	0.1510
20	45	1000	0.2320
50	20	500	0.063
50	20	1000	0.1139
50	45	500	0.0635
50	45	1000	0.2103

One can observe that lower initial dye concentration, higher rotational bed speeds and larger temperatures determine higher rate constant values. Comparison with other literature data is difficult to make because rotating bed systems have not been often used for adsorption process. However, one study investigated adsorption of Basic Yellow 2 dye on activated carbon, in a rotating bed with recirculation, to assess the positive influence of a centrifugal field on adsorption. The authors reported at 1000 rpm bed rotational speed, for an initial dye concentration of 85 mg/L, a rate constant of $1.7005 \times 10^{-2} \text{ min}^{-1}$ [7].

Screening tests

Utilizing a screening process [8], the study examines also the impact of different parameters on color reduction, establishing the most important ones. Using Minitab software, a full factorial design was performed with four dependent variables initial dye concentration, rotational bed speed, aqueous solution temperature and operating time and the response function, the removal efficiency. The obtained Pareto chart being is presented in figure 6. Rotational speed can be identified as the factor exerting the largest influence in reducing color, while temperature and the operation time interval occur as following significant influencing criteria.

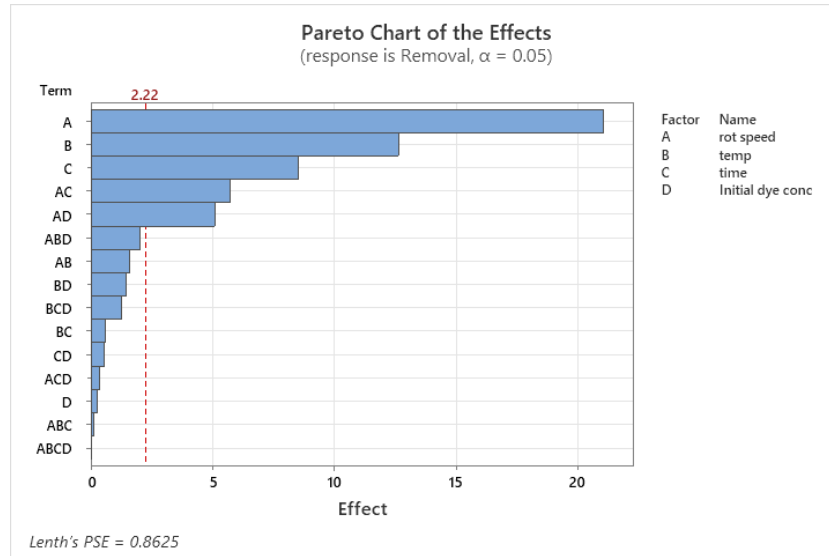


Fig.6 Pareto chart indicating the order of influence for operating parameters on MB adsorption in a rotating bed containing Aquasorb L27

Modified face centered full factorial design (MFCFFD)

The experimental design of the MFCFFD RSM is based on data shown in table 1.

Linear Model Fitting

The factors were MB initial concentration, solution temperature and rotating bed speed. The dependent variable was the rate constant of the pseudo-first kinetic model.

Design Expert Software was used to create the model for the MFCFFD data. The quality of model fitness was improved by removing the coefficients with p-values higher than 0.05.

In terms of actual variables, the following linear model was obtained:

$$Y = -0.04 - 5.98 \times 10^{-4} \times [\text{MB}] + 3.42 \times 10^{-3} \times T + 1.28 \times 10^{-4} \times \text{RBS} \quad (4)$$

subjected to $20 \leq [\text{MB}] \leq 50$ [mg/L]; $20 \leq T \leq 45$ [°C]; $500 \leq \text{Rotational bed speed} \leq 1000$ [RPM].

Table 2 shows the statistics indicators of the proposed model based only on the significant terms.

Table 2

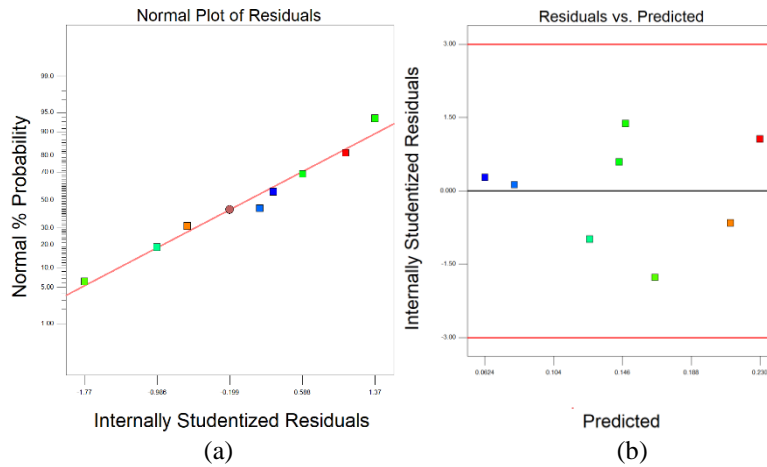
Model statistics

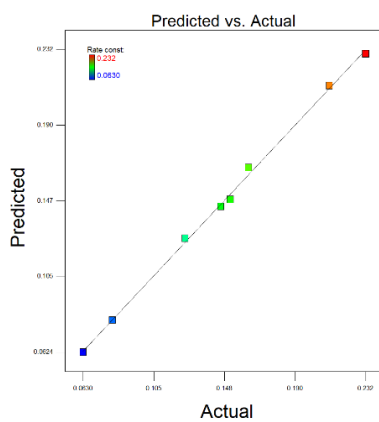
Response	Y, %
Model p value	<0.0001
Model F value	806
Model F-tab	5.343
R^2	0.998
R_{adj}^2	0.997
R_{pred}^2	0.993

The model describing the investigated adsorption process presents an F-value one hundred fifty times higher than the F critical value (tabulated value), thus emphasizing that the model terms have strong effect on the response. Also, the low p-value means that most of variations in response are explained by the suggested regression equation.

The constant rate of the pseudo-first kinetic model is described by the main factors: initial concentration of dye, temperature and rotational bed speed.

Normal probability and residual plots (figure 7) were employed to validate the model.

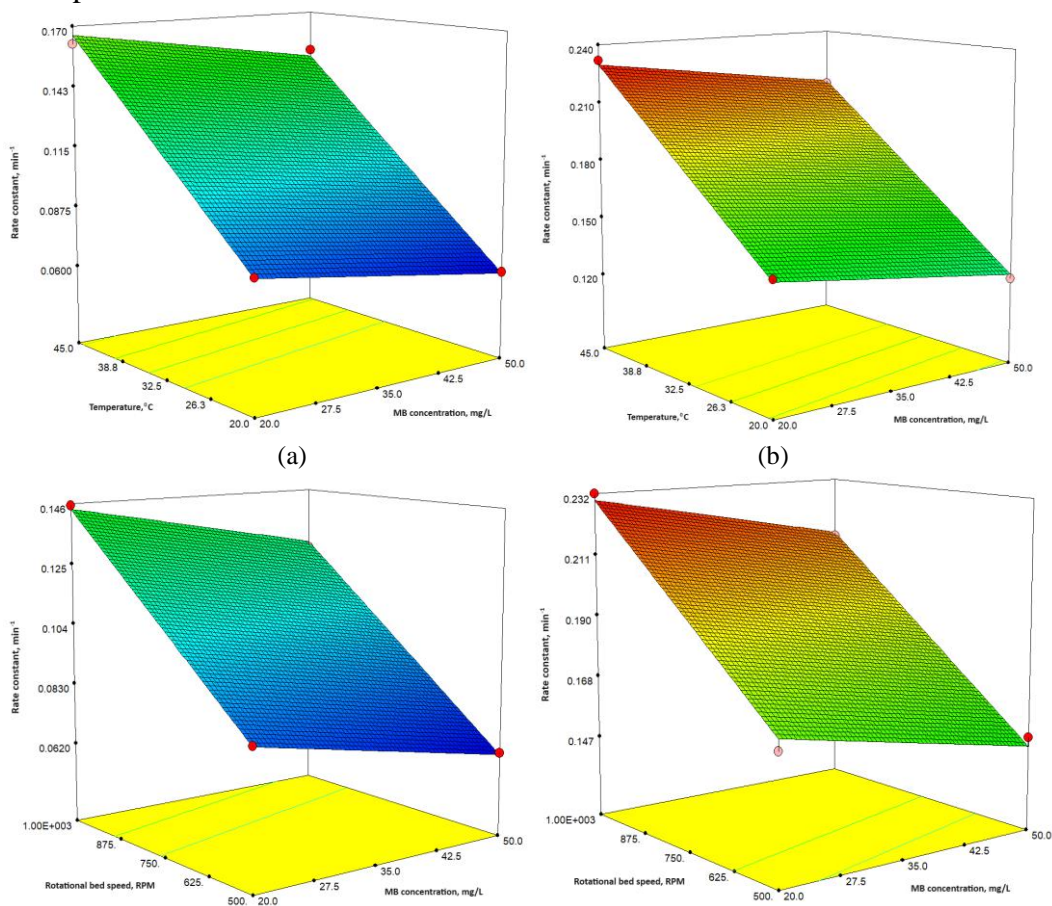




(c)

Fig. 7 Normal probability plot (a); residual plot (b); predicted vs. experimental data plot (c) (Blue fill – low value; green – average value; red – high value of the response).

Figure 8 shows the response surfaces obtained for the constant rate of MB adsorption.



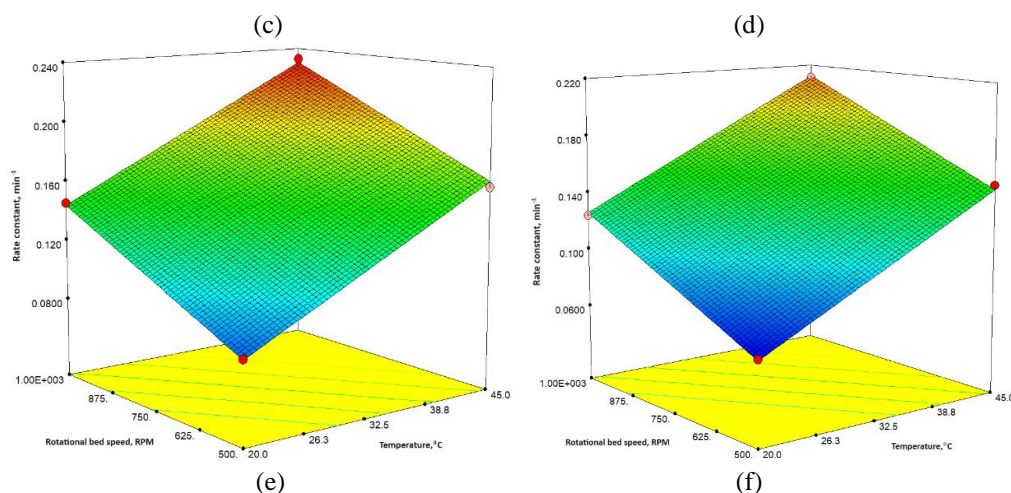


Fig. 8 Response surface of constant rate for MB adsorption as a function of T and [MB] at 500 RPM (a); T and [MB] at 1000 RPM (b); RBS and [MB] at 20°C (c); RBS and [MB] at 20°C (d); RBS and T at 20 mg/L MB (e); RBS and T at 50 mg/L MB (f).

The obtained results show that the rate constant can be accurately predicted by a Modified Face Centered Full Factorial Design RSM.

6. Conclusions

The experimental data revealed a direct correlation between higher rotational speeds and elevated temperatures with increased methylene blue adsorption capacities. The rate of dye uptake by the adsorbent is influenced by the initial concentration of the dye.

The screening investigation highlighted that the bed rotational speed followed by the working temperature and operating time are the most significant parameters affecting the system adsorption capabilities.

A linear model was proposed based on MFCFFD RSM to predict the rate constant for the MB adsorption process on Aquasorb L27, in a self-designed rotating bed system.

REFERENCES

- [1] Guo Q., Zhao Y., Liu Y. Performance and Mechanism of Gas-Solid Adsorption in a Rotating Adsorption Bed, *Chem.Eng.Tech.*, 45, 5 (2022), 844-852.
- [2] Cortes Garcia G.E., van der Schaaf J., Kiss A.A., A review on process intensification in HiGee distillation, *J. Chem. Technol. Biotechnol.*, 92(6) (2017), 1136-1156.
- [3] E Mello M.V.D., Huang H.-M., Systems and methods for deaerating seawater using a rotating packed bed device, U.S. Patent Application 15/211, 284, (2018).

- [4] Guo F., Zheng C., Guo K., Feng Y., Gardner N.C., Hydrodynamics and Mass Transfer in Cross-flow Rotating Packed Bed, *Chem. Eng.Sci.*, 21/22 (1997), 3853.
- [5] Chen, Y.-S., Lin F.-Y., Lin C.-C., Tai C., Liu H.-S. Packing Characteristics for Mass Transfer in a Rotating Packed Bed, *Ind Eng Chem Res.*, 45 (2006). 6846-6853.
- [6] Dávid, E., Secula, M.S., Özdemir, G., Mămăligă, I., Mechanisms of para-chlorophenol adsorption onto activated carbons having different textural and chemical properties, *Desalin. Water Treat.*, 62 (2017), 221-234
- [7] Chia-Chang L., Hwai-Shen L., Adsorption in a Centrifugal Field: Basic Dye Adsorption by Activated Carbon, *Ind. Eng. Chem. Res.*, 39 (2000), 161-167.
- [8] Anderson M.J., Whitcomb P.L., *DOE Simplified. Practical Tool for Effective Experimentation*, 3rd Edition, CRC Press, Boca Raton, Florida, 2015.

CIRCULAR ECONOMY BASED SOLUTIONS DEMONSTRATING THE EFFICIENT RECOVERY OF VALUABLE MATERIAL RESOURCES FROM THE CONSTRUCTION AND DEMOLITION WASTE

Hüseyin İLCAN¹, Emircan ÖZÇELİKCI¹, Mustafa
ŞAHMARAN^{1,*}

¹Department of Civil Engineering, Hacettepe University, 06800, Ankara, Turkey

Abstract

The main objective is to develop and demonstrate novel cost-effective circular smart solutions for an upgraded recovery of secondary building raw materials along the entire circular value chain: from End-of-Life Building materials (EBM) to new building products prepared for circularity and resource-efficiency in built environment. The goal was to enhance the development and demonstration of intelligent solutions that improve the cost-effectiveness, reliability, and performance of quantifying, tracing, and managing EBM. The focus was on designing, developing, and demonstrating cost-effective building products designed for easy disassembly and resource efficiency, encompassing both materials and energy. This involved substituting significant portions (30-100 wt.%) of virgin raw materials with high-purity recycled building materials. The results obtained demonstrate the feasibility of establishing a circular economy within the built environment through the integration of waste recycling practices into construction materials. As a result, tons of idle EBM will be transformed into value-added products, reducing environmental burdens associated with construction activities.

Key words: circular economy, waste recycling, environment, resources and sustainability.

1. Introduction

In recent years, construction activities carried out globally to meet the structural needs of the increasing population and to renovate aging infrastructure have resulted in significant amounts of Construction and Demolition Waste (CDW) being generated worldwide, and this trend continues. From a quantitative standpoint, in Europe alone, this amounts to around 350 million tons of construction, renovation, and demolition waste [1], while globally it exceeds 10 billion tons [2]. However, it can be said that countries face serious challenges in dealing with such significant amounts of generated waste. Many countries either stack these types of waste in clean landfill sites or attempt to utilize them in low-

¹ Corresponding author: sahmaran@hacettepe.edu.tr

technology applications such as road sub-base or foundation filling [3]. However, considering the volume of waste generated, it is undeniable that there is a necessity to evaluate these wastes in higher quantities and with added value. The possibility of these wastes causing soil, water, and air pollution in landfill sites, as well as concerns such as the occupation of clean agricultural areas by waste, have prompted actions to be taken for the management of these wastes [4, 5]. Furthermore, given the current environmental burdens associated with the construction sector, this issue becomes even more urgent.

As it is widely known, concrete is the second most consumed material globally after water [6]. Due to its extensive use, efforts have been intensified in recent years to develop green concrete, addressing issues such as depletion of natural resources, high emissions, and energy consumption associated with energy-intensive materials. In this context, various steps have been taken, including reducing clinker content, decreasing cement dosage, and substituting waste-based mineral additives for cement. In addition to these efforts, steps have begun to be taken to facilitate the valorization of the substantial amount of generated waste by incorporating CDW as a supplementary material in cement and utilizing recycled concrete aggregates (RCA) in concrete mixtures instead of natural aggregates (NA). This shift aims to transition from a linear economy model to a circular economy model in the construction sector, enabling the attainment of high value-added transformations in the built environment.

Considering that aggregates typically make up 60-75% by volume and 80-85% by weight of Portland cement concrete mixes, efforts have been made to incorporate RCA as a substitute for natural aggregates to facilitate recycling. However, it's important to note that the properties of RCA differ significantly from those of NA, leading to variations in the fresh and hardened properties of concretes produced with these aggregates. In studies focusing on workability, the slump values of concrete made with RCA differ from those made with NA due to the considerably higher water absorption capacity of RCA. For instance, Topcu [7] observed a slump of 75 mm in concrete made with RCA compared to 100 mm in concrete made with NA. Moreover, Poon et al. [8] noted a decrease in slump value with an increase in RCA content, attributing this to the moisture content of RCA. Furthermore, the addition of RCA generally results in a reduction in compressive strength compared to concrete made with NA. Various studies have reported reductions in compressive strength ranging from 20% to as much as 40%. For instance, Topçu and Sengel [9] observed a decrease of 33% in C16 concrete and 23.5% in C20 concrete compared to normal concrete. Similarly, Etxeberria et al. [10] found that concrete made with 100% coarse RCA exhibited compressive strength 20-25% lower than normal concrete. However, it has been demonstrated that using RCA up to 30% does not significantly affect compressive strength. These differences in properties are attributed to the adhered mortar on

RCA, which is permeable and has high water absorption, leading to reduced porosity and decreased bond strength at the aggregate-matrix interface.

Research on the substitution of CDW into cementitious systems is relatively limited compared to its use as aggregate. Naceri and Hamina [11] conducted a study to assess the effects of waste brick as a partial replacement for cement in mortar. Different proportions of clinker were replaced with waste brick (0%, 5%, 10%, 15%, and 20%) by weight of the cement. Results indicated that the grinding time of cement remained unchanged for 5% brick replacement but decreased by 5% for 10% brick replacement and by 10% for 15% and 20% brick replacement. Specific gravity values tended to decrease by 0.9%, 3.1%, 4.4%, and 5% compared to the reference sample at replacement rates of 5%, 10%, 15%, and 20%, respectively. Moreover, an increase in waste brick content led to an increase in water demand for normal consistency of the cement paste. Setting times decreased proportionally with the increase in waste brick quantity, while an increase in waste brick content resulted in higher shrinkage values. The mechanical performance of samples decreased at 7 and 28 days with an increase in waste brick replacement rate; however, higher strength and resistance values were observed at 90 days in mixtures with brick replacement rates up to 10% due to variations in SiO_2 and Al_2O_3 content and the CaO/SiO_2 ratio. In another study, Arif et al. [12] examined the feasibility of utilizing Waste Brick Powder (WBP) as a substitute for cement in concrete, with replacement levels set at 5% and 10% compared to standard concrete. The findings indicated an improvement in workability, attributed to the particle size and shape of WBP. With round edges and smooth surfaces, WBP particles act as lubricants in the mix, enhancing flowability. The decrease in density is linked to the lower density of WBP. Moreover, the increase in compressive, split tensile, and flexural strengths suggests an enhancement in concrete quality due to WBP inclusion, attributed to the compact structure of the specimens resulting from the presence of pozzolanic products in concrete voids.

Considering all these studies, researchers have conducted studies specifically focusing on the valuable reuse of end-of-life building materials, particularly CDW, in the construction sector. In this context, the design of green concrete containing waste materials such as waste containing cement and RCA has been developed, and a building has been constructed using this developed material. During this process, the technical properties of the developed mixtures were examined, and decisions were made regarding their use. As a result of this study, the aim is to promote the widespread use of waste materials in the built environment as valuable additions through the circular economy model. The results of this research are expected to enrich existing literature by demonstrating the feasibility of utilizing such waste materials in construction building materials.

2. Experimental

Materials

As part of the study, waste-incorporated cement was employed to formulate and refine recipes for green concrete. This cement was formulated using a blend of materials including 68% by weight of CEM I 42.5R ordinary Portland cement (OPC), and 32% by weight of CDW. Moreover, RCA were utilized as aggregates to enhance the recycling rate of the system. Concrete waste samples were processed through a laboratory jaw crusher with two different settings to obtain fine and coarse recycled aggregates. Subsequently, the aggregates were separated into fine and coarse fractions using sieves. Table 1 presents the mixture designs incorporating waste-based cement and RCA at different ratios.

Table 1

Mixture formulation for the cement-based mixture

	RC A Rep. (%)	Waste- incorporate d Cement	FNA	CNA	FRCA	CRCA	Water	SP	w/c
M1	75	310.8	187.9	270.5	563.7	811.5	230	5.83	0.74
	90		75.16	108.2	676.44	973.8		6.66	
	100		0	0	751.6	1082		7.5	
M2	75	425.9	167.525	262	502.575	786	230	5.83	0.54
	90		67.01	104.8	603.09	943.2		7.5	
	100		0	0	670.1	1048		8.33	

Note: Units are given in kg/m³. FNA: Fine Natural Aggregate, CNA: Coarse Natural Aggregate, FRCA: Fine Recycled Concrete Aggregate, CRCA: Coarse Recycled Concrete Aggregate, SP: Superplasticizer.

Procedure

Following the casting, the samples were molded and submerged in a water tank until the testing day. Within the study's scope, three cubic specimens with dimensions of 100×100×100 mm were prepared for each concrete mixture at 28 days to assess compressive strength. The compressive strength test was conducted on these cubic specimens using a 100-ton capacity testing machine, following ASTM C39 standards, at a loading speed of 0.9 kN/sec. The average compressive strength result was calculated from the results of the three specimens tested. Similarly, three-cylinder specimens with dimensions of Ø100×50 mm were prepared for each concrete mixture at 28 days to determine splitting-tensile strength. The splitting-tensile strength test followed the same procedure as the compressive strength test, and the average splitting-tensile strength result was

obtained from the three specimens tested. Representative image of the specimen can be found in figure 1.



Fig. 1. Digital image of the representative specimens

3. Results and discussions

The 28-day compressive strength results of the mixtures utilizing waste-incorporated cement and NA/RCAs are depicted in Fig 2. For M1 coded specimens, surprisingly, the mixture containing 100% RCA yielded the highest compressive strength result, contrary to expectations, as the inclusion of RCA typically leads to a reduction in compressive strength. This unexpected finding may be attributed to that aluminosilicate-based brick waste and concrete waste with high calcium content may exhibit pozzolanic characteristics at later ages, contributing to the compressive strength. This phenomenon could also be attributed to the elevated water absorption capacity of the recycled aggregate, which might absorb a significant portion of free water in the system during the early stages, potentially resulting in a rise in compressive strength up to a certain threshold [13], as the water/binder ratio was quite high in initial stage. Furthermore, the RCAs utilized in this study were sourced from cubic samples that exhibited notably high strength. The anticipated negative impact of the RCAs might not be readily discernible, given their own robust structural properties with other advantages it offers. Also, it is possible that the RCAs may retain unreacted cement, potentially facilitating the formation of additional gel. Contrastingly, in the case of the M2 coded specimens, an increase in RCA content led to a decrease in compressive strength, unlike the trend observed in M1 coded specimens. This phenomenon can be attributed to the reduced water-to-binder ratio characteristic of M2 coded specimens. Consequently, the beneficial effects of higher RCA content in absorbing free water within the matrix are diminished, resulting in a reduction in strength. This occurrence is due to the inherent robust strength of natural aggregate and its lower probability of interfacial transition zone (ITZ) formation.

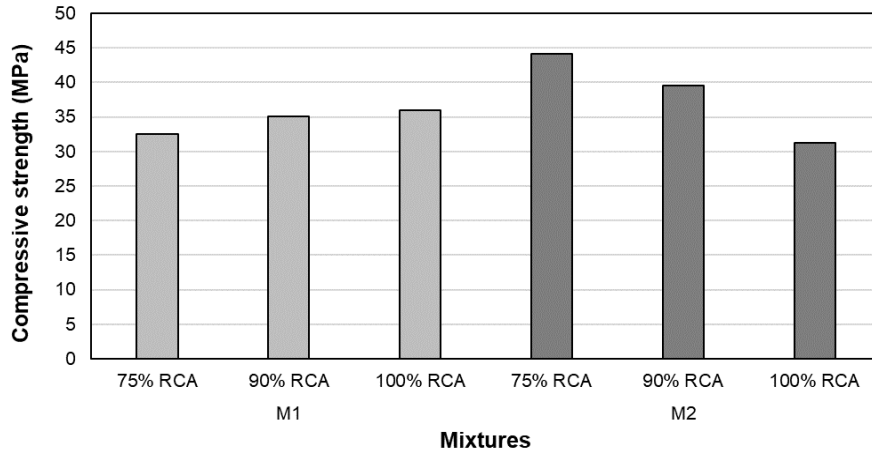


Fig. 2. 28-day compressive strength test results

The 28-day splitting-tensile strength results of the mixtures utilizing waste-incorporated cement and NA/RCA are depicted in Fig 3. Like the trend observed in compressive strength, a comparable pattern was noted concerning the RCA content. Similar factors likely contributed to these results. A higher water-to-binder ratio in the matrix could lead to a less compact structure for mixtures without RCA for the M1 coded specimens. As the RCA content increases in the matrix, the recycled aggregates may absorb the free water in the matrix, resulting in denser structures. In the case of the M2 coded specimens, this scenario takes a reverse turn since the overall matrix water-to-binder ratio is comparatively lower. The addition of more RCA may lead to the formation of secondary ITZ within the matrix, resulting in additional weaknesses and ultimately contributing to a reduction in strength.

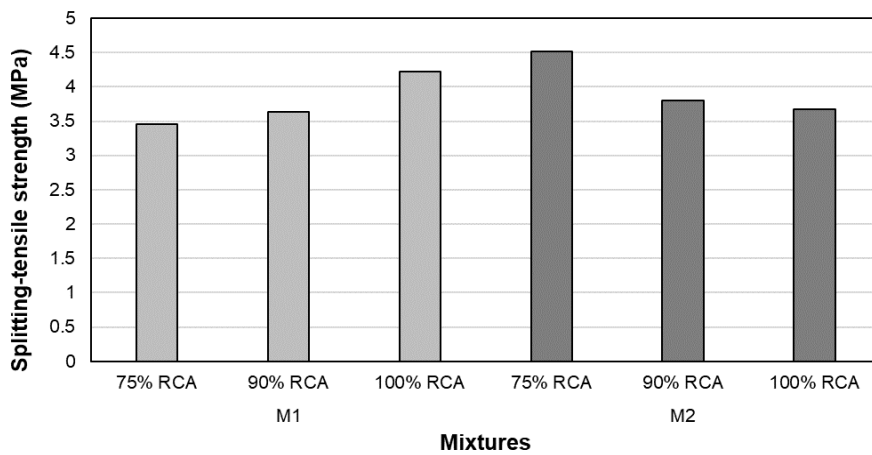


Fig. 3. 28-day splitting tensile strength test results

The findings revealed that CDWs can effectively serve as raw materials in construction materials, exhibiting performance comparable to their virgin counterparts while meeting relevant standards. Utilizing waste materials as value-added raw materials in the built environment facilitates the adoption of a circular economy model in the construction sector. This demonstrates the potential to reintegrate millions of tons of waste currently occupying landfill sites back into the economy. Such practices not only address global pollution issues stemming from these wastes but also reclaim land space for alternative uses. Furthermore, it provides valuable resources for new construction endeavors. Leveraging these research findings, the structure depicted in Figure 4 was constructed using building materials containing CDWs, illustrating the feasibility of integrating EBMs into the built environment.



Fig. 4. Building materials containing CDWs, beginning stages

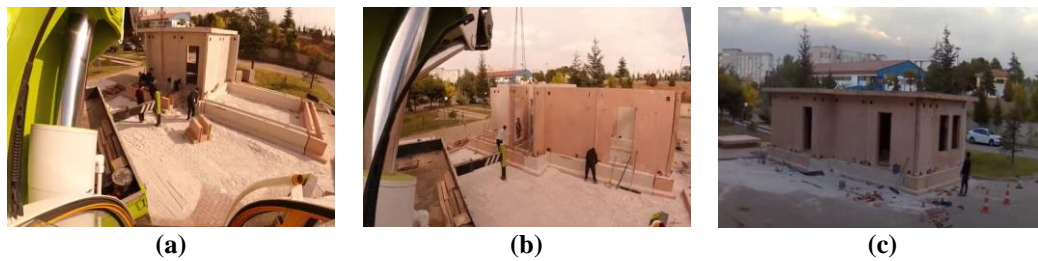


Fig. 5. Building materials containing CDWs, closing structure

4. Conclusions

The findings of this study are poised to significantly advance the adoption of the circular economy within the building industry. This will be accomplished by developing innovative tools for circular reverse logistics and employing advanced technologies for manufacturing high-value secondary raw materials. These endeavors are geared towards instilling market confidence and fostering widespread acceptance of recycled EBMs. This will enable the promotion of extensive utilization of waste materials as valuable contributions in the built environment through the circular economy model. The outcomes of this study are

anticipated to enhance current literature by showcasing the practicality of incorporating these waste materials into construction building materials.

Acknowledgement

The authors gratefully acknowledge the European Union's Horizon 2020 Research and Innovation Programme's financial assistance under Grant Agreement No: 869336 and Acronym: ICEBERG.

REFERENCES

- [1] Deloitte, Resource Efficient Use of Mixed Wastes-Improving management of C&DW, 2017
- [2] Wu H., Zuo J., Zillante G., Wang, J., Yuan H., Status quo and future directions of construction and demolition waste research: A critical review. *Journal of Cleaner Production*, 240, (2019), 118163.
- [3] Şahin O., İlcan H., Ateşli A.T., Kul A., Yıldırım G., Şahmaran M., Construction and demolition waste-based geopolymers suited for use in 3-dimensional additive manufacturing. *Cement and Concrete Composites*, 121, (2021), 104088.
- [4] Poon C.S., Ann T.W., Ng, L.H., On-site sorting of construction and demolition waste in Hong Kong, *Resources, conservation and recycling*, 32, 2, (2001), 157-172.
- [5] Wu Z., Ann T.W., Shen L., Investigating the determinants of contractor's construction and demolition waste management behavior in Mainland China, *Waste management*, 60, (2017), 290-300.
- [6] Aitcin P.C., Cements of yesterday and today: Concrete of tomorrow, *Cement and Concrete research*, 30, 9, (2000), 1349-1359.
- [7] Topcu, I.B., Physical and mechanical properties of concretes produced with waste concrete. *Cement and concrete research*, 27, 12, (1997), 1817-1823.
- [8] Poon C.S., Shui Z.H., Lam L., Fok H., Kou S.C., Influence of moisture states of natural and recycled aggregates on the slump and compressive strength of concrete, *Cement and concrete research*, 34, 1, (2004), 31-36.
- [9] Topcu I.B., Şengel S., Properties of concretes produced with waste concrete aggregate, *Cement and concrete research*, 34, 8, (2004), 1307-1312.
- [10] Etxeberria M., Mari A.R., Vázquez E., Recycled aggregate concrete as structural material, *Materials and structures*, 40, (2007), 529-541.
- [11] Naceri A., Hamina M.C., Use of waste brick as a partial replacement of cement in mortar, *Waste management*, 29, 8, (2009), 2378-2384.
- [12] Arif R., Khatab A., Kırgız M.S., Khan R.B.N., Tayyab S., Khan R.A., Anwar W., Arshad, M.T., Experimental analysis on partial replacement of cement with brick powder in concrete, *Case Studies in Construction Materials*, 15, (2021). e00749.
- [13] González-Fontelbo B., Martínez-Abella F., Recycled aggregates concrete: aggregate and mix properties., *Materiales de construcción*, 55, 279, (2005), 53-66.

GLYCEROL CONVERSION TO LACTIC ACID: PROCESS ANALYSIS

Andreea MANOLACHE¹, Ana M. BREZOIU¹, Ionuț BANU^{1*}

¹Department of Chemical and Biochemical Engineering, Faculty of Chemical Engineering and Biotechnologies, National University of Science and Technology POLITEHNICA Bucharest, Romania

Abstract

With the increased biodiesel production, there is a considerable amount of glycerol obtained as byproduct which can be easily converted into another valuable compounds including lactic acid. In this work, a thorough analysis of lactic acid process synthesis from glycerol was performed. Considering a plant with a production capacity of 30000 t/year, the mass and thermal balance, along with the characteristics of the main equipment were determined and used for the economic evaluation of the process. The CAPEX and OPEX values evaluated for this process allowed us to determine a production price of 1.64 \$/kg for a 80 % wt. lactic acid solution.

Key words: Glycerol valorization, lactic acid, process modeling, commercial simulator

1. Introduction

The interest in lactic acid is related to its high added value. In addition, it is generally recognized as safe (GRAS), considered harmless by the US Food and Drug Administration, has a market with high potential growth, can be produced alternatively by both chemical and biochemical (fermentation) processes and can be synthesized from a wide variety of waste-type raw materials [1]. The first company to produce lactic acid through chemical synthesis was Monsanto (Texas, USA) in 1963. They produced 40% of the lactic acid (4500 tonnes) consumed in the U.S. Sterling Chemicals also produced lactic acid through synthesis, which ended its production in early 1990. In the east, Musashino Chemical used this technology, but recently also switched the production process to the fermentative route [2]. The largest markets for lactic acid are represented by the United States of America, Western Europe and the Asia-Pacific region, which are key producers and consumers on a global scale. Lactic acid production was supported in the past by a small number of companies, such as PURAC and Nature Works LLC, but now there are several major companies in Asia producing lactic acid. PURAC was responsible

¹ Corresponding author: ionut.banu@upb.ro

for 45% of global production in 2014, Henan JINDAN for 15% and CARGILL for 5%. PURAC operates production facilities in the USA, the Netherlands, Spain, Brazil, and Thailand and is the largest producer of lactic acid in the world with a capacity of approximately 350 000 tonnes/yr. The Brazil production plant located in Campos dos Goytacazes/RJ, produces lactic acid from sugar cane, being responsible for meeting the demand of the Latin American market. Global production of lactic acid was 1220 kilotons in 2016 (figure 1). With a growth rate of 16.2%, this demand is expected to reach 1960 kilotons by 2025 - equivalent to \$9.8 billion in the global market [3]. Currently, the main producers of lactic acid include Archer Daniels Midland Company and NatureWorks LLC (USA), Purac (Netherlands), Galactic S.A. (Belgium) and several Chinese companies, including CCA (Changzhou) Biochemical Co. Ltd., Henan Jindan Lactic Acid Co. Ltd. and Musashino Chemical Co. Ltd. [1].

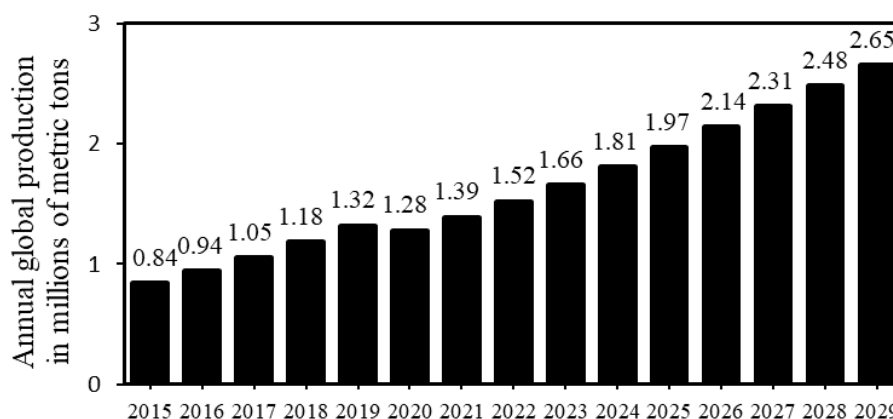


Fig. 1 Global annual production of lactic acid (2015 to 2021) with a forecast for 2022 to 2029 [4].

Lactic acid can be produced either through fermentation, a process called lactic acid fermentation or chemically, the latter producing a racemic mixture of D/L-lactic acid. Lactic acid is usually produced from the fermentation of sugars in the presence of lactic acid bacteria, the latter being the chosen as an alternative at industrial level [3]. The production of lactic acid by chemical synthesis using lactonitrile as raw material (a by-product of the acrylonitrile process) was proposed in 1863 by Wislicenus and involves the following reactions: hydrocyanic acid (HCN) is contacted with liquid acetaldehyde ($\text{CH}_3\text{-CHO}$) in the presence of a basic catalyst at high pressure to produce lactonitrile. Then, the lactonitrile is recovered, purified by distillation, and hydrolyzed using sulfuric acid (H_2SO_4) to give lactic acid ($\text{CH}_3\text{-CH(OH)-COOH}$) and ammonium salt ($(\text{NH}_4)_2\text{SO}_4$). Further, lactic acid is esterified with methanol ($\text{CH}_3\text{-OH}$), and the formed methyl lactate ($\text{CH}_3\text{-CH(OH)-COOCH}_3$) is recovered, purified by distillation, and hydrolyzed in acidic solution

to produce lactic acid and methanol. The methanol is then separated by distillation and recycled [2].

In the last decades, there has been a high interest in the development of synthesis processes based on renewable raw materials. One of these processes uses glycerol as a raw material [5]. Glycerol is the main by-product of transesterification, saponification and hydrolysis of fats and oils. The booming development of the oleochemical industry has resulted in a high production and altogether low prices of glycerol, drawing considerable attention to this abundant but valuable chemical. In particular, the remarkable growth of biodiesel industries, caused by strict environmental regulations as well as oil supply uncertainties and price fluctuations, has intensified the research for reliable glycerol utilization technologies [6]. Glycerol can be converted to lactic acid and other products of interest by processes that occur at high temperatures and pressures. The hydrothermal process can be carried out in the presence of a hydroxide-type catalyst (NaOH or KOH) or in heterogeneous catalysis using a wide range of metal oxides as catalyst (Ca, Cu, Ni, Au, Zn oxides) - table 1 [7]. The conversion of glycerol into lactic acid (or its lactate) through the alkaline process takes place through reactions R-1 and R-2. After the formation of lactic acid, the product will instantly react with the base present in the solution, forming sodium lactate which protects lactic acid from decomposition or polymerization [8].

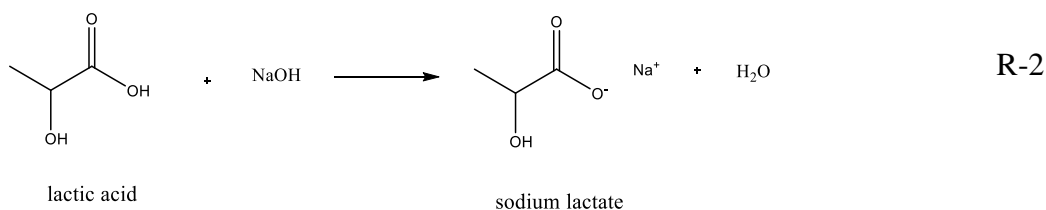
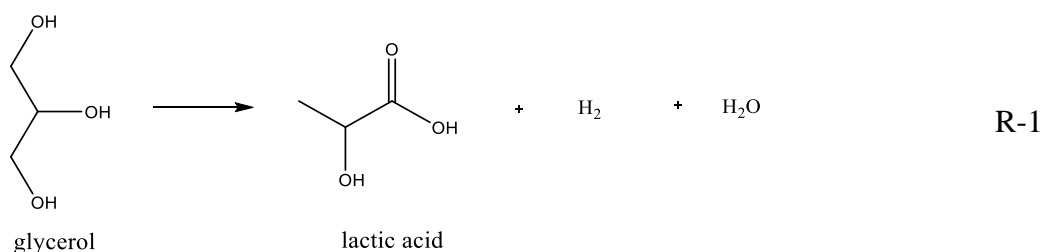


Table 1

Catalysts used in the hydrothermal conversion of glycerol to lactic acid.

Type	Catalyst	Glycerol conversion	Lactic acid selectivity	Conditions	Ref.
<i>Heterogeneous on the support</i>	N _{0.3} /graphite	95.1	88	NaOH/glycerol =1.1:1 230 °C; 2h	[9]
	Cu/hydroxyapatite	91	90		[10]
	Cu/MgO	90	89		[10]
	30%CuO/ZrO ₂	67.5	85	NaOH/glycerol = 1: 1.4 14 bar N ₂ ; 160 °C; 6 h	[11]
	Ni-Co/CeO ₂	86	87	NaOH: 15 mmol; 160 °C; 20 bar N ₂ ; Levulinic acid - H ₂ acceptor	[12]
	Pt/C	80	80	NaOH/glycerol =1.8:1; 180 °C; 20 bar He; 8h	[13]
	Pd/C	99	46	NaOH/glycerol =1.1:1; 230 °C; 3h	[14]
<i>Heterogeneous unsupported</i>	Cu ₂ O	92.5	89.1	NaOH/glycerol=1.2:1; 230 °C; 2h	[15]
	CaO	97.8	40.8	CaO/ glycerol=0.3:1; 77-290 °C; 2.5 h	[16]
	Cu nanoparticles	77.3	83.5	1000 rpm; NaOH/glycerol=1.1:1; substrate/Cu=25.4:1; 240 °C; 2 h	[17]
<i>Homogenous</i>	NaOH	9.8	39.5	1000 rpm; NaOH/glycerol=1.1:1; 240 °C; 2 h	[17]

In this work, a thorough analysis of lactic acid obtaining process from glycerol was carried out, in a continuous reactor over a copper-based catalyst in an alkaline medium. The process involved the obtaining of sodium lactate salt, its conversion to lactic acid, as well as separating the process byproduct with a high purity to be further marketed. A four-pass multi-tubular heat exchanger that preheats the glycerol solution was designed for which the geometrical characteristics were chosen, the partial coefficients were determined based on specific criteria equations and the transfer area was verified by rigorous evaluation of the total heat transfer coefficient. To evaluate the production price of the lactic acid, the geometrical characteristics of the main equipment were also evaluated.

2. Lactic acid production plant design

In this work it was proposed a process flowsheet (given in figure 2) with a production capacity of 30 000 tons per year of 80 % wt. lactic acid solution. The process was divided into three sections: a reaction section where glycerol is converted to sodium lactate, one for lactic acid purification and recovery, and the latter one for resulting byproducts separation. Besides lactic acid, other important products are obtained with high purity including propylene glycol and diglycerol.

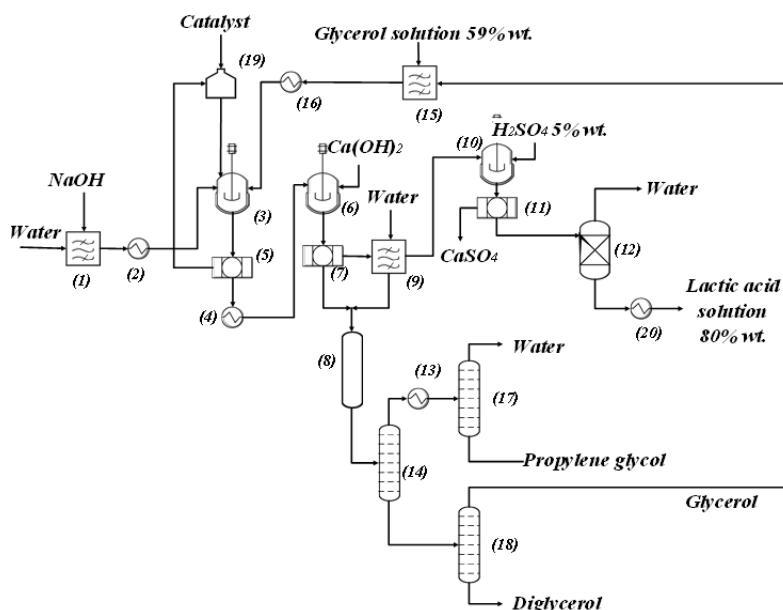


Fig. 2 Process flowsheet for glycerol conversion to lactic acid (1) - vessel for mixing the sodium hydroxide solution; (2), (4), (13), (16), (20) - heat exchangers; (3) - lactic acid reactor; (6) - precipitation reactor; (10) - lactic acid acidification reactor; (5),(7),(11) – filters; (8) - ion exchange column; (12) – evaporator; (15) – glycerol mixing vessel; (14),(17), (18) - rectification columns; (19) – catalyst tank.

A 65% wt. glycerol solution is introduced into the autoclave type reactor with mechanical stirring (3) at the reaction temperature of 240 °C, where the conversion to lactic acid took place, together with a series of by-products such as acetic acid, propylene glycol and diglycerol. As a catalyst, copper nanoparticles were used, in an alkaline environment, obtained by an excess of sodium hydroxide solution of 1:1.1 (molar ratio), which prevents lactic acid polymerization through its conversion to sodium lactate. Also, the acetic acid present in the reactor effluent was then converted into the corresponding sodium salt. From the reaction mixture, the catalyst is recovered in filter (5), and then the separation of sodium lactate from

the other products, was performed through a precipitation reaction with calcium hydroxide in the reactor (6), with the obtaining of the corresponding lactic and acetic acids salts. Further, in the filter (7), the calcium lactate is separated and remained in the precipitate stream based on solubility differences.

The calcium lactate was washed in the equipment (9) and acidified with a 5% wt. sulfuric acid solution in the autoclave (10), where the lactic acid is recovered, and the formed gypsum was removed through a filtration process (11). Diluted lactic acid solution obtained was introduced into an evaporator where it was concentrated to the desired 80% wt. value.

Unreacted glycerol, excess hydroxide, propylene glycol, water, diglycerol, calcium acetate and traces of calcium lactate found in the wastewater and the filtrate separated from (7) are further passed on an ion exchange column (8) over an acid resin capable of retaining cations (sodium hydroxide, calcium lactate, calcium acetate). Thus, the remaining products, i.e. water, propylene glycol, diglycerol and glycerol are separated using three distillation columns. In the first column (17), water and propylene glycol are separated at the top of the column from the glycerol-diglycerol mixture that separates at the bottom of the column. Thus, each binary mixture is separated into a subsequent column. In column (19), propylene glycol, the useful product is separated from water at the base of the column. In column (20), diglycerol is mainly separated as a heavy volatile product, thus the glycerin obtained at the top of the column will be recycled in the process, being mixed with cold glycerol used as raw material.

3. Mass balance

The mass balance was performed for each process operation, considering all the conditions and reactions including precipitation and purification reactions with calcium hydroxide and sulfuric acid respectively, the filtration steps with an assumption that a 20% wt. of each compound will remain in the precipitate. Because the acetic acid reacts with sodium hydroxide and then with the strong acid resulting its calcium salt, a separation both calcium salts (acetate and lactate) was required based on their solubilities ($s_{CL} = 48\text{g/L}$ and $s_{CA} = 347\text{ g/L}$) [18, 19]. For the calcium lactate washing step was assumed that the precipitate will remain with 20% wt. water. The ion exchange step used a resin that retained the cations, meaning sodium hydroxide and traces of calcium salts were separated before the byproducts enter the first distillation column (14). The overall process mass balance is presented in

Table 2.

Table 2

Overall mass balance for lactic acid production plant			
Inlet flows	kg/hr	Outlet flows	kg/hr
NaOH	4038.9	Lactic acid 80% wt.	3925.4
Water	58864.1	Water	60154.5
Glycerol 59% wt.	6535.2	CaSO ₄	2965.9
Ca(OH) ₂	2123.8	Propylene glycol	437.8
H ₂ SO ₄ 5% wt.	2137.2	Diglycerol	1303.4
		Resin retained substances	4279.3
TOTAL	73099.3	TOTAL	73099.3

3.1. Lactic acid reactor mass balance

The mass balance for the lactic acid reactor and the products selectivities as given by Zavrazhnov et al. [17] were considered as shown in Table 3.

Table 3

Reaction mixture composition in the lactic acid reactor outlets [17]					
Substrate	Conversion, x_G (%)	Selectivity, σ (%)			
		DG	LA	PG	AA
Glycerol	77.3	11.0	78.3	8.1	2.6

Where DG-diglycerol, LA-lactic acid, PG-propylene glycol, AA-acetic acid.

To determine the molar feed rate of glycerol $D_{M,G}^0$, its conversion $x_G=0.773$, the annual production capacity for the reactor $P_a=40000$ tonnes/year, the annual operation time $H=8000$ hr/year and the molar mass of lactic acid $M_{LA}=90$ kmol/kg were taken into account, first calculating the molar flow of lactic acid at the exit of the reactor $D_M^{LA}D_m^{LA}$.

The amounts of required sodium hydroxide and catalyst were calculated based on initial molar ratios, $D_{M,G}^0:D_{M,NaOH}^0 = 1 : 1.1$ and $D_{M,G}^0:D_{M,cat}^0 = 25.4 : 1$. Considering that the glycerin that will be introduced into the reactor in the form of an aqueous solution, a concentration of 65% wt. was proposed from which the water flow was calculated. The water needed for sodium hydroxide solution was proposed to be doubled. For the products formed in the conversion process of glycerol to lactic acid, selectivity values reported in literature were considered, being mentioned in Table 3. The obtained reactor mass balance is shown in Table 4.

$$D_M^{LA} = \frac{D_m^{LA}}{M_{LA}} = \frac{P_a}{H} \quad (1)$$

$$\sigma_{LA} = \frac{D_M^{LA}}{D_{M_G}^0 - D_{M_G}} \quad (2)$$

$$D_{M_G} = D_{M_G}^0 (1 - x_G) \quad (3)$$

$$D_M^j = \sigma_j \cdot (D_{M_G}^0 - D_{M_G}) \quad (4)$$

Where: D_M^{LA} -lactic acid molar flow in the reactor effluent, kmol/hr;
 M_{LA} - lactic acid molar mass, kg/kmol;
 D_{M_G} -glycerin molar flow in the reactor effluent, kmol/hr;
 $D_{M_G}^0$ - glycerin molar flow in the reactor feed, kmol/hr;
 σ_{LA} -lactic acid selectivity from glycerin;
 x_G - glycerin conversion.

Table 4

Mass balance for the lactic acid reactor

Inlet flows	kg/hr	Outlet flows	kg/hr
NaOH 65% wt.	121116.7	Sodium lactate	7777.8
Glycerol	8444.96	Diglycerol	1620.2
Copper nanoparticles	229.5	Propylene glycol	456
Water (glycerol solution)	4547.4	Sodium acetate	189.1
Filtrate traces (20%)	6277.3	Glycerol	2396.3
		H ₂ O	17395.9
		NaOH	1461.1
		Copper nanoparticles	229.5
Total flow (kg/h)	31615.8	Total flow (kg/h)	31615.8

3.2. Byproducts separation mass balance

The separation of the by-products was carried out in the Aspen Plus v10 simulator using NRTL property package, given the non-ideal character of the liquid mixture. The separation was carried out considering the boiling points presented in Table 5. Considering the high boiling points for glycerol and diglycerol, the separation of these products was performed in vacuum. In the first rectification column (COL-1), the propylene glycol and water mixture were separated in the distillate from glycerol and diglycerol, based on their boiling temperatures. COL-2 is separating 99.9% mol. propylene as waste while COL-3 is separating glycerol with 99.9% mol. purity as mostly light volatile component (figure 3).

Table 5

By-products boiling points at atmospheric pressure

Byproduct compound	Water	Propylene glycol	Diglycerol	Glycerol
Boiling point, °C	100	187	407	290

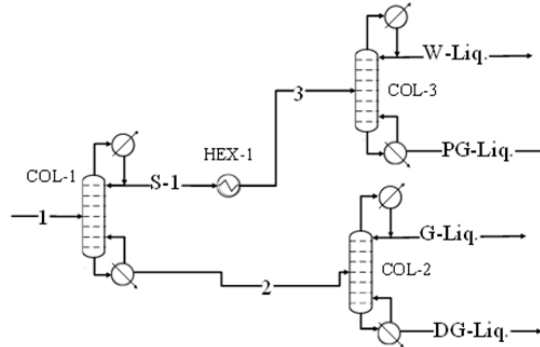
**Fig. 3** Byproducts separation process design simulation

Table 6

Mass balance for byproducts separation units

		1	2	3	DG-Liq.	G-Liq.	PG-Liq.	W-Liq.
From			COL-1	HEX-1	COL-2	COL-2	COL-3	COL-3
To		COL-1	COL-2	COL-3				
Phase		Liquid Phase						
	Units							
Temperature	°C	25	204.15	50	320.75	160.82	181.83	99.65
Pressure	Bar	1	0.05	1	0.03	0.01	1	1
Mass Flows	kg/hr	$2.04 \cdot 10^4$	$3.21 \cdot 10^3$	$1.71 \cdot 10^4$	$1.30 \cdot 10^3$	$1.91 \cdot 10^3$	$4.38 \cdot 10^2$	$1.67 \cdot 10^4$
DG	kg/hr	$1.30 \cdot 10^3$	$1.30 \cdot 10^3$	$7.37 \cdot 10^{-34}$	$1.30 \cdot 10^3$	$1.01 \cdot 10^{-22}$	0	0
PG	kg/hr	$4.37 \cdot 10^2$	$4.37 \cdot 10^{-2}$	$4.37 \cdot 10^2$	$3.66 \cdot 10^{-11}$	$4.37 \cdot 10^{-2}$	$4.37 \cdot 10^2$	$1.21 \cdot 10^{-4}$
W	kg/hr	$1.67 \cdot 10^4$	$5.03 \cdot 10^{-19}$	$1.67 \cdot 10^4$	0	0	1.04	$1.67 \cdot 10^4$
G	kg/hr	$1.92 \cdot 10^3$	$1.92 \cdot 10^3$	$2.88 \cdot 10^{-9}$	7.26	$1.91 \cdot 10^3$	$2.88 \cdot 10^{-9}$	$8.30 \cdot 10^{-38}$

Where G – glycerol, DG – diglycerol, PG – propylene glycol, W – water, COL-1, COL-2 and COL-3 – first, second and third distillation column respectively, HEX-1 – heat exchanger (13), 2 – water and propylene glycol stream, 3 – glycerol and diglycerol stream, G-Liq., DG-Liq., W-Liq., PG-Liq. – glycerol, diglycerol, water and propylene glycol stream, respectively.

3.3. Lactic acid evaporation mass balance

For the 80% wt. lactic acid solution, an evaporator was modeled as a condenser free RADFRAC distillation column in Aspen Plus v10 and the mass balance is presented in table 7 while the separation scheme in figure 4.

Table 7

Lactic acid evaporator mass balance			
Inlet flows	kg/hr	Outlet flows	kg/hr
<i>Mixture</i>		<i>LA-Liq.</i>	
Lactic acid	3056.58	Lactic acid	3056.58
Water	34754.11	Water in solution	764.14
		<i>W-Vap.</i>	
		Evaporated water	33989.97
TOTAL	37810.69	TOTAL	37810.69

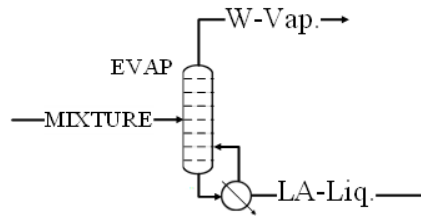


Fig. 4 Lactic acid evaporator scheme.

4. Heat balance

The heat balance was evaluated for heat exchangers, distillation columns and evaporator to determine the utilities flow rates. The results are shown in Table 8 and Table 9. The corresponding mass and heat flow rates were calculated according to the specific heat balance equations (5)-(6), while the utilities were chosen in agreement with inlet and outlet fluid temperatures.

$$Q = D_m^j \cdot cp_j \cdot \Delta T_j = D_m^{steam} \cdot r_{steam} \quad (5)$$

$$Q = D_m^j \cdot cp_j \cdot \Delta T_j = D_m^{water} \cdot cp_w \cdot \Delta T_w \quad (6)$$

Where: Q - heat flow, kW;

D_m^j – mass flow of j species, kg/s;

cp_j - specific heat of j species, J/(kg·K);

ΔT_j - temperature difference for j compound, K;
 r_{steam} – latent heat of vaporization of steam, J/kg;
 cp_w - specific heat for water, J/(kg·K);
 ΔT_w – water temperature difference, K;

Table 8

Utilities flows needed in the heat exchangers

Equipment	Utility	Flow, kg/s	Q, kW
Heat exchanger (2)	Steam 260 °C	1.16	1909
Heat exchanger (4)	Cold water 10 °C	18	5713
Heat exchanger (16)	Steam 260 °C	1.39	2032
Heat exchanger (20)	Steam 100 °C	0.23	184.2
Heat exchanger (13)	Cold water 10 °C	1.02	507.5

Table 9

Utilities flow rates for the rectification columns

Column	Role	Utility	Mass flowrate, kg/s	Q, kW
(14)	Condenser	Cold water 10 °C	551	23041
	Reboiler	Steam 250 °C	13.6	23299
(17)	Condenser	Cold water 10 °C	502	20981
	Reboiler	Steam 250 °C	12.8	22030
(18)	Condenser	Cold water 10 °C	45.8	1915
	Reboiler	Oil	21	1886
(12)	Reboiler	Steam 125 °C	10.97	23992

Sodium hydroxide dissolution in water is accompanied by an important release of heat (exothermic effect) therefore it is mandatory to determine the increase in temperature resulting from mixing the strong base with water, using the enthalpy of dissolution of sodium hydroxide $\Delta H_{\text{NaOH}}^{\text{diss}} = -44.51 \frac{\text{kJ}}{\text{mol}}$ [20]. The solution temperature increased with 88.74 °C, consequently the final temperature was 108.74 °C, which was further heated to the reaction temperature of 240 °C in the heat exchanger (2).

$$Q = \frac{D_{\text{m}}^{\text{NaOH}}}{M_{\text{NaOH}}} \cdot \Delta H_{\text{NaOH}}^{\text{diss}} \quad (7)$$

$$\Delta T = \frac{Q}{cp_{\text{H}_2\text{O}} \cdot Dm_{\text{sol}}} \quad (8)$$

Where: Q – dissolution heatflow, kJ/s;
 ΔT – solution temperature increase, K;
 cp_{H_2O} – water specific heat, kJ/(kg·K)
 $D_m^{sol G}$ – glycerin solution mass flow, kg/s;

The recycled glycerol from the top product of COL-2 having a temperature of 160.82 °C was mixed with fresh glycerol and the final temperature of the solution was also calculated. Since the specific heat of the final glycerol mixture depends on the temperature of the mixture (unknown), temperature correlations for glycerol and water specific heat in 20-160 °C temperature range at 1 bar pressure were obtained and used in heat balance equations for evaluating the temperature at the effluent of the mixture mixing vessel. Thus, the final temperature of the glycerol mixture to be heated before entering the reactor was determined to be approximately 37 °C.

$$(D_m^{fresh}) \cdot cp_{fresh} \cdot T_1 + D_m^{rec G} \cdot cp_G \cdot T_2 = (D_m^{sol G}) \cdot cp_{sol G} \cdot T_f \quad (9)$$

Where: D_m^{fresh} – fresh glycerol solution mass flow, kg/s;
 cp_{fresh} – fresh glycerol solution specific heat, kJ/(kg·K);
 $D_m^{rec G}$ – recycled glycerol mass flow, kg/s;
 $D_m^{sol G}$ – glycerol solution mass flow, kg/s;
 $cp_{sol G}$ – glycerol solution specific heat, kJ/(kg·K);
 T_j –fresh glycerin solution -1, of recycled glycerin -2 or final temperature -f, K

5. Design of glycerol solution heat exchanger

The heat exchanger (16) which heated the 65 %wt. glycerol from $T_1=37$ °C to the reaction temperature $T_2=240$ °C, using 47 bar steam (260 °C) has been designed. Rigorous calculations have been performed and the standard characteristics of the chosen heat exchanger are presented in Table 10. The value of Re number is below 2300, the flow regime being classified as laminar flow for the 65% wt. glycerol solution.

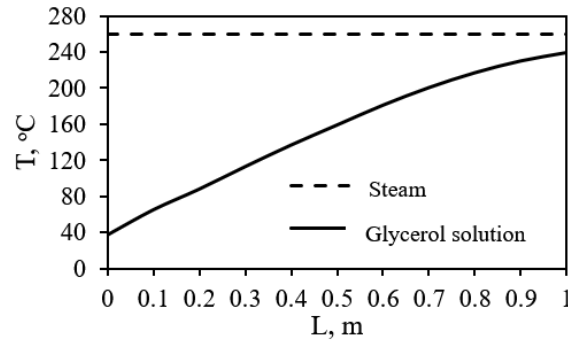


Fig. 5 Diagram of temperature variation along the glycerol solution heating exchanger.

A total heat transfer coefficient K of $200 \text{ W}/(\text{m}^2 \cdot \text{K})$ was proposed, for which the heat transfer area (A) was calculated using equation (10), resulting a value of 136.7 m^2 and this was standardized according to the literature [21]. A four-pass heat-exchanger was chosen to increase the velocity on the tube side and the main characteristics of the heat exchanger are mentioned in Table 10.

$$A = \frac{Q}{K \cdot \Delta T_m} \quad (10)$$

$$\Delta T_m = \frac{(T_{\text{steam}} - T_1) - (T_{\text{steam}} - T_2)}{\ln \frac{(T_{\text{steam}} - T_1)}{(T_{\text{steam}} - T_2)}} \quad (11)$$

Where: A –heat transfer area, m^2

K – proposed total coefficient of heat transfer, $\text{W}/(\text{m}^2 \cdot \text{K})$;

T_1, T_2 – glycerol solution feed and effluent temperatures, K ;

ΔT_m –logarithmic mean temperature difference, K ;

T_{steam} – steam temperature, K ;

Table 10.

Standard characteristics of the chosen multitubular heat exchanger [21]

A_{ST} m^2	D_n mm	δ_p mm	d_e mm	d_i mm	N	L mm	N
137	1400	2	20	16	2408	1000	4

Where A_{ST} –standardized area, D_n –shell diameter, δ_p –wall thickness, d_e, d_i – outer and inner tubes diameter respectively, n –tubes number, L –tubes length, N –pass number.

For the heat exchanger sizing, it is necessary to evaluate the mixture, steam and condensate properties (specific heat, density, conductivity, viscosity) over the temperature range, properties that were extracted from the AspenPlus v10 simulator and presented in Table 11 and Table 12.

Table 11

Average properties of glycerol-water (65%wt.) solution at 23 bar

D_{mix} kg/s	$c_{p\ mix}$ J/(kg · K)	η_{mix} Pa · s	λ_{mix} W/(m · K)	ρ_{mix} kg/m ³
3.61	3142.23	$1.29 \cdot 10^{-2}$	0.564	1090.07

Table 12

Steam and condensate properties at 47 bar and 260 °C					
Γ_{steam} J/kg	ρ_{steam} kg/m ³	c_{pcond} J/(kg · K)	η_{cond} Pa · s	λ_{cond} W/(m · K)	ρ_{cond} kg/m ³
$1.65 \cdot 10^6$	23.82	5586.2	$1.12 \cdot 10^{-4}$	0.542	814.8

Then, using the criterial equation were determined the partial heat transfer coefficients considering that the glycerol solution flows on the tube side and the steam on the shell side.

$$w_{mix} = \frac{D_{mix} \cdot N \cdot 4}{\rho_{mix} \cdot n \cdot \pi \cdot d_i^2} \quad (12)$$

$$Re_{mix} = \frac{w_{mix} \cdot \rho_{mix} \cdot d_i}{\eta_{mix}} \quad (13)$$

$$Pr_{mix} = \frac{c_{p_{mix}} \cdot \eta_{mix}}{\lambda_{mix}} \quad (14)$$

$$B = \frac{Re_{mix} \cdot Pr_{mix} \cdot d_i}{L} \quad (15)$$

$$Nu_{mix} = \left[3,65 + \frac{0,0688 \cdot B}{1 + 0,045 \cdot B^{0,66}} \right] \quad (16)$$

$$\alpha_{mix} = \frac{Nu_{mix} \cdot \lambda_{mix}}{d_i} \quad (17)$$

Where: w_{mix} - glycerol solution velocity, m/s;
 D_{mix} - glycerol solution mass flow, kg/s;
 N - passes number;
 n – tubes number;
 d_i -pipes internal diameter, m;
 L -pipes length, m;
 ρ_{mix} –glycerol solution density, kg/m³;
 η_{mix} - glycerol solution dynamic viscosity, kg/(m·s);
 $c_{p_{mix}}$ - glycerol solution specific heat, J/(kg·K);
 λ_{mix} - glycerol solution thermal conductivity, W/(m·K);
 $Re_{mix}, Pr_{mix}, Nu_{mix}$ - Reynolds, Prandtl, Nusselt glycerol solution criteria;
 α_{mix} - glycerol solution partial coefficient of heat transfer, W/(m²·K).

Thus, the Nu number value is 5.5 from which the partial coefficient of heat transfer for the fluid flowing on the tube side, α_{mix} was calculated with equation (17), having a value of $194 \frac{W}{m^2 \cdot K}$. The steam partial coefficient of heat transfer was

determined with the equation (18) using the properties from Table 14. The partial coefficient of heat transfer for the steam was $18869 \frac{W}{m^2 \cdot K}$. The Reynolds number for steam is determined by equation (19), resulting a value of 20.57, where Γ_{steam} is evaluated by equation (20).

$$\alpha_{\text{steam}} = 1.19 \cdot \text{Re}_{\text{cond}}^{-\frac{1}{3}} \cdot \left(\frac{\eta_{\text{cond}}^2}{\lambda_{\text{cond}}^3 \cdot \rho_{\text{cond}}^2 \cdot g} \right)^{-\frac{1}{3}} \quad (18)$$

$$\text{Re}_{\text{cond}} = \frac{4 \cdot \Gamma_{\text{steam}}}{\eta_{\text{cond}}} \quad (19)$$

$$\Gamma_{\text{steam}} = \frac{D_m^{\text{steam}}}{n \cdot L} \quad (20)$$

Where: D_m^{steam} - steam mass flow, kg/s;
 n –number of tubes;
 L-pipe length, m;
 ρ_{cond} –condensate density, kg/m³;
 η_{cond} - condensate dynamic viscosity, kg/(m·s);
 λ_{cond} - condensate thermal conductivity, W/(m·K);
 Re_{cond} – Reynolds number for condensate;
 Γ_{steam} - mass velocity per unit length, kg/(m·s);
 α_{steam} - steam partial coefficient of heat transfer, W/(m²·K).

Due to laminar flow on the tube side, the correction of the glycerol solution partial heat transfer coefficient was also considered and performed according to equations (21)-(24) which also considered the viscosities ratio. Firstly, a wall temperature near steam (fluid 1) was proposed as $t_{p1}=259 \text{ } ^\circ\text{C}$, then thermal flow q_1 was determined and further used for wall temperature near cold fluid (fluid 2) t_{p2} determination. The viscosities at the average temperature of the material $\eta_2(t_{m2})$, respectively at the temperature of the wall on near glycerin solution $\eta_2(t_{p2})$, were determined with regression equation (25) function of temperature as shown in **Error! Reference source not found..** The results are presented in Table 13.

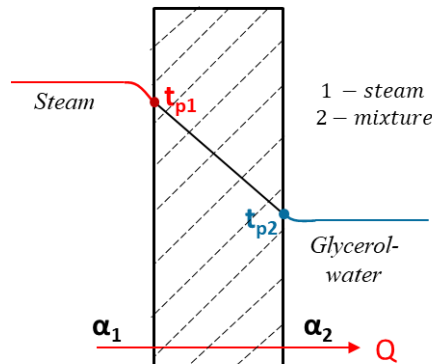


Fig. 6 Thermal transfer through heat exchanger pipe wall.

$$q_1 = \alpha_1 \cdot (t_{m1} - t_{p1}) \quad (21)$$

$$t_{p2} = t_{p1} - q_1 \cdot \frac{\delta_p}{\lambda_p} \quad (22)$$

$$q_2 = \alpha_2 \cdot \left(\frac{\eta_2(t_{m2})}{\eta_2(t_{p2})} \right)^{0.14} \cdot (t_{p2} - t_{m2}) \quad (23)$$

$$\alpha_{2cor} = \alpha_2 \cdot \left(\frac{\eta_2(t_{m2})}{\eta_2(t_{p2})} \right)^{0.14} \quad (24)$$

$$\eta_2(t_i) = x_G \cdot 61463.67 \cdot t_i^{-3.31} + x_{H_2O} \cdot 0.0329 \cdot t_i^{-1.038} \quad (25)$$

Where: q_1, q_2 -hot and cold fluid thermal flow, W/m^2 ;
 α_1 - steam partial coefficient of heat transfer, $W/(m^2 \cdot K)$;
 t_{m1} – steam average temperature, K;
 t_{m2} – glycerol-water solution average temperature, K;
 t_{p1} – steam wall temperature, K;
 t_{p2} – glycerol-water solution wall temperature, K;
 $\eta_2(t_{m2})$ - glycerol solution dynamic viscosity at the average temperature, $kg/(m \cdot s)$;
 $\eta_2(t_{p2})$ - glycerol solution dynamic viscosity at the wall temperature, $kg/(m \cdot s)$;
 δ_p -wall thickness, m;
 λ_p -steel thermal conductivity, $W/(m \cdot K)$;
 α_2 - glycerol-water solution partial coefficient of heat transfer, $W/(m^2 \cdot K)$;
 α_{2cor} - corrected glycerol-water solution partial coefficient of heat transfer, $W/(m^2 \cdot K)$.

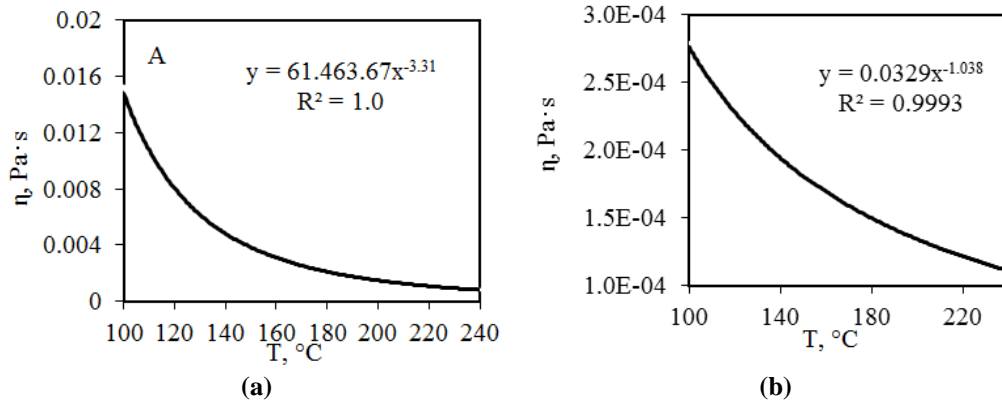


Fig. 7. Glycerol (a) and water (b) viscosity dependence on the temperature.

Table 13

Mixture viscosities at respective temperatures, heat fluxes and corrected partial heat transfer coefficient

$\eta_2(t_{m2}) \text{ Pa} \cdot \text{s}$	$q_1 \text{ W/m}^2$	$t_{p2} \text{ } ^\circ\text{C}$	$\eta_2(t_{p2}) \text{ Pa} \cdot \text{s}$	$q_2 \text{ W/m}^2$	$\alpha_{2cor}, \text{ W/(m}^2 \cdot \text{K)}$
$1.5 \cdot 10^{-3}$	29554.9	257	$2.5 \cdot 10^{-4}$	29554.9	249.1

The total heat transfer coefficient was calculated by equation (26) and compared with the proposed one, where $\delta_p=2$ mm and represents the wall thickness, $\lambda_p=46.5 \text{ W/(m} \cdot \text{K)}$ [21] and represents the thermal conductivity of the steel wall and r_{cr1} and r_{cr2} are the thermal resistances of crusts for condensate and organic fluid [21], and the obtained value was $K_{calc} = 214.6 \frac{\text{W}}{\text{m}^2 \cdot \text{K}}$. The required transfer area for the process to take place has a value of $A_{nec}=127.5 \text{ m}^2$, and the area excess was 6.3%, which makes this multitubular heat exchanger with four passes compliant.

$$K_{calc} = \frac{1}{\frac{1}{\alpha_{2cor}} + \frac{\delta_p}{\lambda_p} + r_{cr1} + r_{cr2} + \frac{1}{\alpha_1}} \quad (26)$$

Where: δ_p - wall thickness, m;

λ_p - steel thermal conductivity, $\text{W/(m} \cdot \text{K)}$;

α_1 - steam partial coefficient of heat transfer, $\text{W/(m}^2 \cdot \text{K)}$;

α_{2cor} - corrected glycerol-water solution partial coefficient of heat transfer, $\text{W/(m}^2 \cdot \text{K)}$;

r_{cr1}, r_{cr2} - thermal resistances of crusts for condensate and organic fluid, $(\text{m}^2 \cdot \text{K})/\text{W}$;

K_{calc} - calculated total coefficient of heat transfer, $\text{W/(m}^2 \cdot \text{K)}$;

The diameters of the inlet and outlet connections for both the mixture and the heat agent were determined with equation (27), where ρ_j – the mixture or heat

agent density of the mixture at the inlet and outlet temperature respectively (kg/m^3), w_j - the speed that it was considered 2 m/s for liquids and 10 m/s for steam, D_m^j - the mass flow rate of the mixture or thermal agent (kg/s). These diameters were standardized according to [21] and the obtained velocities were checked with these standardized diameter values to ensure having values specific for liquid or vapor like phase. The obtained results are presented in Table 14.

$$d_{\text{in/out}} = \sqrt{\frac{4 \cdot D_m^j}{\pi \cdot \rho_j \cdot w_j}} \quad (27)$$

Table 14

The values of mass flow rates, temperatures, densities, velocities and pipe diameter for the inlet and outlet of the mixture and the heat agent.

Fluid	D_m kg/s	Inlet				Outlet			
		T °C	ρ kg/m ³	w m/s	d_{in} mm	T °C	ρ kg/m ³	w m/s	d_{out} mm
Mixture	3.61	37	1159	1.87	46	240	1001.4	1.91	49
Steam	1.39	260	23.82	9.61	88	260	814.81	1.88	34

The pressure drop in the pipes was determined with equation (28) and the hydraulic resistances (ξ_i) for the five zones of the exchanger were considered (Fig. 8). The results for the hydraulic resistances as well for the 5 zones of the heat exchanger are presented in Table 15 and were calculated accordingly. The obtained value of the pressure drop was $\Delta p = 48.7 \text{ Pa}$.

$$\Delta p = \left(\lambda_f \cdot \frac{L}{d_i} + \sum_i N_i \cdot \xi_i \right) \cdot \frac{w_{\text{mix}}^2}{2} \cdot \rho_{\text{mix}} \quad (28)$$

$$\lambda_f = \frac{64}{Re_{\text{mix}}} \quad (29)$$

Where: λ_f – friction coefficient;

N_i – number of hydraulic resistance;

L - pipes length, m;

d_i - pipes internal diameter, m;

ρ_{mix} – glycerol solution density, kg/m^3 ;

ξ_i – hydraulic resistance;

w_{mix} - glycerol solution velocity, m/s;

Re_{mix} - Reynolds glycerol solution number;

Δp – pressure drop for glycerol solution, Pa.

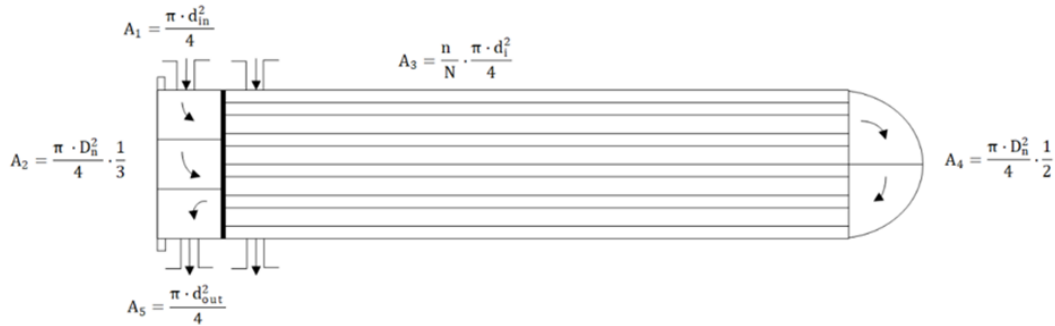


Fig. 8 Diagram of the four-pass heat exchanger with the five zones of different area exemplified.

Table 15

The areas and hydraulic resistances values for the five zones of the heat exchanger

Heat exchanger zones	A_i, m^2	ξ_i
1	0.0017	0.9968
2	0.5131	0.3821
3	0.1210	0.1079
4	0.7697	0.8427
5	0.0019	0.4988

6. Economic evaluation of the lactic acid synthesis plant

The economic evaluation for the proposed process flowsheet for lactic acid production from glycerol consists of two parts, the CAPEX and OPEX terms from equation (30). In

Table 16 is presented the total annual cost for materials, Table 17 contains the utilities required for the plant equipment. For the CAPEX, the equipment cost was analyzed using Aspen Plus v10 or CapCost economic tools, meaning the vessels, the heat exchangers, the columns, the filters, the evaporator were pre-sized, and all the prices are mentioned in Table 18. For the OPEX, the cost for the raw materials and utilities was considered. The valuable products prices were considered in agreement with their purity, 1.9 \$/kg for lactic acid, 1.5 \$/kg for propylene glycol and 2 \$/kg for diglycerol. Considering that the payback period of the investment was considered 10 years, the calculations carried out led to a production price of the finished products of 1.64 \$/kg demonstrating that the proposed process scheme is economically feasible.

$$TIC = \frac{CAPEX}{PBP} + OPEX \quad (30)$$

$$Production_{cost} = \frac{\left(OPEX + \frac{CAPEX}{PBP}\right)_{year} \$}{(D_m^{PG} + D_m^{DG} + D_m^{LA})_{year} \frac{kg}{year}} \quad (31)$$

Where: $Production_{cost}$ - Production cost, \$/kg;

$CAPEX$ – Capital cost, \$;

$OPEX$ – Operational cost, \$/yr;

TIC – Total investment cost, \$/yr;

PBP – Payback period, yr;

D_m^j - Mass flow of j species, kg/yr.

Table 16

Materials cost

Raw material	Amount (kg/year)	Price (\$/kg)	Total price (\$/year)
Glycerol	$5.23 \cdot 10^7$	0.2	$1.05 \cdot 10^7$
NaOH	$3.23 \cdot 10^7$	0.3	$9.69 \cdot 10^6$
Ca(OH) ₂	$1.70 \cdot 10^7$	0.3	$5.10 \cdot 10^6$
H ₂ SO ₄	$1.71 \cdot 10^7$	0.3	$5.13 \cdot 10^6$
TOTAL			$3.04 \cdot 10^7$

Table 17

Utilities cost

Equipment	Utility	Total price (\$/year)
Heat exchangers	Steam	$6.28 \cdot 10^5$
	Electricity	$2.46 \cdot 10^7$
Distillation columns	Steam & electricity	$4.28 \cdot 10^6$
Evaporator	Steam & electricity	$1.46 \cdot 10^6$
TOTAL		$3.10 \cdot 10^7$

Table 18

Equipment cost

Equipment	Type	Total cost (\$)
(3)	Vessel	413.000
(1)		46.800
(9)		70.100
(6)		107.000
(10)		218.000
(15)		59.900
(14), (17), (18)	Distillation columns	4.280.000
(12)	Evaporator	1.460.000
(5), (7), (11)	Filters	1.500.000
(16)	Shell&Tube Heat exchanger	254.000
(2)		68.900

(4)		134.000
(20)		57.000
(13)		60.000
(8)	DIAION™ SK104H resin	1.328.400
TOTAL		10.057.100

8. Conclusions

In this paper the process of converting glycerin into lactic acid was analyzed from a technological point of view. This product represents a versatile substance in terms of uses in different industrial fields such as the food, cosmetics and polymer synthesis industries. The process involves three sections, a reaction section where lactic acid is obtained in the form of sodium lactate, a section for purification and recovery of lactic acid, and a section for the separation of the resulting secondary products. In addition to lactic acid, the product of interest, this process also yields propylene glycol and diglycerol as high purity finished products that are marketed. Performing the material balance for each unit operation, either classically or with the help of the Aspen Plus v10 simulator, a mass flow rate of 80% wt. lactic acid solution of 3820.72 kg/h is obtained from this process, which allows reaching the production capacity of 30 000 tonnes/yr at 8000 h/yr of continuous operation. From the heat balance, utility flows for heating or cooling operations and thermal flows were determined. The temperature of the mixture resulting from the dissolution of sodium hydroxide (108.7°C) was necessary as preheating the feed of the reaction stage and the final temperature of the glycerol solution (37 °C) essential for sizing the heat exchanger thermally integrated because was considered a heat recovery from the separated pure glycerol.

REFERENCES

- [1] Castillo Martinez F.A., Balciunas E.M., Salgado J.M., Domínguez González J.M., Converti A., Oliveira R.P.d.S., Lactic acid properties, applications and production: A review, *Trends in Food Science & Technology*, 30 (1), (2013), 70-83.
- [2] Komesu A., Oliveira J., Martins L., Maciel M., Filho R., Lactic Acid Production to Purification: A Review, *BioResources*, 12, (2017), 4364-4383.
- [3] Arcanjo M.R.A., Silva I.J., Cavalcante C.L., Iglesias J., Morales G., Paniagua M., Melero J.A., Vieira R.S., Glycerol valorization: conversion to lactic acid by heterogeneous catalysis and separation by ion exchange chromatography, *Biofuels, Bioproducts and Biorefining*, 14 (2), (2019), 357-370.
- [4] <https://www.grandviewresearch.com/industry-analysis/lactic-acid-and-poly-lactic-acid-market>, accessed 23/06/2023.
- [5] Ramirez-Lopez C A., Ramirez-Lopez J. R., Fernandez-Santos M., Gomez-Jimenez Aberasturi O., Alonso-Vicario A., Torrecilla-Soria J., Synthesis of Lactic Acid by Alkaline

- Hydrothermal Conversion of Glycerol at High Glycerol Concentration, *Industrial & Engineering Chemistry Research*, 49, (2010), 6270-6278.
- [6] Jalal Sahandi P., Kazemeini M., Sadjadi S., Simulation of continuous catalytic conversion of glycerol into lactic acid in a microreactor system: A CFD study, *Journal of Industrial and Engineering Chemistry*, 104, (2021), 258-271.
- [7] Rodrigues A.K.O., Maia D.L.H., Fernandes F.A.N., Production of Lactic Acid from Glycerol by Applying an Alkaline Hydrothermal Process Using Homogeneous Catalysts and High Glycerol Concentration, *Brazilian Journal of Chemical Engineering*, 32, 3, (2015), 749-755.
- [8] Chen, L., Conversion of Glycerol to Lactic Acid under Low Corrosive Conditions with Homogeneous and Heterogeneous Catalysts, Master's Thesis, University of Tennessee, 2011.
- [9] Yin H., Yin H., Wang A., Shen L., Catalytic conversion of glycerol to lactic acid over graphite-supported nickel nanoparticles and reaction kinetics, *Journal of Industrial and Engineering Chemistry*, 57, (2018), 226-235.
- [10] Yin H., Zhang C., Yin H., Gao D., She, L., Wang A., Hydrothermal conversion of glycerol to lactic acid catalyzed by Cu/hydroxyapatite, Cu/MgO, and Cu/ZrO₂ and reaction kinetics, *Chemical Engineering Journal*, 288, (2016), 332-343.
- [11] Yang G. Y., Ke Y. H., Ren H.F., Liu C. L., Yang R. Z., Dong W. S., The conversion of glycerol to lactic acid catalyzed by ZrO₂-supported CuO catalysts, *Chemical Engineering Journal*, 283, (2016), 759-767.
- [12] Tang Z., Cao H., Tao Y., Heeres H.J., Pescarmona P.P., Transfer hydrogenation from glycerol over a Ni-Co/CeO₂ catalyst: A highly efficient and sustainable route to produce lactic acid, *Applied Catalysis B: Environmental*, (2020), 263.
- [13] Ftouni J., Villandier N., Auneau F., Besson M., Djakovitch L., Pinel C., From glycerol to lactic acid under inert conditions in the presence of platinum-based catalysts: The influence of support, *Catalysis Today*, 257, (2015), 267-273.
- [14] Marques F.L., Oliveirab A.C., Mendes Filhoc J., Rodríguez-Castellón E., Cavalcante Jr. C.L., Vieira R.S., Synthesis of lactic acid from glycerol using a Pd/C catalyst, *Fuel Processing Technology*, 138, (2015), 228-235.
- [15] Shen L., Yin H., Yin H., Liu S., Wang A., Conversion of Glycerol to Lactic Acid Catalyzed by Different-Sized Cu₂O Nanoparticles in NaOH Aqueous Solution, *Journal of Nanoscience and Nanotechnology*, 17, (2017), 780-788.
- [16] Chen L., Ren S., Ye Philip X., Lactic acid production from glycerol using CaO as solid base catalyst, *Fuel Processing Technology*, 120, (2014), 40-47.
- [17] Zavrazhnov S., Esipovich A., Zlobin S., Belousov A., Vorotyntsev A., Mechanism Analysis and Kinetic Modelling of Cu NPs Catalysed Glycerol Conversion into Lactic Acid, *Catalysts*, 9(3), 2019.
- [18] <https://pubchem.ncbi.nlm.nih.gov/compound/13144>, accessed 12/03/2023.
- [19] <https://pubchem.ncbi.nlm.nih.gov/compound/6116#section=Structures>, accessed 12/03/2023.
- [20] [https://chem.libretexts.org/Bookshelves/Introductory_Chemistry/Introductory_Chemistry_\(CK-12\)/17%3A_Thermochemistry/17.13%3A_Heat_of_Solution](https://chem.libretexts.org/Bookshelves/Introductory_Chemistry/Introductory_Chemistry_(CK-12)/17%3A_Thermochemistry/17.13%3A_Heat_of_Solution), accessed 11/06/2023.
- [21] Floarea O., Jinescu Gh., Balaban C., Dima R., Vasilescu P., Operatii si Utilaje în Industria Chimica, Ed. Didactica și Pedagogica, Bucharest, 1980.

MODELING AND OPTIMIZATION OF A PROPYLENE GLYCOL PRODUCTION PLANT

Angela G. MAREȘ^{1,2}, Romuald GYÖRGY^{1*}, Adina GAVRILĂ², Ionuț BANU¹

¹Department of Chemical and Biochemical Engineering, Faculty of Chemical Engineering and Biotechnologies, POLITEHNICA Bucharest

²Department of Bioresources and Polymer Science, Faculty of Chemical Engineering and Biotechnologies, POLITEHNICA Bucharest

Abstract

In this work, an analysis of a glycerol hydrogenolysis plant to manufacture propanediol was carried out, considering a production capacity of 30000 t/yr. Mass and heat balances, sizing of the main equipment and the economic evaluation were performed using Aspen Plus v10 commercial simulator. The behavior of the tri-phase hydrogenolysis reactor was analyzed both at the catalyst particle scale and at the catalyst bed scale. A rigorous optimization study using Aspen Plus and MATLAB was carried out and the Total Annual Cost for the separation section was minimized by using the feed tray position and total number of trays as decision variables. The economic evaluation confirmed the feasibility of the proposed process flowsheet.

Key words: Glycerol valorization, process analysis, process modeling, economic evaluation

1. Introduction

Glycerol is a valuable raw material, both in terms of the significant quantity obtained as a by-product from transesterification and saponification processes in the biodiesel and soap industries, and due to its potential for chemical and biotechnological transformation into value added chemicals with applications in several fields [1]. In the global market, glycerol occupied a volume of \$2.5 billion in 2018 and is expected to grow to \$3.3 billion by 2023, with a CAGR (compound annual growth rate) of 5.7%. Most of the glycerol that is supplied to the market is derived from the biodiesel fuel industry. The biofuels market experienced a decline in 2020 because of the COVID-19 pandemic but is expected to reach 40 million tons per year in the next 3 years. As a result, approximately 6.3 million tons of crude glycerol will be produced by 2025 [2].

1,2-Propanediol is a versatile, colorless, odorless and non-toxic organic compound that is widely used in various industries such as food and pharmaceuticals, its low toxicity making it suitable for various applications

¹ Corresponding author: romuald.gyorgy@upb.ro

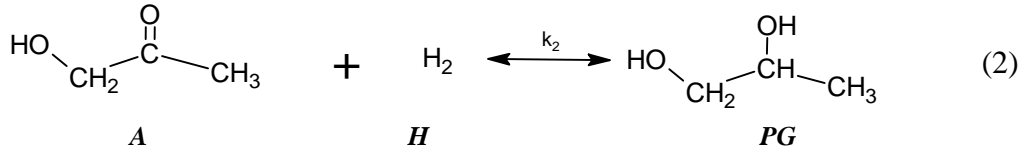
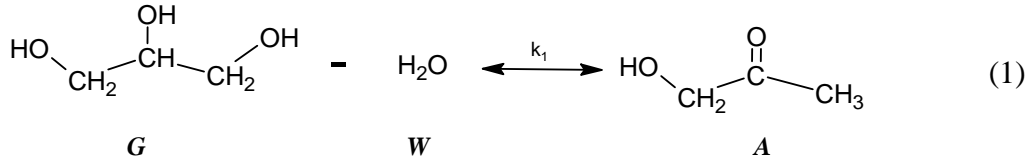
including those involving direct contact with the human body [3]. The global propylene glycol market expanded steadily during the period 2015-2022 and reached 1900 thousand tons per year and is expected to continue to grow at a CAGR (“compound annual growth rate”) of 5.26% until 2035, up to an expected 3800 thousand tons per year. (20) Data Bridge Market Research predicted that the global propylene glycol market (which was \$4.29 billion in 2022) would reach \$6.10 billion by 2030, at a CAGR of about 4.5% [4]. Propylene glycol can be produced from a variety of raw materials. It is currently obtained as the main product of the industrial hydration synthesis of propylene oxide; at the same time, technologies based on the conversion of renewable raw materials such as hydrogenation of lactic acid, hydrogenolysis of glycerol or thermal conversion of carbohydrates are also being pursued [5].

The isothermal conversion of glycerol to propanediol involves carrying out the hydrogenolysis reaction in a trickle-bed reactor at high pressure with a considerable excess of hydrogen. Studies on glycerol hydrogenolysis over a range of Cu-ZnO-Al₂O₃ catalysts of different composition have been reported in the literature. Glycerol conversion from 33.2% to 81.5% and selectivity in propylene glycol from 71.9% to 93.9% were obtained. The high selectivity in propylene glycol indicates that Cu-ZnO-Al₂O₃ is an efficient catalyst for the hydrogenolysis reaction of glycerol to propylene glycol [6].

In the following sections the evaluation of an industrial process for manufacturing propylene glycol from glycerol will be presented. The chemical reaction takes place in a trickle-bed reactor under isothermal conditions at high pressure. The performance of hydrogenolysis reaction was examined by solving the material and heat balances along the catalyst bed, as well as at the catalyst particle scale. Finally, the total annual cost (TAC) of the plant and the production price of propylene glycol were estimated by means of rigorous calculations in Aspen Plus v10.

2. Process kinetics and thermodynamics

In the case of hydrogenolysis of glycerol to propylene glycol, a column reactor with a fixed catalyst bed is used, with glycerol as the liquid phase and hydrogen as the gas phase. One of the main elements required for the design and analysis of a chemical reactor is the kinetics of the process. In our case, a kinetic model for the glycerol hydrogenolysis process from the literature was considered, which takes into account reactions (1) and (2) [6]. Langmuir-Hinshelwood rate expressions for reactions (1) and (2) are given by relations (3) and (4).



Where: **G**, glycerol; **A**, acetol; **W**, water; **PG**, propylene glycol; **H**, hydrogen.

$$r_1 = \frac{k_1 \cdot b_G \cdot c_G}{1 + b_G \cdot c_G + b_A \cdot c_A + b_{PG} \cdot c_{PG}} \quad \frac{\text{kmol}}{\text{kg}_{\text{cat}} \cdot \text{s}} \quad (3)$$

$$r_2 = \frac{k_2 \cdot b_A \cdot c_A \cdot b_H \cdot P_H}{(1 + b_G \cdot c_G + b_A \cdot c_A + b_{PG} \cdot c_{PG}) \cdot (1 + \sqrt{b_H \cdot P_H})^2} \quad \frac{\text{kmol}}{\text{kg}_{\text{cat}} \cdot \text{s}} \quad (4)$$

Where: c_G , c_A , c_{PG} - molar concentrations of glycerol, acetol and propylene glycol, kmol/m^3 ; P_H - hydrogen partial pressure, MPa; k_1 and k_2 - rate constants, $\text{mol}/(\text{g} \cdot \text{s})$; b_G , b_A , b_{PG} , b_H - adsorption equilibrium constants, m^3/mol .

The rate constants and equilibrium constants are determined with relations (5) and (6) based on the kinetic parameters given in table 1

$$k_i = k_i^0 \exp \left[\frac{-E_i}{R_g \cdot T} \right], \quad i = 1, 2 \quad (5)$$

$$b_j = b_j^0 \exp \left[\frac{Q_j}{R_g \cdot T} \right], \quad j = G, A, W, PG \quad (6)$$

Where: E_i - activation energy of reaction i , kJ/mol ; Q_j - enthalpy of adsorption of species j , kJ/mol .

Table 1

Kinetic parameters of the glycerol hydrogenolysis process [6]

	Pre-exponential factor	Activation energy, kJ/mol
$k_1, \text{mol}/(\text{g} \cdot \text{s})$	$1.54 \cdot 10^4$	86.56
$k_2, \text{mol}/(\text{g} \cdot \text{s})$	$7.16 \cdot 10^3$	57.8
$b_G, \text{m}^3/\text{mol}$	$2.22 \cdot 10^{-3}$	36.42
$b_A, \text{m}^3/\text{mol}$	$8.73 \cdot 10^{-3}$	25.94
$b_{PG}, \text{m}^3/\text{mol}$	$5.80 \cdot 10^{-3}$	25.77
$b_H, 1/\text{MPa}$	$1.86 \cdot 10^{-5}$	36.24

The resulting components from the reaction section have distinct boiling points (given in table 2), enabling more efficient separation. The mixture was analyzed using Aspen Properties facilities and no azeotropic points were determined. Considering these aspects, high purity performance can be achieved by using classical separation techniques.

Table 2

Molar masses and boiling temperatures of the compounds involved in the process.

Component	Molecular weight, M _w , g/mol	Boiling point, T _f , °C
Glycerol (G)	92	292
Hydrogen (H)	2	-253
Propylene glycol (PG)	76	188
Water (W)	18	100
Acetol (A)	74	146

3. Reactor modelling

The kinetic model proposed in the literature by Zhou et al. [6] was developed in operating condition in which the physical steps have a negligible influence on the process kinetics. To accurately determine the characteristics of an industrial reactor (catalyst bed volume, reactor diameter), it is important to consider the behavior of the chemical transformation at the catalyst particle scale. One of the physical phenomena that significantly influences process performance is internal diffusion, which can be important for catalyst particle sizes in the millimeters range.

Evaluation of the influence of internal diffusion, at the catalyst particle scale

For the evaluation of internal diffusion, an isothermal catalyst particle was considered for which mass balance equations were written, according to relation (7). For each chemical species j , one such mass balance equation was written. An important feature of these equations is that they have boundary conditions, one at the particle center, whereas the second at the surface. In order to be able to solve these second order differential equations, each of them was transformed into a system of first order differential equations with attached boundary conditions. This system of 8 differential equations was solved in MATLAB using the function bvp4c.

$$\frac{1}{r^2} \cdot \frac{d}{dr} \cdot \left(r^2 \cdot D_{ef} \cdot \frac{dC_j}{dr} \right) - v_{Rj} = 0 \quad \begin{array}{l} r = 0 \quad \frac{dC_j}{dr} = 0 \\ r = R_p \quad C_j = C_{jL} \end{array} \quad j = G, A, W, PG \quad (7)$$

Where: C_j - concentration of species j in the porous catalyst particle, kmol/m³; v_{Rj} - transformation rate of species j , kmol/(kg_{cat}·s); D_{ef} - effective diffusion coefficient, cm²/s.

The chemical transformation performance at the catalyst particle scale was evaluated using effectiveness factors calculated by relation (8), representing the ratio of the average species transformation rate within the catalyst particle to the species transformation rate at the catalyst particle surface. The average species transformation rate inside the catalyst grain was calculated taking into account the particle characteristics shown in table 3 by relation (9), and the values of the required diffusion coefficients in the balance equations were calculated using the Tyn and Calus correlation (10) [7].

$$\eta_j = \frac{\overline{v_{Rj}}}{v_{Rj,S}} \quad (8)$$

$$\overline{v_{Rj}} = \frac{3}{R_p^3} \cdot \int_0^{R_p} r^2 \cdot v_{Rj}(r) dr \quad (9)$$

$$D_{j,G} = 8,93 \cdot 10^{-8} \cdot \frac{V_j^{0,267}}{V_G^{0,433}} \cdot \frac{T}{\eta_G} \quad (10)$$

$$D_{ef} = \frac{\varepsilon_p}{\tau} \cdot \overline{D_{j,G}} \quad (11)$$

Where: η_j - the effectiveness factor of species j ; $\overline{v_{Rj}}$ - average transformation rate of species j within the catalyst particle, kmol/(kg_{cat}·s); $v_{Rj,S}$ - transformation rate of species j at the catalyst outer surface, kmol/(kg_{cat}·s); D_{ef} - effective diffusion coefficient, cm²/s.

Table 3

Structural characteristics of catalyst particle			
Catalyst particle density, ρ_p , g/cm ³	Catalyst particle radius, R_p , mm	Voids fraction in the particle, ε_p	Tortuosity factor, τ
1825	2	0.5	4

The effective diffusion coefficient is averaged, and a typical value for it is $4 \cdot 10^{-6}$ cm²/s. Together with the solution of the mass balance equations, species concentration profiles were obtained with respect to radial position within the catalyst particle. The simulation was carried out considering the typical values presented in table 4.

Table 4

Operating conditions used for simulating the concentration profiles in the catalyst particle

T, K	Surface concentration of species j , $C_{j,s}$, kmol/m ³				P, bar	d_p , mm
	<i>G</i>	<i>A</i>	<i>W</i>	<i>PD</i>		
493	9.51	0.139	1.36	1.22	40	2

Variations in species concentrations are observed: the concentration of glycerol decreases from the surface to the interior of the granule, also the concentration of acetol decreases as it is consumed during the reaction, and the concentration of propylene glycol increases from the interior of the granule towards the surface, this having the highest value in the center of the catalyst granule, where the reaction product is formed.

The influence of internal diffusion evaluated at the granule level must also be considered at the catalyst bed level. One approach would be to integrate the balance equations at each position along the reactor, which would be laborious, another approach is to correlate the effectiveness factors with an empirical model to account for their variations along the catalyst bed.

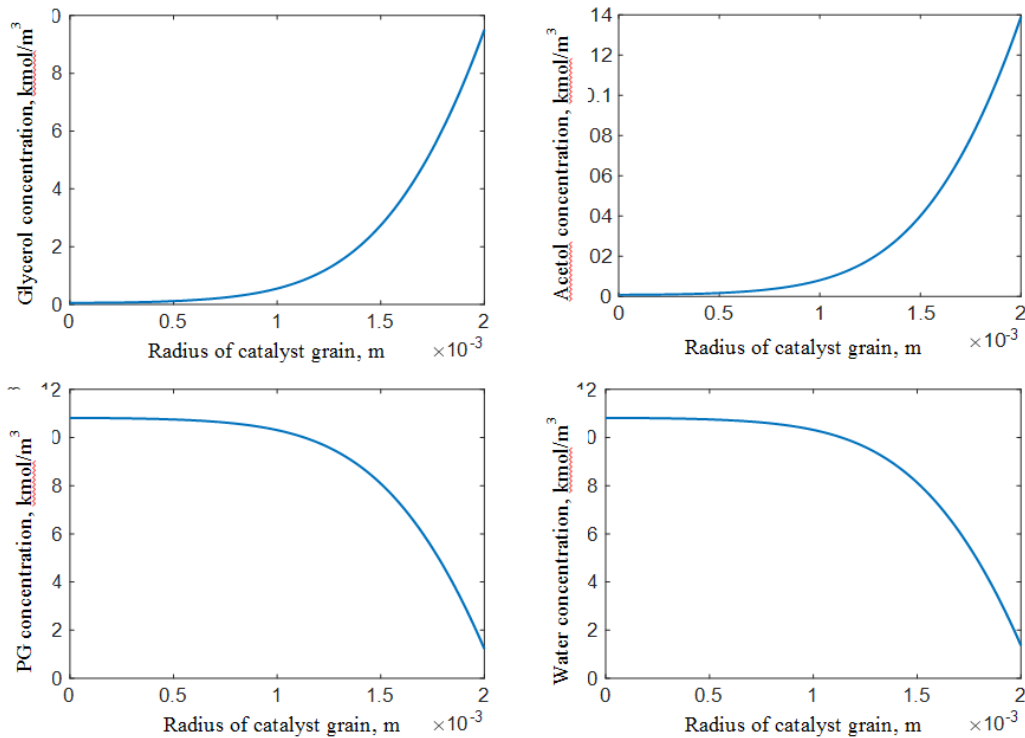


Fig.1. Concentration profiles in the catalyst particle

Following simulation in MATLAB, typical values for the efficiency factors were obtained under various conditions of temperature, pressure, concentrations

and at various catalyst grain diameters and presented in table 5. According to these values one can stress that the internal diffusion has an important effect on the process kinetics because the values of the efficiency factors are relatively small.

Table 5

Effectiveness factors values calculated in typical operating conditions

T, K	Surface concentration of species j , C _j , kmol/m ³				P, bar	d _p , m	η ₁	η ₂
	G	A	W	PG				
493	9.51	0.139	1.36	1.22	30	2·10 ⁻³	0.215	0.215
493	9.51	0.127	1.36	1.23	40	2·10 ⁻³	0.215	0.233
493	9.51	0.119	1.36	1.24	50	2·10 ⁻³	0.215	0.247
513	5.14	0.102	5.73	5.62	30	1·10 ⁻³	0.271	0.211
513	7.85	0.140	3.02	2.88	40	2·10 ⁻³	0.201	0.170
473	9.75	0.105	1.12	1.02	30	3·10 ⁻³	0.159	0.209

In order to be able to correlate the effectiveness factors with the operating conditions, a large number of simulations of the catalyst particle were performed using multiple sets of values for the surface boundary conditions, and an empirical model was obtained (12) in which the effectiveness factors were correlated with the independent variables by multi-linear regression. The coefficients b₀, ...7, are presented in table 6.

$$\eta_i = b_0 + b_1 \cdot T + b_2 \cdot C_G + b_3 \cdot C_A + b_4 \cdot C_W + b_5 \cdot C_{PD} + b_6 \cdot P + b_7 \cdot d_p \quad i = 1, 2 \quad (12)$$

Table 6

Correlation equation coefficients for calculating the effectiveness factors.

	b ₀	b ₁	b ₂	b ₃	b ₄	b ₅	b ₆	b ₇
η ₁	23.07	-6.9·10 ⁻⁴	-2.06	31.02	32.63	30.57	3.3·10 ⁻⁴	-24.15
η ₂	-2.97	-2.65·10 ⁻³	0.42	7.88	8.05	-7.64	1.46·10 ⁻³	-24.61

The adequacy of the empirical models given by equation (12) with the rigorous simulations results can be visually assessed from the parity diagrams given in figure 2.

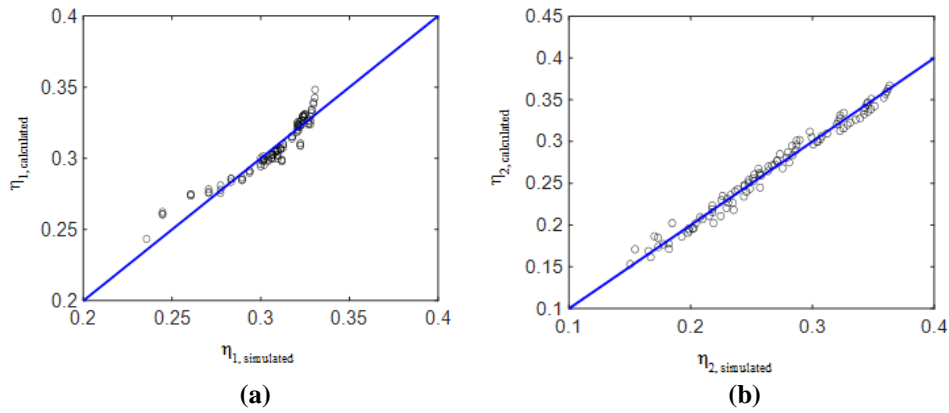


Fig. 2 Effectiveness factor parity diagrams: a) the first reaction (1) and b) the second reaction (2)

Process analysis at the catalyst bed scale

The next step in determining the length of the catalytic layer is to integrate the mathematical model of the reactor. The liquid flow velocity through the catalytic layer is considered from the literature for a similar reactor [8]. The mass balance equations (13) and (14) were used to simulate the behavior of the catalytic reactor.

$$\frac{d\xi_i}{dz} = \sum_{i=1}^r v_{i,j} \cdot d\xi_i = S_T \cdot v_{Ri} \cdot \rho_{sc} \quad (13)$$

$$\frac{d\xi_i}{dz} = \frac{D_{V,GL}^0}{u_L} \cdot v_{Ri} \cdot \rho_{sc} \quad \begin{matrix} z = 0 & \xi_i = 0 \\ i = 1, 2 \end{matrix} \quad (14)$$

$$u_L = 7.522 \cdot 10^{-3}, \quad \frac{cm}{s}, [8] \quad (15)$$

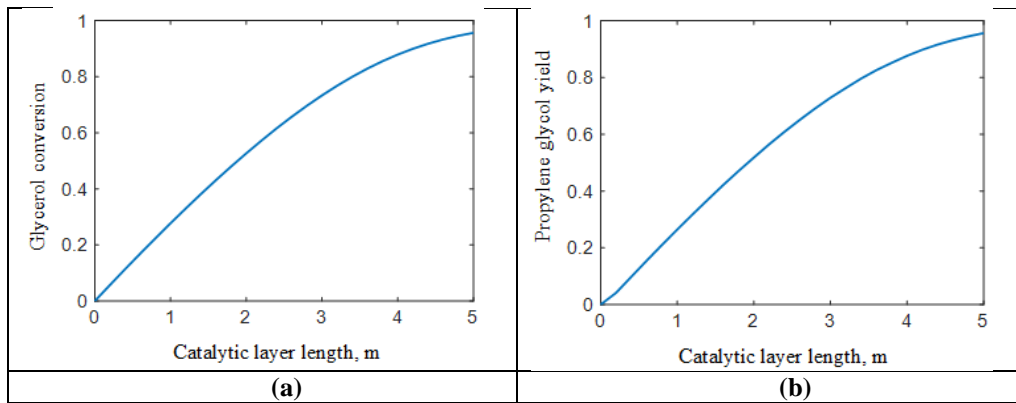


Fig. 3. Variation of glycerol conversion (a) and propylene glycol yield (b) along the catalytic layer

Considering both the influence of internal diffusion and the concentration variation along the reactor, a reactor length of 5 m was determined by successive simulation studies, and it is observed that both a high glycerol conversion of 96% and a high propylene glycol yield of 96% are obtained in this reactor.

4. Process description

Based on the aspects evidenced in the previous paragraphs, a conceptual design of a plant with a production capacity of 30,000 metric tons of propylene glycol per year was performed. The mass and thermal balances were carried out using Aspen Plus v10 process simulator. The proposed process flowsheet is presented in figure 4.

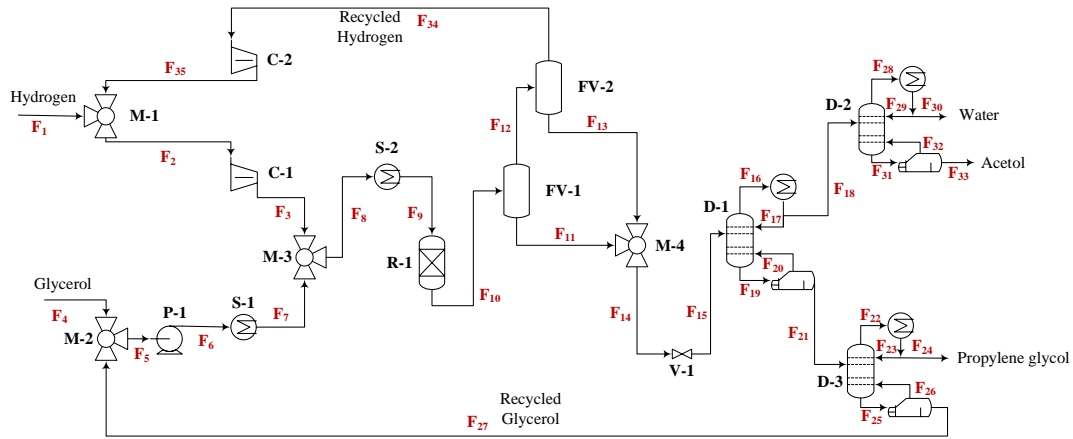


Fig. 4. Flowsheet of the proposed process

Freshly fed glycerol at 25 °C and 1 bar pressure is mixed with the recirculated glycerol flow and pumped at 40 bar pressure and heated to 220 °C reaction temperature in a tubular heat exchanger S-1, using steam as hot utility. After the glycerol is brought to operating conditions, it is mixed with the hydrogen stream and fed into the R-1 reactor.

The fresh hydrogen, from industrial sources, is supplied at a temperature of 25 °C and a pressure of 20 bar. It is then mixed with the recirculated hydrogen flow and compressed to the reaction pressure of 40 bar. Since the compression operation also increases the temperature of hydrogen, resulting in a value close to the reaction temperature, the compressed hydrogen stream is directly mixed with the glycerol stream, with no additional heat transfer operations. Hydrogen is fed in excess, at a molar ratio of 5:1 to glycerol. The reaction mixture is heterogeneous, with hydrogen in the gas phase and glycerol in the liquid phase. The pressure of 40 bar in the reactor is high enough to achieve efficient contact between the reactant phases and

thus chemical transformation takes place in the fixed-bed catalytic reactor R-1 over Cu-Zn/Alumina catalyst.

After the chemical transformation, the main reaction products from the reactor are propylene glycol, acetol and water as by-products, and unreacted glycerol and unreacted hydrogen. The operations following the reaction are grouped in the separation section, which starts with a series of flash separators (FV-1 and FV-2). These are designed to remove the excess hydrogen from the reaction effluent. The separated hydrogen is recirculated and mixed with the freshly fed hydrogen stream in the compression stage.

The resulting liquid phase from the reactor is collected from both flash separators and combined by a mixing operation M-4. This is followed by a depressurization stage resulting in a liquid stream that is fed into the series of separation columns. The first distillation column, D-1, separates water and acetol at the top and glycerol and propylene glycol at the bottom. The pressure in the condenser is 0.5 bar and the temperature is 82.3 °C; the temperature in the reboiler is 177.2 °C. The second distillation column, D-2, separates water at the top and acetol at the bottom; pressure in the condenser is 1 bar, temperature 99.6 °C and temperature in the reboiler 133.3 °C. The third distillation column, D-3, separates propylene glycol at the top and (unreacted) glycerol at the bottom. The pressure in the condenser is 0.02 bar, the temperature is 92.1 °C and the temperature in the reboiler 173.2 °C.

Propylene glycol, water and acetol are separated with high purities and do not require further treatment. The separated glycerol from the third distillation column, D-3, is recirculated and mixed with fresh glycerol before being fed back into the reactor.

5. Results and discussions

Material and heat balance

The feed rates of the raw materials were evaluated considering the annual production, the annual operating time of the plant and the information on the selectivity of the chemical transformation. Using the previously considered annual production of $P = 30000$ t/year and the annual operating time of $H = 8000$ h/year, the mass and molar flow rate of propylene glycol were calculated with relations (16) and (17) and (17).

$$D_{m,PG} = \frac{P_a}{H}, kg/h \quad \text{Propylene glycol mass flow rate} \quad (16)$$

$$D_{M,PG} = \frac{D_{m,PG}}{M_{PG}}, kmol/h \quad \text{Propylene glycol molar flow rate} \quad (17)$$

$$D_{m,PG} = \frac{30000 \text{ t/year}}{8000 \text{ h/year} \cdot 1000} = 3750 \frac{kg}{h} \quad (18)$$

$$D_{M,PG} = \frac{3750 \text{ kg/h}}{76 \text{ g/mol}} = 49,34 \frac{kmol}{h} \quad (19)$$

Reactor Mass Balance

For the hydrogenolysis process, the Cu/ZnO/Al₂O₃ catalyst with a Cu/Zn/Al molar ratio of 1:1:0.5 was considered, for which the selectivity of glycerol conversion to propylene glycol is $\sigma_G=93.4\%$ [6]. The feed molar ratio between hydrogen and glycerol is 5. Considering these aspects, the feed mass flow rates of the raw materials were determined. For the dehydrogenation reaction of glycerol to acetol, a conversion of $X_G = 96 \%$ was considered, and for the hydrogenation reaction of acetol to propylene glycol, a conversion of $X_A = 93 \%$ was considered.

Table 7

Mass balance for the chemical reaction stage.

Species flow rate	Inlet	Outlet
	Mass flow in F9 stream	Mass flow in F10 stream
$D_{m,G}$ (kg/h)	5100	204
$D_{m,H}$ (kg/h)	663	563.29
$D_{m,PG}$ (kg/h)	38.02	3801.85
$D_{m,W}$ (kg/h)	2.67	960.41
$D_{m,A}$ (kg/h)	1.66	275.79
Total (kg/h)	5805.35	5805.35

Distillation column material balance

Table 8

Material balance for D-3 distillation column.

Species	Inlet		Outlet			
	Molar flow in F22 stream (kmol/h)	x_F	Molar flow in F24 stream (kmol/h)	x_D	Molar flow in F24 stream (kmol/h)	x_W
G	2.22	0.0425	0	0	2.22	0.8160
H	0	0	0	0	0	0
PG	49.96	0.9575	49.46	1.0000	0.50	0.1840
W	0	0	0	0	0	0
A	0	0	0	0	0	0
Total	52.17	1	49.46	1	2.71	1

Material balance for the overall unit

All material flows into and out of the process flowsheet are considered for the overall material balance according to relation (20):

$$D_{m,F3} + D_{m,F7} = D_{m,34} + D_{m,F30} + D_{m,F33} + D_{m,F24} + D_{m,F27} \quad (20)$$

Table 9

Overall material balance for the proposed process.

Species flow rate	Inlet		Outlet				
	F3	F7	F34	F30	F33	F24	F27
$D_{m,G}$ (kg/h)	0	5100	0	0	0	0	204.00
$D_{m,H}$ (kg/h)	663	0	563.29	0	0	0	0
$D_{m,PG}$ (kg/h)	0	38.01	0	0.40	0	3763.43	38.01
$D_{m,W}$ (kg/h)	0	0	0	9.58	948.16	0	0
$D_{m,A}$ (kg/h)	0	0	0	271.40	2.74	0	0
Total (kg/h)	5801.01		5801.01				

Heat balance

Heat balances were carried out for the heating or cooling stages of the material streams, for the purpose of determining the flow rate of the used cold and hot utilities.

Table 10

Results for the heat balance.

Equipment	Utility type	Thermal agent flow rates, kg/s
S-1	Steam	0.357
S-3	Cold water	0.137
Reboiler D-1 column	Steam	0.89
Reboiler D-2 column	Steam	3.26
Reboiler D-3 column	Steam	0.82
Condenser D-1 column	Cold water	10.55
Condenser D-2 column	Cold water	45.91
Condenser D-2 column	Cold water	13.72

Economic evaluation

The total annual cost was found by summing the annual cost of raw materials, the annual cost of utilities, and the annual operating cost (which includes employee salaries and statutory payments). The annual cost of depreciation is also added to this amount.

The initial investment capital was spread over the lifetime of the plant through a depreciation schedule. A depreciation period of 10 years was considered for the plant.

The cost of equipment accounts for the largest share of direct costs. The following are relationships that can be used to estimate the costs of major equipment.

Pressure vessels, columns, and reactors:

$$\text{Cost of purchase}(\$) = \frac{M\&S}{280} \cdot (957.9 \cdot D^{1.066} \cdot H^{0.82} \cdot F_c) \quad (21)$$

Where, D is the diameter, H is the height, factor $F_c = F_m - F_p$, where F_m is a material characteristic constant and F_p is a pressure-dependent factor [9], calculated using equation (21)

$$F_p = 1 + 0.0074 \cdot \left(\frac{P}{[bar]} - 3.48 \right) + 0.00023 \cdot \left(\frac{P}{[bar]} - 3.48 \right)^2 \quad (22)$$

Heat exchangers (with shell and tubes)

$$\text{Cost of purchase}(\$) = \frac{M\&S}{280} \cdot (474.7 \cdot A^{0.65} \cdot F_c) \quad (23)$$

Where, A is the heat transfer area in m² and 20<A<500 m² for each sleeve. F_c=F_m-(F_d+F_p), where F_m, F_d, F_p are correction factors for material, construction type and operating pressure [9].

Compressor

$$\text{Cost of purchase}(\$) = \frac{M\&S}{280} \cdot (664.1 \cdot P^{0.82} \cdot F_c) \quad (24)$$

Where: P is the braking power in kW, with 25<P<750 kW; F_c is a correction factor depending on the type of compressor [9].

In the following, simulation results related to operating costs, raw material costs, utility costs, equipment costs, benefits obtained from the marketing of the obtained products and profit will be presented.

Table 11

Costs determined from the simulation of the economic analysis.

Initial investment capital, \$	11.1·10 ⁶	Payback period, years	10
Total annual cost, \$	41.9·10 ⁶	Annual depreciation cost, \$	1.11·10 ⁶
Annual cost of raw materials, \$	22.0·10 ⁶	Profit on sale of products, \$	49.1·10 ⁶
Annual cost of utilities, \$	1.12·10 ⁶	Annual profit, \$	7.20·10 ⁶

Table 12

Cost of utilities.

	Quantity	Unit of measure	Cost per hour, \$/h	Cost per year \$/year
Steam 40 bar	34·10 ⁶	kJ/h	27.43	2.20·10 ⁵
Cold water	32·10 ⁶	kJ/h	84.92	7.41·10 ⁵
Electricity	353.95	kW	6.75	5.93·10 ⁴

Table 13

Cost and prices of raw materials and products involved in the process.

	Mass flow, kg/h	Mass flow, kg/year	Price, \$/kg	Annual price, \$/kg
Freshly fueled hydrogen	99.7	$7.98 \cdot 10^5$	3	$2.39 \cdot 10^6$
Freshly fed glycerol	4896	$39.2 \cdot 10^6$	0.5	$19.6 \cdot 10^6$
Total cost of raw materials				$22 \cdot 10^6$
Acetol	281.4	$2.25 \cdot 10^6$	1.2	$2.70 \cdot 10^6$
Propylene glycol	3764	$30 \cdot 10^6$	1.4	$42.2 \cdot 10^6$
Total profit from sale of products				$45 \cdot 10^6$

Table 14

Cost of major equipment.

Compressor C-1	$3.11 \cdot 10^6$	D-3 column condenser	$1.16 \cdot 10^5$
Pump P-1	$1.60 \cdot 10^5$	D-1 column cooler	$1.26 \cdot 10^5$
Reactor R-1	$3.49 \cdot 10^5$	Column D-2 cooler	$1.77 \cdot 10^5$
Separator FV-1	$1.64 \cdot 10^5$	Column D-3 cooler	$1.15 \cdot 10^5$
Separator FV-2	$1.42 \cdot 10^5$	Column D-1 reflux vessel	$1.44 \cdot 10^5$
Distillation column D-1	$4.82 \cdot 10^5$	Column D-2 reflux vessel	$1.16 \cdot 10^5$
Distillation column D-2	$4.75 \cdot 10^5$	Column reflux vessel D-3	$1.15 \cdot 10^5$
Distillation column D-3	$6.18 \cdot 10^5$	Column reflux pump D-1	$3.88 \cdot 10^4$
Condenser of column D-1	$8.99 \cdot 10^4$	Column reflux pump D-2	$4.25 \cdot 10^4$
Condenser of column D-2	$1.23 \cdot 10^5$	Column reflux pump D-3	$4.29 \cdot 10^4$

The specific consumptions characteristic of the hydrogenolysis plant are illustrated in table 15.

The price per kilogram of propylene glycol produced was calculated by relating the annual operating cost of the plant to its productivity. For one tons of propylene glycol of 99.5% purity, a company producing chemicals for cosmetic and pharmaceutical applications in China charges \$1800 [10]. Given the high purity of propylene glycol from the glycerol hydrogenolysis plant and the competitive market price of the product, estimated at 1400 \$/t, the proposed process is feasible.

Table 15

Specific consumption of utilities and raw materials.

	Quantity	Unit of measurement	Quantity of product, kg	Specific consumption	Unit of measurement
Freshly fed hydrogen	99.7	kg	3764	0.026	kg/kg
Freshly fed glycerol	4896	kg		1.301	kg/kg
Steam 40 bar	$2.1 \cdot 10^4$	kg		5.568	kg/kg
Cold water	$2.79 \cdot 10^5$	kg		74.165	kg/kg
Electricity	354.95	kW		0.094	kW/kg

Economic optimization

The separation section of the proposed process was optimized using total annual cost (TAC) minimization as the objective function. 6 decision variables influencing TAC were identified, namely the total number of distillation stages and the position of the feed stage for each distillation column in the separation section: D-1, D-2, and D-3. The investment cost included the column shell, trays, and heat exchangers (condenser and reboiler), calculated as previously described in the economic evaluation section. The operating cost comprised only the (hot and cold) utility expenses for the thermal agents used in the heat exchangers.

To enable the evaluation of the large number of simulations (*i.e.*, total and feed stage configurations) required for cost minimization, the process flowsheet was connected to and controlled by MATLAB using the component object model interface. Using this approach, the values of the decision variables were first sent to Aspen Plus and written to the appropriate fields, including tray sizing and column hydraulics utilities; then, the simulation was run to solve the mass and heat balance equations; finally, equipment size, together with pressure, temperature, and utility flowrates were read from the simulation using MATLAB code, and combined into a corresponding TAC value.

The optimization was performed using the genetic algorithm implemented by the *ga* function in MATLAB. A total of 9141 configurations were evaluated, resulting in optimal values for the objective functions listed in Compared with the base case, the total annual cost of the separation section was reduced from \$1.08 million to about \$0.55 million.

Table 15

Optimal values for the decision variables minimizing the total annual cost of the separation section.

Distillation column	D-1	D-2	D-3
Feed stage	4	16	3
Total number of stages	8	19	4

6. Conclusions

Propylene glycol is a compound with numerous industrial applications, and low toxicity and environmental hazard. The development of a technological process to produce propylene glycol (which uses a by-product considered as technical waste as a raw material) is a step towards a more sustainable future based on sustainability and green principles.

In this work a propylene glycol synthesis plant from glycerol with a production capacity of 30,000 t/year was designed from the technological point of view.

The hydrogenolysis reaction proceeds in two steps: dehydration of glycerol to acetol (hydroxy acetone) and hydrogenation of acetol to propylene glycol. In order to obtain important values of glycerol conversion and selectivity to propylene glycol, a Cu/ZnO/Al₂O₃ catalyst and a hydrogen-to-glycerol molar ratio of 5:1 was used. The chemical transformation takes place in a fixed-bed three-phase reactor. Based on a kinetic model proposed by Zhou et al [6], the glycerol analysis was carried out both at the catalyst particle and catalyst bed scales. The results showed an important influence of internal diffusion. Considering the influence of internal diffusion along the catalyst bed, a reactor diameter of 1.73 m and a catalyst bed length of 5 m were determined. Rigorous simulations of the chemical transformation, both at the catalyst and reactor scales, resulted in a high glycerol conversion of 96%, and a significant yield in propylene glycol of 96%.

Following the economic analysis, carried out after the mass and heat balances of the main equipment in the proposed process scheme, performed with the Aspen Plus v10 process simulator, an initial investment cost for such a plant was estimated at \$11 million and an annual operating cost of \$42 million. Comparing the estimated price for propylene glycol of 1.4 \$/kg with the market recovery price of 1.8 \$/kg showed the economic feasibility of the proposed process flowsheet.

Therefore, due to the competitive market price of propylene glycol resulting from the economic analysis and the benefits of using a technology based on renewable raw materials, the development and implementation of a glycerol hydrogenolysis plant to obtain propylene glycol is feasible.

REFERENCES

- [1] Chozhavendhan S., Karthiga Devi G., Jayamuthunagai J., Bharathiraja B., *Horizons in Bioprocess Engineering*; R. Pogaku (editor), *Conversion of glycerol to valuable products*, Springer International Publishing, 157–169, 2019.
- [2] Attarbach T., Kingsley M.D., Spallina V., New trends on crude glycerol purification: A review, *Fuel*, 340, (2023), 1-19.
- [3] Okolie J.A., *Review. Insights on production mechanism and industrial applications of renewable propylene glycol*, iScience, 1-19, 2022
- [4] *Global Propylene Glycol Market – Industry Trends and Forecast to 2029*. <https://www.databridgemarketresearch.com/reports/global-propylene-glycol-market> (accessed 13 July 2023).
- [5] Nanda M.R., Yuan Z., Qin W., Xu C., Recent advancements in catalytic conversion of glycerol into propylene glycol: A review, *Catalysis Reviews - Science and Engineering*, 58 3, (2016), 309–336.
- [6] Li Z.X., Zeng T., Hong W., Cheng Z., Yuan W., Kinetics of hydrogenolysis of glycerol to propylene glycol over Cu-ZnO-Al₂O₃ catalysts, *Chinese Journal of Chemical Engineering*, 18, 3, (2010), 384–390.
- [7] Reid R.C., Prausnitz J.M., Poling B. E., *The properties of gases and liquids*, McGraw-Hill, 1987.
- [8] Korsten H., Hofmann U., Three-Phase Reactor Model for Hydrotreating in Pilot Trickle-Bed Reactors, *AIChE Journal*, 42, 5, (1996), 1350-1360.
- [9] Dimian A.C., Bildea C.S., Kiss A.A., *Integrated Design and Simulation Of Chemical Processes*, Elsevier, 2003.
- [10] 99.5 % Propylene Glycol. https://www.alibaba.com/product-detail/99-5-Propylene-Glycol-usp-Bulk_1600264323034.html?spm=a2700.7724857.0.0.5b583edaMI431A (accessed June 30, 2023).

MODELING OF VOLATILE ORGANIC COMPOUNDS FLOW RATE PRODUCED IN PAINTING INSTALLATIONS FROM AUTOMOTIVE INDUSTRY

Ionuț A. POPA¹, Oana C. PÂRVULESCU¹, Petre CHIPURICI¹,
Tănase DOBRE^{1,2,*}

¹National University of Science and Technology
Politehnica Bucharest, 1-7 Gheorghe Polizu St., 011061
Bucharest, ROMANIA

²Technical Sciences Academy of Romania, 26 Dacia Blvd.,
030167 Bucharest, Romania

Abstract

A mathematical modeling of the flow rate evolution of volatile organic compounds obtained from tunnel drying of a freshly painted surface.

Key words: bacterial volatile organic compounds, coating in the automotive industry, paints in the automotive industry, mathematical modelling

1. Introduction

Painting techniques in the automotive industry have evolved a lot in the last century due to the rapid evolution of technology. If at first the painting is done manually by brushing the surface of the vehicle, polishing and sanding, and its duration was a few weeks, from the desire to reduce the production time of a car, solutions were sought that would offer faster drying and hardening, thus resulting in enamels. However, due to limited raw materials, it gave way to synthetic chemicals [1]. Thus, the application of multiple layers of primer was introduced, which was later replaced by dip coatings, a more automated process, but dangerous due to the solvent emission of solvent-based paints. Then was proposed anodic deposition coatings, based largely on maleinated polybutadiene resins, which were quickly replaced by cathodic ones due to the better corrosion protection of their modified epoxy resin scaffolds and polyurethane-based reactive crosslinkers [1].

Today, most clearcoats in Europe are based on a two-component (2K-) formulation consisting of an acrylic resin with OH functions and a reactive polyurethane crosslinker. The rest of the world still prefers single-component

¹ Corresponding author: tghdobre@gmail.com

technology based on acrylic resins and melamine crosslinkers [2]. Even though the cost of the basecoat/clearcoat paint process was prohibitive for less expensive automobile lines, it was used on more expensive, high-end automobiles. The environment in vehicle painting factories is contaminated by volatile organic compounds released after the application and drying of the paint on the vehicle surface [1]. The specialized literature presents experimental results and states that the following volatile organic compounds are most often released by using car paints: m/p-xylene, toluene, ethylbenzene and o-xylene [3]. Apart from these, other species of volatile organic compounds are also found in much smaller quantities such as: Butylacetate, Methylchloride, Acrylonitrile, 1-Butene, Octane, n-Propylbenzene, m-Ethyltoluene, p-Ethyltoluene, 1,3,5-Trimethylbenzene, o-Ethyltoluene, 1,2,3-Trimethylbenzene, 1,2,4-Trimethylbenzene [4]. However, the variety of aromatic species represents 96.9% of paint emissions from car factories [3]. The interest in the present work is to determine the flow rate of organic volatile compounds (VOC) produced by a dyeing installation with continuous operation. A car paint has in its composition a pigment, a binder, a film agent, a filler, additives, a special pigment and as a VOC precursor, a lot of solvent. During the drying phase of the waxed part, the vaporization of the solvent as VOC in the warm circulated air circulated through the drying tunnel causes it to become charged with VOC.

2. Modeling

The physical model considered is that of a metal piece with a surface S thickness δ that is covered with a film of thickness δ_{fo} that enters the tunnel at a constant speed, w . Here occurs the piece heating and solvent vaporization from the paint in the air stream, that flows counter currently with the piece movement, so that at the exit from the tunnel there is no more solvent in the paint film. A simultaneous process of mass and heat takes place in the tunnel.

With figure 1 we introduce the description of phenomenology associated with drying of paint deposited on piece of known surface. It insists to shows that here we have simultaneous heat and mass transfer. The right part of figure gives the temperature and COV concentration profiles near to paint surface when the piece is in current position x in the tunnel.

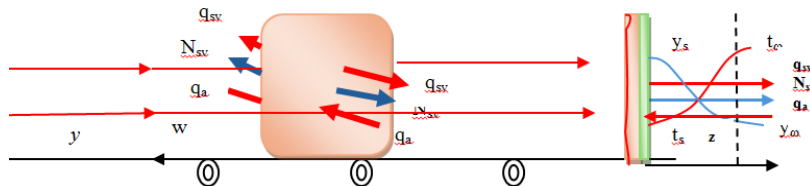


Fig. 1. Phenomenology of paint drying in a hot air tunnel

Considering this figure, the current specific flow rate of vaporized VOC is written as it is shown in relation (1). The vapor specific flow takes with it the heat

specific flow q_{sv} , expressed here by relation (2). The plate heating is characterized by air transfer flux (specific flow rate) to the piece, where paint is in drying (3).

$$N_{sv} = k_y (y_s - y_\infty) \quad (1)$$

$$q_{sv} = h^{vs} N_{sv} \quad (2)$$

$$q_a = \alpha_g (t_\infty - t) \quad (3)$$

The transfer analogy [7, 8] can be considered for mass transfer coefficient k_y and the heat transfer coefficient from the air to the piece α_g . So that k_y is expressed by relating it to the heat transfer coefficient (4).

$$k_y = \frac{k_g}{C} = \frac{\alpha_g}{C \rho_g c_{pg}} \quad (4)$$

A relationship from the literature [5, 6] was thus chosen, here specified in the form (5), where the coefficients a , m and l_c have the specifications in table 1.

$$\alpha_g = a \left(\frac{t_a - t}{l_c} \right)^m \quad (5)$$

Table 1

Values for parameters of relation (5)

Crt. no.	Parameter	Vertical surface	Horizontal upper surface	Horizontal lower surface
1	a	1.420	1.320	1.520
2	m	0.250	0.250	0.330
3	l_c	0.112	0.055	0.055

The molar fraction of VOC on the surface of the paint, y_s , is expressed as a function of the molar fraction of the solvent in the paint, x , and the temperature of piece, t , according Raoult's law and vapor pressure dependence upon t through the Antoine relation. That is shown by relation (6), where $\gamma(x)$ is the solvent activity

coefficient in the paint. It is recognized in (6) that A, B, C represent Antoine constants for vapor pressure of solvent from paint composition:

$$y_s = \frac{\gamma(x)x P_{sVOC}}{p} = \frac{\gamma(x)x}{p} 10^{\left(A - \frac{B}{t+C}\right)} \quad (6)$$

A mathematical model of tunnel paint drying describes how the solvent concentration (molar fraction) in the paint decreases along the tunnel, respectively how this concentration increases in the drying air. The following focuses on these problems. For a time interval $d\tau$, when the surface S advances from $x - dx$ to x the paint layer solvent loss is related to the vaporization flux through the relation (7). Considering that molar fraction of solvent in paint and paint film thickness evolve in time (7) goes into (8).

$$-\frac{d\left(\frac{S\rho_{pt} \delta x}{M_{pt}}\right)}{d\tau} = SN_{sv}(x, t, y_{\infty}) \quad (7)$$

$$y_s = \frac{\gamma(x)x P_{sVOC}}{p} = \frac{\gamma(x)x}{p} 10^{\left(A - \frac{B}{t+C}\right)} \quad (8)$$

The relationship between δ and x can be accepted to be linear (9) as it is shown below, where δ_f is the thickness of dry paint and k is a proportionality constant. With this consideration the relation (8) becomes to (10), respectively (11) if it replaces $d\tau$ with dy/w .

$$\delta = \delta_f(1 + kx) \quad (9)$$

$$\frac{dx}{d\tau} = -\frac{M_{pt}}{\rho_{pt}} \frac{N_{sv}(x, t, y_{\infty})}{\delta_f(1 + (1+k)x)} \quad (10)$$

$$\frac{dx}{dy} = -\frac{M_{pt}}{w\rho_{pt}} \frac{N_{sv}(x, t, y_{\infty})}{\delta_f(1 + (1+k)x)} \quad (11)$$

To establish the model equation that shows how the temperature of the part evolves along the drying tunnel, it is assumed to have a high thermal conductivity, so that the heat received spreads quickly throughout its mass. With this consideration, the thermal balance in time from τ to $\tau + d\tau$ take the expression from relation (12).

$$-\frac{d\left(m_p^c p^t\right)}{d\tau} = S(q_a(t, t_\infty) - q_{sv}(x, t, y_\infty)) \quad (12)$$

The processing of relation (12) goes to final expression (13) respectively (14) for piece temperature state.

$$-\frac{d\left(m_p^c p^t\right)}{d\tau} = S(q_a(t, t_\infty) - q_{sv}(x, t, y_\infty)) \quad (13)$$

$$-\frac{d t}{d y} = \frac{1}{\delta_p \rho_p^c p^w} (q_a(t, t_\infty) - q_{sv}(x, t, y_\infty)) \quad (14)$$

To complete the model, it is also necessary to determine how the air temperature and VOC concentrations change along the tunnel. If H is the drying piece characteristic length, then when it moves from y to $y + dy$, it takes heat and discharges solvent vapors. The balance for the air loading with caps thus has the expression from the relation (15):

$$\frac{d y_\infty}{d y} = \frac{H M_g}{G_{vg} \rho_g} N_{sv}(x, t, y_\infty) \quad (15)$$

The balance for the air heat loss, when the painted piece moves from y to $y + dy$, leads to the differential equation (16), which completes the paint tunnel drying mathematical model. So, the drying paint model for a mobile piece in a tunnel where hot air is in a countercurrent contains the differential equations (11), (14), (15) and respectively (16) together with consistent expressions N_{sv} , q_a , q_{sv} and initial conditions that show the state of model differential equations variables at one of the ends of the tunnel. These conditions are written here for hot air entering the tunnel. Here air does not contain VOCs, the piece is almost dry, and it have a temperature close to that of hot air (17):

$$-\frac{d t_{\infty}}{dy} = \frac{HM}{G_{vg} \rho_g c_{pg}} (q_a - q_{sv}) \quad (16)$$

$$y = y_t, x = 0.001, t_{\infty} = t_{ain}, y_{\infty} = 0, t = t_{\infty} - 0.5 \quad (17)$$

The case in which the numerical integration is done from the piece entrance into tunnel has the main condition that here the paint of piece has the solvent molar fraction corresponding to paint application layer. Also, here the entrance piece temperature is that of the paint application environment. This is the case that was used in the simulations performed to prove the model functioning and its ability to analyze the investigated process.

3. Results and discussions

As is customary [9] in the case of process analysis through simulation, all quantities involved in the model must be specified by numerical values or by expressions depending on the state model variables. Table 2 shows the quantities with fixed values respectively those that were varied (process factors). Those effects are found in the simulations given with figure 2 and figure 3.

Table 2

Values of quantities involved in drying model of paint from a piece moving in a tunnel.

	Considered quantities/ symbol	Value	SI units
1	Air flow rate in drying tunnel, G_{vg}	0.01, 0.015, 0.02	m ³ /s
2	Flow area of tunnel, A	1	m ²
3	Air density, ρ_g	1.29	kg/m ³
4	Air specific heat, c_{pg}	1000	J/(kg grd)
5	Piece characteristic length, H	1	m
6	Piece specific heat, c_p	450	J/(kg grd)
7	Piece thickness, δ_p	0.001	m
8	Dried paint thickness, δf	0.0001	m
9	Piece material density, ρ_p	7500	kg/m ³
10	Mean molecular mass of paint, M_p	90	kg/kmol
11	Air pressure in tunnel, p	1	atm
12	Velocity of piece in tunnel, w	0.035, 0.04, 0.045	m/s
13	Solvent Antoine constants, A, B, C	6.9546, 1170.9, 226.23	-, grd, grd
14	Imposed solvent in air exit, $y_{\infty ex}$	0.045	Kmol _s /kmol _{am}
15	Molar fraction in paint at input, x_{in}	0.35	Kmol _s /kmol _{pt}
16	Air molecular mass, M_g	28	kg/kmol

Figure 2 shows the effect of movement piece velocity in the tunnel on the state along of tunnel of solvent concentration of in the paint, on solvent concentration in the air respectively on the piece and air temperature. Figure 3 differs from Figure 2 in that here the effect of the air flow rate in the tunnel on the state of the same variables is analyzed.

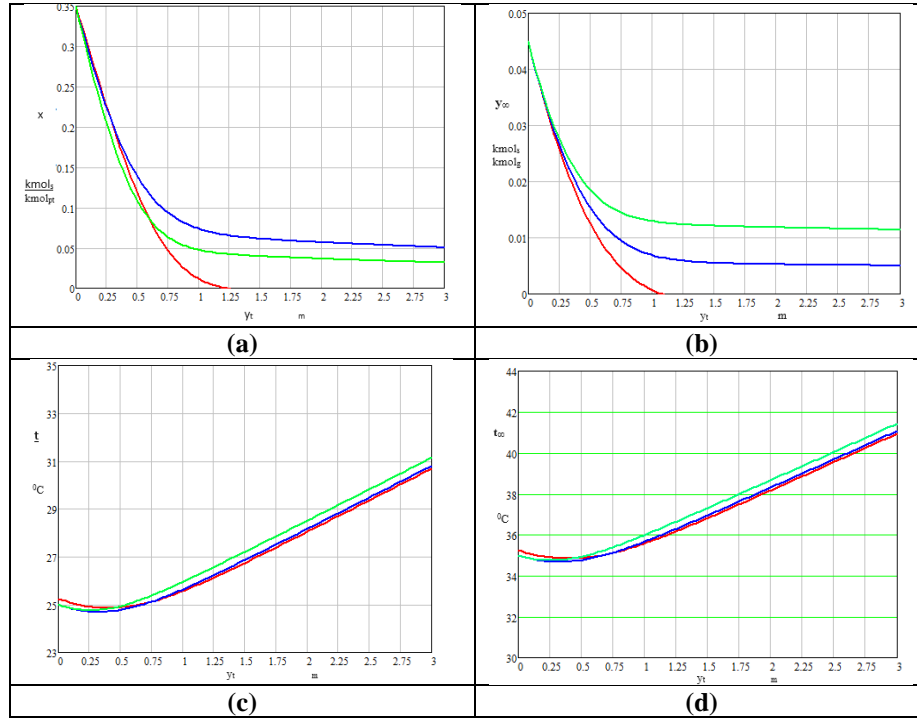


Fig. 2. State of x , y_∞ , t and respectively t_∞ along of tunnel length for various piece movement velocity (red - 0.045 m/s, blue - 0.04 m/s, green - 0.035 m/s, $G_{vg} = 0.015$ m³/s)

The first thing that needs to be said is that we give here simulations that require that the air coming out has a molar fraction of solvent vapors of 0.045 kmol_s/kmol_g when painted piece entering in tunnel. The reason for this consideration would be that it is desired to start the solvent vaporization from paint with an acceptable specific flow rate, not how high it could be. In these conditions, we find that the influence of the piece movement speed through the tunnel has an interesting influence on the paint drying. Appears that the drying becomes good when the piece movement speed is around 0.045 m/s and the air flow rate through the tunnel is 0.015 m³/s. It is interesting that at lower piece movement speed the air entering in the tunnel must have more or less vaporized solvent with a temperature around of 41 °C (figure 2, t_∞ vs. y_t).

Figures 2 and 3 show that in this simultaneous mass and heat transfer problem, the mass transfer intensity is strong along the tunnel length of up to 1.5 m, while the heat transfer is active along the entire length of the tunnel.

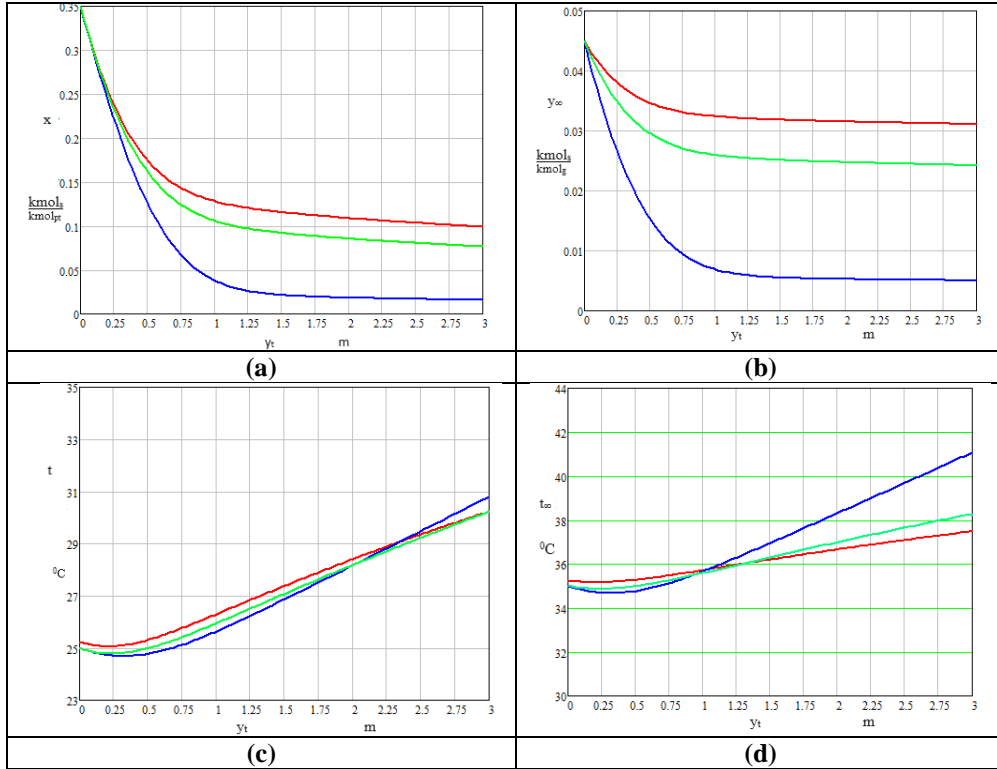


Fig. 2. State of x , y_{∞} , t and respectively t_{∞} along of tunnel length for various air flow rate in the tunnel (red - 0.035 m³/s, green - 0.025 m³/s, blue - 0.015 m³/s, $w = 0.04$ m/s)

Considering what was specified, namely that the air leaving the tunnel should have a VOC content with a molar fraction of 0.45, it can be seen, from figure 3 that the air introduced must contain more and more VOCs as the air flow rate through the tunnel grow. This causes the solvent vaporization driving force to be quickly brought to zero. The one shown in figure 3 for the dependencies x vs. y_t and y_{∞} vs. y_t is thus explained. The temperature t and the temperature t_{∞} evolve along the tunnel in a manner like what was shown in relation to figure 2. The results obtained through the given simulations are in agreement with those reported in similar works [10].

6. Conclusions

The problem of the simultaneous mass and heat transfer that occurs during the paint drying of a car piece in a countercurrent circulation drying tunnel was

analyzed. The developed mathematical model contains four ordinary differential equations near to data, expressions and initial conditions requested by model detailing. Considering that is imposed to have VOC content in the gas exiting from tunnel at the level of 0.045 molar fraction was simulated the influence of car piece movement velocity and of air flow rate through the tunnel on the state along the tunnel of VOC molar fraction in paint, of VOC molar fraction in gas, on car piece temperature and on gas temperature.

REFERENCES

- [1] Streitberger H.J., Dossel K.F., *Automotive Paints and Coatings - Introduction*, WILEY-VCH Verlag GmbH & Co. KGaA, Weinheim, 2008,
- [2] Akafuah N.K., Poozesh S., Salaimah A., Patrick G., Lawler K., Saito K, *Evolution of the Automotive Body Coating Process*, MDPI, 6, 24, (2016).
- [3] Yuan B., Shao M., Lu S., Wang B., Source profiles of volatile organic compounds associated with solvent use in Beijing, China, *Atmospheric Environment*, 44, 5, (2010), 1919-1926.
- [4] Song M.Y., Chun H., Species and characteristics of volatile organic compounds emitted from an auto-repair painting workshop, *Scientific Reports*, 11, 16586, (2021).
- [5] Bird B. R., Stewart E. W., Lightfoot N. E., *Transport Phenomena, Chapter 14, Paragraph 14.6*, 442-443, Second Edition, John Wiley & Sons, Inc., 2002.
- [6] Leca A., Pop M.G., Prisecaru I., Neaga C., Zidaru Gh., Musatescu V., Isbasoiu E.C., *Calculation guide. Tables, nomograms and thermotechnical formulas*, vol. II, 71, Technical Publishing House, Bucharest, 1987.
- [7] Floarea O., Dima R., *Mass Transfer and Specific Equipment, Chapter: Transfer Phenomena Analogy*, Didactic and Pedagogic House, Bucharest, 1984.
- [8] Welty J., *Fundamentals of momentum heat and mass transfer*, John Wiley & Sons Inc, 2021.
- [9] Dobre T., Sanchez J. M., *Chemical Engineering Modelling Simulation and Similitude*, Wiley VCH, 2007.
- [10] Oueslati H., Mabrouk B S., Mami A., Dynamic Modelling and Performance Optimization-Based Sliding Mode Control of Process Drying in a Convective Tunnel Dryer, *International Journal of System Dynamics Applications*, 10, 4, (2011), 1-11.

THE INFLUENCE OF MASS TRANSPORT ON THE ELECTROCRYSTALLISATION PROCESS

Valeria DANILOVA¹, Liliana LAZAR^{1*}, Florin BANDRABUR¹, Ioan MĂMĂLIĞĂ¹

¹Gheorghe Asachi Technical University of Iasi,
Cristofor Simionescu Chemical Engineering and Environmental
Protection Faculty, Iasi, ROMANIA

Abstract

Electrocrystallisation is an essential elemental process used for deposition of metals from aqueous electrolytes. In an electrolyte solution, ion-solvent interactions and ion-ion interactions can take place, the predominant ones being of the ion-ion type. The mass transport of ions through the electrolyte can limit the rate of the electrode process based on reduction of metal ions. The speed of this elementary process depends on the value of current density and becomes significant if the electrolyte is operated at relatively high current densities. The higher the electrode polarizations for the elementary electrocrystallization process, the better the quality of the cathodic deposits can be.

Key words: cooper, electrode overpotential, electrolytes electroplating.

1. Introduction

The transport of ions takes place by their displacement as a result of migration processes, when there is a potential gradient between two points of the electrolyte that causes the displacement of ions in the electric field. Along with migration processes, diffusion processes can occur when there is a concentration gradient, and convection processes can occur when there is a temperature gradient [1, 2]. For electrolytes used in the electrochemical deposition of metals (electroplating technology), the total electrode overpotential is the sum of the mass transport overpotentials, the activation overpotential generated by charge transfer, the reaction overpotential specific to possible slow chemical reactions, and the crystallization overpotential (the formation and growth of solid-phase nuclei from the cathodic deposit) [3, 4].

Mass transport can limit the speed of electrode processes, its rate depends on the current density value of the electrolyte. In the case of slow electrochemical reactions that take place at low and very low current densities, the concentration difference between the bulk of the electrolyte and the immediate vicinity of the electrode-electrolyte interface is small, resulting in mass transport not being the determining factor for reaction rate. Fast electrochemical reactions, carried out at

* Corresponding author: lillazar@ch.tuiasi.ro, lillazar@yahoo.com

high current densities, can be limited by the rate of mass transport to the electrode [1, 3, 5].

The electrode overpotential corresponding to mass transport, expressed through the limiting current density [1, 3], can be calculated using the following formula:

$$\eta_d = -\frac{R \cdot T}{z_i \cdot F} \cdot \ln \left(1 - \frac{i}{i_d} \right), [\text{V}] \quad (1)$$

Quality electroplated deposits consist of numerous fine crystals that provide the resulting layer with adhesion, minimal porosity, hardness, and as uniform a thickness as possible. In this case, the rate of formation of solid-phase nucleating center is much higher than their growth rate. In principle, the higher the electrode polarizations from a particular electrolyte, the better the quality of the cathodic deposits can be [3, 6].

2. Modeling

Ionic flow in electrolyte solutions

In the case of ionic transport due to diffusive field, the velocity equation for the unidirectional movement of a species j has the form:

$$v_{j,x} = k_j \cdot \frac{d\mu_j}{dx} \quad (2)$$

Also considering the convective component of the solution velocity on the x (v_x) direction, relation (2) becomes:

$$v_{j,x} = -k_j \cdot \frac{d\mu_j}{dx} + v_x \quad (3)$$

In an electrochemical reactor, the chemical potential (μ_j) depends on the activity of species j (a_j) according to the expression:

$$\mu_j = \mu_{j,0} + RT \cdot \ln(a_j) \quad (4)$$

respectively, on the electric state of the system, for which the dependence potential is:

$$\left(\frac{\partial \mu_j}{\partial \phi_s} \right)_{C_j} = z_j F \quad (5)$$

Equation (5) shows that for a solution of constant concentration, the chemical potential variation registered in diffusive transport is also associated with an electric transport. Therefore, the variation in chemical potential is given by the function $\mu_j = f(C_j, \phi_s)$, whose derivative is:

$$\frac{d\mu_j}{dx} = \left(\frac{\partial \mu_j}{\partial C_j} \right)_{\phi_s} \cdot \frac{dC_j}{dx} + \left(\frac{\partial \mu_j}{\partial \phi_s} \right)_{C_j} \cdot \frac{d\phi_s}{dx} \quad (6)$$

The first partial derivative can be obtained by differentiating the equation of chemical potential with the assumption that the activity of the species j (a_j) is equal to molar concentration (C_j):

$$\left(\frac{\partial \mu_j}{\partial C_j} \right) = \frac{\partial}{\partial C_j} [\mu_j^0 - RT \cdot \ln(C_j)] = \frac{RT}{C_j} \quad (7)$$

Replacing the equations (5) and (7) to equation (6) we obtain:

$$\frac{d\mu_j}{dx} = \frac{RT}{C_j} \cdot \frac{dC_j}{dx} + z_j F \cdot \frac{d\phi_s}{dx} \quad (8)$$

From (3) and (8) results that the rate of ion movement j on x direction:

$$v_{j,x} = -k_j \cdot \frac{RT}{C_j} \cdot \frac{dC_j}{dx} - k_j \cdot z_j F \cdot \frac{d\phi_s}{dx} + v_x \quad (9)$$

The number of moles of component j that passes through the normal surface unit in the x -direction, in the time unit represents its transported flow ($N_{j,x}$), for which the calculation relationship is:

$$N_{j,x} = v_{j,x} C_j = -k_j \cdot RT \cdot \frac{dC_j}{dx} - k_j \cdot C_j \cdot z_j F \cdot \frac{d\phi_s}{dx} + C_j \cdot v_x \quad (10)$$

Relation (10) is the base for calculating the ion transport in steady state regime.

Replacing the term $k_j \cdot RT$ from equation (10) with the diffusion coefficient D_j ,

we obtained:

$$N_{j,x} = -D_j \cdot \frac{dC_j}{dx} - \frac{D_j \cdot C_j \cdot z_j F}{RT} \cdot \frac{d\phi_s}{dx} + C_j \cdot v_x \quad (11)$$

The three terms of equation (10) represent the ionic flows of diffusion, migration, and convection. Maintaining the electroneutrality of the solution requires verifying the relationship:

$$\sum(z_j \cdot C_j) = 0 \quad (12)$$

Even if equations (11) and (12) have a general character, they are not sufficient for the complete description of ion behaviour in an electrochemical reactor, because the concentration of ions changes through the reactions that take place and these transformations must be evaluated quantitatively through mass balance [3, 8]. The variation of convection velocity with position and time can only be evaluated by applying the fluid dynamics equations. Finally, the flux at the electrode interface can be expressed by means of the current density.

We consider the case of an aqueous electrolyte solution with concentration C . Between the concentration of the electrolyte and that of its ions there is the relationship:

$$C = \frac{C_+}{n_+} = \frac{C_-}{n_-} \quad (13)$$

and the electroneutrality will be equal to:

$$z_+ C_+ + z_- C_- = 0 \quad (14)$$

In the absence of convection ($v_x = 0$), the flux equations for the salt ions can be written for a one-dimensional process in the form:

$$N_+ = -D_+ \cdot \frac{dC_+}{dx} - \frac{D_+ \cdot C_+ \cdot z_+ F}{RT} \cdot \frac{d\phi_s}{dx} \quad (15)$$

$$N_- = -D_- \cdot \frac{dC_-}{dx} - \frac{D_- \cdot C_- \cdot z_- F}{RT} \cdot \frac{d\phi_s}{dx} \quad (16)$$

Substituting the ion concentration from equations (14) and (15) using equation (12) and ordering the terms, results:

$$\frac{N_+}{n_+} = -D_+ \cdot \frac{dC}{dx} - \frac{D_+ \cdot C \cdot z_+ F}{RT} \cdot \frac{d\phi_s}{dx} \quad (17)$$

$$\frac{N_-}{n_-} = -D_- \cdot \frac{dC}{dx} - \frac{D_- \cdot C \cdot z_- F}{RT} \cdot \frac{d\phi_s}{dx} \quad (18)$$

The terms on the left-hand side of equations (17) and (18) represent the ionic fluxes, which are equal. Thus, by equating the two equations, we obtain:

$$(D_+ - D_-) \cdot \frac{dC}{dx} = \frac{C \cdot F}{RT} \cdot \frac{d\phi_s}{dx} (D_- \cdot z_- - D_+ \cdot z_+) \quad (19)$$

The gradient of the potential can be eliminated between equations (15) and (16) and equation (19), obtaining:

$$N = \left(\frac{N_+}{n_+} = \frac{N_-}{n_-} \right) = - \frac{D_+ \cdot D_- (z_+ - z_-)}{D_+ \cdot z_+ - D_- \cdot z_-} \cdot \frac{dC}{dx} \quad (20)$$

Comparing equation (20) with the electrolyte flow expressed as a function on the experimental diffusion coefficient, D_{exp} :

$$N = -D_{exp} \frac{dC}{dx} \quad (21)$$

it can be observed that, in the case of ionic transport, the diffusion coefficient is given by the expression:

$$D_{exp} = \frac{D_+ \cdot D_- (z_+ - z_-)}{D_+ \cdot z_+ - D_- \cdot z_-} \quad (22)$$

Ion transport in a binary electrolyte solution

We will consider the mono-directional ionic transport in the case of a solution containing a binary electrolyte, in which case the functional schematic principle is presented in figure 1. In this electrochemical reactor, the cations are discharge at the cathode located at distance $x = 0$, and the anions are discharge only at the anode located at the $x = d$.

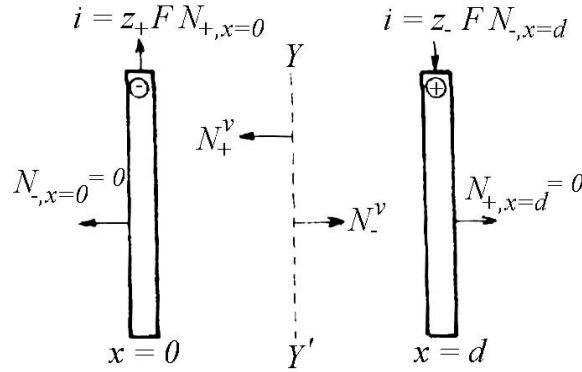


Fig. 1 Mono-directional ionic transport in a binary electrolyte [1, 3].

In the absence of convection ($v_x = 0$), the ion fluxes at each electrode can be written based on equations (15) and (16) as follows:

$$(N_+)_{x=0} = -D_+ \left(\frac{dC_+}{dx} \right)_{x=0} - \frac{D_+ \cdot C_+ \cdot z_+ F}{RT} \left(\frac{d\phi_s}{dx} \right)_{x=0} \quad (23)$$

$$(N_-)_{x=0} = -D_- \left(\frac{dC_-}{dx} \right)_{x=0} - \frac{D_- \cdot C_- \cdot z_- F}{RT} \left(\frac{d\phi_s}{dx} \right)_{x=0} \quad (24)$$

Since no anion is discharged at the cathode, $(N_-)_{x=0} = 0$, and the internal potential gradient of the solution is equal to:

$$\left(\frac{d\phi_s}{dx} \right)_{x=0} = - \frac{RT}{C_- z_- F} \left(\frac{dC_-}{dx} \right)_{x=0} \quad (25)$$

Combining equations (23) and (25) and eliminating (C_-) and its derivative using equation (14) we obtained:

$$(N_+)_{x=0} = -D_+ \left(\frac{dC_+}{dx} \right)_{x=0} + D_+ \frac{z_+}{z_-} \left(\frac{dC_+}{dx} \right)_{x=0} \quad \text{respectively}$$

$$(N_+)_{x=0} = -D_+ \left(1 - \frac{z_+}{z_-} \right) \cdot \left(\frac{dC_+}{dx} \right)_{x=0} \quad (26)$$

By comparing the flux expressed by equation (26) and the cation flux obtained in the absence of an electric field but having the same concentration gradient (equations 20 and 21), it is shown that:

$$N_+ = -D_{exp} \left(\frac{dC_+}{dx} \right)_{x=0} \quad (27)$$

conditions under which equation (26) becomes in the form:

$$\begin{aligned} (N_+)_{x=0} &= -\frac{D_+ \cdot D_- (z_+ - z_-)}{D_+ \cdot z_+ - D_- \cdot z_-} \cdot \frac{D_- \cdot z_- - D_+ \cdot z_+}{D_- \cdot z_-} \left(\frac{dC}{dx} \right)_{x=0} \quad \text{respectively} \\ (N_+)_{x=0} &= D_{exp} \frac{D_- \cdot z_- - D_+ \cdot z_+}{D_- \cdot z_-} \left(\frac{dC}{dx} \right)_{x=0} \end{aligned} \quad (28)$$

Because the term $\frac{D_- \cdot z_- - D_+ \cdot z_+}{D_- \cdot z_-} > 1$, the electrolyte flux increases in the presence of an electric field.

The current passing through the electrochemical reactor

To establish the current passing through the reactor, expressions are written that give the current density as a function of the ionic flux to the two electrodes:

$$i_+ = z_+ F \cdot (N_+)_{x=0} \quad (29)$$

$$i_- = z_- F \cdot (N_-)_{x=d} \quad (30)$$

Considering the ion transport through section YY' (figure 1) under the condition in which the convective component of ion transport through the reactor is zero ($v_x = 0$) at all points in the reactor, in the volume zone of the solution there is no concentration gradient, and therefore transport is solely due to migration. Therefore, the flux of transported ions is written by means of the expressions:

$$N_-^v = -\frac{D_-^v \cdot C_-^v \cdot z_- F}{RT} \left(\frac{d\phi_s^v}{dx} \right) \quad (31)$$

$$N_+^v = -\frac{D_+^v \cdot C_+^v \cdot z_+ F}{RT} \left(\frac{d\phi_s^v}{dx} \right) \quad (32)$$

The total current that crosses the section YY' per time unit is equal to the current carried by ions represent the partial current densities:

$$i = z_+ F \cdot N_+^v + z_- F \cdot N_-^v \quad (33)$$

where i_+ and i_- represent the partial current densities: we

$$i_+ = z_+ F \cdot N_+^v \quad (34)$$

$$i_- = z_- F \cdot N_-^v \quad (35)$$

From equations (33), (34) and (35) we obtained the transport number of cations, and respectively the transport number of anions:

$$\frac{i_+}{i} = \frac{z_+ \cdot N_+^v}{z_+ \cdot N_+^v + z_- \cdot N_-^v} = t_+ \quad (36)$$

$$\frac{i_-}{i} = \frac{z_- \cdot N_-^v}{z_+ \cdot N_+^v + z_- \cdot N_-^v} = t_- \quad (37)$$

The sum of the transport numbers has the value:

$$t_+ + t_- = 1 \quad (38)$$

From the ratio based of equations (31) and (32) and the application of the condition electroneutrality, it can be written as:

$$\frac{N_+^v}{N_-^v} = \frac{-D_+^v}{-D_-^v} \quad (39)$$

and, correspondingly, the transport numbers of the ions will be equal to

$$t_+ = \frac{z_+ \cdot D_+^v}{z_- \cdot D_-^v - z_+ \cdot D_+^v} \quad (40)$$

$$t_- = \frac{z_- \cdot D_-^v}{z_- \cdot D_-^v - z_+ \cdot D_+^v} \quad (41)$$

Because migration fluxes can be precisely expressed when the concentrations and diffusivities of the ions are known, and the transport numbers are conditioned by the same quantities. Equation (28) contains a transport number defined by the values of D_+ și D_- at $x = 0$. It can be expressed with the relation:

$$(t_-)_{x=0} = 1 - (t_+)_{x=0} = \frac{z_- \cdot D_-}{z_- \cdot D_- - z_+ \cdot D_+} \quad (42)$$

Combining the equations (28), (29) and (42), the cathodic current density during the electrolysis of a binary electrolyte solution is expressed through the expression:

$$\frac{i}{z_+ F} = - \frac{D_{exp}}{1 - (t_+)_{x=0}} \cdot \left(\frac{dC_+}{dx} \right)_{x=0} \quad (43)$$

For calculating the parameters D_+ , D_{exp} și $(t_+)_{x=0}$ the concentration must be known $(C_+)_{x=0}$.

In practice, it would be more practical to use the values of D_{exp} , at the volume concentration, and accept that the calculated transport number from these does not vary with concentration. This simplifying assumption is acceptable for various electrolytic systems [1, 8].

Using the anion flux, an equivalent expression for the anodic current density can be deduced:

$$\frac{i}{z_- F} = - \frac{D_{exp}}{1 - (t_-)_{x=d}} \cdot \left(\frac{dC_-}{dx} \right)_{x=d} \quad (44)$$

in which the anion transport number was evaluated using the ion diffusibility for $x = d$.

3. Results and discussions

The verification of the mass transport influence on the electrochemical process parameters was carried out in the case of electrochemical deposition of copper using two types of electrolytes:

(a) *cyanuric electrolytes*, for which the current density is less than 10 A/dm², are characterized by exceptional penetrating power, the deposits having a fine structure, special adhesion, and uniform thickness [9]; the main cathodic process following which copper is deposited can be represented by the reactions:





(b) *sulphate electrolytes*, for which the current density is higher than 100 A/dm² even reaching 1500 A/dm²; these electrolytes are characterized by high chemical stability, high current efficiencies, but with relatively low penetrating power, with deposits exhibiting a coarse structure [9]; the main cathodic process following which copper is deposited can be represented by the reactions:



While using the *cyanuric electrolytes*, the ion from which copper will deposit on the cathode corresponds to monovalent copper. (Cu^+). Ion Cu^+ originates from the dissociation of complex ions $\text{Cu}(\text{CN})_3^{2-}$ and $\text{Cu}(\text{CN})_2^-$. The dissociation process takes place at a very slow rate, both in the volume of the electrolyte and in the immediate vicinity of the cathode. The limiting rate stage for the cathodic process is mass transfer (concentration polarization). This is experimentally reflected by the value of the cathodic potential, which is by 1 V more electronegative rather the potential shown when using acidic electrolytes. If we consider the deposition of copper according to the mechanism described by reactions (46), the minimum speed is given by the charge transfer process. But even in this case, the high electrochemical polarization has a favourable effect on the quality of the galvanic deposition. From *acidic electrolytes based on copper sulphate*, the ion that discharged at the cathode Cu^{2+} . The electrochemical equivalent of this ion is two times lower than that of the Cu^+ ion. Consequently, the calculated values for the mass transfer overpotential, at various current densities, are half the values recorded when using cyanide electrolyte [1, 3, 9].

The verification of this hypothesis is carried out by studying the influence of the ratio i/i_d in a range of 0,7 – 0,99 for electrodeposition of monovalent copper (Cu^+), respectively for electrodeposition of divalent copper (Cu^{2+}). The temperature range was considered between 18 – 25 °C, specific to operating condition for cyanuric and sulphate electrolytes for copper electrodeposition.

In figure 2 and figure 3 the graph displays the calculated data for the electrode overpotential (rel. 1) corresponding to the mass transport depending on the ratio i/i_d . According to these aspects, theoretically may be assumed that *the electrodepositions made from cyanide electrolytes will have superior quality compared to electrodepositions obtained from acidic electrolytes* [1, 3, 10].

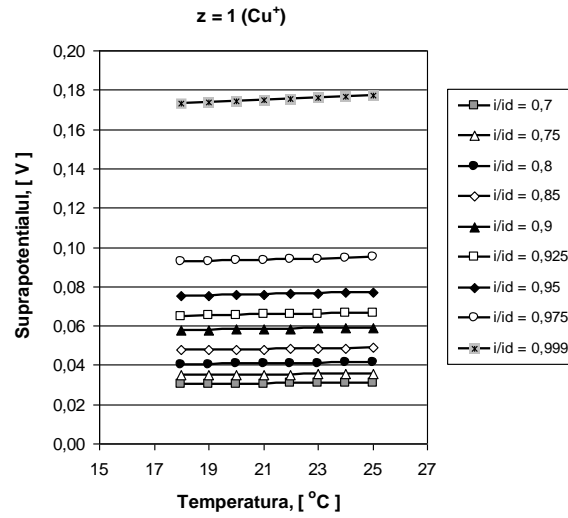


Fig. 2. Influence of the ratio i/i_d on mass transfer overpotential: *cyanuric electrolytes*

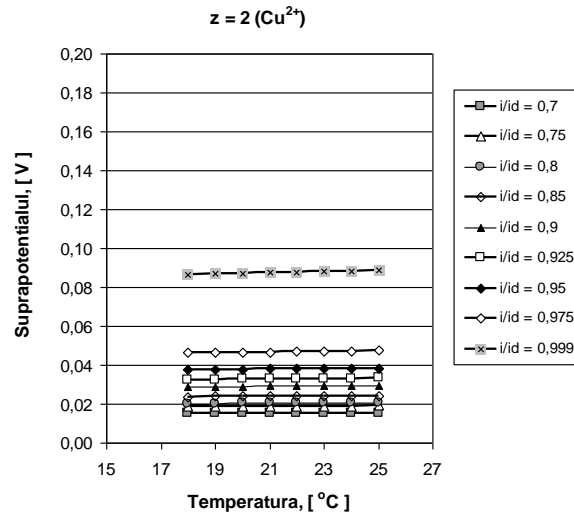


Fig. 3. Influence of the ratio i/i_d on mass transfer overpotential: *sulphate electrolytes*

4. Conclusions

Quality galvanic deposits are formed by numerous, fine crystals, which give the resulting layer adhesion, porosity as low as possible, hardness and a thickness as uniform as possible. The speed of formation of solid phase nuclei is much higher than their growth rate. The higher the electrode polarizations in deposits from a particular electrolyte, the better the quality of the cathodic deposits can be.

The calculations of the transfer overpotential for cyanuric electrolytes and sulphate electrolytes characteristic for copper electrodeposition was performed for the range of $i/i_d = 0,7 - 0,99$ and temperature range between $18 - 25$ °C. The electrodeposition of Cu^+ , for cyanide electrolytes, the mass transfer overpotential value is twice as large as that corresponding to the deposition of Cu^{2+} from acidic electrolytes. The high values of mass transfer overpotential that occur in the case of cyanide electrolytes ensure the formation of quality deposits. For this reason, cyanide electrolytes are preferred over acidic ones, even though it requires a technological step for wastewater treatment.

Notations: F – Faraday constant; z_j – electronic charge of the species j ; $v_{j,x}$ – velocity of ion movement j in the direction x ; $d\mu/dx$ – chemical potential gradient; k_j – a proportionality constant; $\mu_{j,0}$ – standard chemical potential of the species j ; ϕ_s – internal potential of the solution; z_+ și z_- – charges of cations and anions, with the sign of z_- being negative; n_+ și n_- – number of cations and respectively anions provided by a salt molecule; ν – an exponent referring to the volume of the electrolyte; t_+ – transport number of the cation, defined as the fraction of the total current transported by the migration of cations in the volume zero of the electrolyte solution; i_d – diffusion – limited current.

REFERENCES

- [1] Oniciu, L., Constantinescu, C., *Electrochimie și coroziune*, Editura Didactică și Pedagogică, București, 1982.
- [2] Scott, K., *Electrochemical Reaction Engineering*, Academic Press, Londra, 1991.
- [3] Choo R.T.C., Toguri J.M., El-Sherik A.M., Erb U., Mass transfer and electrocrystallization analyses of nanocrystalline nickel production by pulse plating, *Journal of Applied Electrochemistry*, 25, (1995), 384-403.
- [4] Vural Y., Ma L., Ingham D.B., Pourkashanian M., Comparison of the multicomponent mass transfer models for the prediction of the concentration overpotential for solid oxide fuel cell anodes, *Journal of Power Sources*, 195, (2010), 4893-4904.
- [5] Feng D., Bao C., Gao T., Prediction of overpotential and concentration profiles in solid oxide fuel cell based on improved analytical model of charge and mass transfer, *Journal of Power Sources*, 449, (2020), 227499.
- [6] Okagaki J., Hsu W.L., Chisaka M., Yoo E., Matsuda H., Daiguji H., Simple method of determining the ion transport parameters of binary liquid electrolytes, *Journal of Electroanalytical Chemistry*, 929, (2023), 117105.
- [7] Pereira J., Souza R., Moita A., Moreira A., Nanofluids and ionic fluids as liquid electrodes: An overview on their properties and potential applications, *Processes*, 11, (2023), 3189.
- [8] Mainar A.R., Iruin E., Colmenares L.C., Kvasha A., de Meatza I., Bengoechea M., Leonet O., Boyano I., Zhang Z., Blazquez J.A., An overview of progress in electrolytes for secondary zinc-air batteries and other storage systems based on zinc, *Journal of Energy Storage*, 15, (2018), 304-328.
- [9] Firoiu, C., *Tehnologia proceselor electrochimice*, Editura Didactică și Pedagogică, București, 1983.
- [10] Low C.T.J., Ponce de Leon C., Walsh F.C., Electrodeposition of copper from mixed sulphate-chloride acidic electrolytes at a rotating disc electrode, *The International Journal of Surface Engineering and Coatings*, 92, (2014), 281-288.

ASSESSMENT OF HEAVY METAL CONTAMINATION ON AGRICULTURAL SOILS IN THE VICINITY OF A HISTORICALLY POLLUTED AREA IN TURDA, CLUJ COUNTY

Alexandra I. CRĂCIUN¹, Carmen A. ROBA*¹, Maria BIZĂU-CÂRSTEA¹,
Alexandru OZUNU¹

¹ Faculty of Environmental Science and Engineering, University of Babeş-Bolyai,
30 Fantanele Street, RO-400294, Cluj-Napoca, Romania

Abstract

Heavy metal contaminated soils in Romania have gained the attention of experts, due to the recent environmental regulations set for contaminated sites. To evaluate such an area in Turda (Cluj County), a chemical assessment was conducted in the proximity of a former chemical plant. The total metal content was determined in various soil samples collected from the study site. The analyses were performed with flame atomic absorption spectrometry. To evaluate the potential environmental risk, the bioavailable fraction was also analyzed to be correlated with possible plant uptake. Principles of the sequential extraction technique were considered for the evaluation of the mobile forms of heavy metals. The results were confronted with the Romanian environmental legislation and increased metal contamination was observed in the analyzed soil samples. At the same time, a potential level of soil contamination with bioavailable forms of heavy metals (in particular Cu, Zn, Cd) was indicated by the chemical assessment.

Key words: soil, contamination, heavy metals, historical pollution, total fraction, bioavailable fraction, risk.

1. Introduction

Heavy metals are defined as a group of elements that have an atomic number greater than 20, an atomic density greater than 5 g/cm³ and must exhibit the properties of a metal. These metals exhibit certain characteristics, such as toxicity and bioaccumulation, that differentiate them from other chemical elements [1]. The presence of heavy metals in the environment is of great ecological importance due to their toxicity at certain concentrations, translocation through food chains and non-biodegradability which is responsible for their accumulation in the biosphere. Soil is a vital natural resource for sustaining human needs for food supply and is a life-supporting environment. Once plants are grown on land polluted with heavy metals, they can absorb heavy metals as

¹ Corresponding author: carmen.roba@ubbcluj.ro

mobile ions from the soil solution through their roots or by uptake. Absorbed metals bioaccumulate in the roots, stems, fruits, berries and leaves of plants. Some heavy metals, such as As, Cd, Hg and Pb, are particularly dangerous to plants, animals and humans [2]. In Romania, there are various sources of heavy metal contamination, mainly from anthropogenic activities. Results from studies over the last ten years show that soil is significantly affected by this type of pollution [3]. The current investigation was conducted to assess the impact of heavy metal contamination on agricultural lands near the former chemical plant. The aim of the research is to determine the potential for contamination and bioaccumulation of heavy metals in soil associated with industrial activity. To evaluate potential risks to human health, ecosystem health, and food safety, a sequential analysis of the total and bioavailable fractions of heavy metals in soil was deemed necessary.

2. Experimental

The selection of soil sampling points was carried out in accordance with Annex 3 of the Romanian Order No. 184/1997. For the determination of physico-chemical parameters, a 1:5 aqueous extract (soil-distilled water) was used, followed by agitation, settling, and filtration. The measurements were performed by using the WTW-multi 350i multiparameter device. Moisture content was determined by drying the samples in an oven at 105°C for 24 hours. For the determination of heavy metals, the samples were dried in an oven, ground, sieved, weighed, mineralized with aqua regia (HCl:HNO₃ 3:1) for 8 hours, and heated on a sand bath for 2 hours. Analysis was performed using flame atomic absorption spectrometry (AAS-F) with the assistance of the AAS ZEE nit 700 Analytik Jena instrument. To determine the bioavailable fraction (SR ISO 14870:2001), a method of extracting oligoelements from soil samples using a diethylenetriaminepentaacetic acid (DTPA) buffer solution was used. The assessment of the degree of heavy metal soil contamination was performed using specific factors.

3. Results and discussions

In order to assess the level of heavy metal contamination, the values of the total concentrations were interpreted with the legislative thresholds of Order No. 756/1997, established by Romania. Samples taken from the chemical plant site (Samples 1-5) were compared with the less sensitive type of use, representing the area of industrial activity, and the remaining samples (Samples 6-25) were compared with the sensitive use being related to agricultural areas.

Possible contamination with **Cu** was identified in samples taken from soil where industrial activities occurred, showing exceedances of alert and intervention thresholds. **Ni** exceeded all normal values according to the law, and **Cr** showed exceedances in samples taken from sensitive agricultural land, approaching the intervention threshold. The total fraction of **Zn** exceeds both the alert and intervention thresholds for sensitive uses, as well as in the vicinity of the chemical plant, and the total fraction of **Cd** presents high values for sensitive land use. Regarding **Fe** concentrations, no significant differences or fluctuations were observed, considered normal for the respective area. Considering that **control samples** (P6-9) were collected from rural agricultural land, outside the area considered affected by possible pollution generated by the former chemical plant, and they fall below the normal values, a level of heavy metal contamination can be observed in the other investigated areas.

Table 1

Sample no.	TOTAL FRACTION (mg/kg)						BIOAVAILABLE FRACTION (mg/kg)					
	Cu	Ni	Cr	Zn	Cd	Fe	Cu	Ni	Cr	Zn	Cd	Fe
1	81	56	27	162	1	4063	9	2	1	19	0	33
2	2474	39	26	2716	2	4057	145	1	1	161	0	12
3	494	13	29	524	1	3973	53	0	1	127	0	6
4	46	39	29	142	1	4073	6	1	0	8	0	17
5	71	39	26	997	1	4194	8	1	1	16	0	24
6	34	67	34	145	1	4077	4	2	0	5	0	29
7	39	49	67	115	1	4190	9	2	0	14	0	22
8	32	46	96	120	1	4073	3	3	1	7	0	21
9	39	60	8	153	1	4073	4	4	2	3	0	27
10	61	39	16	474	1	4097	9	0	3	6	0	23
11	50	49	38	159	1	4107	6	1	5	4	0	24
12	121	27	23	537	2	4070	18	1	5	31	0	27
13	53	47	23	507	1	4093	7	0	1	5	0	23
14	54	71	22	490	1	4090	7	0	1	4	0	23
15	53	100	19	301	1	4087	6	1	1	17	0	27
16	41	14	34	137	2	4030	7	1	1	4	0	36
17	52	31	59	134	2	4057	4	1	1	2	0	17
18	40	23	97	140	1	4040	3	1	0	4	0	21
19	629	56	103	10027	7	4127	49	1	0	144	1	38
20	84	23	8	2103	2	4003	7	1	2	10	0	20
21	121	16	23	607	2	4077	22	2	3	18	0	34
22	56	49	41	294	1	4017	4	3	6	5	0	25
23	55	37	32	271	1	4080	4	2	0	3	0	23

Assessment of heavy metal contamination on agricultural soils in the vicinity of a historically polluted area in Turda, Cluj COUNTY

Sample no.	TOTAL FRACTION (mg/kg)						BIOAVAILABLE FRACTION (mg/kg)					
	Cu	Ni	Cr	Zn	Cd	Fe	Cu	Ni	Cr	Zn	Cd	Fe
24	47	15	26	136	1	4037	4	2	0	4	0	24
25	53	45	23	817	1	4020	10	1	0	18	0	46
Reference values for heavy metals in soil (Romanian Ord. no. 756/03.11.1997)												
Element	Normal Values	ALERT THRESHOLD				INTERVENTION THRESHOLD						
		Sensitive land use		Less sensitive land use		Sensitive land use		Less sensitive land use				
Cu	20	100		250		200		500				
Ni	20	75		200		150		500				
Cr	30	100		300		300		600				
Zn	100	300		700		600		1500				
Cd	1	3		5		5		10				

Following the investigations regarding the contamination of agricultural lands in the industrial area of Turda municipality, the results highlight a potential level of soil contamination with bioaccumulative heavy metals (in particular **Cu**, **Zn**, **Cd**) in the studied area, as a result of historical pollution generated by past industrial activities. According to the obtained data, a significant level of bioaccumulation is highlighted in certain soil samples for Cu, Cr, Zn, and Cd.

Table 2

Calculation of specific factors to identify the degree of soil contamination

Sample no.	GEOACUMULATION INDEX (Igeo)						ECOLOGICAL RISK INDEX (Er)				
	Igeo_Cu	Igeo_Ni	Igeo_Cr	Igeo_Zn	Igeo_Cd	Igeo_Fe	Er_Cu	Er_Ni	Er_Cr	Er_Zn	Er_Cd
1	1.1	0.9	-0.9	0.6	2.6	-0.4	16.15	13.93	1.56	2.29	185.78
2	6	0.4	-1	4.7	4	-0.4	494.73	9.73	1.49	38.25	470.88
3	3.7	-1.2	-0.8	2.3	2.5	-0.4	98.73	3.23	1.68	7.38	169.18
4	0.3	0.4	-0.8	0.4	2.3	-0.4	9.28	9.72	1.68	2	144.56
5	0.9	0.4	-1	3.2	2.9	-0.3	14.2	9.68	1.5	14.04	226.67
6	-0.1	1.2	-0.6	0.4	2.1	-0.4	6.76	16.85	1.94	2.04	128.5
7	0	0.7	0.4	0.1	2.6	-0.3	7.71	12.22	3.84	1.62	187.89
8	-0.2	0.6	0.9	0.2	2.4	-0.4	6.38	11.55	5.49	1.69	163.06
9	0.1	1	-2.7	0.5	2.2	-0.4	7.78	15.1	0.47	2.15	135.51
10	0.7	0.4	-1.8	2.2	3	-0.4	12.14	9.87	0.89	6.67	241.43
11	0.4	0.7	-0.4	0.6	3.3	-0.4	10.09	12.21	2.2	2.24	290.07
12	1.7	-0.2	-1.2	2.3	3.4	-0.4	24.15	6.74	1.34	7.56	325.24
13	0.5	0.7	-1.2	2.3	3	-0.4	10.63	11.8	1.3	7.14	236.26
14	0.5	1.2	-1.2	2.2	3	-0.4	10.83	17.71	1.28	6.91	243.06
15	0.5	1.7	-1.5	1.5	3.1	-0.4	10.68	25.09	1.08	4.23	251.84

Sample no.	GEOACUMULATION INDEX (Igeo)						ECOLOGICAL RISK INDEX (Er)				
	Igeo_Cu	Igeo_Ni	Igeo_Cr	Igeo_Zn	Igeo_Cd	Igeo_Fe	Er_Cu	Er_Ni	Er_Cr	Er_Zn	Er_Cd
16	0.1	-1.1	-0.6	0.4	3.5	-0.4	8.2	3.54	1.93	1.93	345.24
17	0.5	0	0.2	0.3	3.5	-0.4	10.43	7.75	3.37	1.88	335.03
18	0.1	-0.4	0.9	0.4	3.3	-0.4	8	5.64	5.52	1.97	290.27
19	4.1	0.9	1	6.6	5.5	-0.3	125.73	14.01	5.87	141.23	1346.26
20	1.2	-0.4	-2.7	4.3	3.6	-0.4	16.75	5.75	0.48	29.62	355.58
21	1.7	-0.9	-1.2	2.5	3.6	-0.4	24.17	4.02	1.3	8.54	361.63
22	0.6	0.7	-0.4	1.5	3.3	-0.4	11.1	12.15	2.33	4.14	293.06
23	0.6	0.3	-0.7	1.3	2.7	-0.4	11.07	9.34	1.8	3.81	191.29
24	0.3	-1	-1	0.4	2.1	-0.4	9.31	3.67	1.47	1.92	129.18
25	0.5	0.6	-1.2	2.9	2.1	-0.4	10.67	11.2	1.32	11.5	130.41
LIMITS (Brişan et al., 2022)	practically uncontaminated (Igeo<0)						low potential ecological risk (Er < 40)				
	uncontaminated to moderately contaminated (Igeo = 0-1)						moderate potential ecological risk (40 < Er < 80)				
	moderately contaminated (Igeo = 1-2)						considerable potential ecological risk (80 < Er < 160)				
	moderately to highly contaminated (Igeo = 2-3)						high potential ecological risk (160 < Er < 320)				
	highly contaminated (Igeo = 3-4)						very high ecological risk (Er > 320)				
	highly to extremely contaminated (Igeo = 4-5)										
	extremely contaminated (Igeo>5)										

Calculating the **geoaccumulation index**, we can observe high Igeo values in the range $1 \leq Igeo \leq 4$ and $Igeo > 5$. These values indicate a significant accumulation of heavy metals in the soil, especially in the case of Samples 2, 19 and 20 for copper, zinc and cadmium, which may be the result of the industrial activity of the chemical plant. It can be considered that in the past the former chemical plant released heavy metals into the environment through its industrial processes.

The results of the **potential ecological risk index assessment** show that the order of risk of heavy metal pollution in soil in the study area is $Cd > Zn > Cu > Fe$. Heavy metal pollution in soil is at a considerable to very high ecological risk level. The cadmium content is significant mainly in the vicinity of the industrial platform and agricultural land near the former industrial waste landfill from the former chemical plant [4].

Analyzing these values, it can be considered that the activity of the former chemical plant can be a major pollution risk factor both in the industrial area and extended off-site, with exceedance areas being in the chemical plant site and in the agricultural land near the industrial area.

4. Conclusions

The accumulation of heavy metals in the soil near the former chemical plant may be a consequence of historical soil pollution. Heavy metals, including copper, cadmium, lead, mercury, chromium, zinc and others analyzed, can persist in the soil for long periods of time and pose significant risks to the environment and human health. This finding carries important implications for the decision-making process of authorities regarding soil management, remediation, and risk assessment. It can be assumed that conducting detailed investigations in the industrial area of Turda city, with particular emphasis on the zones near the former chemical plant, is crucial to determine the extent and impact of heavy metal contamination. By implementing sustainable strategies, it is possible to protect both human health and the integrity of the environment against the adverse effects of this form of contamination. It is necessary to develop a monitoring system for these areas, as well as a method for a more precise assessment of the effects of these metals on human health [5]. Detailed investigations of this area, monitoring and analysis of specific heavy metal concentrations in soil can provide essential information for risk assessment and prioritization of remediation and protection of human health and the environment.

REFERENCES

- [1] Cîmpeanu, C., Vârsta, A., *Metalele grele în mediul înconjurător*, Editura Valahia University Press, 2011.
- [2] Nyiramigisha, P., Komariah, S., *Harmful Impacts of Heavy Metal Contamination in the Soil and Crops Grown Around Dumpsites*, 9, 2021.
- [3] Iosob, G.A., Bute, A., Calara, M., Antal-Tremurici, A., Benchea, C.M., Bouruc, D., Avasiloaiei, D.I., Muscalu, *Heavy metals contamination of soil and vegetables in three regions from Romania: A review*, Studies and Research, Vasile Alecsandri University of Bacău, 2020.
- [4] Zhao, G., Ma, Y., Liu, Y., Cheng, J., Wang, X., *Source analysis and ecological risk assessment of heavy metals in farmland soils around heavy metal industry in Anxin County*, *Scientific Reports*, 12, 10562, (2022)
- [5] Brișan, N., Roba, C., Bălc, R., Ulinici, S., Oltean, V.I., Boar, F., *Heavy metals concentration in different species of trees, shrubs and the associated soils from urban area of Cluj-Napoca, România*, *Ecological and environmental chemistry: 2022*, Ed. 7, 3-4 martie 2022, Chișinău, Republica Moldova, Centrul Editorial-Poligrafic al USM, Ediția 7, 2, 2022

EFFECT OF SURFACE ROUGHNESS OF CO-CR ALLOY MODIFIED BY HYDROXYAPATITE COATING

Hussein F. HUSSEIN^{1*}, Farqad R. SAEED², Jihad G. ABDULQADER³, Shaalan B. AHMED⁴

¹Ministry of Science and Technology, Baghdad, Iraq

Abstract

The effects of roughness on cobalt-chromium-molybdenum substrate were investigated to improve the quality of hydroxyapatite (HA) coating as well as enhance the cell responses. Blasting process used to roughing the substrates surface by using a different alumina particles size (19, 45, 110, and 250) μm then coated with HAp using sol-gel coating by spin coating technique. Analysis of surface morphology, crystal structure and chemical composition of surface with HA coating were analyzed using field-emission scanning electron microscopy and characterized by energy dispersive X-ray spectroscopy. However, the bioactivity and stabilization of thin films were analyzed by immersing implants in the simulated body fluid (SBF) then analyzed by scanning electron microscopy and characterized by X-ray spectroscopy to investigate the transformations in surface morphology and crystal structure after 7, 14, 21 days.

Key words: Hydroxyapatite, Co-Cr alloy, X-ray spectroscopy, SEM, thin film.

1. Introduction

Since the need of closer attention to use biomaterials in the human body is increased, especially when the human body may experience for some damage or not responded for implants, thought was being given to devising better materials and alloys, given there a significant properties to strengthen the achievement of its objectives, that this was because of human could not to fabricate tissues or organs corresponded strictly what's in his structure, It started with used a known metals down to materials and alloys to fully perform its functions, as well as its ability to function as efficiently as possible to interact with tissue surrounding it appropriately, to attain a better standard of biocompatibility and Bioactivity [1, 2]. The biomedical revolution has resulted in the industrial and technical development of materials used widely such as Co-based alloys and Ti-based alloys [3]. It is noted that most applications of medical depend on titanium according to it had an excellence property such as low density adequately,

* Corresponding author: husseinalaubi@live.co.uk

significant corrosion resistance, acceptable biocompatibility but in return, ions of Al and V elements released from implants which can lead serious health problems like the toxicity which may affect various tissues, in addition, to unacceptable mechanical resistance for kind of applications and decomposition maybe happen in implants [4, 5]. The biomedical revolution has resulted in the industrial and technical development of materials used widely such as Co-based alloys and Ti-based alloys [3]. Conversely, the properties of Co-Cr based alloy such as superior strength, high hardness, high wear feature, good corrosion resistance and biocompatibility enabled it to engage into the biomedical world as materials in orthopaedic and dental implants [6, 7].

Hydroxyapatite (HAp), most stable calcium phosphate compound and also one of the bone components with morphology and chemical composition $\text{Ca}_{10}(\text{PO}_4)_6(\text{OH})_2$ similar to human hydroxyapatite, used to coat the surface of alloys in accomplishing these requirements of osteointegration and biocompatibility which lead to serve to strengthen the role of medical implants, through the capability to be adhesion and bond to bone (bone bonding ability), consequently, to improve osteoconductivity of metallic implants, also it has a larger role of preventing any physio-chemical ionic reactions to occur and forming a protective layer [9, 10]. In any case, it had been noted the failure of implant during coating as result of HAp layer breakdown from implant surface when contact with tissue [11, 12].

The searchers have produced numerous studies concerning the HA coating on Co-Cr alloy, which was aimed to overcome these challenges through the use surface modification techniques like sand blasting, grit blasting and thermal oxidation to increase the surface roughness of metal with the aim to improve adhesion strength of HA coating [14]. Various methods were utilized to achieve a good coating HA onto Co-Cr alloys implants such as sol-gel [13], electrochemical deposition [12], sputtering process [15], plasma spraying [16], biomimetic [16], despite the importance of the sol-gel technique in terms simplicity in the processing and utilization, low-cost and coating affectivity for complex shaped implants [17, 18].

2. Experimental

2.1 The Selection and the Process

This segment included the materials which used in the synthesis, coating and deposition by sol - gel technique as follows:

1. Specimens of cobalt – chromium – molybdenum-based alloys as plates form with dimensions 5 x 5 mm and thickness 2, 2.5 mm respectively.
2. The surface of plates blasted with Al_2O_3 particles by using blasting

process which have specific sizes (29, 45, 110 and 250 μm) to produce surface roughness for each specimen.

3. Hydroxyapatite solution prepared by using sol-gel technique which used:
 - 98% of Triethylphosphate $\text{P}(\text{OCH}_2\text{CH}_3)_3$ according to Sigma-Aldrich Inc., St.Louis, MO.
 - Ethanol ($\text{CH}_3\text{CH}_2\text{OH}$).
 - deionized wate.
 - 99% Calcium nitrate hydrate ($\text{Ca}(\text{NO}_3)_2 \cdot 4\text{H}_2\text{O}$) according to Sigma-Aldrich Inc., St.Louis, MO.
 - Ammonia solution
4. A Spin Coater from Laurell model WS-650 used to coat the specimens.

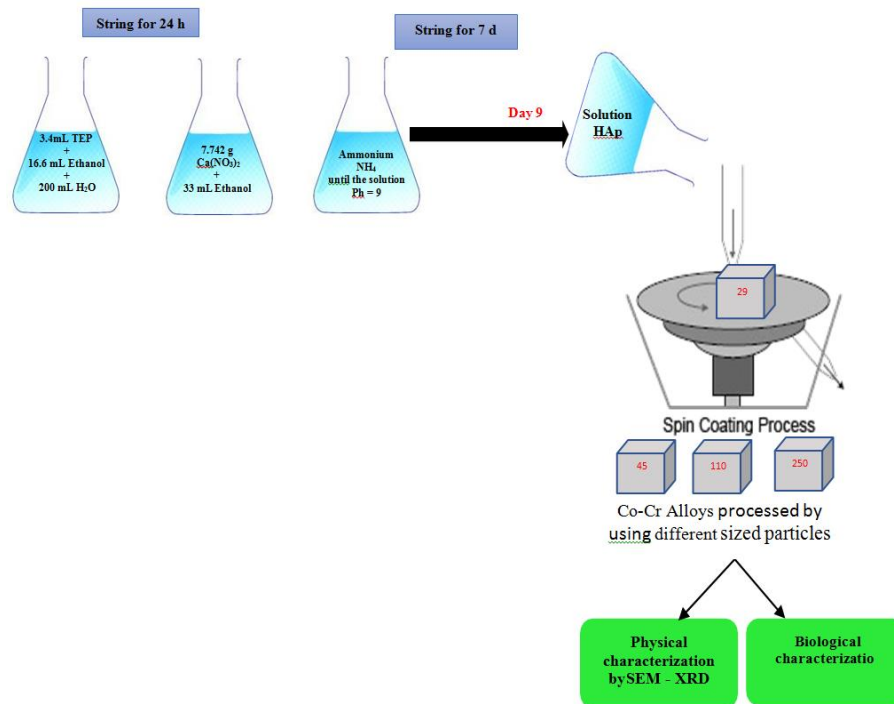


Fig. 1. Coating technological workflow

2.2 The materials of coating process

Sol-gel technique used to produce HAp solution which preferred for spinning coating and obtained the thin films on material surfaces, synthesis of HAp solution was prepared according to the follow steps:

- Distilled water added to 1 mole to tri-ethyl-phosphate (TEP) in ethanol under continuous stirring for 24 h to ensure the homogenous of solution.

- The homogenous solution added to 1 mole of calcium nitrate in ethanol while ensuring the relative of calcium/phosphor about 1.67, then the solution left under continuous stirring for 24 h until the PH reached to 9 by Ammonium additional.
- The solution formed was left to be homogenized for 7 days.

After receiving the solution of Hydroxyapatite, spinning coating method used to coated cobalt-chromium – molybdenum alloys with 20 layers of solution at a speed 2000 rpm for 5 sec for every layer of coating, after every deposited layer, the films were dried at 80 °C for 10 min on a heating plate, the specimens coded after dried as shown in table 1 below.

An electronic scanning microscope (SEM) manufactured of FEI Quanta™ used to studying the morphology and microstructure of the formed surface films after coating of specimens of Cobalt-Chromium alloys with hydroxyapatite, which it's characterized:

1. Images of the formed films topography made by the resultant secondary electron beam with (30 keV) energy.

2. Detection of crystal structure for coated films by using a PANalytical Empyrean model diffractometer equipped with a hybrid mono-chromator (2xGe 220) on the side and a parallel plate collimator mounted on the Pixel 3D detector on the diffracted side.

3. The microstructure of alloys indicated by Grazing Incidence X-ray Diffraction (GIXRD) measurements at room temperature with an incidence angle of $\omega = 0.5^\circ$ for Bragg angle values of 20 between 10° and 80° , using Cu K α radiation with $\lambda = 1.5406 \text{ \AA}$ (40 mA and 45 kV).

4. The elemental composition of the coating was identified using Energy Dispersive Spectroscopy (EDS).

Table 1

Code of Co-Cr coated with HAp				
Alloy	Co-Cr	Co-Cr	Co-Cr	Co-Cr
Size of blasting particles (μm)	29	45	110	250
Code	HAp_29 ^{Co-Cr}	HAp_45 ^{Co-Cr}	HAp_110 ^{Co-Cr}	HAp_250 ^{Co-Cr}

3. Results and discussions

3.1 X-ray characterization (XRD)

X-ray diffraction (XRD) is a technique used in materials science for determining the atomic and molecular structure characterizing crystalline materials. This analysis was used to investigate the crystallinity of the film

deposited on the surface of the Co-Cr alloys by hydroxyapatite coated on different roughness of Co-Cr alloy surface.

In figure 2, the samples HAp_29^{Co-Cr} -HAp_250^{Co-Cr} and HAp_Ag_29^{Co-Cr} - HAp_Ag_250^{Co-Cr} which analyzed by X-ray diffraction spectra, it can be observed that HAp_29^{Co-cr} has a precipitation of de-calcium phosphate $\text{CaHPO}_4 \cdot 2\text{H}_2\text{O}$ as monoclinic crystal structure similar to those of gypsum [19] combined with Hexagonal crystal structure of Co ion (ASTM sheets 00-056-1217). While HAp_45^{Co-Cr} has a Calcium Phosphide Ca_5P_8 with monoclinic crystal structure according to ASTM sheets 00-048-1825 combined with hexagonal crystal structure of Co and P ions according to ASTM sheets 04-015-9495 and 00-056-1217 respectively.

In the case of diffraction spectra obtained for HAp_110^{Co-Cr} and HAp_250^{Co-Cr}, it can be seen that samples exhibit lower crystallinity compared to HAp_29^{Co-Cr} and HAp_45^{Co-Cr}, which is demonstrated by the intensity of smaller high diffraction lines.

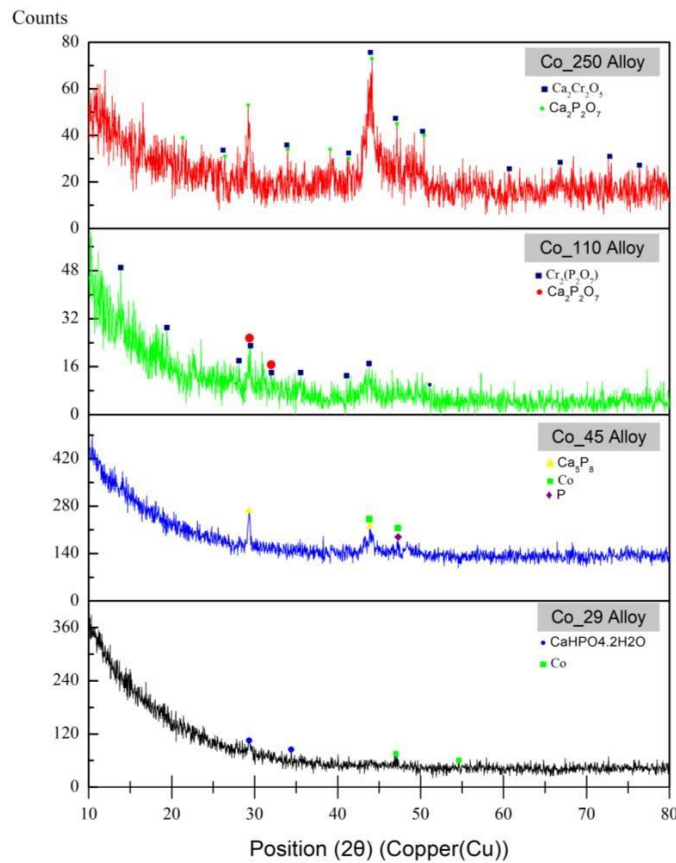


Fig. 2. Compared XRD Spectra for all samples of HApCo-Cr with different roughness of Co-Cr surfaces.

XRD Spectra for both, revealed that the crystal structure $\gamma\text{-Ca}_2\text{P}_2\text{O}_7$ obtained of $\text{HAp}_{110}^{\text{Co-Cr}}$ and $\text{HAp}_{250}^{\text{Co-Cr}}$ as intermediate products for Calcium Phosphate of hydroxyapatite formed according to ASTM datasheets 00-003-0605, indicating that deposition has been successful. It should be noted that the samples of $\text{HAp}_{110}^{\text{Co-Cr}}$ contain chromium phosphate $\text{Cr}_2(\text{P}_2\text{O}_7)$ as oxide interlayer as protective layer with monoclinic crystal structure according to ASTM datasheets 00-003-0605, while $\text{HAp}_{250}^{\text{Co-Cr}}$ contain to Calcium Phosphate $\text{Ca}_2\text{P}_2\text{O}_7$ and Calcium chromium oxide $\text{Ca}_2\text{Cr}_2\text{O}_5$ as oxide interlayer with Orthorhombic crystal structure according to ASTM datasheets 00-066-0840.

It can be observed that calcium phosphate $\text{CaHPO}_4 \cdot 2\text{H}_2\text{O}$ and Calcium Phosphide Ca_5P_8 formed with low roughness compared with Calcium Phosphate $\gamma\text{-Ca}_2\text{P}_2\text{O}_7$ with high roughness which is represented the best formed as a thin layer were deposited which could lead to a better bio-inerrability [20]

3.2 Electronic Scanning (SEM)

Electronic Scanning Microscopy (SEM) is an investigative method that can provide relevant information about the structure and state of the material surfaces. This analysis was used to investigate the morphological characteristics of the hydroxyapatite film deposited on the surface of the Co-Cr alloys.

3.2.1 SEM analysis of uncoated Co-Cr

Figure 3 shows the SEM data obtained of Co-Cr alloy samples for surface morphology at different surface roughness of Co-Cr alloys used as a substrate for the deposition of thin films of hydroxyapatite. It can clearly be seen that; the roughness of the samples increases with the increase of ball size as result of crystal growth.

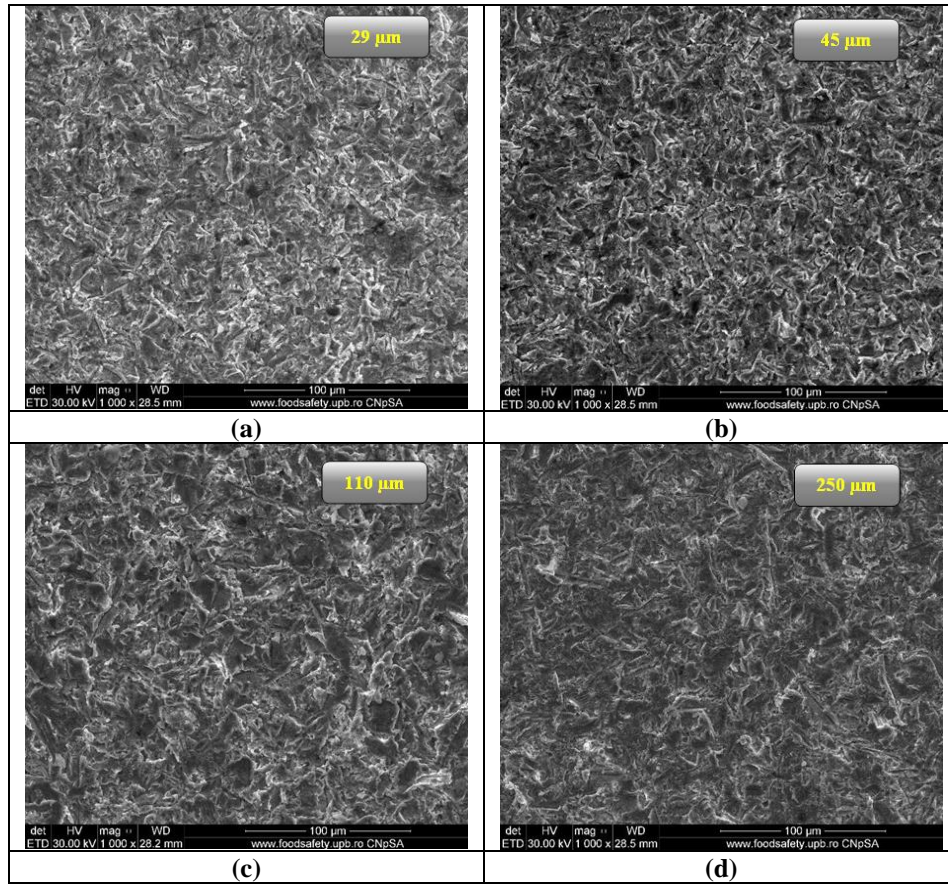


Fig. 3. SEM micrographs of Co-Cr alloy with different roughness

3.2.2 SEM analysis of un-doped samples HAp_29Co-Cr, HAp_45Co-Cr, HAp_110 Co-Cr, HAp_250 Co-Cr

It can be observed that micrographs obtained of samples HAp_29^{Co-C}, HAp_45^{Co-C}, HAp_110^{Co-C}, HAp_250^{Co-C} contain a uniform deposited layer on the surface of Co-Cr alloys, as result of hydroxyapatite decomposition to compounds of calcium phosphate which is distributed with different crystal structures in all the recesses formed by balls halls of different sizes (29, 45, 110, 250μm).

It can be seen polyhedral forms for layer morphology of hydroxyapatite deposition, for HAp_29^{Co-Cr} in figure (4) shows the morphology of the starting de-calcium phosphate (brushite) like those of gypsum which formed by typical homogeneous crystals, whose XRD data were previously reported elsewhere. While HAp_45^{Co-Cr} contain a penta-calcium octaphosphate structure as calcium phosphate as shown in fig (5), for HAp_110^{Co-Cr} contain γ -Ca₂P₂O₇ and

$\text{Cr}_2(\text{P}_2\text{O}_7)$ shows spheroids morphology distributed in $\gamma\text{-Ca}_2\text{P}_2\text{O}_7$ as smaller crystallites are formed shown in figure 6 for $\text{HAp}_{250}^{\text{Co-Cr}}$ shows in figure 7 contain $\text{Ca}_2\text{P}_2\text{O}_7$ and $\text{Ca}_2\text{Cr}_2\text{O}_5$ as spheroids morphology. However, there were no marked differences in the distribution of cells on the top surface of samples from the different groups of balls sizes (29, 45, 110, 250 μm).

EDAX analysis performed of Co-Cr alloy samples, with phosphate ceramic layers which have been deposited using the spin coating method simultaneously confirms the uniform distribution of the specific species found, such as Aluminum, Calcium, Cobalt, Chromium and Molybdenum characteristic of the solution submitted.

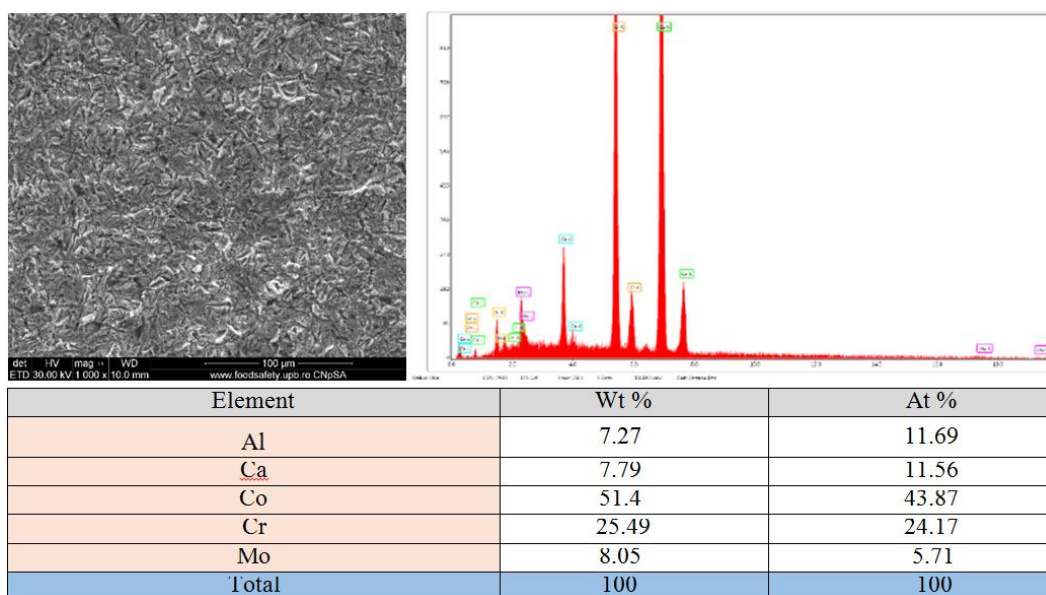


Fig. 4. SEM and EDAX of $\text{HAp}_{29}^{\text{Co-C}}$ sample

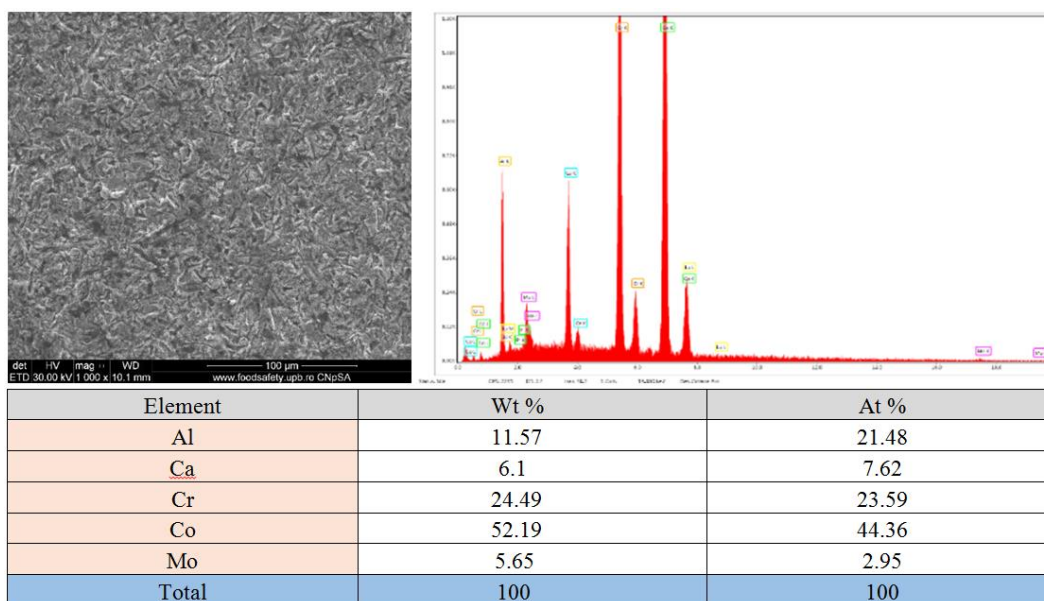


Fig. 5. SEM and EDX of HAp₄₅Co-Cr sample

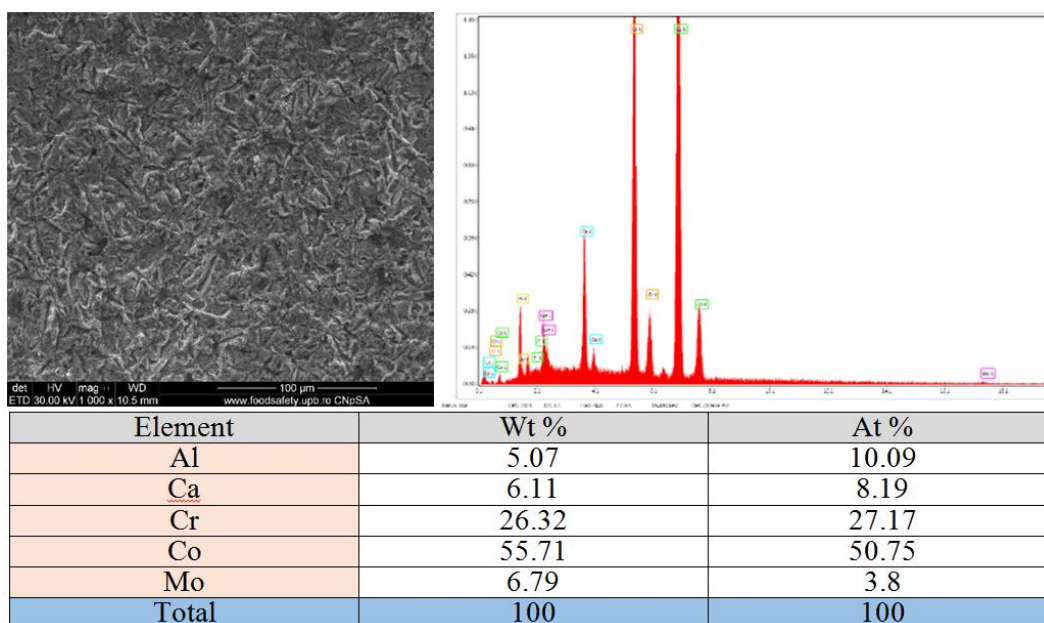


Fig. 6. SEM and EDAX of HAp₁₁₀Co-Cr sample

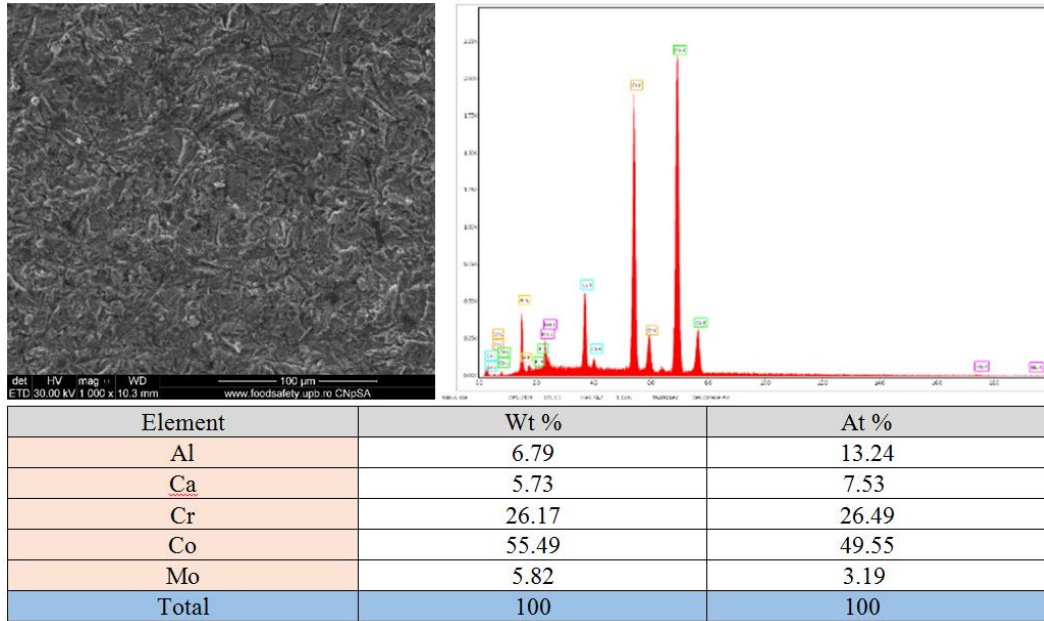


Fig. 7. SEM and EDAX of HAp_250^{Co-Cr} sample

3.3 Stabilization of thin films in SBF

The method of coating with HAp can be based on practical biomimicry by immersing implants in the simulated body fluid (SBF), which is an equal inorganic composition with the pH and temperature of the human blood plasma.

The surface morphology of the spinning coated specimens was observed by a field scanning electron microscope and X-ray spectra (XRD) analysis was performed.

3.3.1 X-ray Diffraction Analysis of samples HAp_29^{Co-Cr}, HAp_45^{Co-Cr}, HAp_110^{Co-Cr}, HAp_250^{Co-Cr} after 7, 14, 28 days of immersion in SBF.

In table 2, showed the data that's been gathered from X-ray diffraction spectra of HAp_29^{Co-Cr}, HAp_45^{Co-Cr}, HAp_110^{Co-Cr}, HAp_250^{Co-Cr} analyzing after 7, 14, 21 days of immersion in SBF. it be noticed after 7 days of immersion in SBF, that HAp_29^{Co-Cr} and HAp_45^{Co-Cr} have a hydroxyapatite film with hexagonal crystal of calcium phosphate hydroxide $\text{Ca}_5(\text{PO}_4)_3(\text{OH})$ according to ASTM datasheets 01-086-0740 and $\text{Ca}_4(\text{PO}_4)_2\text{O}$ as tetra-calcium di-phosphate monoxide, crystallizes in the monoclinic according to ASTM datasheets 01-084-9872 for HAp_45^{Co-Cr}, but with HAp_29^{Co-Cr} it crystallized with calcium

phosphate hydroxide $\text{Ca}_5(\text{PO}_4)_3(\text{OH})$, then the HAp_45^{Co-Cr} for intensity of diffraction lines for $\text{Ca}_4(\text{PO}_4)_2\text{O}$ decreases with increased roughness. While the samples of HAp_110^{Co-Cr} and HAp_250^{Co-Cr}, both of them exhibit lower crystallinity compared to HAp_29^{Co-Cr} and HAp_45^{Co-Cr}, which is demonstrated by the intensity of smaller high diffraction lines, since the analyzed layer of HAp_110^{Co-Cr} and HAp_250^{Co-Cr} have shown the same formed of calcium phosphate $\text{Ca}_3(\text{PO}_4)_2$ with rhombohedra crystal structure according to ASTM datasheets 04-010-5151, indicating that stabilization of film has been good calcium phosphate TCP $\text{Ca}_3(\text{PO}_4)_2$, has long been considered as an excellent biomaterial to promote bone repairs and implant [21].

On the other hand, for samples after 14 days of immersion in SBF, it can be noticed that HAp_45^{Co-Cr} formed of Calcium chromium oxide CaCr_2O_4 as Orthorhombic crystal according to ASTM datasheets 04-007-4990 that was also evidence of reaction of chromium from the alloys in SBF with released P, Cr ion as Orthorhombic and cubic crystal structures according to ASTM datasheets 03-065-2491 and 04-021-2342 respectively, while HAp_110^{Co-Cr} it crystallized with tri-calcium phosphate $\text{Ca}_3(\text{PO}_4)_2$, as rhombohedral crystal structure according to ASTM datasheets 04-010-5151 besides Co and Cr ion as tetragonal and cubic crystal structures according to ASTM datasheets 01-078-4003 and 04-021-2342 for intensity of diffraction lines for $\text{Ca}_3(\text{PO}_4)_2$ decreases with increased roughness. It can be seen that sample of HAp_250^{Co-Cr}, exhibit lower crystallinity which is demonstrated by the intensity of smaller high diffraction lines, since the analyzed layer of HAp_250^{Co-Cr} have shown to formed calcium hydroxide $\text{Ca}(\text{OH})_2$ with Hexagonal crystal structure according to ASTM datasheets 01-073-6988 as portlandite responsible for the bioactivity and biocompatibility, thus means the precipitates of calcium hydroxide $\text{Ca}(\text{OH})_2$ has been good, besides Co ion released as tetragonal crystal structure according to ASTM datasheets 01-078- 4003.

By the looks of the samples after 21 days of immersion in SBF as result of initially attracted of Calcium ion to the negatively charged interface between the HAp coating and solution which observed with HAp after 21 days, the calcium formed at the interface combines with phosphate ions, consequently forming apatite nuclei.

With the increase of immersion time, a large amount of calcium ions and phosphate ions are attracted to the HAp coatings to form apatite precipitates $\text{Ca}_3(\text{PO}_4)_2$, Ca_5P_8 , $\text{C}_{10}(\text{PO}_4)_6\text{O}$

Table 2

The effect of different ball sizes (roughness) on HApCo-Cr compound after and before immersion in SBF

Ball Sizes μm	HAp in SBF for different periods times (days)											
	0			7			14			21		
	Chemical Formula	Compound name	Crystal system	Chemical Formula	Compound name	Crystal system	Chemical Formula	Compound name	Crystal system	Chemical Formula	Compound name	Crystal system
29	$\text{CaHPO}_4 \cdot 2\text{H}_2\text{O}$ Co	Dicalcium Phosphate	Monoclinic	$\text{Ca}_5(\text{PO}_4)_3(\text{OH})$	Calcium Phosphate oxide	Hexagonal				$\text{Ca}_3(\text{PO}_4)_2$	Tricalcium	Rhombohedral
45	$\text{Ca}_5\text{P}_3\text{CoP}$	Calcium phosphate Cobalt Phosphate	Monoclinic Cubic Cubic	$\text{Ca}_4(\text{PO}_4)_2\text{O}$	Tetracalcium diphosphate monoxide	Monoclinic	CaCr_2O_4 P Cr	Calcium chromium oxide Phosphorus Chromium	Orthorhombic Cubic Cubic	CoCr CrCoP	Chromium cobalt Chromium cobalt phosphide	Cubic Orthorhombic
110	$\text{Ca}_3\text{P}_2\text{O}_7$ $\text{Cr}_2(\text{P}_2\text{O}_7)$	Calcium Phosphate Chromium phosphate	Unknown Monoclinic	$\text{Ca}_3(\text{PO}_4)_2$	Calcium phosphate	Rhombohedral	$\text{Ca}_3(\text{PO}_4)_2\text{CoCr}$	Tricalcium phosphate Cobalt Chromium	Rhombohedral Tetragonal Cubic	Ca_3P_3 $\text{C}_{10}(\text{PO}_4)_6\text{O}$	Calcium phosphate Calcium phosphate oxide	Monoclinic Hexagonal
250	$\text{Ca}_2\text{P}_2\text{O}_7$ $\text{Ca}_2\text{Cr}_2\text{O}_5$	Calcium Phosphate Calcium chromium oxide	Unknown Orthorhombic	$\text{Ca}_3(\text{PO}_4)_2$	Calcium phosphate	Rhombohedral	$\text{Ca}(\text{OH})_2$ Co	Calcium hydroxide Cobalt	Hexagonal Tetragonal	$\text{Ca}_3(\text{PO}_4)_2$ CrCo	Tricalcium Chromium cobalt	Rhombohedral Orthorhombic

3.3.2 Scanning Electron Microscopy (SEM)

In figure 8, clarifying the SEM data obtained of sample HAp₂₉^{Co-Cr}, HAp₄₅^{Co-Cr}, HAp₁₁₀^{Co-Cr}, HAp₂₅₀^{Co-Cr} after 7, 14, 21 days of immersion in SBF.

According to SEM micrographs which performed after 7 days of immersion in SBF for HAp, it can be seen that the calcium phosphate ceramics (biological apatite) film has developed quantitatively at the same time of presenting a homogeneous arrangement on the surface of the Co-Cr alloys. This is an indication of high activity of hydroxyapatite in contact with physiological fluid in the human body. It's best with comparison, it can be said that HAp₂₅₀^{Co-Cr} shows the best development of the formed film, so the roughness is directly involved in the stability of thin films.

While the samples after 14 days of immersion in SBF, it can be seen that the different films are formed with HAp different roughness, chromium oxide layer for

HAp₂₉^{Co-Cr} and phosphate ceramic film with ions released have a more significant development on the surface of the Co-Cr alloy substrate than the micrographs obtained 7 days after immersion, as well as HAp₁₁₀^{Co-Cr} and HAp₂₅₀^{Co-Cr} give a good morphology than others HAp

As well as in the case of samples analyzed after 21 days of immersion in SBF, Focus of the success of deposition and growth of hydroxyapatite on Co-Cr substrate is , being homogeneous with oxide layers

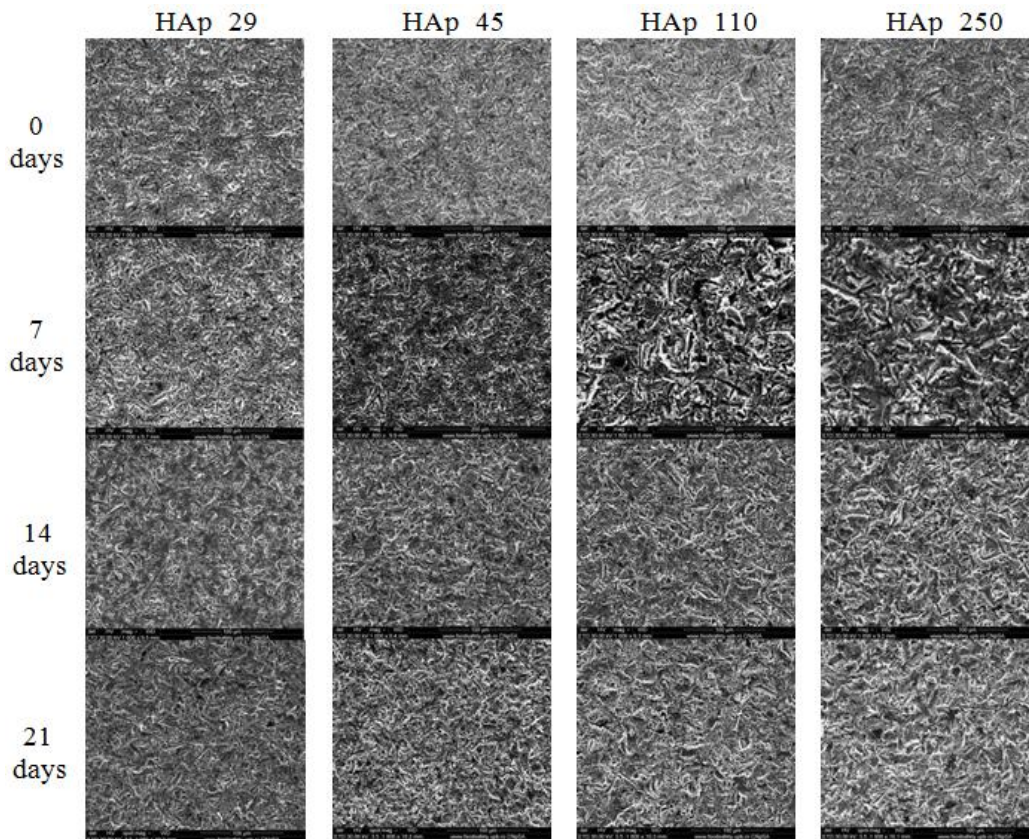


Fig. 8. SEM micrographs, registered for HAp₂₉^{Co-Cr}, HAp₄₅^{Co-Cr}, HAp₁₁₀^{Co-Cr}, HAp₂₅₀^{Co-Cr} after 7, 14, 21 days of immersion in SBF respectively.

4. Conclusions

1. As can be seen from the above, the roughness which synthesized by blasting process contributed to enhances the adhesive between Co-Cr surface and ceramic (HAp) bonding successfully.
2. It is important to note that, increasing the surface roughness led to form a crystal structures differ from one to the other which work to promote the affectivity of surface when coated with HAp

3. The samples of HAp_110^{Co-Cr} and HAp_250^{Co-Cr} exhibit lower crystallinity compared to HAp_29^{Co-Cr} and HAp_45^{Co-Cr}, which is demonstrated by the intensity of smaller high diffraction line of Ca₂P₂O₇ this can be attributed to the fact that Calcium Phosphate of hydroxyapatite was formed in holes due to the larger size of the particles.
4. The deposited layer formed on the surface of Co-Cr alloy is uniform and distributed in all the recesses.
5. EDAX analysis performed of Co-Cr alloy samples, with phosphate ceramic layers which have been deposited using the spin coating method simultaneously confirms the uniform distribution of the specific species found, such as Aluminum, Calcium, Cobalt, Chromium and Molybdenum characteristic of the solution submitted.
6. Based on the SEM results of 21 days immersion in SBF, the morphology of Tricalcium phosphate crystal formed with β -TCP which has a more stable structure and higher biodegradation, faster degradation rate and higher solubility. Consequently, lead to increase the biocompatibility.
7. According to XRD result, which indicated the pure HAP is not yet formed, as it was observed a different compositions of calcium phosphate peaks, for most samples with different roughness However, for 21 days immersion in SBF, there were also Ca₃(PO₄)₂ peaks for HAp_250^{Co-Cr}.

REFERENCES

- [1] Chen F.M., Liu X., Advancing biomaterials of human origin for tissue engineering HHS Public Access Author manuscript, *Prog Polym Sci*, vol. 53, (2016), 86–168.
- [2] Ratner B.D., *A History of Biomaterials*, Biomater. Sci. An Introd. to Mater. Third Ed., 2013.
- [3] Zhang L.C., Chen L.Y., A Review on Biomedical Titanium Alloys: Recent Progress and Prospect, *Adv. Eng. Mater.*, 21, 4, (2019), 1–29.
- [4] Khorasani A.M., Goldberg M., Doeven E.H., Littlefair G., Titanium in biomedical applications—properties and fabrication: A review, *Journal of Biomaterials and Tissue Engineering*, 5, 8, (2015), 593–619.
- [5] Li Y., Yang C., Zhao H., Qu S., Li X., Li Y., New Developments of Ti-Based Alloys for Biomedical Applications, *Materilas*, 7, (2014), 1709–1800.
- [6] Dănilă E., Bounegru I., Benea L., Chiriac A., Improving Biocompatibility of Co-Cr Alloy Used in Dentistry by Surface Modification with Electrochemical methods - Corrosion of Untreated Co-Cr Alloy in Solution with Different pH, *Dunarea de Jos*, N, 2, (2014), 54–59.
- [7] Liu R., Li X., Hu X., Dong H., Surface modification of a medical grade Co-Cr-Mo alloy by low-temperature plasma surface alloying with nitrogen and carbon, *Surf. Coatings Technol.*, 232, (2013), 906–911.
- [8] Vechietti F.A., Muniz N.O., Rezwan K., Schumacher M., Gelinsky M., Dos Santos L.A.L., Influence of cobalt chromium alloy surface modification on the roughness and wettability behavior of pine oil/hydroxyapatite as coating, *Mater. Res. Express*, 6, 2, (2018), 025401.

- [9] Jeong J., Kim J.H., Shim J.H., Hwang N.S., and Heo C.Y., Bioactive calcium phosphate materials and applications in bone regeneration, *Biomater. Res.*, 23, 1, (2019), 1–11.
- [10] Erdem U. *et al.*, Hydroxyapatite-based nanoparticles as a coating material for the dentine surface: An antibacterial and toxicological effect, *Ceram. Int.*, 46, 1, (2020), 270–280.
- [11] Wang L. N., J. L. Luo, Preparation of hydroxyapatite coating on CoCrMo implant using an effective electrochemically assisted deposition pretreatment, *Mater. Charact.*, 62, 11, (2011), 1076–1086.
- [12] Ayu M. *et al.*, Surface Modification on CoCrMo Alloy to Improve the Adhesion Strength of Hydroxyapatite Coating, *Procedia Eng.*, 184, (2017), 399–408.
- [13] Huynh V., Ngo N.K., Golden, T.D., Surface Activation and Pretreatments for Biocompatible Metals and Alloys Used in Biomedical Applications, *Int. J. Biomater.*, 2019.
- [14] Oje A.M., Ogwu A.A., Chromium oxide coatings with the potential for eliminating the risk of chromium ion release in orthopaedic implants, *R. Soc. Open Sci.*, 4, 7, (2017).
- [15] Dehghanghadikolaei A., Fotovvati B., Coating techniques for functional enhancement of metal implants for bone replacement: A review, *Materials (Basel)*, 12, 11, (2019).
- [16] Kheimehsari, H., Izman S., Shirdar M.R., Effects of HA-Coating on the Surface Morphology and Corrosion Behavior of a Co-Cr-Based Implant in Different Conditions, *J. Mater. Eng. Perform.*, 24, 6, (2015), 2294–2302.
- [17] Beevers C.A., The crystal structure of dicalcium phosphate dihydrate, $\text{CaHPO}_4 \cdot 2\text{H}_2\text{O}$, *Acta Crystallogr.*, 11, 4, (1958), 273–277.
- [18] Habraken W., Habibovic P., Epple M., Böhner M., Calcium phosphates in biomedical applications: Materials for the future? *Mater. Today*, 19, 2, (2016), 69–87.
- [19] Bisaria H., Patra B.B., Mohanty S., Surface modification during hydroxyapatite powder mixed electric discharge machining of metallic biomaterials: a review, *Surface Engineering*, 38, 7–9, 2022.
- [20] Liao S., Yang L., Zhang Q., Zheng B., Yang C., Zheng J., Zou D., Song Z., Effect of annealing on the mechanical properties and cytocompatibility of CoCrMo alloy with tantalum coating, *Surface and Coating Technology*, 469, 2023.
- [21] Yan X., Cao W., Li H., Biomedical Alloys and Physical Surface Modifications: A Mini-Review, *Materials*, 15, 1, 66, 2021.

ETHANOLIC EXTRACTION OF URSOLIC ACID BY CONVENTIONAL METHODS

Vasile STAICU^{1,2*} Justinian A. TOMESCU^{1,2}, Mihaela NEAGU², Daniela IONESCU², Cristina MANEA², Ioan CALINESCU¹

¹Faculty of Chemical Engineering and Biotechnologies, National University of Science and Technology Politehnica Bucharest, 1-7 Gheorghe Polizu St., 011061 Bucharest Romania

²S.C. Hofigal Export Import S.A., 2, 4 Intr. Serelor St., 042124 Bucharest, Romania

Abstract

This study describes the main three conventional methods of extraction of bioactive compounds from medicinal plants, namely: simple maceration, extraction with mechanical agitation and percolation. The technological steps necessary for extraction and the devices used are presented. The results obtained for the ethanolic extraction of ursolic/oleanolic acid from rosemary and sages using the 3 extraction procedures mentioned above are rendered. The results refer to the dry extract rich in ursolic/oleanolic acid, obtained by precipitation with warm water of the concentrated extracts. The dry extract allows obtaining, together with some traditional plants, a phytotherapeutic, incapsulable product, intended for the treatment of prostate and bladder diseases.

Key words: ursolic/oleanolic acid, maceration, percolation, extraction with mechanical agitation

1. Introduction

Ursolic acid and its isomer oleanolic acid (AU/AO) is a natural pentacyclic hydroxy-terpenoid, which has sedative, anti-inflammatory activity [1, 2], antimicrobial [3], it lowers blood sugar [4], it reduces blood fat and increases immunity [5].

As an antioxidant it is used in medicine, cosmetics and as an emulsifier in food [6]. AU/AO is naturally present in vegetarian foods and herbs (rosemary, sage, thyme, etc.) AU/AO improves skin and hair health, treats wrinkles and age spots, inhibits the action of the enzyme elastase in the skin, inhibits cyclooxygenase, inflammation (inflammatory) enzymes and lipoxygenase.

* Corresponding author: vasile.staicu@yahoo.ro

It is soluble in methanol, ethanol, it has the chemical formula: $C_{30}H_{48}O_3$ (see figure 1) and molecular weight = 456.7 g/mol. The main worldwide supplier is the Chinese company SHAANXI NHC Technology CO., LTD, (email: cxj@hnikes.com)

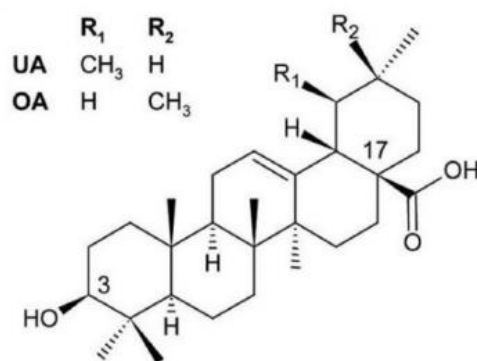


Fig. 1. Ursolic/oleanolic acid [7]

Ethanolic vegetable extracts, as a source generating ursolic acid, are products obtained by ethanol extraction of ursolic/oleanolic acid from plants, followed by evaporation of the solution to the concentration or consistency indicated by the pharmacopoeia or working procedure. The extraction mechanism depends on the extraction process, the solvent used and the nature of the plant material [8, 9]

Usually, dry vegetable raw materials are used. Through the drying operation, plant cells contract, the cell membrane breaks, the protoplasm in the cells gradually concentrates and dries, irreversible precipitation occurs that makes osmosis and diffusion processes difficult. For some vegetable raw materials, the component substances are coupled together into poorly soluble products (glyco-tannins, glyco-proteins, flavo-proteins). As a result, the dried plant material is prepared for extraction, through preliminary operations that favor the transfer of bioactive compounds from the plant material into the solvent. Therefore, the plant is subjected to grinding, pre-wetting or fermentation with plant enzymes.

Regarding the extraction process, the most common way of plant depletion is simple contact consisting in treating a quantity of plant once with a set amount of solvent, under conditions of time, agitation and variable temperature. The process of fractional percolation (multiple contact) is also often encountered, for this using percolator batteries. Regarding the choice of solvent used, its selectivity, physical properties (density, viscosity), chemical reactivity, corrosivity, toxicity, flammability, cost, recovery possibilities and costs as well as solubility of bioactive compounds are considered [8, 9]. The extraction yield is higher as the plant is on finer ground, the contact surface is larger, and the duration of the operation and the

renewal of the solvent are longer. The beneficial action of extracts rich in ursolic/oleanolic acid is higher as the content in active principles of the plant extract is higher. Conventional methods of obtaining ursolic/oleanolic acid aimed to produce a solution rich in ursolic/oleanolic acid, which, diluted 1:1 with warm water at 50-55 °C, lead to a precipitate, then after filtration and drying it results in a dry extract rich in the two components [10].

The dry extract can be added in an incapsulable mixture with other traditional herbs (little flowered puffball - *Epilobium parviflorum*, thorn - *Xanthium spinosum*, passiflora - *Passiflora incarnata*, dead nettle - *Lamium album*, small nettle - *Urtica urens*, nettle root - *Urtica dioica*, pumpkin seeds - *Cucurbita maxima*, in pressed seeds - flaxseed, milk thistle pressed seeds - *Silybum marianum* etc.) in order to obtain a food supplement with anti-inflammatory and antitumor activity [11, 12] The mentioned plants contain biologically active compounds such as: flavones, polyphenols, sitosterols, lectins, lignans, vitamins and minerals that, together with ursolic acid, act synergistically against inflammation of the prostate and bladder.

2. Experimental

The main conventional methods used for ethanolic extraction of ursolic/oleanolic acid are simple maceration (simple contact), extraction with mechanical agitation and fractional percolation.

Maceration is a simple extraction method that is performed in stainless steel vessels, of conical shape, provided with a feed mouth at the top and a drain/spill valve at the bottom. The plant is introduced ground to powder granulation at room temperature and after adding the solvent make a daily intermittent shaking of the mixture. The extraction can take 5-7 days, the solution is drained and added again to the top, in case of maceration with recirculation. Finally, after maceration and draining of the liquid solution, it is filtered through silk cloth and left to mature for another 7 days, after which it is sent for analysis. The resulting residue is sent to the compost farm or boiled additionally to produce liquid fertilizers. The final solutions can focus on rotavapor, and the recovered ethanol is reintroduced into the technological process. The procedure requires large amounts of solvent, has low efficiency and a long extraction time. To increase the reaction efficiency, decrease the extraction time and production costs, extraction by maceration, assisted by ultrasound/microwave, can be performed.

Extraction with mechanical agitation requires much shorter reaction times than simple maceration (about 1.5 - 2 hours) and requires agitation operation with the top stirrer, with low speed, 20 - 60 revolutions/min. It produces higher extraction yields compared to the maceration process and lower costs.

Simple percolation is an extraction process in which the solvent slowly passes through a layer of ground plant, under the action of gravity, entraining the active principles ceded by the plant product by osmosis, diffusion or dissolution, operation that is performed in a tronconic vessel, as in figure 2. For fractional percolation, several percolators are used, the collected fraction (called percolate) is used to extract the plant from the next vessel of the technological flow, and so on. Fractional percolation is performed in a battery of 4 tronconic maceration vessels, like the one in figure 2 below, or in separation funnels (in the laboratory). All 4 pots are loaded with equal amounts of plant, ground to a grain of 1-2 mm (so as not to clog the plant layer), over which equal amounts of solvent are added. Allow 2-3 days to macerate, with intermittent stirring, then add a warm quantity of fresh solvent from above to vessel 1 and turn on the bottom tap at a drip rate of 1-2 drops per second.



Fig. 2. Semi-industrial percolator (own source)

After consuming the solvent, allow another period to drain for an additional emptying of the solvent from the plant. Fraction 1, harvested, is added over vessel

2, on top and repeat the collection operation, and so on. To deplete the plant, the process can be resumed with the addition of fresh solvent to vessel 1. If the extraction vessel, the percolator, is larger and the amount of plant subjected to extraction in a percolator is greater than 1 kg (for example 2-3 kg), a drip rate of 5-6 drops per second is chosen, so that for each kg of plant we have a drip rate of 5-6 mL per minute [13]. The extraction is completed when the resulting solution is discolored. The residue from each pot is pressed to squeeze the plant, and the resulting waste is sent to the compost farm or boiled additionally to produce liquid fertilizers. The final solutions can focus on rotavapor, and the recovered ethanol is reintroduced into the technological process. The procedure has high efficiency and a short extraction time, compared to simple maceration. Regardless of the extraction process used, after obtaining the final solution, filter the solution through silk cloth or filter paper, then concentrate the solution with solvent recovery, see figure 3 [13], store the concentrated extract (for attachment to the support) or perform the additional dilution operation with warm water at 50-55 °C and obtaining the dry extract rich in active compounds (ursolic/oleanolic acid).

Materials

All reagents used were purchased from VWR Chemicals, of chromatographic purity. The ethanol is of pharmaceutical grade, and purified water was used for precipitation.

The plant raw materials, rosemary and sage, come from the Hofigal micro-farm. The equipment used: maceration vessels, percolators and separation funnels are provided by the Hofigal research laboratory.

For the preparation of the working samples were used: Partner AS 310.R2 analytical balance, Biovita-DEH600D artificial dryer, Retch GM-200 laboratory mill, Retch AS 200 Basic sieve machine. For the preparation of samples for analysis were used: Elmasonic ultrasonic bath P 180 H, Elma, Julabo TW8 water bath, Ortoalresa 21 R centrifuge, Buchi R-300 rotavapor, equipped with B-300 Base water bath, V-300 vacuum pump and F-308 chiller chiller, VWR MB 160 thermobalance, WTW CR 3200 thermoreactor, Milli-Q Direct-8 water purification system, MultiVap 10 nitrogen concentrator (Lab Tech).

Procedure

The starting material, rosemary and dry extract were analyzed by HPLC to determine the ursolic/oleanolic acid content of each sample. Figure 3 shows the proposed flow chart for the extraction of medicinal plant compounds.

For the plant, rosemary, 1 g sample was weighed to the analytical balance, add 50 ml MeOH, ultrasound for 30 min on Elmasonic, filter, concentrate to dryness

on the concentrator in nitrogen atmosphere MultiVap 10 (Lab Tech), redissolve in 10 ml of MeOH, filter through PTFE 0.2 µm filter and inject into the HPLC system. If necessary, dilute 1:10. For the dry extract, weigh 0.1 g sample to the analytical balance, dissolve in 10 mL MeOH by ultrasonication for 2 min, filter through PTFE 0.2 µm and inject into the HPLC system. If necessary, dilute 1:10 or 1:5.

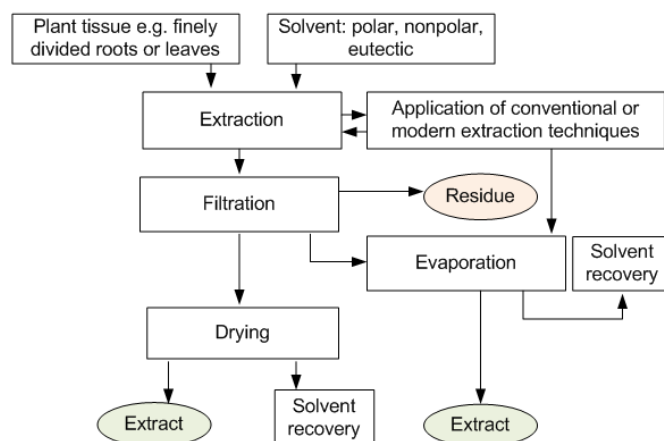


Fig. 3. Technological flow for the extraction of compounds from medicinal plants [13]

HPLC analysis was performed with Thermo Fisher Scientific Vanquish Core HPLC system, equipped with a Vanquish Core Dual Pump C (VC-P32-A-01), Vanquish Split autosampler (VC-A12-A-02), Vanquish column compartment (VC-C10-A-03), and Vanquish™ Diode Array Detector (VC-D11-A-01), the separation column was ZORBAX Eclipse Plus C18 (4.6 x 150 mm, 3.5µm). The detection reached a wavelength of 210nm. The method used is modified and adapted from Chen, Xia, 2003[14], for HPLC analysis of rosemary ursolic acid.

3. Results and discussions

3.1. Extraction of ursolic/oleanolic acid from rosemary

The results of the extraction of ursolic/oleanolic acid from rosemary, by conventional methods, are shown below, in table 1. Equation (1) is applicable to both table 1 and table 2.

$$\%Total^* = \frac{Q_{de}}{Q_{pu}} \times 100 \quad (1)$$

where:

Q_{de} = Quantity of dry extract (g)

Q_{pu} = Quantity of plant used (g).

Table 1

The dry extract obtained from rosemary, %, conventional methods.

No crt	Name of the plant	The method used	Technological flow	P1 (g)	P2 (g)	P3 (g)	Total dry extract (g)	Total* (%)
0	1	2	3	4	5	6	7	8
1	Rosemary, plant powder, 200 g	Simple maceration. 3 samples are obtained, P1,P2,P3 after 3 successive extractions in the same vessel	P1.Fresh ethanol, 96%=1,0 L, Time=4 days. Extract obtained=400 mL. Dry extract obtained=3.36g. P2.Fresh ethanol,96%=200 mL. Time=2 days. Extract obtained=100 mL.Dry extract =0.56g P3. Fresh ethanol, 96%=100 mL. Time= 2 days. Extract obtained= 200 mL, with the squeeze of the residue. Dry extract= 0.80 g. 300 g of powdered rosemary is used, which is extracted with 2 L ethanol 96%.Extract obtinut=1.7 L. Concentration 4:1. Precipitation with hot water	3\,36	0.56	0.80	4.72	2.36
2	Rosemary, plant powder, 300 g	Mechanical stirring, 1.5 hours		-	-	-	15.62	5.2
3	Rosemary, granulation 1.5 mm, 1.4 kg	Percolation with 4 separation funnels	Funnel 1(2000 mL)=400 g +1,2 L ethanol 96%.Funnel 2(2000 mL)=400 g +1,2 L ethanol 96%.Funnel 3(1000 mL)=300 g+ 800 mL ethanol 96%. Funnel 4(1000 mL)=300 g +800 mL ethanol 96%. Leave to macerate for 3 days and then add to funnel 1=500 mL ethanol 96%, fresh solvent and percolation begin, 8 h. 2.8 L extract is obtained. Concentrate and precipitate with hot water.	-	-	-	95.92	6.85

3.2. Extraction of ursolic/oleanolic acid from sage

The results of the extraction of ursolic/oleanolic acid from sage by conventional methods are shown below in table 2.

Table 2

The dry extract obtained from sage, %, conventional methods.

No crt	Name of the plant	The method used	Technological flow	P1 (g)	P2 (g)	P3 (g)	Total (g)	Total* (%)
0	1	2	3	4	5	6	7	8
1	Sage granulation 1 mm 100 g	Simple maceration	Same as rosemary	1.55	0.24	0.35	2.14	2.14
2	Sage granulation 1 mm 100 g	Mechanical stirring 1.5 hours	It is extracted with 800 mL of ethanol 96 %. 600 mL of extract are obtained. Concentration=4:1. Precipitation with hot water.	-	-	-	5.03	5.03
3	Sage granulation 1 mm 1.4 kg	Percolation with 4 separation funnels	Same as rosemary	-	-	-	79.81	5.70

The centralized results in tables 1 and 2 are represented graphically in figure 4, below, which gives us the possibility to easily compare the results obtained for the two studied plants, regarding the values of the dry extract, rich in ursolic/oleanolic acid.

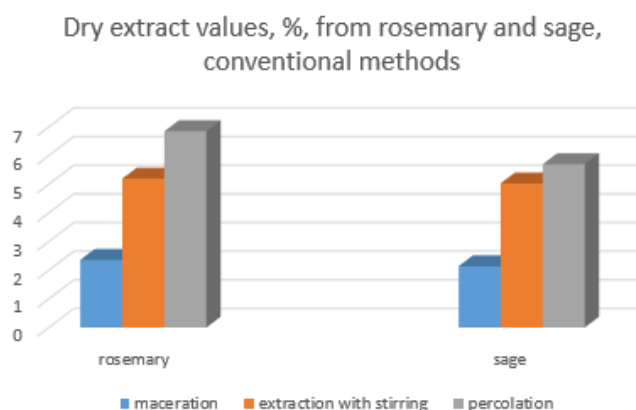


Fig. 4 Results obtained for the dry extract, rich in ursolic/oleanolic acid, %, by conventional methods.

3.3. HPLC analysis

Following the HPLC analysis, the ursolic acid content of the raw material, dry rosemary, was determined, which was 16.06 mg/g and the oleanolic acid content =7.98 mg/g (relative to the dry plant). For rosemary, for the dry extract, sample 3, simple maceration, a value was obtained for ursolic acid of 1.56 mg/g (relative to the dry plant), which represents 10.3 % of the total amount in the plant(as much as extract sample 3 during simple maceration, and the continuation of the process no longer produced results). The HPLC analysis of the samples was performed by the method described in the Experimental chapter [14] and the obtained chromatograms are reproduced below, in figures 5 and 6.

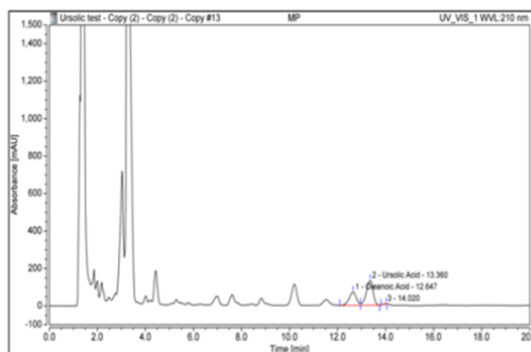


Fig. 5. HPLC chromatogram for raw material, rosemary, dried plant.

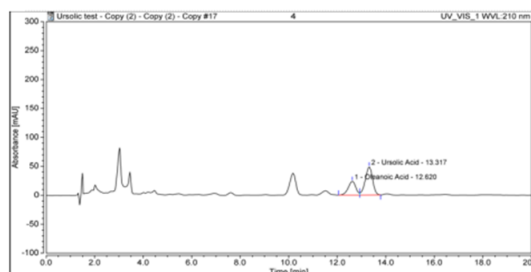


Fig. 6. HPLC chromatogram for dry rosemary extract (sample 3).

3.3. Discussions

Following the experiments carried out to obtain the dry extract of rosemary/sage and the analyses carried out, the results of which are given in the tables, figure 4 and HPLC chromatograms above, the following findings emerge:

a. The value of the dry extract obtained, %, is higher at extraction by percolation than at extraction with mechanical agitation, by at least 10% and 2.5-3 times compared to simple maceration, both rosemary and sage.

b. The results obtained show us that the extraction yield is higher as the plant is finer ground, the contact surface is larger, solvent renewal and plant depletion are higher.

c. The results obtained show us that the values are better at the ethanolic extraction of rosemary, by 10-15%, compared to the ethanolic extraction of sage.

d. The analysis of sample 3, from simple maceration, by HPLC method, to determine the ursolic acid content of the dry extract (1.56 mg/g, relative to the dry plant, i.e. 10.30% of the total ursolic acid content in the plant) led to the cessation of the technological maceration process, as the solvent no longer extracted the active compound.

e. Considering that the raw material, dried rosemary, has a content of 16.06 mg/g ursolic acid (1.6%) and according to literature data [10] the ursolic acid content in the precipitate is at least 18%, we can say that the exhaustion of the rosemary plant, by conventional methods, was made to obtain 8.88% dry extract (the plant remained with 22.86% ursolic acid unextracted). This shows that other, more severe conventional (or unconventional) methods can be found that can deplete the plant. Such a conventional process that can be proposed, for the future, is thermal extraction with mechanical agitation, at temperatures of 40-450C, with thermostat and reaction duration of 2 hours, or improvement of the percolation process (solvent renewal and plant exhaustion)

f. Another proposal, for the future, is to establish a technological flow for the reuse of ethanol resulting from extraction concentration operations, using the thermal extraction process with mechanical agitation or percolation with 2 batteries of separation funnels (2 x 4 = 8 funnels).

4. Conclusions

The need to use conventional methods of extracting ursolic acid from rosemary/sage, in the form of a dry precipitate, has led to simple and cost-free methods of extracting bioactive compounds. These methods allow us to obtain a dry extract that can be added, in an incapsulable mixture, along with other traditional medicinal plants, in order to obtain a dietary supplement with anti-inflammatory and antitumor activity. The final incapsulable mixture contains biologically active compounds such as: flavones, polyphenols, sitosterols, lectins, lignans, vitamins and minerals that, together with ursolic acid, act synergistically against inflammation of the prostate and bladder. It is necessary to improve technologies to find ways to deplete the plant and to reuse the recovered ethanol in the technological process. Not all experiments performed in the experimental part gave satisfactory results, especially extraction by simple maceration. The results of this study show that two of the proposed methods are sustainable and economical

for obtaining bioactive compounds from medicinal plants, in order to develop new dietary supplements.

Acknowledgements

The authors thank for the financial support received through the Human Capital Operational Program, Priority Axis 6 - Education and Skills, Project: Preparation of PhD students and postdoctoral researchers in order to acquire applicative-SMART research skills, MySMIS Code:153734.

REFERENCES

- [1] Nadinic E., Gorzalczany S., Rojo A., Baren C.V., Topical anti-inflammatory activity of *Gentiana alba*, *Fitoterapia*, 70, 2, (1999), 166-171.
- [2] Alvarez M. E., Rotelli A.E., Pelzer L. E., Saad J. R., Giordano O., Phytochemical study and anti-inflammatory properties of *Lampaya Hieronymi* Schum. ex Moldenke, *Farmaco*, 55, 6-7, (2000), 502-505.
- [3] M. A. Collins, H.P.C., Antimicrobial activity of carnosol and ursolic acid: Two anti-oxidant constituents of *Rosmarinus officinalis* L. *Food Microbiol*, 1987. 4: p. 311-315.
- [4] Mourya A., Akhtar A., Ahuja S., Sah S.P., Kumar A., Synergistic action of ursolic acid and metformin in experimental model of insulin resistance and related behavioral alterations, *Eur J Pharmacol*, 835, (2018), 31-40.
- [5] Khwaza V., Opeoluwa O.O., Aderibigbe B.A., Antiviral activities of oleanolic acid and its analogues, *Molecules*, 23, 9, (2018).
- [6] Bai X., Lai T., Zhou T., Li Y., Li X., Zhang H., In Vitro Antioxidant Activities of Phenols and Oleanolic Acid from Mango Peel and Their Cytotoxic Effect on A549 Cell Line, *Molecules*, 23, 6, (2018), 1395.
- [7] Siani A.C., Nakamura M.J., Dos Santos D.S., Mazzei J.L., do Nascimento A.C., Valente L.M., *Efficiency and selectivity of triterpene acid extraction from decoctions and tinctures prepared from apple peels*, *Pharmacogn Mag*, 10 (Suppl 2), S225-31, 2014.
- [8] Stoian S.I., Savopol E., *Extrakte farmaceutice vegetale*, Ed. Medicala, Bucharest, Romania, 1977.
- [9] Smigelschi O., *Revista de chimie*, 32, 2, (1981), 150.
- [10] Yoshida N., Mori C., Sasaki T., *Process for preparing high purity corosolic acid and high purity ursolic acid*, Kenko Corporation, Tokyo-To(JP), Tokiwa Phytochemical Co, Ltd Chiba-Ken(JP): USA, 2006.
- [11] Khwaza V., Oyediji O.O., Aderibigbe B.A., Ursolic Acid-Based Derivatives as Potential Anti-Cancer Agents: An Update, *Int J Mol Sci.*, 21, 16, 2020, 1-27.
- [12] Kashyap D., Sharma A., Tuli H.S., Punia S., Sharma A.K., Ursolic Acid and Oleanolic Acid: Pentacyclic Terpenoids with Promising Anti-Inflammatory Activities, *Recent Pat Inflamm Allergy Drug Discov.*, 10, 1, (2016), 21-33.
- [13] Bitwell C., Indra S.S., Luke C., Kakoma M.K., A review of modern and conventional extraction techniques and their applications for extracting phytochemicals from plants, *Scientific African*, 19, (2023), 1-19.
- [14] Chen J.H., Xia Z.H., Tan R.X., High-performance liquid chromatographic analysis of bioactive triterpene in *Perilla frutescens*, *Journal of Pharmaceutical and Biomedical Analysis*, 32, (2003), 1175-1179.

THERMAL TREATMENT AN GREEN TECHNOLOGY IN MEDICAL WASTE MANAGEMENT

Adela CIOBANU^{1*}, Carmen ROBA¹, Cristina MODOI¹, Alexandru OZUNU¹

¹ Faculty of Environmental Science and Engineering, University of Babeş-Bolyai,
30 Fantanele Street, RO-400294, Cluj-Napoca, Romania

Abstract

Considering the priority of Environmental Protection and Security in the European Union, which is a significant factor for ensuring human health, it is essential to implement and promote various actions aimed at reducing environmental pollution, such as effective waste management strategies.

In literature and in European legislation, hazardous medical waste classification and standard waste classification codes have been given particular importance. The goal of efficient waste management is to minimize the presence of hazardous substances in products and/or substitute hazardous substances with safer alternatives. Due to the potentially detrimental nature of medical waste, there is a need to promote advanced technologies for transforming hazardous medical waste into less hazardous waste. The waste treated in this way can be used through recycling, through co-incineration processes or, as a less sustainable process, stored in the non-hazardous landfill.

The objective of this study is to introduce this thermal treatment technology for hazardous medical waste as a comprehensive business model, effectively integrating all material flows within a circular process aimed at ensuring efficient resource utilization. Consequently, the minimization of thermally treated hazardous medical waste generation is achieved, aligning with the "Best Available Techniques BAT" standards, ultimately contributing to enhancing environmental safety and security.

Key words: medical waste treatment facilities, incineration, sterilization, circular economy, pollution, alternative methods, competitive advantage.

1. Introduction

The action plan for the circular economy includes a policy of "durable products" to support the circular design of all products based on a common methodology and principles. It prioritizes material reduction and reuse before recycling; promotes new business models and establishes minimum requirements to prevent the introduction of environmentally harmful products into the EU market. National legislation (Government Emergency Ordinance 92/202, Government of Romania, 2021) regulates the extended producer responsibility aiming to: reduce waste quantities; reuse waste and recycle it for transformation

¹ Corresponding author: adela.romeghea@ubbcluj.ro

into new valuable products later. Ensuring a healthy environment through selective waste collection is a priority and a legislative requirement. Materials that may initially appear as waste can be treated and reused in various greener ways to avoid unnecessary waste [1]. Recycling is the easiest way to help the environment. Optimal waste recycling means applying all necessary operations before landfilling, thereby reducing or avoiding negative impacts on natural ecosystems [2, 3].

The objective of this work is to present the progress made by Romania in achieving the final elimination of hazardous medical waste through environmentally friendly methods. This paper emphasizes the decision to implement and select those technologies that promote efficient management in the final disposal of hazardous medical waste. Selective collection of medical waste is the determining factor in choosing the technology for their final disposal. Based on national reports, the National Institute of Public Health (INSP) compiles annual reports highlighting that in recent years, more and more economic operators, who previously treated medical waste exclusively through incineration, are beginning to promote thermal treatment technologies that transform a portion of hazardous medical waste into non-hazardous waste with minimal environmental impact [4, 5].

From a financial perspective, microwave thermal treatment is a business model aimed at ensuring a higher degree of sustainability and greater potential for reuse of the products obtained. This supports techniques favorable to the circular economy and investments in it. Authorized economic operators in the relevant market can prevent the generation of hazardous waste by limiting the presence of hazardous substances in products and replacing hazardous substances with "safer" alternatives. Microwave thermal treatment represents an alternative solution to the incineration method for hazardous medical waste. The microwave thermal treatment technology is based on the principle of continuity in the final disposal process of hazardous medical waste, with the generation of raw material for co-incineration [6].

By promoting the concept of the circular economy, this business model offers several benefits to the environment and public health by enhancing competitiveness in the relevant market and fostering innovation. Medical waste treated thermally and used as raw material in co-incineration reduces pressure on natural resources (e.g, biomass), improves raw material supply security, based on analysis bulletins [7].

Generators of hazardous medical waste will have the opportunity to collaborate with holders of sustainable and more innovative technologies, which will enable them to access hazardous medical waste disposal services at fair rates.

This drives economic growth by promoting "safer" job opportunities, protecting personnel handling, and improving quality of life. The hierarchy of

hazardous medical waste management is useful when applied correctly, determining the choice of an optimal method for the final disposal of hazardous medical waste, being the primary priority of the EU, and waste landfills should be the last resort for final disposal. Hazardous medical waste refers to those categories of medical waste that require special handling, storage, transport, and disposal measures, applying management processes directly proportional to the category of hazardous medical waste, depending on the specific nature of the generating healthcare facility [8].

In the specialized literature and European legislation, special importance has been given to the classification of hazardous medical waste and the use of standard codes because, depending on the nature of the medical waste and the presence of harmful content, a specific treatment for final disposal is applied, accepted by the World Health Organization [9].

Environmental auditing and assessment of the impact on the environment, along with identifying the negative aspects of each phase of the life cycle, of hazardous waste final disposal technologies, pave the way for more ecological technologies. These technologies lead to environmental benefits and cost savings compared to the operation costs of hazardous medical waste final disposal technologies, in a comparative analysis: Advantages/Benefits.

Theoretical Considerations at National and International Levels in the Research Field

Romania and the EU are currently dependent on imports of raw materials. The main issues addressed by the European Court of Auditors are presented below (figure 1) (European Court of Auditors).

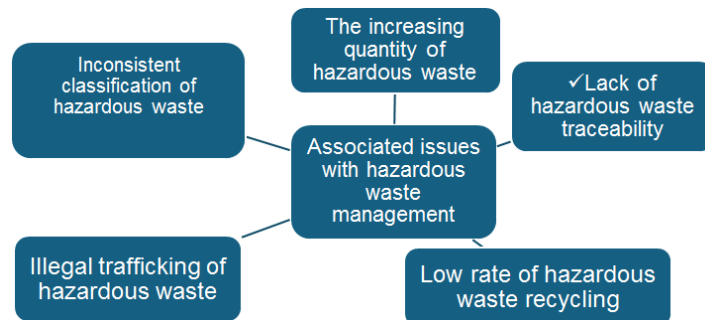


Fig. 1. Aspects of hazardous waste management (source Doc 2/2023) [10].

According to statistics compiled by the Circular Economy Monitoring Framework, Romania has the weakest performance in waste management relative to GDP, waste treatment, and the use of recyclable materials in the economy


(National Strategy for the Circular Economy of Romania - Official Monitor No. 943/27.09.2022)) [11].



Fig. 2. Medical waste classification source [12]

The categories of waste resulting from medical activities, according to the Technical Norms regarding the management of waste resulting from medical activities approved at the national level (Government Decision no. 856 of August 16, 2002), are outlined in table 1.

Table 1
Categories of waste resulting from medical activities (Government Decision no. 856 of August 16, 2002)

Medical waste code	Waste content	Packing type
Sharps waste (code 18 01 01/18 01 03*) 	Disposable needles, sutures, catheters, needles with syringes, cannulas, scalpel blades, pipettes, laboratory glassware or other glassware broken or unused, expired, which has not come into contact with potentially infectious material.	They are collected in rigid plastic containers, yellow in color, resistant to mechanical actions, provided at the top with a special lid that allows the insertion of waste in one direction only. The containers are equipped with a sturdy handle for easy transportation to the temporary storage location and, subsequently, to the final disposal site.

Infectious waste (code 18 01 03*)	as well as viruses, bacteria, parasites, and/or toxins from microorganisms, infusion sets with tubing, containers containing blood or other biological fluids, surgical drapes, gloves, probes, and other disposable materials, compresses, dressings, and other contaminated materials, dialysis membranes, plastic bags for urine collection, used laboratory materials, diapers from patients admitted to healthcare facilities with infectious diseases or infectious disease wards of healthcare facilities, animal carcasses resulting from research and experimentation activities.	They are collected in cardboard boxes lined with yellow polyethylene bags or yellow polyethylene bags marked with the biological hazard symbol.
Anatomical-pathological waste (code 18 01 02/18 01 03*)	Fragments from organs and human organs, anatomical parts, organic fluids, biopsy material resulting from surgical and obstetric operating rooms (fetuses, placentas, etc.), anatomical parts resulting from autopsy laboratories, blood containers, etc. All these wastes are considered infectious and are included in category 18 01 03*.	They are mandatory collected in rigid cardboard boxes, lined inside with polyethylene bags that must be securely sealed, or in boxes made of rigid plastic material with a tightly sealing lid, marked in yellow and specifically designed for this category of waste, marked with the biological hazard symbol.
Waste whose collection and disposal are not subject to special infection prevention measures (code 18 01 04)	Uncontaminated clothing, plaster casts, uncontaminated linens, waste resulting from the treatment/decontamination of infectious waste, containers that have contained medications other than cytotoxic and cytostatic ones, etc.	Non-hazardous waste is collected in black polyethylene bags labeled "Non-hazardous waste". In the absence of these, transparent and colorless polyethylene bags are used.
Chemical waste - except for radioactive waste (code 18 01 06 and 18 01 07)	Solid, liquid, or gaseous chemical substances, acids, bases, halogenated solvents, other types of solvents, organic and inorganic chemicals, including residual products generated during laboratory diagnostics or non-hazardous organic and inorganic chemicals	Chemical waste is collected and packaged in PVC containers with a capacity not exceeding 5 liters for liquid substances and 5 kilograms for solid substances.

	(which do not require specific labeling).	
Pharmaceutical waste - except for radioactive waste (code 18 01 08* and 18 01 09)	Expired medications, solutions for infusion without added traces of infectious hazard, cytotoxic-cytostatic substances, contrast agents without hazardous, toxic, radioactive content, etc., and residues of chemotherapeutic substances, which may be cytotoxic, genotoxic, mutagenic, teratogenic, or carcinogenic.	They are collected separately, in single-use containers that are safe and equipped with lids, which are disposed of separately.

The preparation and specialization of operators in waste treatment facilities are vital for the compliant operation of technologies in the relevant market. To carry out efficient final disposal activities of waste, operators must place acute importance on the technologies they manage, their life cycle, by applying ecological methods, establishing internal and external plans, and procedures that minimize pollution impact on the environment, based on the relationship: potential - performance - process (competitive advantage) [13]

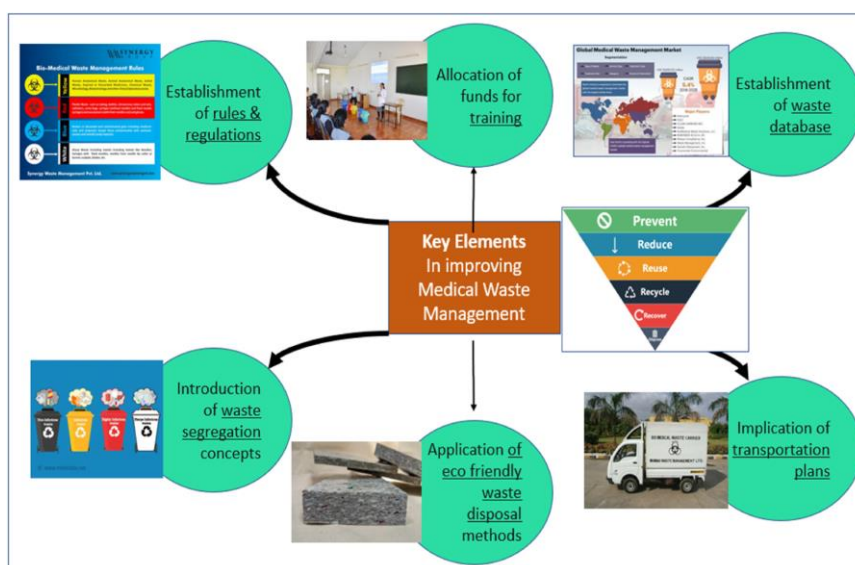


Fig. 3. Key elements for implementing a successful medical waste management system [14]

On the territory of Romania, there are currently 8 waste incineration plants and 16 thermal treatment-sterilization facilities (www.anpm.ro (figure 4)). The representative geographical market of the location of hazardous waste final disposal stations highlights the high costs associated with transporting hazardous

waste to the final disposal stations, which influences both environmental emissions and costs [15].

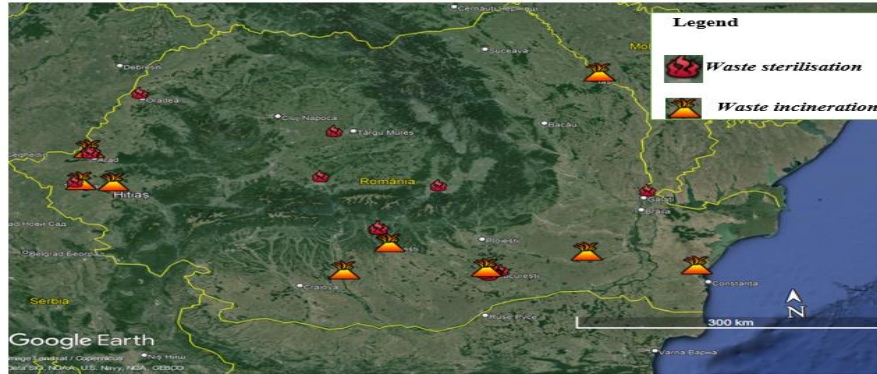


Fig. 4. The map of Romania - Medical waste disposal technologies www.ubbcluj.ro 2024

2. Experimental

Each method of hazardous medical waste disposal depends on numerous factors, including the nature and composition of the medical waste, equipment and facilities, availability of operations and physical maintenance, allocated spaces for the compliant functioning of technologies, access to utilities, possibility of implementing photovoltaic panels, skill set of the employed personnel, legislative regulatory requirements, public acceptability, costs, volume of hazardous medical waste (85% non-hazardous medical waste, 15% hazardous medical waste) [16].

Incineration

Incineration represents a significant risk factor in the occurrence of fires and accidents, impacting both workers and communities, especially during the Covid-19 period when significant quantities of medical waste were incinerated (Lemma et al., 2022). Directive 2001/80/EC on the limitation of emissions of certain pollutants into the air from large combustion plants aims to reduce emissions of sulfur dioxide (SO_2) and nitrogen oxides, ensuring that depositions and concentrations remain below critical loads and levels, including reducing particulate matter emissions.

In figure 5, two of the nationally authorized incinerators (Slobozia and Dolj) are depicted.



Fig. 5. Types of incinerators for hazardous medical waste currently existing in Romania (a - incinerator in Ialomita <https://obiectiv.net/?p=14465>; b - incinerator in Dolj <https://www.gds.ro/Local/2022-01-07/>)

Wastes (sludge or dust) resulting from gas purification systems during the incineration of medical waste are used in the energy industry as alternative fuel in power plants or cogeneration facilities. Additionally, in the cement industry, solid residues can be co-processed in cement factories by adding them to the kilns, where hazardous substances are destroyed, resulting in a safer final product (ANPM, 2019).

Hazardous medical waste thermal treatment

The hazardous medical waste thermal treatment facility (figure 6) operates as a closed system so that throughout the thermal treatment cycle, the waste is not in contact with the atmosphere inside the chamber, starting from the beginning, starting from the loading stage into the equipment and until disposal [14].



Fig. 6. Hazardous medical waste microwave treatment facility <https://www.ecosteryl.com>

There are microwave thermal treatment stations of various capacities available for purchase, which can be acquired based on the specific needs of the waste-generating area (number of hospitals, quantities of waste generated etc.) [17].

From an economic standpoint, this business model of thermal treatment of medical waste using microwave technology in the hazardous medical waste final disposal market is found to be efficient and effective. Microwave thermal treatment transforms hazardous medical waste into non-hazardous waste through more circular solutions, innovative recycling solutions.

The quality of thermally treated medical waste is constantly monitored throughout the entire treatment process, with temperatures being recorded for continuous monitoring. To achieve the status of high-performance technology, analysis bulletins are periodically prepared. Reduction in contamination is determined by evaluating the microbiological degree of contamination of raw (untreated) waste and treated waste. During the test, the total flora of the raw waste before treatment ranged between $2.2 \cdot 10^4$ CFU/g and $1.7 \cdot 10^4$ CFU/g (CFU = colony-forming unit). After treatment, the bacterial content was significantly reduced, with their presence no longer being detected (less than 4 CFU/g). The quality of thermal treatment is verified using a control sample that is introduced into the neutralization flow at the entrance to the action area and recovered at the exit of the sterilized waste. Decontamination quality is checked in real-time, and operating parameters are recorded every 30 seconds (OMS 1729/2012) [18].

From an environmental protection perspective, the suction system in the thermal treatment facility prevents the release of dust from both the feeding bunker and the discharge bunker. Air treatment through washing, disinfection, deodorization, and activated carbon filtration maintains air quality. Noise levels are below the minimum standards currently in force. The efficiency of the technological flow of thermal treatment facilities ranges from 90% to 99%. Waste after thermal treatment becomes inert, with volume reduction of up to 80-90%. During incineration, only about 4-6% ash is produced. (OMS 1729/2012)

Analyzing hazardous medical waste final disposal facilities, it can be observed that the direction is towards supporting ecological installations to maximize ecological, technical, and hazardous waste management safety in relation to the directly served area, directly proportional to the quantities of waste generated in the territory (supply/demand).

Comparative analysis of the advantages and disadvantages derived from the two thermal treatment systems for medical waste in Romania is presented in the table 2.

Table 2

Advantages and disadvantages of thermal sterilization method versus incineration:	
THERMAL STERILIZATION	INCINERATION
Advantages	
➤ Applicability: for waste with codes 18.01.03* and 18.01.01 (representing 80-	➤ Applicability: for the entire class of medical waste (code 18.01).

<p>85% of total medical waste)</p> <ul style="list-style-type: none"> ➤ Does not release harmful gases and substances into the atmosphere or soil. ➤ The waste resulting from thermal treatment is microbiologically inert, shredded, and compacted. 	<ul style="list-style-type: none"> ➤ Direct incineration of waste takes place without the need for preliminary selective waste handling stages. ➤ Energy recovery. ➤ Complex ecological technology ensuring the combustion of both raw waste and resulting pollutants, as well as dry neutralization followed by wet gas neutralization operations; water cooling of ash and its extraction.
DISADVANTAGES	
<ul style="list-style-type: none"> ➤ Presents minimal risks of technical failures associated with power outages or failure of the solar panel system, which can be supplemented by high-power generators. ➤ There is a risk of malfunctioning of the shredding device or waste compactors, which makes the operation of the facility impossible. 	<ul style="list-style-type: none"> ➤ Requires auxiliary materials for the technological gas filtration process: sodium hydroxide, sodium bicarbonate, and activated carbon granules. ➤ Consumption of sanitizing substances used: sodium hypochlorite and/or other disinfectant solutions. ➤ High water consumption: in the technological process, cooling water,

<p>➤ Without energy recovery.</p> <p>[19]</p>	<p>washing water, and sanitation water for equipment within the incineration facility, as well as water needed for cleaning associated spaces.</p> <p>➤ Fuel consumption: liquefied petroleum gases for the pilot flame and natural gases.</p> <p>➤ Lubricants: vaseline and hydraulic oil.</p> <p>➤ Risk of accidents - open flame.</p> <p>➤ Specialized personnel involved in the process, risk of exposure.</p> <p>➤ High electricity consumption.</p> <p>➤ Use of specialized software for automated emission control.</p> <p>➤ Building permit required.</p> <p>(Deepak et al., 2022)</p>
---	--

The result for the elimination of all categories of waste consists of the existence of multiple technologies, with the benefit of energy recovery. Technologies that are economically competitive and have minimal environmental impact are promoted [12].

3. Results and discussions

Microwave thermal treatment is a closed, automated system that is easy to operate, with minimal environmental pollution. According to technical specifications, it is a demountable technology that can be assembled in enclosed spaces and as close as possible to the generation site. Access to utilities can be arranged depending on the area. Drinking water supply can be obtained from a nearby drilled well if there is no water distribution network in the area. Electricity supply can be supplemented by installing photovoltaic panels. After treatment with electromagnetic waves, the resulting medical waste can be stored in landfills as municipal waste. This technology is not suitable for treating blood or chemicals and may produce an unpleasant odor [20].



Fig. 7 Microwave sterilization process shredded (www.ecosterile.com)

The microwave sterilization process (figure 7) is based on electromagnetic waves with a high frequency of 2450 MHz. The principle of treatment with electromagnetic waves is characterized by its absorption by water, fats, and proteins. It is identified by the selective absorption characteristics of energy by microbial cells, placing them in the energetic field of high-frequency electromagnetic wave oscillation. The vibration of the electric field rapidly increases the energy in the cell membrane, leading to cell death, thereby killing the pathogens in medical waste. The moisture content of medical waste has a significant impact on microwave treatment, as does the exposure time and mixing interval of the medical waste.

The information regarding the characteristics of medical waste is necessary to define the typology of equipment required for the treatment of hazardous medical waste. Moisture content is one of the key parameters in the process of hazardous medical waste disposal.

The presence of a high percentage of moisture reduces the calorific value. Increased moisture content in waste will lead to the reproduction and spread of bacteria and sources of infection (table 3 and table 4).

Table 3

Moisture content of medical waste - source [21]

Study category	Plastic %	Biomass %	Synthetic fibers %	Rubber %	Inorganic salts %	Metal se%	Decontamination %	The moisture content of the samples%
Untreated medical waste	4.84	58.52	16.62	4.85	1.78	1.85	100	44.75

Table 4

Classification of medical waste by materials source [21]

Classification material	Major medical supplies
Synthetic fibers	Disposable bed sheets, treatment towels, surgical gowns, surgical caps, masks, surgical drapes, sutures.
Biomass	All types of cotton gauze dressings, absorbent cotton, cotton pads, paper consumables, abdominal belts.
Plastic	Disposable syringes, infusion sets, all types of liquid medications in plastic bags, bottles, negative pressure drainage bags, all types of plastic cannulas, catheters and gags, disposable plastic bags, plastic trays.
Rubber	Surgical rubber gloves, rubber stoppers from all medication bottles.
Inorganic salts	Plaster bandages, all types of liquid medications in vials.
Metals	Surgical knife blades, aluminum seal needles from liquid medication bottles

The calculation of the calorific value demonstrates the usefulness of treating this medical waste thermally through microwaves, as they can be used as raw material for co-incineration [22]

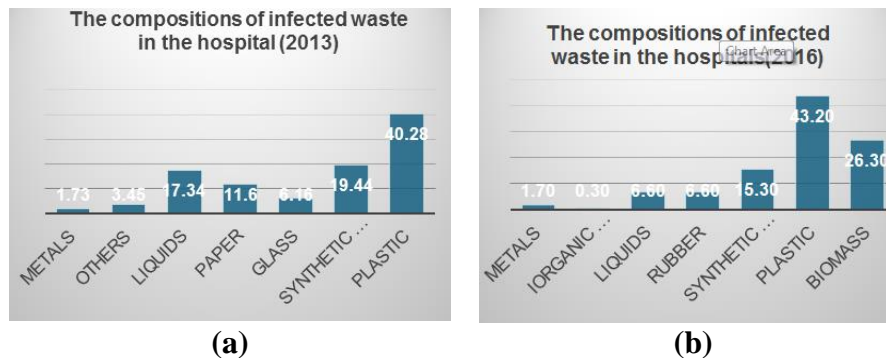


Fig. 8. Classification of medical waste by materials (source a.Ferdowsi et al., 2013) (source b.Zhang et al., 2016)

According to the data provided in table 5, the waste subjected to the thermal treatment process complies with the maximum limits imposed by national legislation (Order 95/2005) for the acceptance of waste in non-hazardous waste landfills. It is worth mentioning that the data are taken from the Test Report (2022) of the economic agent who provided consent for the use of the data.

Table 5

Chemical analysis of the waste sample leached with distilled water at a 1/10 ratio yielded the following results.

Parameter	Measurement unit	Results obtained for the waste sample (shredded)	Criteria for accepting waste at non-hazardous waste landfills (Order 95/2005)
Dry matter	mg / kg s.u	86.2	-
pH		8.49	-
Sulfates	mg / kg s.u	2920	20.000
Chlorides	mg / kg s.u	1695	15.000
Fluorides	mg / kg s.u	123.6	150
DOC	mg / kg s.u	8380	800
DOC(pH=7,85)	mg / kg s.u	8340	800
TDS	mg / kg s.u	1535	60.000
As	mg / kg s.u	0.04	2
Ba	mg / kg s.u	0.91	100
Cd	mg / kg s.u	0.01	1
Cr	mg / kg s.u	0.40	10
Cu	mg / kg s.u	0.35	50
Hg	mg / kg s.u	<0.01	0.20
Mo	mg / kg s.u	0.19	10
Ni	mg / kg s.u	0.26	10
Pb	mg / kg s.u	0.13	10
Sb	mg / kg s.u	0.16	0.70
Se	mg / kg s.u	0.02	0.5
Zn	mg / kg s.u	43.8	50



Biomass is the main carrier of liquid waste, as most medical materials from biomass are cotton bandages, and their main ingredient is cellulose. In the

medical treatment process, most bodily fluids, including blood, liquids, and fluids, are absorbed and stored in the gauze bandages, making them the largest moisture carrier in medical waste.

In conclusion, the bulk density of medical waste is 249 kg/m^3 , and the moisture content is 44.75%. Without information on the density of medical waste, it is not possible to calculate cost-effectiveness per transport unit and final processing capacity of hazardous medical waste [20].

The thermal treatment facility is fully automated, so the operator does not come into contact with medical waste, being equipped with an integrated control panel with a warning system in case of any deficiencies during the process, displaying operating parameters and alerts.

4. Conclusions

The current technology is equipped with rigorous process control systems for the final disposal of hazardous medical waste, with advanced command devices. Legislation requires the authorization of waste disposal stations only if they have self-monitoring software for operating parameters with data transmission to regulatory authorities [8, 20].

To properly manage all medical waste generated by hospitals, it is important for the operator to have both thermal treatment methods and reserve equipment to avoid losses that may occur during maintenance periods, technical failures, or the inability to dispose of all categories of medical waste. (OMS 1226/2012, HG 856/2002)

Typically, especially in the case of hazardous waste, a well-executed waste mixture recipe minimizes the need for auxiliary fuel input, according to the calorific power calculation.

The microwave thermal treatment method is easy to assemble and operates with minimal utility connections. The economic and financial barriers faced by a company aiming to enter the market are represented by high costs associated with equipment acquisition, operation, maintenance, and upkeep [23]. The cost of medical waste recovery and recycling systems is the main obstacle that puts the promotion and implementation of new technologies on hold [22]. Efficient medical waste management involves specialized personnel knowledgeable about the field in the relevant market [24].



Fig. 8. Positive aspects of microwave thermal treatment www.ubb.cluj

We choose microwave thermal treatment for several reasons:

- Efficiency: Microwave technology can efficiently treat hazardous medical waste without requiring pre-treatment or sorting stages.
- Safety: Microwave treatment occurs in a closed environment, protecting operators from risks associated with other methods like incineration.
- Environmental protection: Microwave use reduces emissions of toxic gases and particles into the atmosphere compared to other medical waste treatment methods.
- Flexibility: This technology can be adapted to different capacities and installed in various locations, including areas with limited space.
- Energy savings: Microwave treatment only requires electric power, eliminating the need for gas or other fuels.
- Volume reduction: Microwave treatment can reduce the volume of medical waste, facilitating its management and disposal [16].

The primary outcome of this research article is to present data indicating the attitude and openness of economic operators towards adopting eco-friendly technologies. According to specialized literature, over the past decade, a beneficial approach has been observed regarding the direction and evolution of activities carried out by economic operators in the relevant market. The competitive environment determines a specialized behavior of both the public and private sectors in the provision of collection, transportation, and final disposal services for hazardous medical waste. The existence of supportive policies and funding for industries at the regional level represents the confidence that

economic operators may have in innovative investments contributing to medium and long-term development [25].

REFERENCES

- [1] Agenția Europeană de Mediu, 2021. (2023). Strategia AEM–Eionet 2021–2030. http://eea.europa.eu/ro.file:///C:/Users/Adela%20Romeghea/Desktop/AN%201%202023/strategia_RGB_RO%202021-2030.pdf
- [2] MacNeill, A. J., Hopf, H., Khanuja, A., Alizamir, S., Bilec, M., Eckelman, M. J., Hernandez, L., McGain, F., Simonsen, K., Thiel, C., Young, S., Lagasse, R., & Sherman, J. D. (2020). Transforming The Medical Device Industry: Road Map to A Circular Economy: Study examines a medical device industry transformation. *Health Affairs*, 39(12), 2088–2097. <https://doi.org/10.1377/hlthaff.2020.01118>
- [3] Guvernul Romaniei. (f.a.). PLANUL DE ACTIUNE pentru Strategia națională privind economia circulară Anexa 2. [/www.mmediu.ro/app/webroot/uploads/files/Planul%20de%20actiune%20pentru%20Strategia%20Nationala%20privind%20Economia%20Circulara%20-%20varianta%20finala.PDF](http://www.mmediu.ro/app/webroot/uploads/files/Planul%20de%20actiune%20pentru%20Strategia%20Nationala%20privind%20Economia%20Circulara%20-%20varianta%20finala.PDF)
- [4] INSP BUCURESTI. (2022). Raportul pentru sanatate si mediu 2022. <https://insp.gov.ro/cnmrmc/rapoarte/>
- [5] INSP BUCURESTI. (2021b). Raport pentru sanatate si mediu 2021. <https://insp.gov.ro/cnmrmc/rapoarte/>
- [6] Li, J., Wang, H., Chen, H., Wu, H., Xu, G., Dong, Y., Zhao, Q., & Liu, T. (2023). Comparative thermodynamic and techno-economic analysis of various medical waste-to-hydrogen/methanol pathways based on plasma gasification. *Applied Thermal Engineering*, 221, 119762. <https://doi.org/10.1016/j.applthermaleng.2022.119762>
- [7] Deshmukh, P., & Jagdale, T. (2023). Production of Energy from Waste Material—A Review. În S. Tamane, S. Ghosh, & S. Deshmukh (Ed.), *Proceedings of the International Conference on Applications of Machine Intelligence and Data Analytics (ICAMIDA 2022)* (Vol. 105, pp. 122–129). Atlantis Press International BV. https://doi.org/10.2991/978-94-6463-136-4_13
- [8] Çelik, S., Peker, İ., Gök-Kısa, A. C., & Büyüközkcan, G. (2023). Multi-criteria evaluation of medical waste management process under intuitionistic fuzzy environment: A case study on hospitals in Turkey. *Socio-Economic Planning Sciences*, 86, 101499. <https://doi.org/10.1016/j.seps.2022.101499>
- [9] Sepetis, A., Zaza, P. N., Rizos, F., & Bagos, P. G. (2022). Identifying and Predicting Healthcare Waste Management Costs for an Optimal Sustainable Management System: Evidence from the Greek Public Sector. *International Journal of Environmental Research and Public Health*, 19(16), 9821. <https://doi.org/10.3390/ijerph19169821>
- [10] CURTEA DE CONTURI EUROPEANA. (2023). Acțiunile întreprinse de UE pentru a aborda problema cantității tot mai mari de deșeuri periculoase. www.eca.europa.eu/Lists/ECADocuments/RW23_02/RW_Hazardous_waste_RO.pdf
- [11] M.MEDIU. (2023). Strategia națională privind economia circulară. Romania. file:///C:/Users/Adela%20Romeghea/Desktop/AN%201%202023/Strategia%20Nationala%20Privind%20economia%20circulara%202022%20ANEXA-32.pdf
- [12] Mazzei, H. G., & Specchia, S. (2023). Latest insights on technologies for the treatment of solid medical waste: A review. *Journal of Environmental Chemical Engineering*, 11(2), 109309. <https://doi.org/10.1016/j.jece.2023.109309>

- [13] Alam, O., & Mosharraf, A. (2020). A preliminary life cycle assessment on healthcare waste management in Chittagong City, Bangladesh. *International Journal of Environmental Science and Technology*, 17(3), 1753–1764. <https://doi.org/10.1007/s13762-019-02585-z>
- [14] Wang, H., & Bolan, N. (2023). Review on distribution, fate, and management of potentially toxic elements in incinerated medical wastes. *Environmental Pollution*, 321, 121080. <https://doi.org/10.1016/j.envpol.2023.121080>
- [15] Wawale, S. G., Shabaz, M., Mehbodniya, A., Soni, M., Deb, N., Elashiri, M. A., Dwivedi, Y. D., & Naved, M. (2022). Biomedical Waste Management Using IoT Tracked and Fuzzy Classified Integrated Technique. *Human-centric Computing and Information Sciences*, 12(0), 401–414. <https://doi.org/10.22967/H CIS.2022.12.032>
- [16] Kenny, C., & Priyadarshini, A. (2021). Review of Current Healthcare Waste Management Methods and Their Effect on Global Health. *Healthcare*, 9(3), 284. <https://doi.org/10.3390/healthcare9030284>
- [17] Bolan, S., Padhye, L. P., Kumar, M., Antoniadis, V., Sridharan, S., Tang, Y., Singh, N., Hewawasam, C., Vithanage, M., Singh, L., Rinklebe, J., Song, H., Siddique, K. H. M., Kirkham, M. B., Wang, H., & Bolan, N. (2023). Review on distribution, fate, and management of potentially toxic elements in incinerated medical wastes. *Environmental Pollution*, 321, 121080. <https://doi.org/10.1016/j.envpol.2023.121080>
- [18] INSP BUCURESTI. (2021a). Ghidul deseurilor medicale INSP Bucuresti anul 2020. https://insp.gov.ro/download/cnmrmc/Ghiduri/Igiena%20Mediului%20si%20Apa%20Potabila/Ghid_deseuri_medicale_2021.pdf
- [19] MINISTERUL SANATATII. (f.a.). ORDIN nr. 1.279 din 14 decembrie 2012. <https://legislatie.just.ro/Public/DetaliiDocumentAfis/144282>
- [20] Matalakah, F. (2023). Recycling of hazardous medical waste ash toward cleaner utilization in concrete mixtures. *Journal of Cleaner Production*, 400, 136736. <https://doi.org/10.1016/j.jclepro.2023.136736>
- [21] Xu, L., Dong, K., Zhang, Y., & Li, H. (2020). Comparison and analysis of several medical waste treatment technologies. *IOP Conference Series: Earth and Environmental Science*, 615(1), 012031. <https://doi.org/10.1088/1755-1315/615/1/012031>
- [22] Zhang, L., Wu, L., Tian, F., & Wang, Z. (2016). Retrospection-Simulation-Revision: Approach to the Analysis of the Composition and Characteristics of Medical Waste at a Disaster Relief Site. *PLOS ONE*, 11(7), e0159261. <https://doi.org/10.1371/journal.pone.0159261>
- [23] Ferdowsi, A., Ferdosi, M., & Mehrani, M. (2013). Incineration or Autoclave? A Comparative Study in Isfahan Hospitals Waste Management System (2010). *Materia Socio Medica*, 25(1), 48. <https://doi.org/10.5455/msm.2013.25.48-51>
- [24] Attrah, M., Elmanadely, A., Akter, D., & Rene, E. R. (2022). A Review on Medical Waste Management: Treatment, Recycling, and Disposal Options. *Environments*, 9(11), 146. <https://doi.org/10.3390/environments9110146>
- [25] Zhao, H., Liu, H., Wei, G., Zhang, N., Qiao, H., Gong, Y., Yu, X., Zhou, J., & Wu, Y. (2022). A review on emergency disposal and management of medical waste during the COVID-19 pandemic in China. *Science of The Total Environment*, 810, 152302. <https://doi.org/10.1016/j.scitotenv.2021.152302>
- [26] Jafarzadeh Ghouschi, S., Memarpour Ghiaci, A., Rahnamay Bonab, S., & Ranjbarzadeh, R. (2022). Barriers to circular economy implementation in designing of sustainable medical waste management systems using a new extended decision-making and FMEA models. *Environmental Science and Pollution Research*, 29(53), 79735–79753. <https://doi.org/10.1007/s11356-022-19018-z>

- [27] Bharti, B., Li, H., Ren, Z., Zhu, R., & Zhu, Z. (2022). Recent advances in sterilization and disinfection technology: A review. *Chemosphere*, 308, 136404. <https://doi.org/10.1016/j.chemosphere.2022.136404>
- [28] Consiliul Concurentei. (2019). *RAPORT PRELIMINAR PRIVIND DEȘEURILE MEDICALE*. file:///C:/Users/Adela%20Romeghea/Desktop/AN%201%202023/Raport-preliminar-sectoriala_-deseuri-med_vers-site%20Consiliul%20Concurentei%20iNVESTIGATIE%202019.pdf
- [29] Govindan, K., Nosrati-Abarghoee, S., Nasiri, M. M., & Jolai, F. (2022). Green reverse logistics network design for medical waste management: A circular economy transition through case approach. *Journal of Environmental Management*, 322, 115888. <https://doi.org/10.1016/j.jenvman.2022.115888>

APPLICATION OF (BIO)CHEMICAL ENGINEERING CONCEPTS AND TOOLS TO MODEL GENETIC REGULATORY CIRCUITS (GRCS), AND SOME ESSENTIAL CCM PATHWAYS IN LIVING CELLS FOR THE *IN-SILICO* RE-DESIGN SOME GRCS TO OBTAIN GMOS

Gheorghe MARIA,^{1,2,*}

¹Dept. of Chemical and Biochemical Engineering, National University of Science and Technology Politehnica Bucharest, 1-7 Gheorghe Polizu St., 011061 Bucharest, ROMANIA

²Romanian Academy, Chemical Sciences section., Bucharest 010071, Romania

Abstract

The paper is aiming at reviewing the main math modelling and computational tools developed by Maria [RW5-RW8] to in-silico re-design genetic regulation circuits (GRC) in living cells to get genetically modified micro-organisms (GMOs) of desired characteristics. A number of suggestive case studies are reviewed as well. More specifically, this work is aiming to prove the feasibility and the advantages of using the novel concept to couple extended cell-scale CCM-based (central carbon metabolism) structured deterministic kinetic models with bioreactor classical dynamic models (including macro-scale state variables). The ever-increasing availability of experimental (qualitative and quantitative) information, at the cell metabolism level, but also on the bioreactors' operation necessitates the advancement of a systematic methodology to organise and utilise these data. The resulted hybrid structured modular dynamic (kinetic) models (HSMDM), promoted by the author, were proved to successfully solving more accurately difficult bioengineering problems. In such HSMDM, the cell-scale model part (including nano-level state variables) is linked to the biological reactor macro-scale state variables for improving both model prediction quality and its validity range. In all case studies, there are multiple advantages of using extended HSMDM-s. for the in-silico designed genetically modified (GMOs). In other words, this work presents a holistic "closed loop" approach that facilitates the control of the "in vitro" through the "in silico" development of HSMDM with continuous variables and based on cellular metabolic reaction mechanisms.

• case study *no.1* (hg). HSMDM is used to simulate the dynamics and to optimize the mercury uptake from wastewaters in a semi-continuous (SCR) three-phase fluidized bioreactor (TPFB). Thus, a higher prediction detailing degree is reported, that is prediction of the dynamics of [26(cell species) + 3(bulk species)] vs. only [3 (bulk species)] by a classical macroscopic SCR- TPFB model, while covering a wider range of input mercury loads, with using cloned *E. coli* cells with

¹ Corresponding author: gmaria99m@hotmail.com; https://en.wikipedia.org/wiki/Gheorghe_Maria

various amounts of *mer*-plasmids [**Gmer**]. Also, the model allows predicting the bacteria metabolism adaptation to environmental changes over dozens of cell cycles, and the optimum [**Gmer**] level leading to an optimum mercury uptake without exhausting the cell resources.

- case study no.2 (*trp*). **HSMDM** is used to simulate the dynamics of a fed-batch bioreactor (**FBR**) at both cell- and bulk-phase species levels, aiming to maximize the tryptophan (**TRP**) production. The **HSMDM** realizes a higher prediction detailing degree, by predicting the dynamics of [11(cell species) + 4(bulk species)] vs. only [3 (bulk species)] by a classical macro-level **FBR** model, while covering a wider range of control variables, and various **GMO** *E. coli* cells strains. Eventually this model was used to derive the optimal operating policy of a **FBR** leading to the **TRP** production maximization, by considering a larger number of control variables related to the bioreactor feeding.

- case study no.3 (*succ*). **HSMDM** is used to simultaneously maximize two opposite objectives, that is the production of biomass and of succinate (**SUCC**) in a batch bioreactor (**BR**). By using the **HSMDM** a Pareto-optimal front was generated including the locus of the all-best compromise problem solutions, that is the cell **CCM** optimal fluxes, together with the genes to be *in-silico* removed from the genome (“gene knockout”) to design *E. coli* mutants that simultaneously fulfil the two goals. This approach uses a mixed-integer nonlinear programming (**MINLP**) rule, coupled with an effective adaptive random search to determine the optimal **CCM** metabolic fluxes of the **GMO** in respect to the two goals, and associated to the “gene knockout” strategies. The **MINLP** alternative using the **HSMDM** model is proved to be superior to the linear procedure **MILP** (mixed-integer linear programming) that solves a combinatorial problem in a bi-level optimization approach, of dimensionality sharply increasing with the number of removed genes, rapidly becoming not applicable. Besides, in this case study, the **HSMDM** realizes a higher prediction detailing degree, by predicting the metabolic fluxes dynamics of [72(cell species), involved in 95 reactions + 1(bulk species, i.e. the biomass)] vs. only [1 (bulk species)] by a classical macroscopic **BR** model, while covering a wider range of control variables, and **GMO** *E. coli* strains.

Key words: systems biology; cell metabolism; deterministic modelling; gene expression modelling; genetic regulatory circuits (GRC); Pareto design of *E. coli* to obtain maximum succinate; design cloned *E. coli* to get maximum mercury uptake; design *E. coli* with a genetic switch biosensor; design *E. coli* with a desired glycolytic oscillator; tryptophan synthesis; glycolytic oscillator; Phenyl-alanine synthesis in *E. coli*; kinetic models for the central carbon metabolism (CCM); “whole-cell of variable-volume” (**WCVV**) modelling framework; “hybrid structured modular dynamic (kinetic) models” (**HSMDM**); “modular structured dynamic (kinetic) models” (**MSDKM**)

1. Introduction

The work is a systematized and reasonable short review of the main published contributions of the author in the field of cell metabolic processes simulation related to the central carbon metabolism (**CCM**) and, in particular,

modelling the dynamics of the individual gene expression module of regulatory reactions (**GERM**), and of the genetic regulation circuits (**GRC**) in living cells. Application of the chemical and biochemical engineering (**CBE**), and of the control theory of nonlinear systems (**NSCT**) principles and concepts to the modeling of complex cellular processes on deterministic bases are briefly presented in the reviews papers of Maria [RW1-RW8]. These math dynamic (kinetic) models are essential for understanding and simulating the **CCM**, useful to *in-silico* (that is model-based) re-design of genetically modified micro-organisms (**GMOs**) with applications in industrial biosynthesis, medicine, environmental engineering, vaccine production, biosensors, etc.

A special attention is paid to the authors' contributions related to dynamics simulation of the **GERMs**, and of the **GRCs** in living cells, by promoting a novel cell math modelling framework, that is the so-called "variable-volume-whole-cell" (**WCVV**) models [1-3]. The relatively novel concept of "whole-cell" simulation of cell metabolic processes has been reviewed to prove its advantages when building-up dynamic models of modular structures that can reproduce complex metabolic syntheses inside living cells. The advantages of the more realistic **WCVV** approach are briefly underlined and exemplified when developing kinetic representations of the **GERMs** that control the protein synthesis and homeostasis of the cell metabolic processes. After a brief presentation of the general concepts and particularities of the **WCVV** math (kinetic) modelling, both past and current experience with constructing effective **GERM** models is reviewed, together with some rules used when linking **GERMs** to build-up models for the optimized globally efficient **GRCs**, by using a "building-blocks" strategy, and quantified regulatory performances indices (**P.I.**). These **P.I.s** introduced by Maria [1-3] were evaluated from the analysed cell system response to the simulated dynamic and stationary environmental perturbations.

The topics belongs to the emergent field of **Systems Biology**, defined as "the science of discovering, modelling, understanding and ultimately engineering at the molecular level the dynamic relationships between the biological molecules that define living organisms" (Leroy Hood, Inst. Systems Biology, Seattle). Systems Biology is one of the modern tools, which uses advanced mathematical simulation models for *in-silico* re-design of **GMOs** that possess specific and desired functions and characteristics. The present work makes a short review of the **CBE** principles and deterministic modelling rules used by the Systems Biology for modelling cellular metabolic processes [1-3]. This involves application of the classical **CBE** modelling techniques (mass balance, thermodynamic principles), algorithmic rules, **NSCT** theory, and bioinformatics rules. The metabolic pathway representation with continuous and/or stochastic variables remains the most adequate and preferred representation of the cell processes, the adaptable-size and

structure of the lumped model depending on available information and utilisation scope [rw1-3].

2. Generalities about HSMDM kinetic models

Biologically catalyzed reactions (with enzymes or living cell cultures) can successfully replace complex chemical syntheses, being more selective, by using milder reaction conditions, and generating less waste. As proved by the recent literature, the developed *in-silico* (math-model-based) numerical analysis of such biochemical/biological systems turned out to be a beneficial tool to (i) off-line determine optimal operating policies of complex multi-enzymatic or biological reactors with a higher precision and predictability, or (ii) to design **GMO** of desired characteristics for various uses. This work presents a holistic ‘closed loop’ approach that facilitate the control of the *in vitro* through the *in silico* development of dynamic models for living cell systems, by deriving *hybrid structured modular dynamic (kinetic) models* (**HSMDM**) (with continuous variables, and based on cellular metabolic reaction mechanisms). The ever-increasing availability of experimental (qualitative and quantitative) information about the tremendous complexity of cell metabolic processes, stored in large bio-omics databanks (including genomic, proteomic, metabolomic, fluxomic cell data for various micro-organisms), but also about the bioreactors’ operation necessitates the advancement of a systematic methodology to organise and utilise these data.

This work is aiming to prove the feasibility and the advantages of using the classical and novel concepts and numerical tools of the **CBE** to develop “modular structured dynamic (kinetic) models” (**MSDKM**) of the extended cell-scale **CCM**-based dynamic models (**Fig. 1**), or of the **GRC-s** (**Fig. 2**). These extended cell kinetic models (with cell nano-scale state variables) will be further linked to those of the bioreactor dynamic models (including macro-scale state variables), thus resulting the **HSMDM** math (kinetic) models proved to successfully solve more accurately difficult bioengineering problems, by improving both model prediction quality (detailing degree, precision), and its validity range.

By contrast, the current (classical/default) approach in biochemical engineering and bioengineering practice for solving design, optimization and control problems based on the math models of industrial biological reactors is to use *unstructured* Monod (for cell culture reactor) or Michaelis-Menten (if only enzymatic reactions are retained) global kinetic models by ignoring detailed representations of metabolic cellular processes. The applied engineering rules to develop **MSDKM** and **HSMDM** dynamic math models presented in [RW4-RW6] are similar to those used in the **CBE**, and by the **NSCT**.

The [RW7-RW8] reviews proved, by means of several demonstrative relevant examples, the superiority of using **MSDKM** and **HSMDM** dynamic math models when solving various bioengineering problems, such as: (i) in-silico off-line optimize the operating policy of various types of bioreactors, and (ii) in-silico design/check some **GMO**-s of industrial use able to improve the performances of bioprocesses/bioreactors.

By contrast, by considering only the macroscopic key-variables of the process (biomass, substrate, and product concentrations), the unstructured (apparent, global) math models do not adequately reflect the metabolic changes of the bioreactor biomass, being inadequate to accurately predict the cellular response to the medium disturbances through the self-regulated cellular metabolism over dozens of cell cycles. These classical global/unstructured dynamic models may be satisfactory for an approximate modelling of the biological process, but not for modeling of cellular metabolic processes, and they can not make any correlation between the bioreactor operation and the continuous adaptation of the biomass metabolism to the variable conditions of the bioreactor. Even worst, as proved by the author in previous papers, such global models, or the classical (default) **WCCV** (whole-cell constant-volume modelling framework) cell dynamic models, may lead to biased, wrong, and distorted predictions / conclusions about the **GERM**'s performances, thus making difficult the modular constructions of **GRC**-s by linking individual **GERM**-s, being inappropriate for detailed engineering calculations.

3. The novel **WCVV** math (kinetic) modelling framework of the living cell metabolism

One of reported **major and essential** contribution of Maria [RW1-8] in the theoretical/math modelling of the metabolism in the living cells (single cell analysis), of tremendous importance is the following. The introduction and promotion of a novel math modelling concept / framework to derive cell kinetic models to simulate the cell metabolism, particularly **CCM**, or **GRC**s in a holistic approach (e.g. genetic switches, genetic amplifiers, operons expression). This so-called, “variable-volume-whole-cell” (**WCVV**) approach, ensures cell processes homeostasis, and accurately simulate the individual / holistic **GRC** regulatory properties, by including in a natural way constraints related to the cell system isotonicity, and the variable-volume in relationship to the all-species reaction rates [RW1-4]. Such an isotonicity constraint is required to ensure the cell membrane integrity, but also to preserve the homeostatic properties of the cell system, not by imposing “the total enzyme activity” or the “total enzyme concentration” constraints suggested in the literature [18].

By contrast to the the classical (default) **WCCV** (“whole-cell constant-volume” modelling framework) cell dynamic models, the novel holistic “whole-cell of variable-volume” (**WCVV**) modelling framework introduced, extended, and widely promoted by Maria [RW1-8];[19,20] has been proved to be more realistic and robust, by explicitly including in the model relationships the cell-volume growth, while preserving the cell-osmotic pressure. The added isotonicity constraint by Maria [rw1-3] was proved to be essential for predicting more adequate performance regulatory indices of **GERM-s** and **GRC-s**. The essential part of the **WCVV** approach is to explicitly include the cell variable volume in the metabolic process kinetic model, that is in math terms (**Fig. 3**):

$$\frac{dC_j}{dt} = \frac{d}{dt} \left(\frac{n_j}{V} \right) = \frac{1}{V} \frac{dn_j}{dt} - \frac{n_j}{V} \frac{dV}{dt} = \frac{1}{V} \frac{dn_j}{dt} - DC_j = h_j(C, k, t) \quad (1)$$

(where: C_j , n_j = species “j” concentration, or number of moles; V = cell cytosol volume; t = time; D = cell content dilution rate, due to its volume growth).

By considering the isotonicity (Pfeffers’ law) of the cell system (to preserve the membrane integrity), then, it is possible by derivation of this relationship, to obtain the “instant” cell dilution “ D_i ” to be used when solving the cell dynamic model, instead of the “default” average dilution “ $D = \ln(2)/(\text{cell cycle})$ ”. In math terms this translates in:

$$D_i = \frac{1}{V} \frac{dV}{dt} = \left(\frac{RT}{\pi} \right) \sum_j^{n_s} \left(\frac{1}{V} \frac{dn_j}{dt} \right) \quad (2)$$

$$RT / \pi = 1 / \sum_j C_j = \text{constant (Pfeffers' law)}$$

(where: R = the universal gas constant; T = absolute temperature; π = osmotic pressure; n_s = number of the species (individual or lumped inside the cell)).

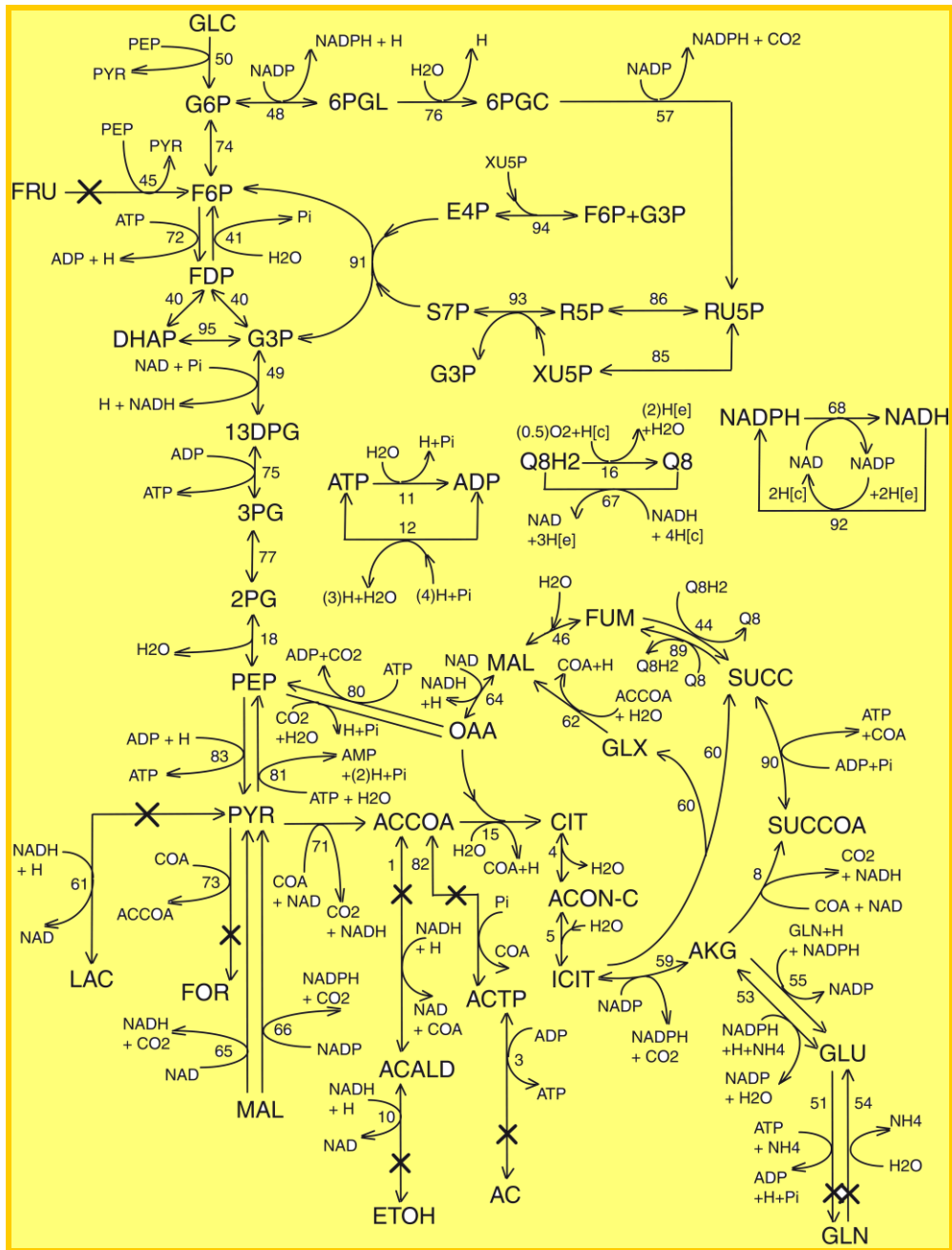


Fig. 1. The **CCM** reduced pathway of *Escherichia coli* after the model of Edwards and Palsson [17]. This “wild” strain includes the PTS-system for GLC import from the environment. Fluxes characterizing the membranar transport $Metabolite[e] \leftrightarrow Metabolite[c]$ and the exchange with environment $[e]: Metabolite \leftrightarrow Metabolite[e]$ have been omitted from the plot ([e]= environment; [c]= cytosol). This is the case of fluxes number: 2(ACALD), 6(AC,H), 9(AKG,H), 14(CO₂),

Application of (bio)chemical engineering concepts and tools to model genetic regulatory circuits (GRCS), and some essential CCM pathways in living cells for the *in-silico* re-design some GRCS to obtain GMOS

17(LAC,H), 19(ETOH,H), 20(AC), 21(ACALD), 22(AKG), 23(CO₂), 24(ETOH), 25(FOR), 26(FRU), 27(FUM), 28(GLC), 29(GLN), 30(GLU), 31(H), 32(H₂O), 33(LAC), 34(MAL), 35(NH₄), 36(O₂), 37(Pi), 38(PYR), 39(SUCC), 42(FOR,H), 43(FOR), 47(FUM,H), 52(GLN,ATP), 56(GLU,H), 58(H₂O), 63(MAL,H), 69(NH₄), 70(O₂), 78(Pi,H), 84(PYR,H), 87(SUCC,2H), 88(SUCC,H). Notations: (Met) = diffusional transport of metabolite Met; (Met,H) = transport of metabolite Met via proton symport; (Met,ATP) = transport of metabolite Met via ABC system. Species abbreviations are explained by [3]. The considered 72 metabolites, the stoichiometry of the 95 numbered reactions, and the net fluxes for specified conditions are given by Maria et al. [3].

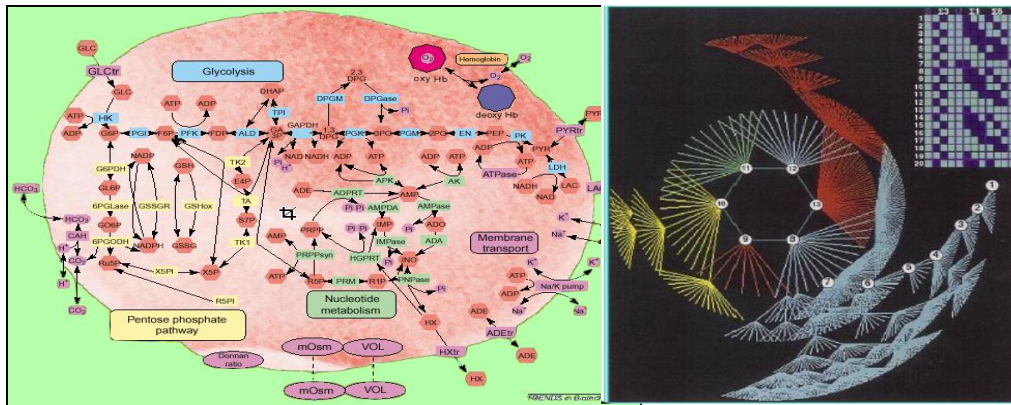


Fig. 2 [Left] Simplified reaction pathway of the **CCM** in *E. coli*. **[Right]** Example of a complex genetic regulatory circuit (**GRC**) in a living cell [RW1-RW4].

This novel modelling framework makes it possible to precisely simulate a lot of cell metabolic effects, such as: relationships between the external conditions, species net synthesis reactions, osmotic pressure, cell content (ballast) influence on smoothing the continuous perturbations in external nutrient concentrations, etc. [RW1-4]. One of the major differences compared to the classical (“default”) approach **WCCV** (of constant cell volume formulation), is the use of the instant cell dilution “**Di**” in the **WCVV** models (eq.2) instead of the “default” average (approximate) dilution $D = \ln(2)/(\text{cell cycle})$. As proved [19,20][RW1-4], this aspect is of major importance for the cell dynamic model prediction accuracy. While the classic **WCCV** cell dynamic models, ensure the holistic cell properties (such as homeostasis, self-regulation of syntheses, and of gene expression, perturbation treatment, etc.), by imposing a lot of constraints (such as “the total enzyme activity”; “total enzyme concentration”, etc.[18]), Maria [rw1-8] promoted inclusion of thermodynamic isotonicity relationships/constraints in the cell kinetic model formulation (**Fig.3**), and, proves step-by-step in a math way how such constraints ensure cellular intrinsic properties in a natural way (that is not derived from artificial hypotheses). Such concepts, and rules translated from **BCE** and **NSCT** principles are explained,

proved, and exemplified by Maria [RW1-4]. The **WCVV** models using modular **GRCs** are successfully used to design **GMOs** of desirable characteristics. Some examples are mentioned below.

By contrast to the novel **WCVV**, the classical (“default”) modelling tools of metabolic cell processes are based on the **WCCV** continuous variable **ODE** dynamic models, which do not explicitly consider the cell volume exponential increase during the cell growth. As proved by Maria et al. [20-22], such a **WCCV** classic approach may lead to wrong, distorted, and biased predictions and conclusions on the **GERM**’s performances, making difficult the modular constructions of **GRCs** by linking individual **GERMs**. Such a conclusion is exemplified in **Figs. 4-6**. The concepts and hypotheses used in the **WCVV** math modelling are explained, proved, and exemplified in detail by Maria [RW1-8]. Their main hypotheses are given in the **Table 1**. Examples include generic **GERM**, **GRC**, **GS** (genetic switches) models for various case studies.

Based on such a novel **WCVV** math modelling formulation, Maria [RW1-8] developed a significant number of notable contributions in bioinformatics and biochemical engineering, as followings:

- 1).- Development of a math “LIBRARY” including “template” kinetic models of the main **GERM** types (self-regulated individual gene expressions). This library is useful to build-up dynamic models of **GRCs**, useful for the *in-silico* design of **GMOs** (**Fig. 7**);
- 4).- Introduction of novel quantitative performance indices (**P.I.**) to characterize the regulation efficiency of **GERMs** related to the external perturbations (dynamic, or stationary) [RW1-8];
- 5).- The use of the novel **WCVV** math modelling framework, and of **GERM**-s **P.I.s** to propose a “building-blocks” strategy and rules to connect **GERM**-s to build-up **GRCs** aiming to obtain modular, deterministic, structured, hybrid kinetic models for various purposes: (a) to simulate the essential parts of the **CCM**, such as: glycolysis, TCA cycle, ATP recovery system, mercury operon expression, Tryptophan operon expression, succinate synthesis, etc., and (b) to simulate and/or design various **GRCs**. Examples include: genetic switches, genetic amplifiers, operons expression. (c) To *in-silico*, off-line derive optimal operating policies of bioreactors, with a higher precision and degree of detail. Some examples are presented in the next section.

The concepts and the basic hypotheses of **WCVV** dynamic modelling framework in living cells are briefly summarized by Maria [RW1-6]. This novel modelling framework **WCVV** is leading to accurately simulate a lot of cell metabolic intrinsic processes, such as the relationships between the external conditions and the inner cell metabolic processes, such as: (i) species net synthesis reactions, (ii) osmotic pressure, (iii) cell content (ballast) influence on smoothing

the continuous perturbations in the external nutrient concentrations, etc. (see examples in [RW1-8]).

4. Examples

Exemplifications of using such modular **HSMDM** models for *in-silico* design of **GMOs**, of desired characteristics, include improving several bioprocesses of industrial interest, that is six case studies of high complexity, extensively described by [RW1-8]:

- 1) *In-silico* design of a genetic switch in *E. coli* with the role of a biosensor [1] (**Figs.8-10**);
- 2) *In-silico* design of a cloned *E. coli* with mercury-plasmids to maximize its capacity of mercury uptake from wastewaters [2-5];
- 3) *In-silico* design of a genetic modified *E. coli* with a maximized capacity of concomitantly production of biomass and succinate (SUCC) [6];
- 4) *In-silico* design of a genetic modified *E. coli* with a modified glycolytic oscillator [1,7-11];
- 5) *In-silico* modulate the operating policy of a **FBR** (fed-batch) bioreactor using a modified *E. coli* (T5 strain of Chen [25,26]) to maximize the production of tryptophan (TRP) [8,9,12-15] (**Figs. TRP1-TRP6**). In the T5 strain the PTS system for the GLC import was replaced with a more efficient one, based on galactose permease/glucokinase GalP/Glk. Such an alternative provides a 73% increase in TRP production compared to a simple batch bioreactor (**BR**), or a non-optimally operated **FBR**. Of this increase, 50% is due to the **GMO** *E. coli* used, the rest being associated with the optimal operating policy of the **FBR**, derived by Maria and Renea [13,15] (with using a variable feeding, with a multi-control variables).
- 6) *In-silico* re-configure the metabolic pathway for Phenyl-alanine synthesis in *E. coli* [16] to maximize its production. That implies to modify the structure and activity of the involved enzymes, and modification of the existing regulatory loops. Searching variables of the formulated mixed-integer nonlinear programming (MINLP) optimization problem are the followings: the regulatory loops (that is integer variables, taking “0” value when the loop has to be deleted, or the value “1” when it has to be retained); the enzyme expression levels (that is continuous variables), and all these in the presence of the stoichiometric and thermodynamic constraints. To solve this complex optimization problem, two contrary objectives are formulated: maximization of the Phenyl-alanine selectivity, with minimization of cell metabolites’ concentration deviations from their homeostatic levels (to avoid an unbalanced cell growth). The elegant solution of the problem is the so-called Pareto-optimal front, which is the locus of the best trade-off between the two

adverse objectives. By choosing two problem solution alternatives from this Pareto-curve [23,24], it is to observe the large differences between the two pathways into the cell, fully achievable by genetic engineering.

A novel math (kinetic) modelling framework of the cell metabolic process. That is [WCVV= "whole-cell, holistic approach of isotonic, variable volume, growing cell systems"]. It is very appropriate to simulate the dynamics of the self-regulation of individual gene expression modules (GERM), and of the genetic regulatory circuits / networks (GRC).

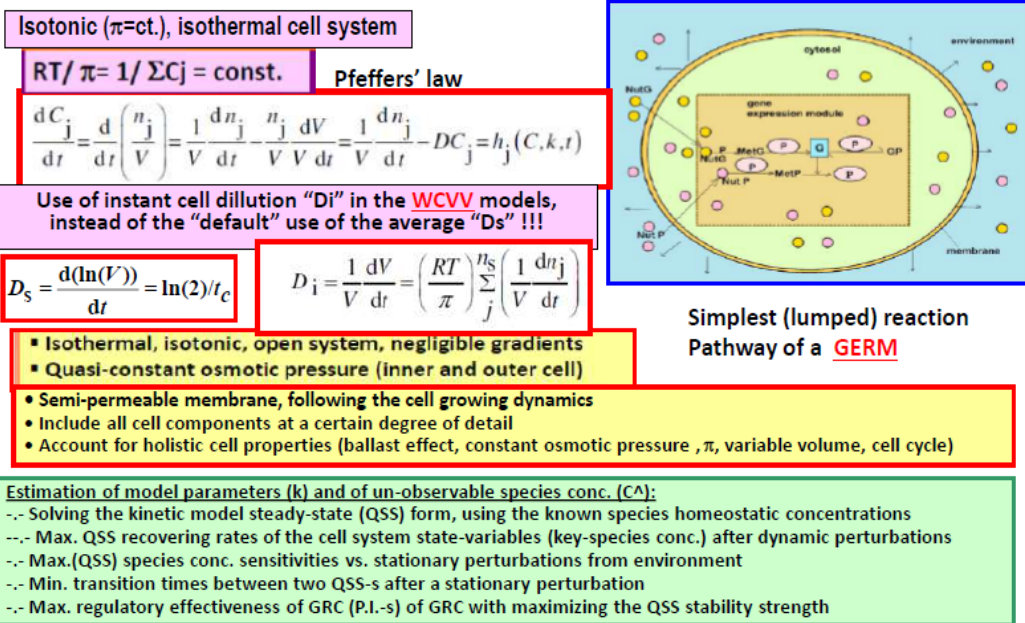


Fig. 3. The essential concepts / relationship hypotheses of the WCVV modelling framework.

Application of (bio)chemical engineering concepts and tools to model genetic regulatory circuits (GRCS), and some essential CCM pathways in living cells for the *in-silico* re-design some GRCS to obtain GMOS

Proving that the classic ("default") math modelling approach (**WCCV**, "constant-cell-volume, non-isotonic system") is **erroneous** compared to the novel **WCVV**, by leading to **distorted simulation results** and conclusions [Maria, *Current Trends in Biomed. Eng. & Biosci.*, 12(2),2018, DOI 10.19080/CTBEB.2018.12.555833].

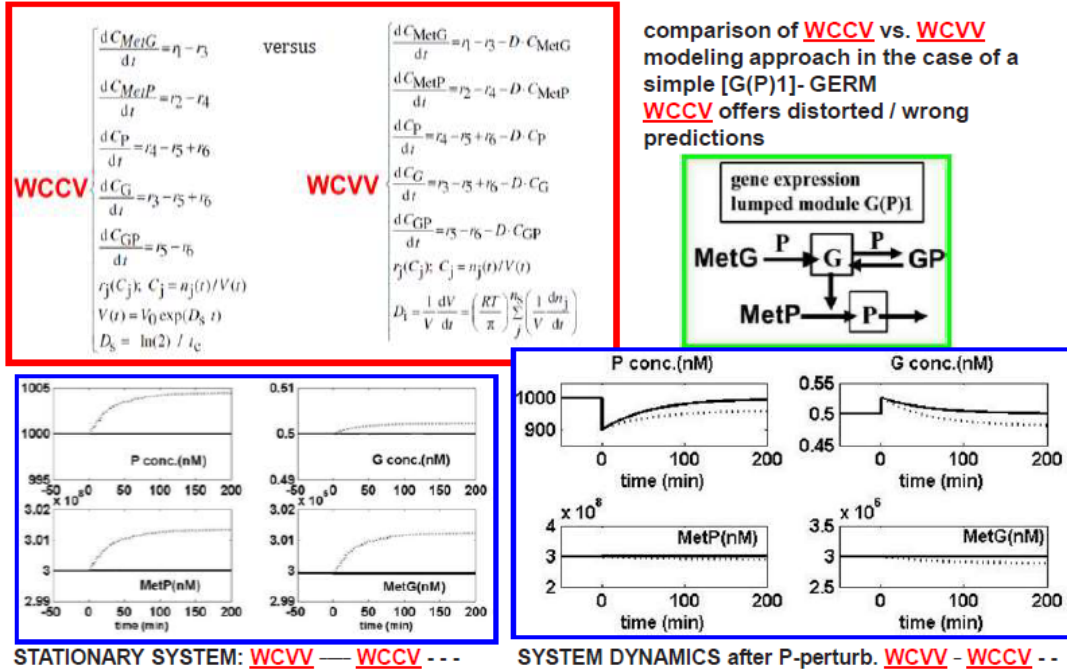
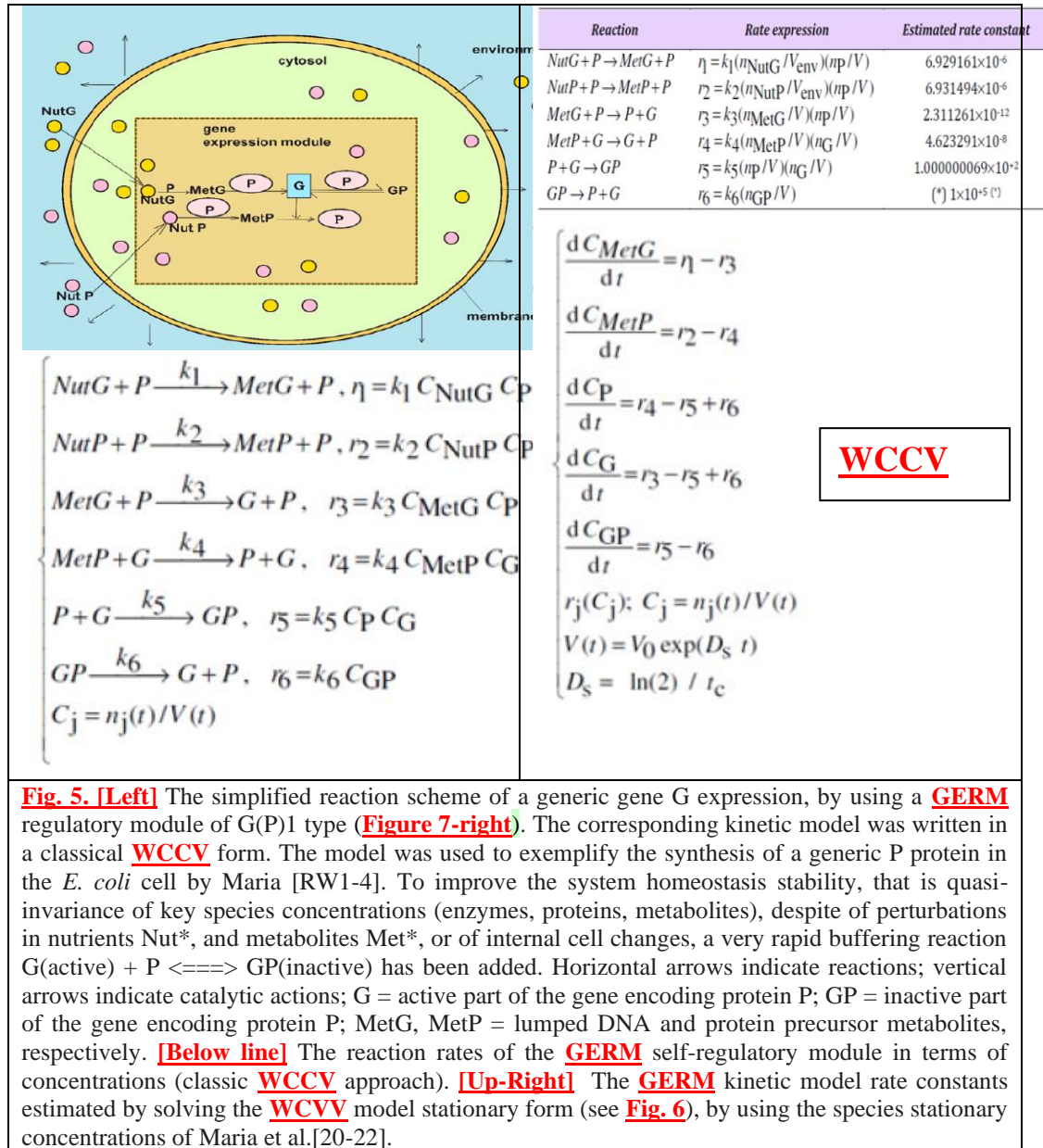
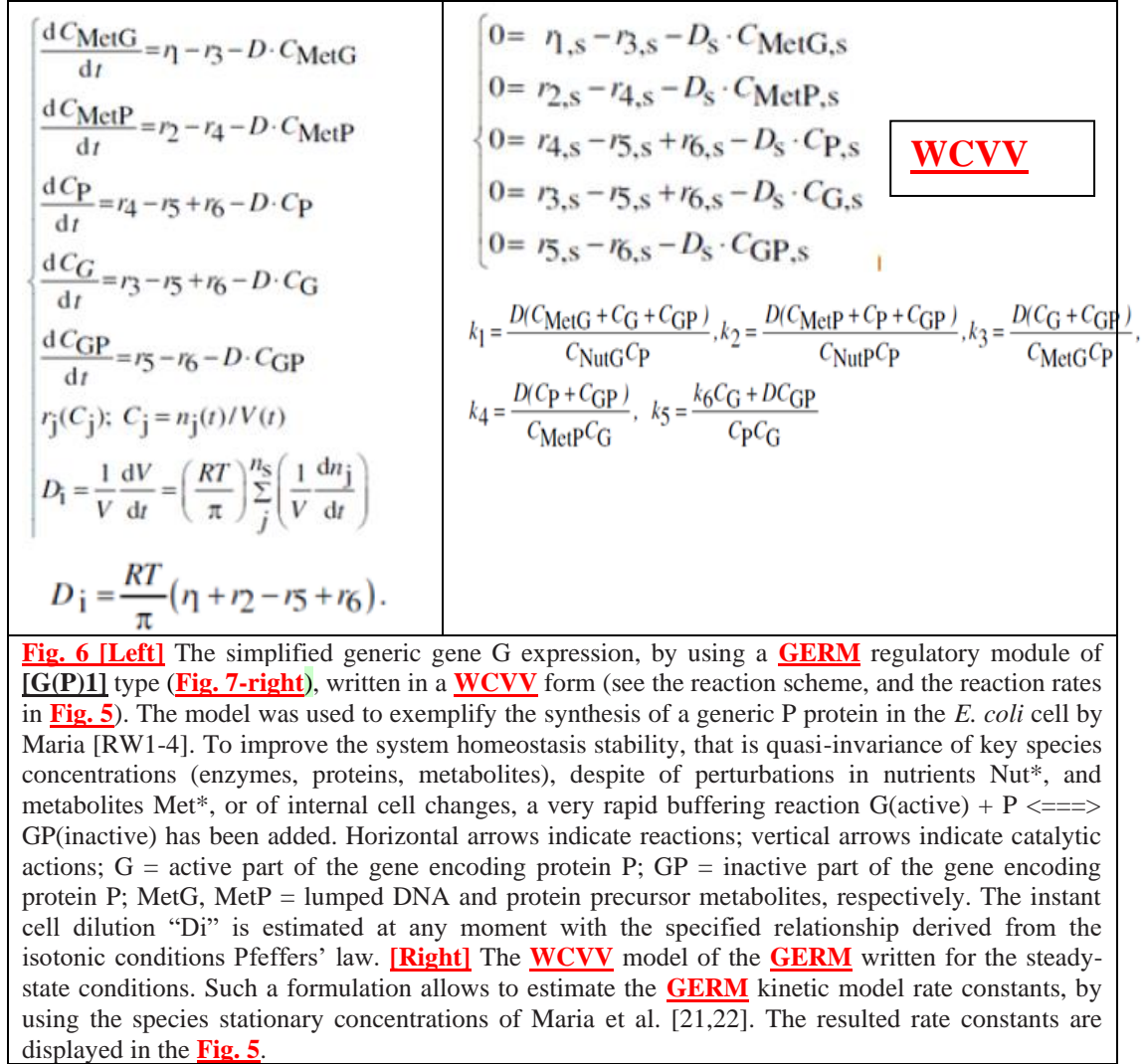


Fig. 4. [top-line] Comparison between **WCVV** and the classical **WCCV** modelling framework in the case of a simple **GERM** kinetic model. **[down-line]** The recovering trajectories over time of the key-species after a dynamic perturbation (-10% in [P]) differ very much. [2].





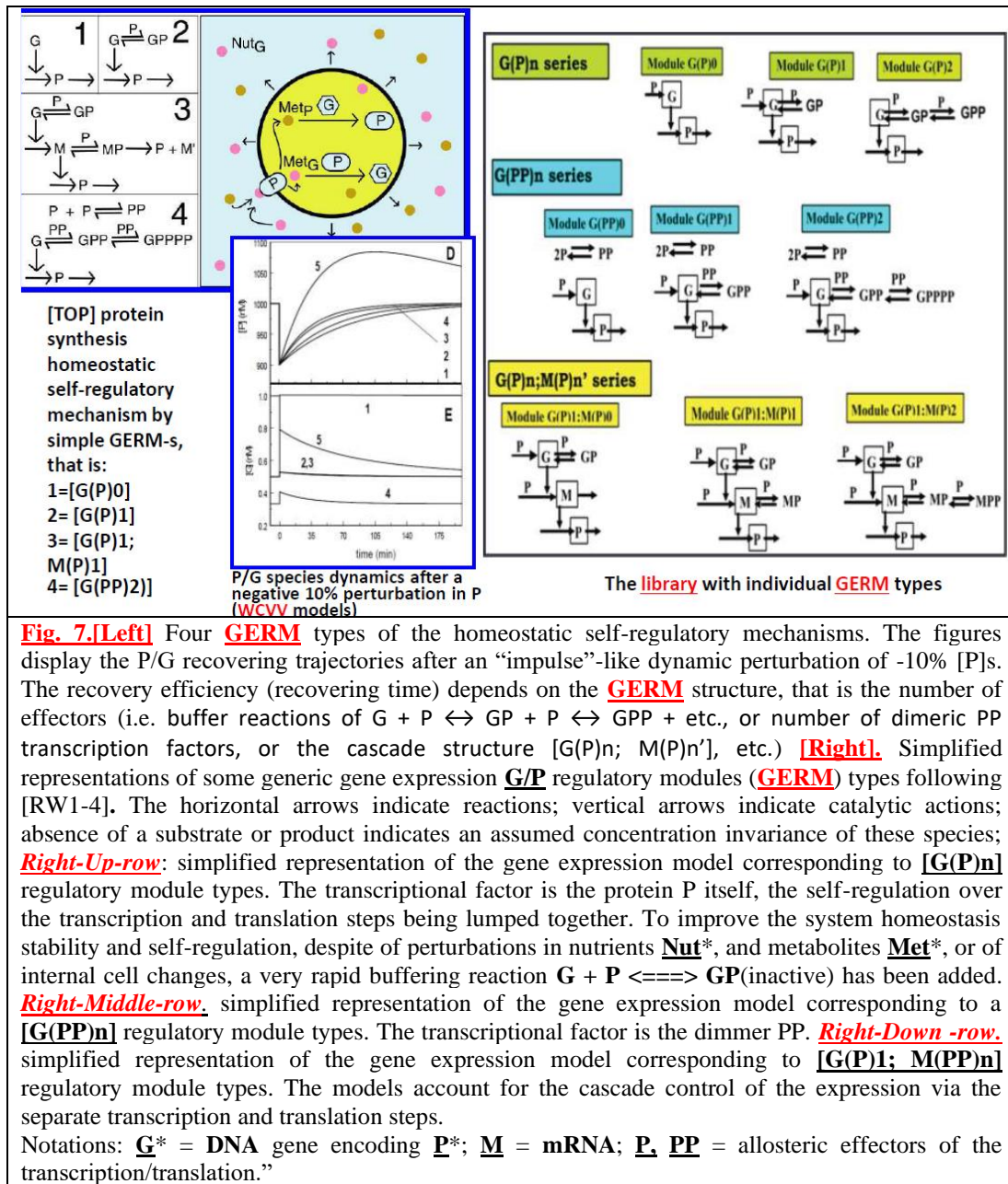


Fig. 7.[Left] Four **GERM** types of the homeostatic self-regulatory mechanisms. The figures display the P/G recovering trajectories after an “impulse”-like dynamic perturbation of -10% [P]s. The recovery efficiency (recovering time) depends on the **GERM** structure, that is the number of effectors (i.e. buffer reactions of $G + P \leftrightarrow GP + P \leftrightarrow GPP + \text{etc.}$, or number of dimeric PP transcription factors, or the cascade structure $[G(P)n; M(P)n']$, etc.) **[Right]**. Simplified representations of some generic gene expression **G/P** regulatory modules (**GERM**) types following [RW1-4]. The horizontal arrows indicate reactions; vertical arrows indicate catalytic actions; absence of a substrate or product indicates an assumed concentration invariance of these species; **Right-Up-row**: simplified representation of the gene expression model corresponding to **[G(P)n]** regulatory module types. The transcriptional factor is the protein P itself, the self-regulation over the transcription and translation steps being lumped together. To improve the system homeostasis stability and self-regulation, despite of perturbations in nutrients **Nut***, and metabolites **Met***, or of internal cell changes, a very rapid buffering reaction $G + P \rightleftharpoons GP(\text{inactive})$ has been added. **Right-Middle-row**: simplified representation of the gene expression model corresponding to a **[G(PP)n]** regulatory module types. The transcriptional factor is the dimmer PP. **Right-Down -row**: simplified representation of the gene expression model corresponding to **[G(P)1; M(PP)n]** regulatory module types. The models account for the cascade control of the expression via the separate transcription and translation steps.

Application of (bio)chemical engineering concepts and tools to model genetic regulatory circuits (GRCS), and some essential CCM pathways in living cells for the *in-silico* re-design some GRCS to obtain GMOS

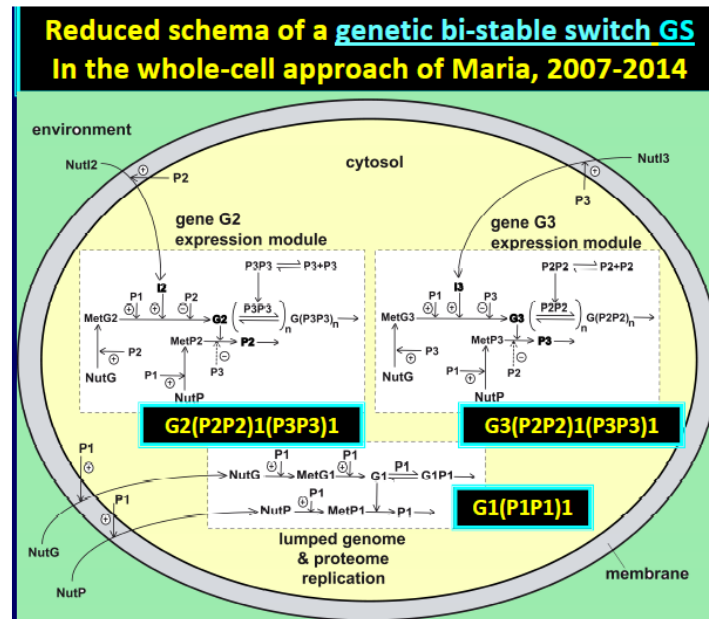


Fig. 8. A generic genetic switch in *E. coli*, with two self- and cross-repressed **GERMs**, of type **[G2(P2P2)1(P3P3)1] + [G3(P2P2)1(P3P3)1]** in the **WCVV** math modelling framework. The lumped **GERM** **[G1(P1)1]** simulate the self-regulation of the genome and proteome replication [rw1-8]. Notations: G*= generic gene, ADN; P*= generic protein; M = mARN; Met = metabolites; Nut = nutrients; I2-3 = internal inducers.

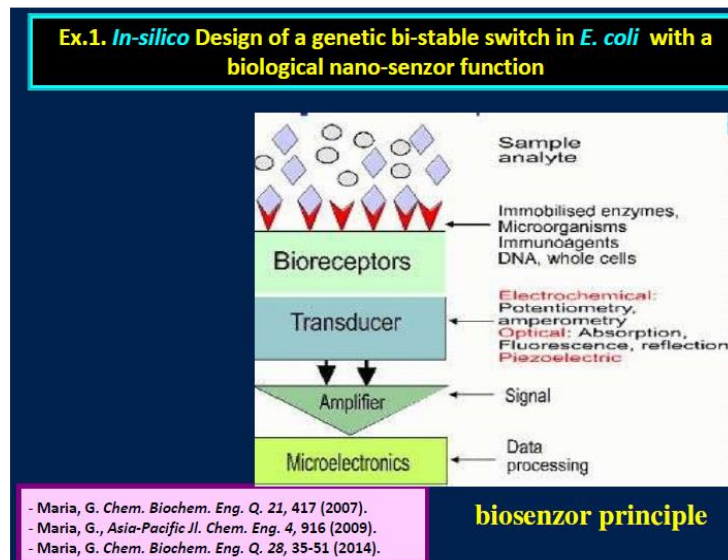


Fig. 9. Principle of a molecular biosensor based on a cellular genetic switch (**Fig. 8, Fig. 10**). The external „Inducer” (I2) generates an over-expression of the cell protein „P2” (the so-called „bio-receptor”) (**Fig. 10**). In turn, this protein will generate a measurable modification of a cell characteristics (fluorescence, etc.). The detection accuracy is very high (inducers in nano-molar concentrations). [RW3-4]

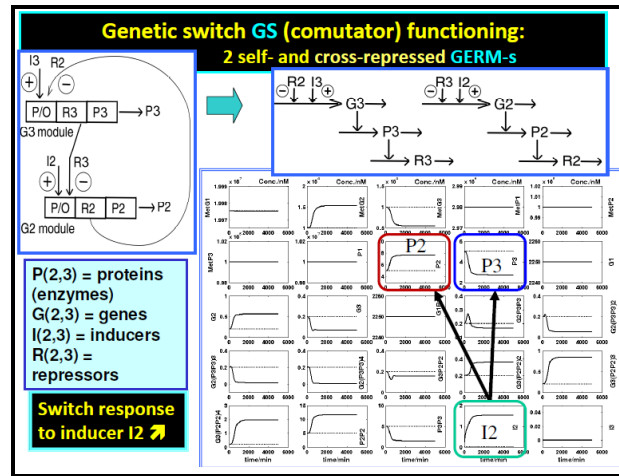


Fig. 10. The principle of a genetic switch: two self- and cross-repressed **GERM**-s [G2/P2+G3/P3] under the **WCVV** modular math modeling approach, with inclusion of clustered proteome/genome replication [G1/P1] (**Fig. 8**). Notations: G= generic gene, DNA; P= generic protein; M = mRNA; Met = metabolite; Nut = nutrient; I2-3 = inducers. Simulation of the dynamics of a genetic switch, in the presence of an external molecular I2 inducer (nano-molar detection level).

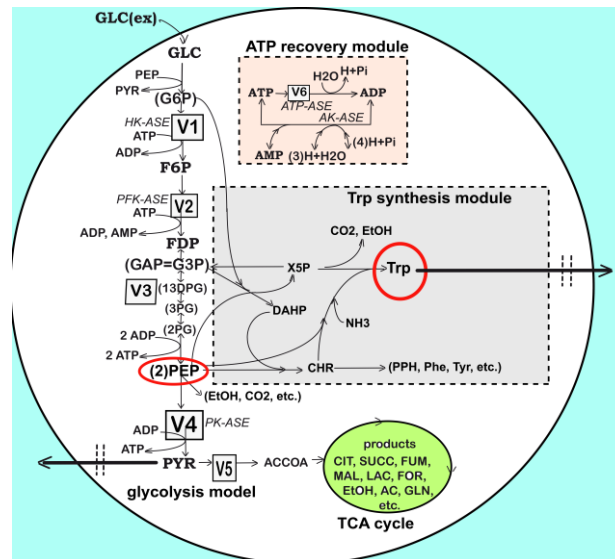


Fig. TRP-1. Simplified representation of glycolysis in *E. coli*, according to Maria [RW3-4, RW7-8]; [9,12-15]). Glycolysis is connected to the tryptophan (TRP) synthesis (gray area) via the common species PEP. This reaction scheme was used by Maria [9,12-15]; [RW3-4, RW7-8] to develop a structured **HMCSD** kinetic model for TRP synthesis. The modular model structure also includes the synthesis of adenosine co-metabolites ATP, ADP, AMP as part of the ATP regeneration system (pink rectangle in the figure). GLC(ex)= glucose in the cellular environment. Species abbreviations are given in [7,8,10]. Species in parentheses are not explicitly included in the glycolysis model. Italics denote enzymes. Squares include notations of the grouped enzymatic reactions V1-V6 included in the glycolysis model [7,8,10].

Application of (bio)chemical engineering concepts and tools to model genetic regulatory circuits (GRCS), and some essential CCM pathways in living cells for the *in-silico* re-design some GRCS to obtain GMOS

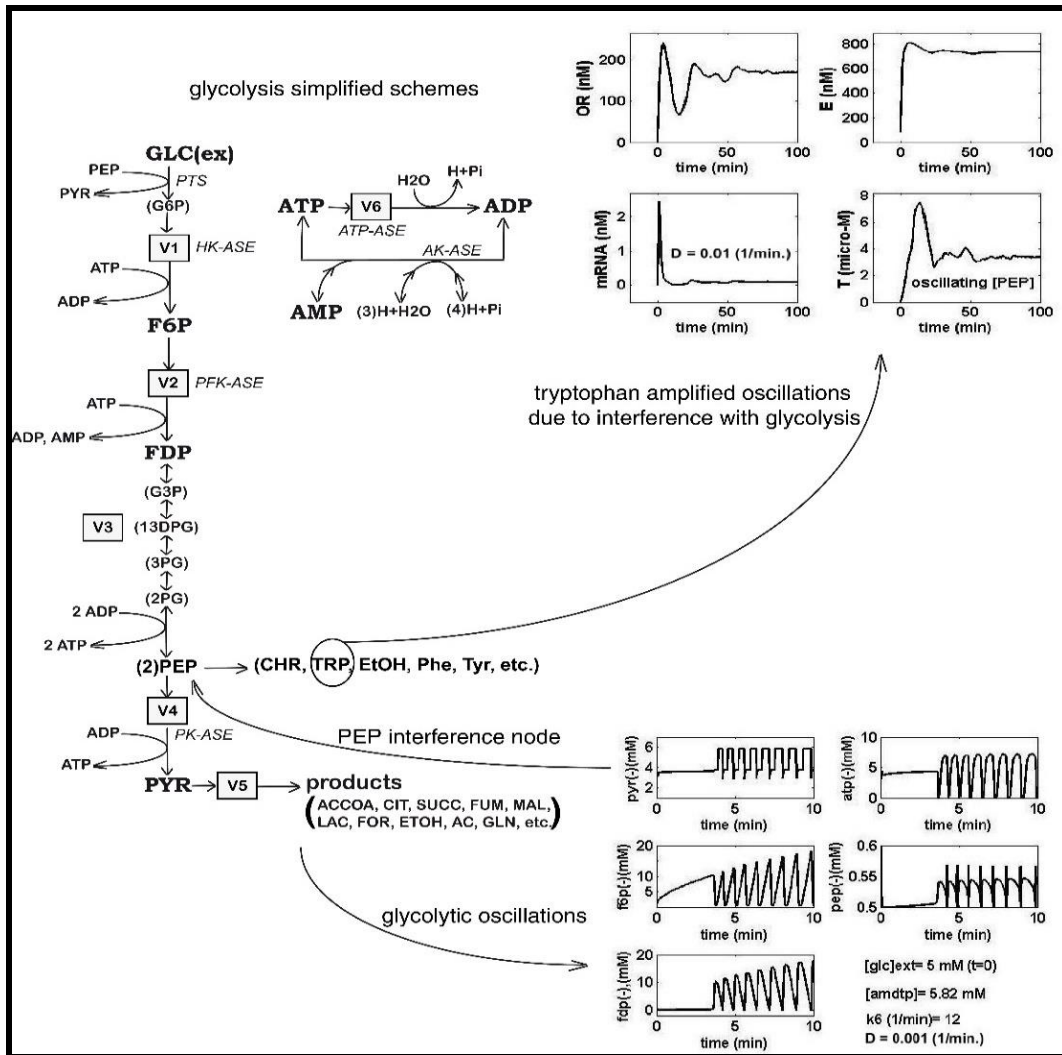


Fig. TRP-2. The link between the oscillating glycolysis and the oscillating TRP operon expression is made through the common species PEP [7-10,12-15]

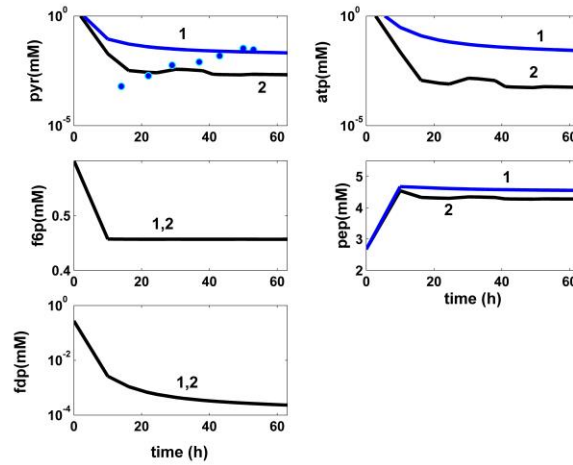


Fig. TRP-3. *In-silico* simulated trajectories (____) for the key glycolytic species (PYR, F6P, FDP, ATP, PEP) in the modified strain T5 of *E. coli* of Chen [25,26], for the **FBR** operated in two alternatives: (i). (2, black) the optimal operating policy *in-silico* obtained by Maria [13,15], i.e. a variable feed flow rate (FL) with a GLC solution of variable concentration; (ii). (1, blue) and the experimental data (•, blue) of Chen [25,26], for a "nominal", non-optimal operating policy [13,15], i.e. a constant feed flow rate (FL) with a GLC solution of constant concentration. Species abbreviations are given by Maria [13,15].

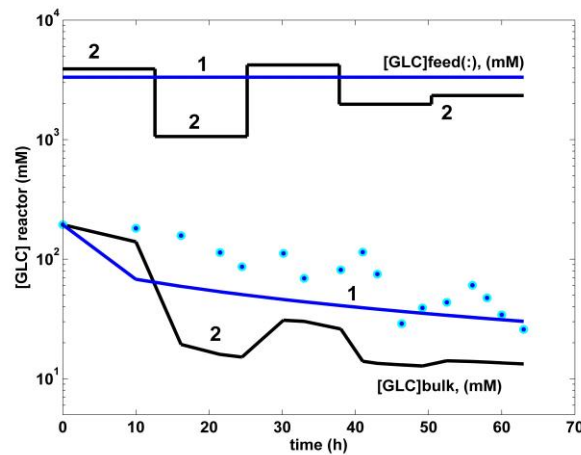


Fig. TRP-4. Top curves. The "time step-wise" optimal feeding policy (2, black) of the GLC concentration in the bioreactor (using $j = 1, \dots, 5$ equal "time-arcs", evenly distributed during the batch, according to Maria [13,15]). This optimal policy is characterized by a variable feed flow rate (FL), and also a variable concentration of GLC solution. The comparison is made with the experimental bioreactor **FBR** (1, blue) operated under non-optimal "nominal" conditions by Chen [25,26], that is with a constant feed flow rate (FL), and with a GLC solution of constant concentration. Both cases use the same modified strain T5 of *E. coli*.

Bottom curves. *In-silico* simulated trajectories (____) for the glucose concentration (GLC) in the bioreactor bulk, for the **FBR** operated in the alternatives (i) or (ii) defined in the **Fig. TRP-3**.

Application of (bio)chemical engineering concepts and tools to model genetic regulatory circuits (GRCS), and some essential CCM pathways in living cells for the *in-silico* re-design some GRCS to obtain GMOS

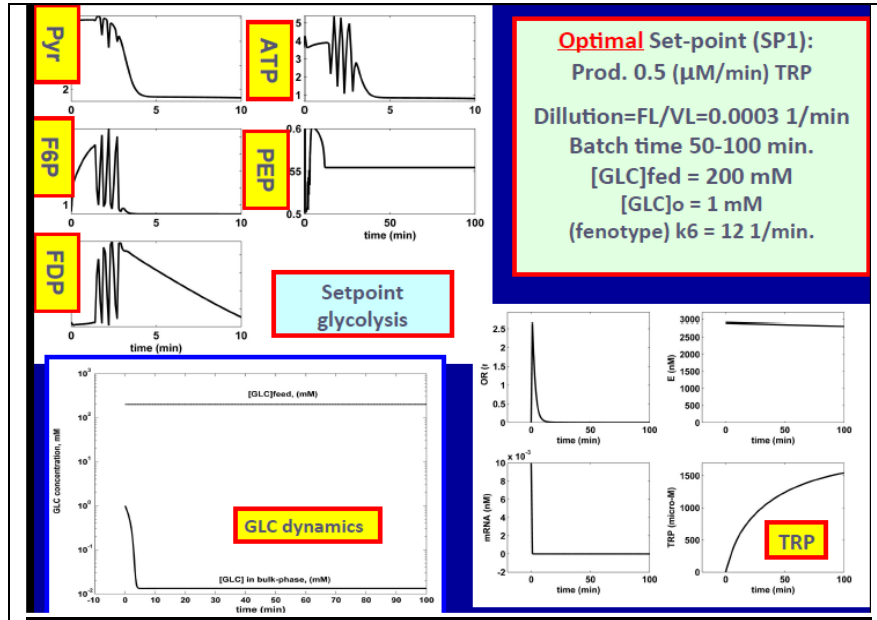


Fig. TRP-5. One of the optimal operating policies (SP = "set-point") of the **FBR** obtained through *in-silico*, *off-line* evaluations. While glycolytic oscillations disappeared (leading to a stationary glycolysis), TRP synthesis reported high yields [8,9,13,15].

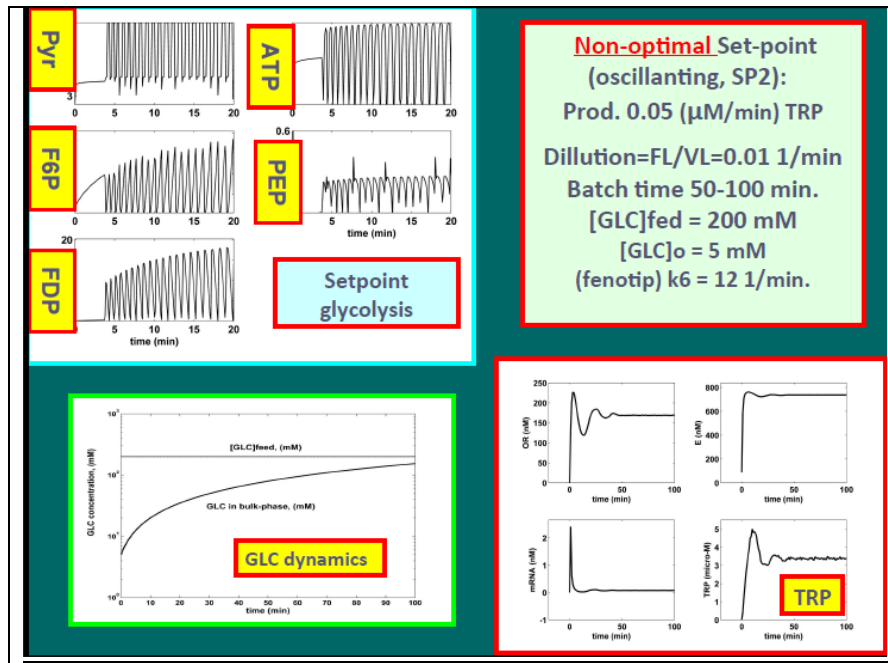


Fig. TRP-6. One of the optimal operating policies (SP = "set-point") of the **FBR** obtained through *in-silico*, *off-line* evaluations. While glycolytic oscillations are stable and present a high frequency, TRP synthesis becomes oscillating, reporting low yields [8,9,13,1

Table 1

The concepts and the basic hypotheses of **WCVV** dynamic modelling framework in living cells of variable volume. [RW1-8].

Mass Balance and State Equations	Remarks
$\frac{dC_j}{dt} = \frac{1}{V} \frac{dn_j}{dt} - D C_j = g_j(C, k)$	continuous variable dynamic model representing the cell growing phase (ca. 80% of the cell cycle)
$\frac{1}{V} \frac{dn_j}{dt} = r_j(C, k) ; j = 1, \dots, n_s$	
$V(t) = \frac{RT}{\pi} \sum_{j=1}^{n_s} n_j(t)$	Pfeffer's law in diluted solutions
$D = \frac{1}{V} \frac{dV}{dt} = \left(\frac{RT}{\pi} \right) \sum_j \left(\frac{1}{V} \frac{dn_j}{dt} \right)$	D = cell content dilution rate = cell volume logarithmic growing rate
$\frac{RT}{\pi} = \frac{V}{\sum_{j=1}^{n_s} n_j} = \frac{1}{\sum_{j=1}^{n_s} C_j} = \frac{1}{\sum_{j=1}^{n_s} C_{jo}}$ constant.	constant osmotic pressure (π) constraint
$\left(\sum_j C_j \right)_{cyt} = \left(\sum_j C_j \right)_{env}$	Derived from the isotonic osmolarity constraint
Hypotheses:	
a. Negligible inner-cell gradients.	
b. Open cell system of uniform content.	
c. Semi-permeable membrane, of negligible volume and resistance to nutrient diffusion, following the cell growing dynamics.	
d. Constant osmotic pressure (the same in cytosol "cyt" and environment "env"), ensuring the membrane integrity ($\pi_{cyt} = \pi_{env} = \text{constant}$).	
e. Nutrient and overall environment species concentration remain unchanged over a cell cycle t_c .	
f. Logarithmic growing rate of average $D_s = \ln(2)/t_c$; volume growth of ; $V = V_0 e^{D_s t}$; t_c = duration of the cell cycle.	
g. Homeostatic stationary growth of $(dC_j / dt)_s = g_j(C_s, k) = 0$.	
h. Perturbations in cell volume are induced by variations in species copynumbers under the isotonic osmolarity constraint: $V_{perturb} / V = (\sum n_j)_{perturb} / (\sum n_j)$.	
Notations: T = absolute temperature; R = universal gas constant; V= cell (cytosol) volume; π = osmotic pressure; C_j = cell species j concentration; n_j = species j number of moles; r_j = j-th reaction rate; t = time; k =rate constant vector; "s" index indicates the stationary state.	

5. Conclusions

As proved by the above case studies above and others (not presented here), kinetic models based on the reaction mechanism, of the HMCSMD hybrid type, formulated in the new WCVV kinetic modelling framework, both introduced and promoted by Maria [rw1-8], even if they are more computationally intensive and require more experimental information, they have proven to be more flexible, and can offer higher quality predictions in terms of precision and degree of detail (number of species considered), being very suitable for a) *in-silico* design of GMOs with desired properties, and b) *in-silico*, off-line optimization with a high precision of industrial bioreactors. This is due to the way by which the structured cellular metabolic processes (with state variables at the nano-molar scale) are explicitly connected with the dynamic processes at the bioreactor level, with macroscopic state variables. These aspects make them increasingly used in engineering evaluations with multiple advantages, as follows:

I.)- Realization of a higher degree of detail and precision of the kinetic model predictions, both at the macro-scopic level (the number of state variables of the bioreactor), and at the nano-scopic level (the dynamics of a large number of cellular species belonging to the CCM).

II.)- Prediction of the key metabolic reaction rates (fluxes) inside the cell. These CCM fluxes (i.e. metabolic reaction rates under stationary, homeostasis conditions) directs the efforts to obtain GMOs with desired characteristics regarding obtaining the desired metabolite (for example TRP in case study 5).

III.)- The HMCSMD hybrid model (which explicitly couples the nano-cellular processes with the macro-scopic processes in the liquid phase of the bioreactor) can predict the adaptation of bacteria metabolism (cell fluxes) to the changes in the bioreactor environment during several tens of cell cycles. The hybrid model can also predict the effect of cell cloning (case study 2) or of GMOs (case study 5) on the efficiency of the bioreactor.

IV.)- Extended HMCSMD models (in WCVV format) can provide predictions with a higher accuracy when used for biochemical engineering calculations (off-line optimization of bioreactor operation), compared to unstructured Michaelis-Menten or Monod models. For example, in case study 5, concerning the maximization of tryptophan production (TRP) in a continuous MASCR (mechanical agitated semi-continuous bioreactor), the HMCSMD hybrid model can predict: (a) an optimal operating policy for a constant feed [rw5-8], or (b) an optimal variable feeding policy (both as flow rate and GLC substrate concentration) of the bioreactor, which is leading to a better TRP-productivity compared to the operation with a constant feeding.

V.)- As presented in the specialized literature [rw1-8], complex MCSMD models can also be used in bioinformatics studies, for example to evaluate the

influence of the bioreactor operating conditions (that is the control variables) on the dynamics of the key species at a cellular nano-scopic scale, and on the cellular fluxes involved in the synthesis of a target metabolite. For case study no. 5, the species and fluxes of interest are those related to glycolysis, the ATP recovery system, and the TRP operon expression. Such evaluations can direct the in-silico design of GMOs with desired characteristics ("motifs").

VI).- As proved by Maria [rw1-8] in example no.2, the HMCSMD models can be used to obtain reduced dynamic models, more accessible to fast engineering calculations, by using specific numerical algorithms to reduce the model and additional kinetic data valid in the analyzed "local" operating area. See [27,28] for nonlinear/general MCSMD models, or [29,30] for linear kinetic models. As a result of such an approach, the complexity of the bioprocess can be described by a sequence of reduced local models "folded" on the real process. The local/reduced models usually include only the key metabolic pathways in order to obtain quickly (on-line), approximately predictions of interest regarding the state of the bioprocess in the bioreactor.

6. Reviews works

- [RW-1]. Maria, G., 2017, *A review of some novel concepts applied to modular modelling of genetic regulatory circuits*, (Juniper publ, Irvine CA, USA), 2017, ISBN (USA) 978-1-946628-03-9. <https://juniperpublishers.com/ebook-info.php>
- [RW-2]. Maria, G., 2017, *Deterministic modelling approach of metabolic processes in living cells - a still powerful tool for representing the metabolic process dynamics*, (Juniper publ, Irvine CA, USA), ISBN 978-1-946628-07-7(USA). <https://juniperpublishers.com/ebook-info.php>
- [RW-3]. Maria, G., 2018, *In-silico design of Genetic Modified Micro-organisms (GMO) of industrial use, by using Systems Biology and (Bio)Chemical Engineering tools*, (Juniper publ, Irvine CA, USA), 2018, ISBN (USA) 978-1-946628-12-1. <https://juniperpublishers.com/ebook-info.php>
- [RW-4]. Maria, G., 2024, Hybrid modular kinetic models linking cell-scale structured CCM reaction pathways to bioreactor macro-scale state variables. Applications for solving bioengineering problems, Juniper publ. Inc., Irvine, California (USA), (300 pages), in-press (galley-proofs).
- [RW-5]. Maria, G., 2023 Application of (bio)chemical engineering concepts and tools to model GRCs, and some essential CCM pathways in living cells. Part 1. Generalities, *Curr Trends in Biomedical Eng & Biosci.*, (Juniper publ, Irvine CA, USA), 22(1), 556080-556104 (2024). DOI: 10.19080/CTBEB.2023.22.556080
- [RW-6]. Maria, G., 2024, Application of (bio)chemical engineering concepts and tools to model GRCs, and some essential CCM pathways in living cells. Part 2. Mathematical modelling framework, *Annals of Reviews & Research*, (Juniper publ, Irvine CA, USA), 10(3), pp. 555790-555835, DOI: 10.19080/ARR.2024.10.555790
- [RW-7]. Maria, G., (2024) Application of (bio)chemical engineering concepts and tools to model GRCs, and some essential CCM pathways in living cells. Part 3. Applications in the bioengineering area, *Archives in Biomedical Engineering & Biotechnology*, (Iris publ,

- San Francisco CA, USA), 7(5), (2024), ABEB MS.ID.000672. DOI: 10.33552/ABEB.2024.07.000672.
- [RW-8]. Maria, G., (2024), Application of (bio)chemical engineering concepts and tools to model GRCs, and some essential CCM pathways in living cells. Part 4. Applications in design some GMO-s, *Annals of Systems Biology*, (Peertechz publ, Los Angeles, USA), 7(1), 001-034, 2024, Article ID: ASB-7-121, <https://doi.org/10.17352/asb.000021>

REFERENCES

- [1] Maria, G., 2014, *Chemical & Biochemical Engineering Quarterly*, 28 (2014), 35-51.
- [2] Maria, G., Luta, I., *Computers & Chemical Eng.*, 58 (2013), 98-115. DOI: 10.1016/j.compchemeng.2013.06.004.
- [3] Maria, G., (2009B), *Chemical and Biochemical Engineering Quarterly*, 23 (2009B), 323-341.
- [4] Maria, G., *Revista de Chimie (Bucharest)*, 61(2010), 172-186.
- [5] Maria, G., Luta, I., Maria, C., *Chemical Papers*, 67 (2013), 1364–1375. DOI: 10.2478/s11696-013-0403-z.
- [6] Maria, G., Xu, Z., Sun, J., *Chemical & Biochemical Engineering Quarterly*, 25 (2011), 403-424.
- [7] Maria, G., *Chemical & Biochemical Engineering Quarterly*, 28 (2014), 509-529. doi: 10.15255/CABEQ.2014.2002
- [8] Maria, G., *Frontiers in Chemistry*, 8 (2020c), 526679-526693. doi: 10.3389/fchem.2020.526679.
- [9] Maria, G., Gijiu, C.L., Maria, C., Tociu, C., *Computers & Chemical Engineering*, 108 (2018a), 395-407. <https://doi.org/10.1016/j.compchemeng.2017.10.003>.
- [10] Maria, G., Mihalachi, M., Gijiu, C.L., *Chemical and Biochemical Engineering Quarterly*, 32 (2018b), 523-533. doi: 10.15255/CABEQ.2018.1300.
- [11] Maria, G., Mihalachi, M., Gijiu, C.L., *U.P.B. Sci. Bull., Series B - Chemie*, 80 (2018e), 27-38.
- [12] Maria, G., Mihalachi, M., Gijiu, C.L., *Chemical Eng. Res. and Design*, 135 (2018), 207-221. [HTTPS://doi.org/10.1016/j.cherd.2018.05.011](https://doi.org/10.1016/j.cherd.2018.05.011)
- [13] Maria, G., *Computers & Chemical Engineering*, 153 (2021), 107450-107466. <https://doi.org/10.1016/j.compchemeng.2021.107450>
- [14] Mihalachi, M., Maria, G., *U.P.B. Sci. Bull., Series B - Chemie*, 81 (2019), 29-36, <http://www.scientificbulletin.upb.ro/>.
- [15] Maria, G., Renea, L., (2021), *Bioengineering-Basel*, 8 (2021), 210-247. <https://doi.org/10.3390/bioengineering8120210>
- [16] Hatzimanikatis, V., Floudas, C.A., Bailey, J.E., *AIChE J.*, 42 (1996), 1277-1292.
- [17] Edwards, J.S.; Palsson, B.O., *Proc. Natl. Acad. Sci. USA*, 97 (2000), 5528-5533, doi: 10.1073/pnas.97.10.5528
- [18] Heinrich, R., Schuster, S., *The regulation of cellular systems*, Chapman & Hall, NY, 1996.
- [19] Maria, G., Scoban, A., *Revista de Chimie (Bucharest)*, 68 (2017), 3027-3037.
- [20] Maria, G., Scoban, A., *Revista de Chimie (Bucharest)*, 69 (2018), 259-266.
- [21] Maria, G., Maria, C., Tociu, C., *UPB Bull. Sci., series B*, 79 (2017), 3-19.
- [22] Maria, G., Gijiu, C.L., Maria, C., Tociu, C., Mihalachi, M., *Current Trends in Biomedical Engineering & Biosciences*, 12 (2018), CTBEB.MS.ID.555833, DOI: 10.19080/CTBEB.2018.12.555833.
- [23] Maria, G., Crisan, M., *J. Process Control.*, 53 (2017), 95-105. DOI: 10.1016/j.jprocont.2017.02.004

- [24] Rao, S.S., Engineering optimization – Theory and practice, Wiley, New York, 2009.
- [25] Chen, M. et al., Metabolic Eng. Commun., 12 (2021), e00167.
<https://doi.org/10.1016/j.mec.2021.e00167>
- [26] Chen, M., PhD thesis, TU Hamburg, 2020.
- [27] Maria, G., Algoritmi numerici de simplificare a modelelor cinetice ale proceselor chimice și biochimice, Printech, Bucharest, 2019 (815 pagini).
- [28] Edwards et al., Comp. & Chem. Eng., 22 (1998), 239-246.
- [29] Maria, G., Chemical Engineering Science, 60, (2005), 1709-1723,
[doi:10.1016/j.ces.2004.11.009](https://doi.org/10.1016/j.ces.2004.11.009).
- [30] Martinez, E.C., Beltramini, L.J., Chem. Eng. Sci., 45 (1990), 2103-2108,
[https://doi.org/10.1016/0009-2509\(90\)80083-Q](https://doi.org/10.1016/0009-2509(90)80083-Q)